PLASMA TRANSPORT IN A MAGNETIC MULTICUSP NEGATIVE HYDROGEN ION SOURCE

DISSERTATION

Ricky G. Jones
Captain, USAF

AFIT/DS/ENP/91-02

DEPARTMENT OF THE AIR FORCE
AIR UNIVERSITY
AIR FORCE INSTITUTE OF TECHNOLOGY

Wright-Patterson Air Force Base, Ohio

AFIT/DS/ENP/91-02

PLASMA TRANSPORT IN A MAGNETIC MULTICUSP NEGATIVE HYDROGEN ION SOURCE

DISSERTATION

Ricky G. Jones
Captain, USAF

AFIT/DS/ENP/91-02

Approved for public release; distribution unlimited

AFIT/DS/ENP/91-02

PLASMA TRANSPORT IN A MAGNETIC MULTICUSP NEGATIVE HYDROGEN ION SOURCE

DISSERTATION

Presented to the Faculty of the School of Engineering
of the Air Force Institute of Technology
Air University
In Partial Fulfillment of the
Requirements for the Degree of
Doctor of Philosophy

Ricky G. Jones, B.S., M.S.
Captain, USAF

December 1991

AFIT/DS/ENP/91-02

PLASMA TRANSPORT IN A MAGNETIC MULTICUSP NEGATIVE HYDROGEN ION SOURCE

Hicky G. Jones, B.S., M.S.
Captain, USAF

Approved:

Wm. F. Bailey — 27 Nov '91
William F. Bailey, Chairman

Alan Garscadden — 3 DEC '91
Alan Garscadden

Alan V. Lair — 27 Nov '91
Alan V. Lair

Accepted:

Robert A. Calico, Jr.
Dean, School of Engineering

Preface

The purpose of this work was to examine the transport of charged plasma constituents across the magnetic picket fence (filter) in negative hydrogen ion sources. The plasma flux and the rate at which thermal electrons in the source are cooled as they cross the filter affect the production and destruction rates for negative hydrogen ions. Thus, an understanding of thermal electron transport through the filter is key to optimizing negative hydrogen ion yields. One of the successes of this work was to derive an equation which correctly predicts the variation of electron cooling with flux through the magnetic filter. But the actual mechanism for electron diffusion remains something of a mystery. The magnitude of electron flux through the filter is an indication that the diffusion may be driven by ion acoustic or related turbulence associated with gradients in density and temperature in the filter region.

Also important are the transport of high energy electrons (from hot filaments) and the three positively charged ion species present in the source through the filter. High energy electrons in the extraction chamber of a negative hydrogen ion source may strip negative hydrogen ions of their excess electrons, while the distribution of positive ion species will affect *via* wall neutralization processes the production rate for vibrationally excited hydrogen molecules (from which negative hydrogen ions are produced) and the negative hydrogen ion/positive ion mutual neutralization rate. The transport of positive ions through the filter appears to be well described by an equation that assumes that ion motion is collisionless. The transport of energetic electrons, like that of thermal

electrons, proceeds at an anomalous rate, indicating that microinstabilities may be enhancing diffusion.

Negative hydrogen ions extracted from the source will be accelerated then stripped of their excess electrons to form energetic neutral hydrogen ion beams. These beams can be used to heat fusion plasmas and in space-based weapon systems.

Several people were of great help to me in performing this research. I want to thank first my wife Karen and my sons Christopher and Geoffrey for encouraging me to complete this dissertation and for making home a superior place to work - far superior to the officially sanctioned work environment. I also want to thank my faculty advisor, Dr William Bailey, for his careful attention to the details upon which my arguments rest, and Mr Joe Marshall for repeatedly drawing vivid verbal pictures of how miserable my future would be if I failed to graduate.

Table of Contents

List of Figures

List of Tables

Abstract

An analysis of plasma transport through the magnetic filter in magnetic multicusp tandem negative hydrogen ion sources was conducted. The objectives of the study were to 1) assess the rate of thermal electron transport through the magnetic filter, 2) analyze the scaling of thermal electron diffusion with plasma electrode bias voltage and magnetic filter induction and hence determine the mechanism of thermal electron diffusion, 3) explain the observed variations of thermal electron cooling with plasma electrode bias voltage as a function of thermal electron flux through the magnetic filter, 4) describe the transport of energetic electrons through the magnetic filter, and 5) model the transport of positive ion species through the magnetic filter and calculate the relative percentages of extracted positive ion species.

The rate of thermal electron transport through the magnetic filter was found to be one to three orders of magnitude higher, depending upon discharge parameters, than the rate expected from classical collisional transport theory. Thermal electron flux through the filter is known to scale as the inverse square of the magnetic induction. Although the collision frequency temperature dependence could not be determined from the data, the flux variation was best described using a Coulomb-like temperature gradient drag term. Theoretically, the candidate thermal electron diffusion mechanism consistent with these results is scattering from weak ion sound or related turbulence.

Thermal electron energy flux loss through the magnetic filter was found to be due to 1) inelastic collisions with neutral molecular hydrogen at low values of thermal electron flux and 2) plasma potential variations at high values of the thermal electron flux. An equation was derived which correctly reproduces the observed variation of the ratio of source to extraction chamber plasma densities as a function of the ratio of source to extraction chamber thermal electron temperatures.

The flux of primary electrons through the filter was shown to be one order of magnitude higher than the classical collisional rate. Positive ion species transport was modelled assuming ballistic flow rather than diffusion through the filter. Relevant ion production and loss mechanisms were used in conjunction with the transport model to calculate extracted positive ion species percentages. Results were found to be in reasonable agreement with experiment.

PLASMA TRANSPORT IN A MAGNETIC MULTICUSP NEGATIVE HYDROGEN ION SOURCE

Chapter I - Introduction

Preliminary Remarks

An outline of this effort to model charged particle transport through the magnetic filter in H^- sources will be presented in the final section of this chapter. First, H^- sources will be described in detail: the motivation for producing H^- in abundance will be given, and the configuration of a typical H^- source described. Variations in plasma density and electron temperature with various discharge parameters will be presented, followed by an overview of H^- production and loss mechanisms. Results of recent efforts to model H^- sources will be summarized. Then the transport problem itself and the relevant parameter space will be described.

In the H^- sources of interest here, the primary physical process resulting in the production of H^- is dissociative attachment of low energy electrons to vibrationally excited hydrogen molecules ($H_2(v) + e \rightarrow H + H^-$) (Bacal, 1988). This reaction is thought to occur predominantly in the volume of the plasma rather than at a surface, hence the name "volume" source. In a volume source with a magnetic filter, H^- is produced in abundance in a region called the target chamber which is mag-

netically shielded from the region where electrons and positive ions are produced. The H^- production rate in the target chamber is a function of low energy electron density and temperature, while H^- loss is due to mutual neutralization with positive ions. Plainly, a comprehensive H^- source model must provide for the computation of electron transport and cooling rates and positive ion transport rates across the magnetic filter into the target chamber.

Description of Volumes Sources

Motivation. H^- sources are required for the generation of intense neutral hydrogen beams with energies in excess of 150 keV per nucleon to heat magnetically confined fusion plasmas. Actually, negative ionic deuterium, D^-, is preferred to H^-, since it is one of the reactants in the deuterium-tritium fusion reactions. Some estimates require deuterium energies of 400 keV to achieve sufficient penetration of the confined plasma prior to ionization of the injected neutral deuterium atoms (Forrester, 1987). The neutral beams must have current densities between 10 and 100 mA/cm^2 (Hiskes, 1984: 1927) for this purpose.

In addition to heating fusion plasmas, neutral beams have the potential to be employed in space-based weapon systems (Forrester, 1987). The atomic hydrogen beam energy required to disarm the electronics of a nuclear warhead is approximately 100 MeV per nucleon (McKee, 1986).

Negative ions are preferred to positive ions for beam formation because beam energies must be high. The neutralization efficiency of positive ions is very low at high energies: the charge exchange cross

section drops rapidly at energies above 100 keV/nucleon, resulting in a neutralization efficiency of about 20%. For negative ions, the neutralization efficiency at the same energy is about 60% with a gas stripping target, while a plasma stripping target can improve this to about 85% (Figure 1-1) (Walther, 1988).

History. Interest in the generation of negative hydrogen ion beams began with Ehler's work in 1965 when a high current (> 40 mA) beam of negative ions was extracted from a Penning source. Since that time, three methods for producing negative hydrogen ions have been considered: the double charge exchange process which converts a proton beam into a negative ion beam; the bombardment of a cesiated surface by a plasma rich in H^+ (known as a surface plasma source); and the generation of negative hydrogen ions in the volume of a plasma. Double charge exchange sources produce large negative ion currents, but beam cross sections are necessarily large, resulting in low current densities. These sources also leak gas into the accelerator vacuum, thus degrading beam quality. Surface-plasma sources have been operated successfully since 1971 when intense negative ion yields were observed after cesium vapor was injected into an arc discharge by Soviet researchers in Novosibirsk. To date, these devices have produced beam currents on the order of 1 ampere, and current densities roughly 1 A/cm^2 (Wells, 1981).

Interest in the production of negative hydrogen ions in the volume of a plasma was sparked by the discovery by Bacal and Hamilton in 1979 that negative hydrogen ions can be created in copious amounts in a hot plasma hydrogen discharge (Leung, 1983). Experiments at

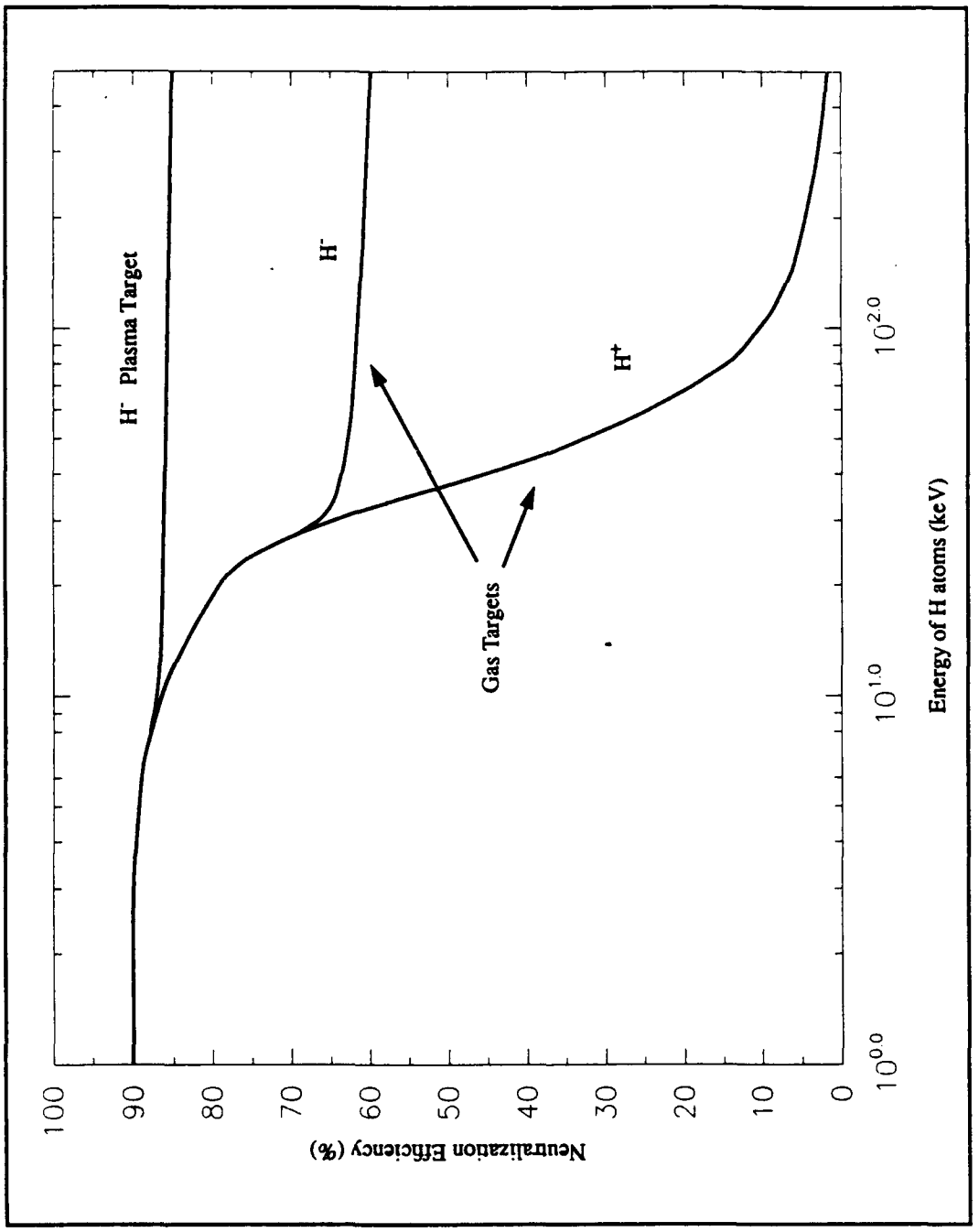

Figure 1-1: Maximum Neutral Fraction vs Beam Energy

Ecole Polytechnique in France in 1976-77 had produced measurements of H^- density in a diffusion-type plasma (with glass walls and no magnetic wall shielding) 100 times larger than that computed from cross sections then known for H^- production and loss. Relative to the other production methods, production in the volume of a discharge should have the advantage of creating a relatively quiescent beam at high current densities (Bacal, 1982). Indeed, the prime advantage of the volume source is that it produces H^- at very low temperatures (Ehlers, 1990).

Configuration. Details of the physical configuration of H^- volume sources will be given in Figures 1-2 through 1-4. Typically, a volume source consists of a stainless steel cylinder about 20 cm in diameter and 30 cm in length, although there has been one important variation on this shape: a source with rectangular walls, 55 cm by 31 cm by 20 cm in dimensions (Holmes, 1987). (Where reference to the source shape is necessary, the rectangular parallelepiped source will be referred to as the box source.)

In the cylindrical source (Figures 1-2 (Ehlers (1982b) and 1-3 (Ehlers, 1982a)), samarium cobalt magnets are mounted along the external surface in grooves carved to within millimeters of the plasma volume. These magnets produce fields in excess of 1 kilogauss near the walls but a very weak field near the chamber center and are placed to form cusp lines parallel to the cylinder axis with the north and south magnetic poles alternately facing the plasma. Magnets are also placed on the circular face of the cylinder opposite the extraction opening (Ehlers, 1981). Through this face also are introduced several fine (0.05 cm in diameter) tungsten filaments (Ehlers, 1982b).

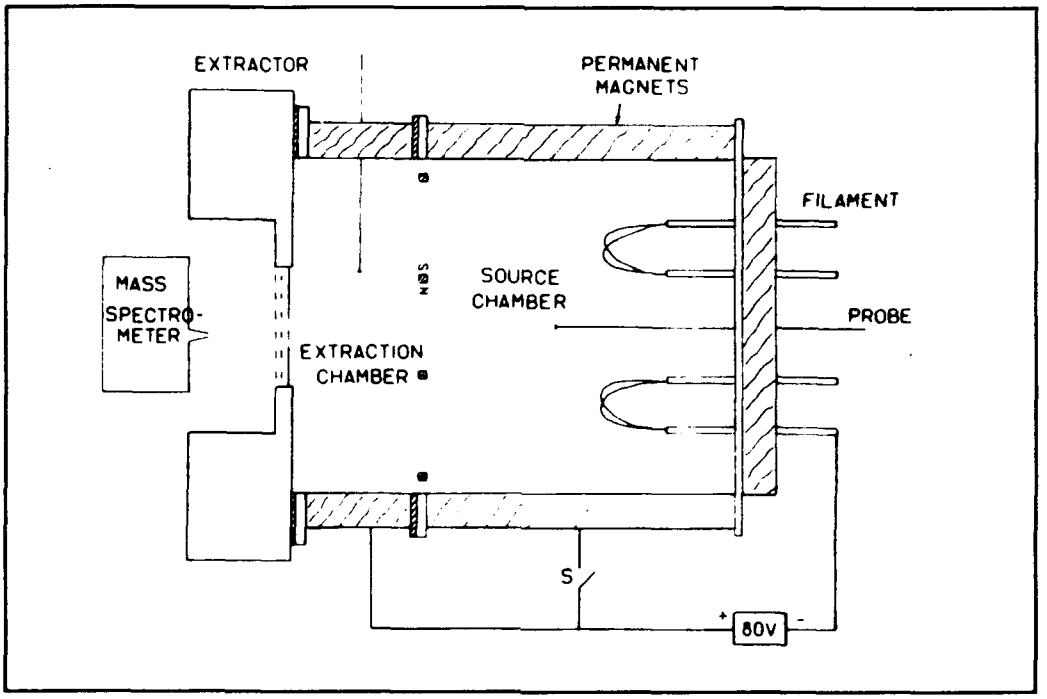

Figure 1-2: Cylindrical Source

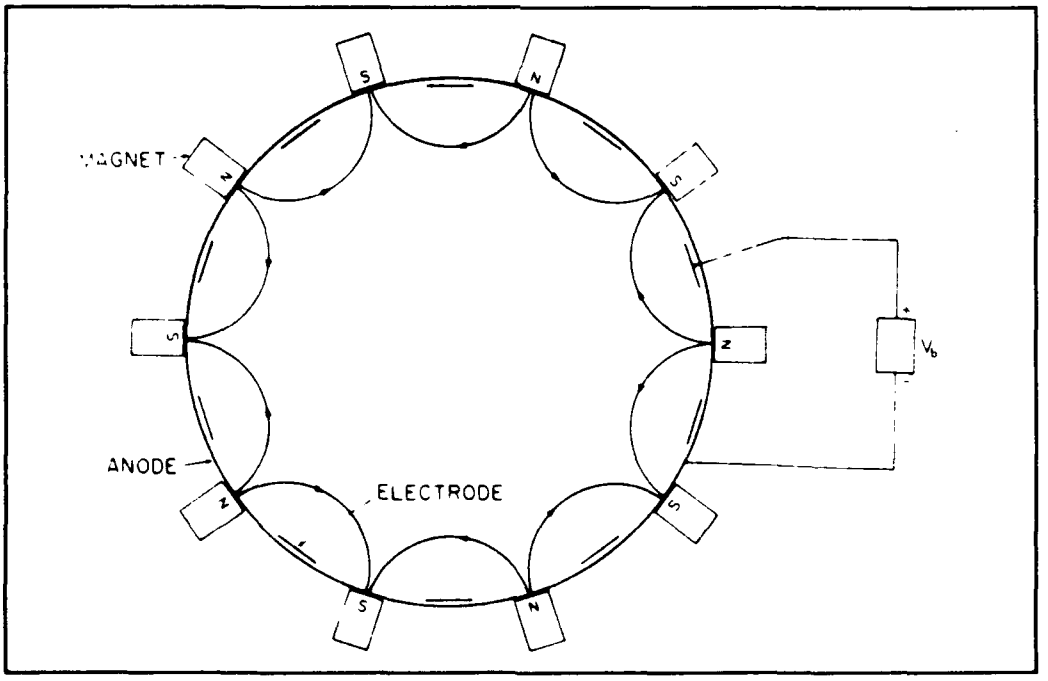

Figure 1-3: Wall Magnets on Cylindrical Source

In the box source, the external magnets do not extend the length of the device. They are positioned in a checkerboard pattern, with north and south poles alternately facing the plasma. Here, also, tungsten filaments are introduced through one wall (see Figure 1-4) (Holmes, 1987).

Sources with Filters. In the type of negative ion source most relevant to this research, the tandem magnetic multicusp device, the interior is divided into two chambers by a magnetic filter which allows the motion of ions and low temperature (< 1 eV) electrons from one chamber, called the source chamber, to the second, known as the target or extraction chamber. The filter thus enhances H^- production by separating the plasma into a source region where energetic electrons excite vibrational energy levels of H_2 and a target chamber where cold electrons dissociate vibrationally excited H_2 into H^- and H. In a cylindrical source, the magnetic filter field can be formed by inserting a bank of magnets into the source parallel to the plasma electrode (Figure 1-2) (Ehlers, 1981) or by introducing two banks of current-carrying wires into the same plane (Holmes, 1982b; Bezverbaja, 1988). When the field is produced by permanent magnets, the maximum field strength is typically less than 100 gauss (Ehlers, 1981). When the field is produced by current-carrying wires, the strength is adjustable (Holmes, 1982b).

In a box source, the magnetic filter field is created by two rows of bar magnets on the exterior of the source which form rows of north or south poles parallel to the long axis of the source. The field has a maximum value on the center plane of the source of about 60 gauss, although, of course, this depends on the strength of the wall confinement magnets (Holmes, 1987).

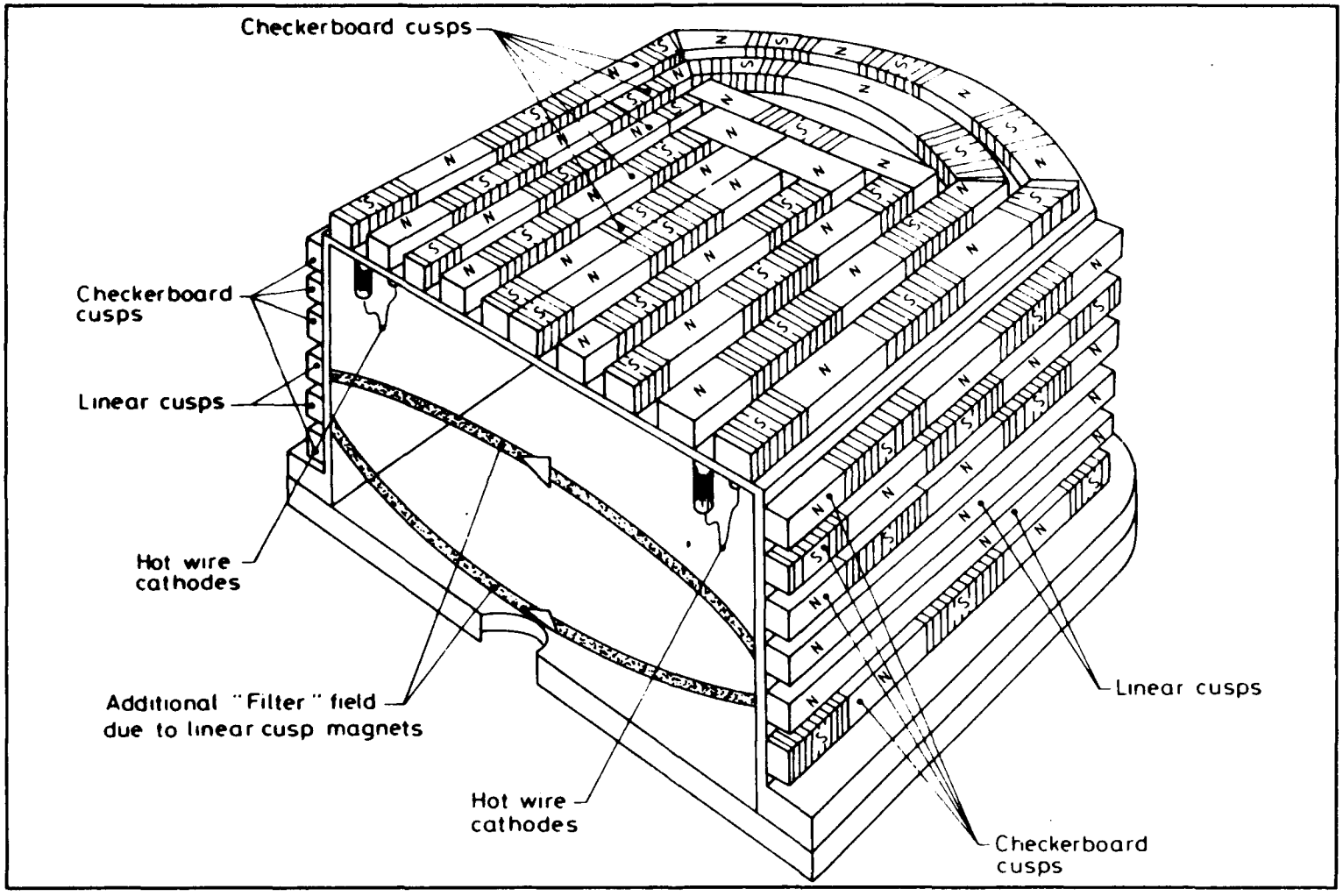

Figure 1-4: Box Source

In the source chamber, thermionic electrons from filaments are accelerated to energies of about 100 eV and interact with the neutral gas to form the plasma and excite the hydrogen molecules into higher vibrational levels (Bacal, 1988). The electron energy distribution function has a high energy tail with a high concentration of electrons with energies in excess of 25 eV (Hiskes, 1987). The target chamber has no or very few high energy electrons (Hopkins, 1988) and a low (< 1 eV) electron temperature. In both chambers the plasma is confined by the use of magnets at the walls. The wall magnets increase the efficiency of the discharge by reflecting the high energy electrons back into the plasma and by limiting plasma losses to the cusp lines. And even on the cusp lines, electrons are subject to mirror-like confinement (Bacal, 1988). Leung and Ehlers have shown that plasma confinement is superior for a line-cusp magnet geometry (as in a cylindrical source) to that of a checkerboard magnet configuration (Leung, 1984a).

One wall in the target chamber generally left free of magnetic shielding is the target chamber end plate or plasma electrode. H^- is extracted through apertures bored in the end plate. In most experiments, the plasma electrode voltage can be varied independently of the voltage on the other walls.

The confinement of the plasma by wall magnets allows the production of a relatively high density plasma at low pressures. (Pressures in the typical H^- volume sources to be discussed in this work are on the order of 1 mTorr (Ehlers, 1981).) The situation of relatively high plasma densities (10^{11} cm^{-3}) with low neutral densities (10^{13} cm^{-3}) results in a high utilization efficiency. A high gas utilization efficiency is

indicative of a low relative density of neutrals in the acceleration channel of a beam (where H^- ions are accelerated after extraction from the source). Neutrals in the acceleration channel may transfer charge with the ions in the beam, degrade beam quality, or cause other undesirable effects (Forrester, 1987). In addition, low neutral pressure diminishes the rate for the stripping process $H_2 + H^- \rightarrow H_2 + H + e$ within the source itself, which can be major loss mechanism for H^- (Wadhera, 1984). Leung has shown that the presence of a magnetic filter reduces the optimum operating pressure of the source by a factor of 2 (Leung, 1985b).

Plasma Density and Potential Profile Dependence on Extraction Electrode Bias Voltage. The magnetic filter serves to produce a region of low plasma density, resulting in a significant reduction in the electron component of an extracted beam (York, 1984). The reduction in plasma density is most significant when the end plate of the target chamber has a small positive bias voltage (Ehlers, 1982b). In that case, the profile of the plasma potential in the extraction chamber (Figure 1-5) is fairly flat (Leung, 1984b), so that H^- moves easily to the end plate where it can be extracted. Since the energy of H^- upon formation is only about 0.17 eV (Wadhera, 1984), reduction of the retarding potential is an important consideration.

Electron Temperature Dependence on Magnetic Filter Field Strength. As stated above, the magnetic filter also reduces the electron temperature in the target chamber below that in the source chamber (Ehlers, 1981). The reduction in electron temperature can also occur along the field lines when the plasma is separated by a magnetic mirror field

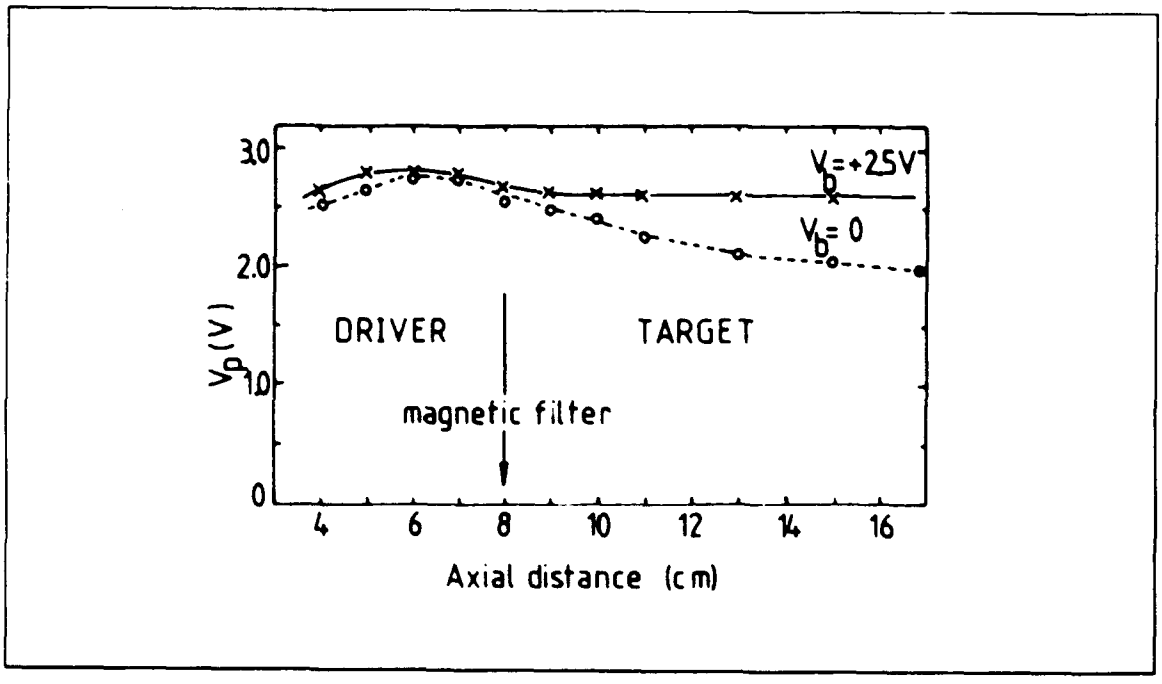

Figure 1-5: Plasma Potential Profile with Variable Extraction Electrode Potential

(Brynoff, 1988). Leung has investigated the dependence of the electron temperature in the target chamber on both the bias voltage on the end plate and the magnetic filter field strength. The target chamber electron temperature dependence on magnetic filter induction is fairly weak, but it would appear that the temperature reduction is more pronounced for the strong filter. Holmes has measured the dependence of extraction chamber electron temperature with the magnetic flux. His results are displayed in Figure 1-6.

Electron Temperature Dependence on Extraction Electrode Bias Voltage. As for the dependence upon target chamber end plate voltage, V_b, the temperature reduction was most pronounced (the source chamber electron temperature being about 1.4 eV, while the target chamber temperature fell to 0.4 eV) for low bias voltages (V_b = 0). The target cham-

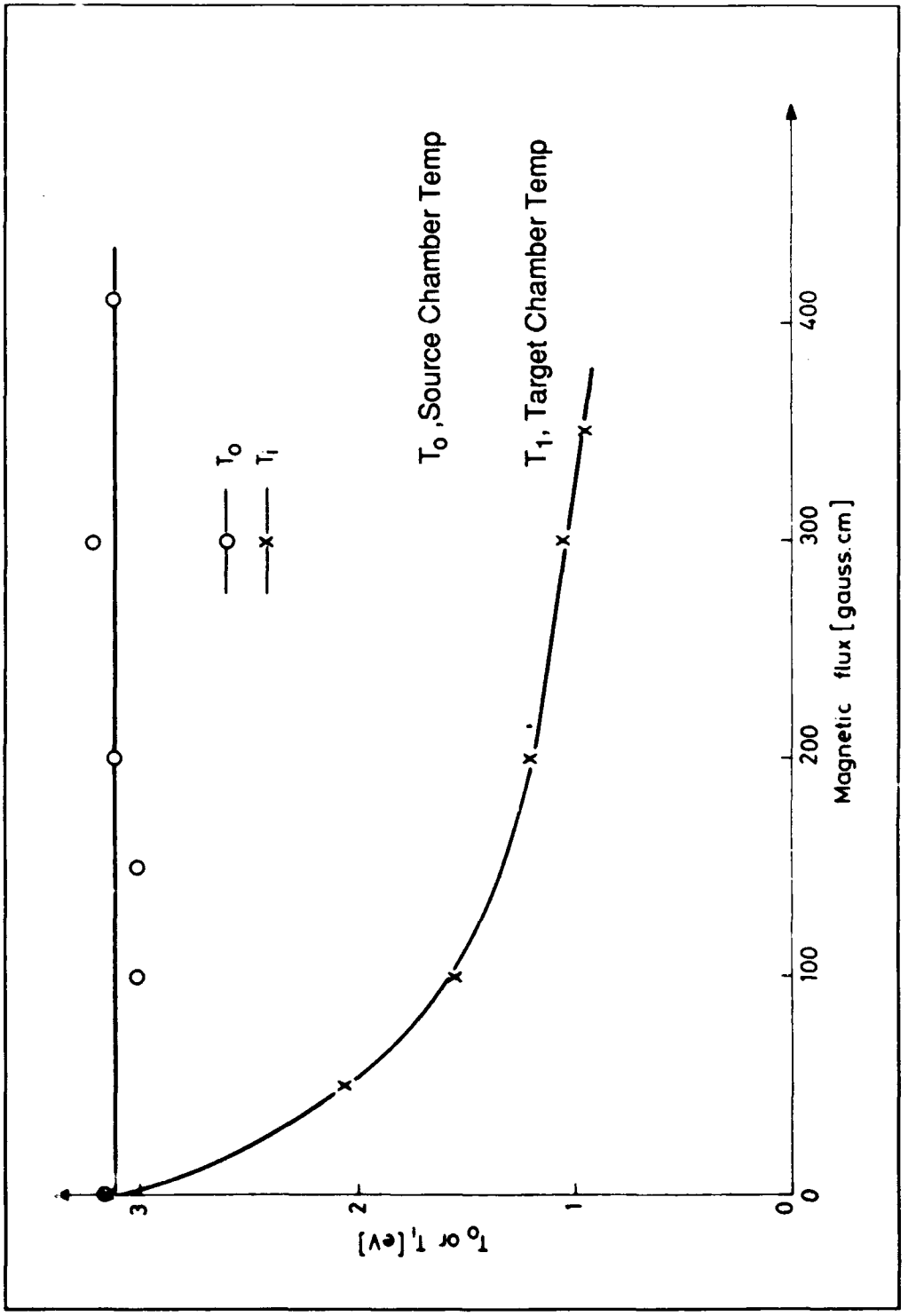

Figure 1-6: Variation of Electron Temperatures with Magnetic Flux

ber electron temperature rose slowly with increasing V_b, becoming about 0.5 eV at V_b = 2 V (Leung, 1983). Leung's Langmuir probe traces appear here as Figures 1-7 and 1-8. Figure 1-7 shows the variation for a "weak" magnetic filter, while Figure 1-8 is for a "strong" filter. The magnetic flux for the "strong" filter was twice that for the "weak" filter.

Plasma Density Dependence on Magnetic Filter Field Strength. The behavior of the plasma density with magnetic field strength is less clear. Holmes has shown that, for V_b = 0, the source chamber plasma density rises linearly with increasing magnetic flux (which varies as the magnetic field strength) while the target chamber density stays constant (Holmes, 1982a). Figure 1-9 displays Holmes' measurement of this variation. But while the Langmuir probe traces in Leung's paper indicate a rising source chamber density with magnetic filter field strength, they also indicate a fall in target chamber plasma densities for V_b > 0 (Leung, 1983).

Electron Temperature Variation with Discharge Current. According to Holmes, the electron temperature in the source chamber rises from about 3 eV for a discharge current, I_d, of 10 amperes to about 6 eV when I_d = 40 amperes. But the target chamber electron temperature rises only from 1.0 eV to perhaps 1.5 eV for the same discharge current variation. These measurements were made with a magnetic flux of 300 G cm, and here, as above with Holmes, V_b = 0 (Holmes, 1982a). Holmes' result appears here as Figure 1-10.

Plasma Density Variation with Discharge Current. Holmes also measured the variation of plasma density with the discharge current for the same magnetic flux. He found that the source chamber plasma density rose by a factor of 3 to 4 over the range of discharge currents, while

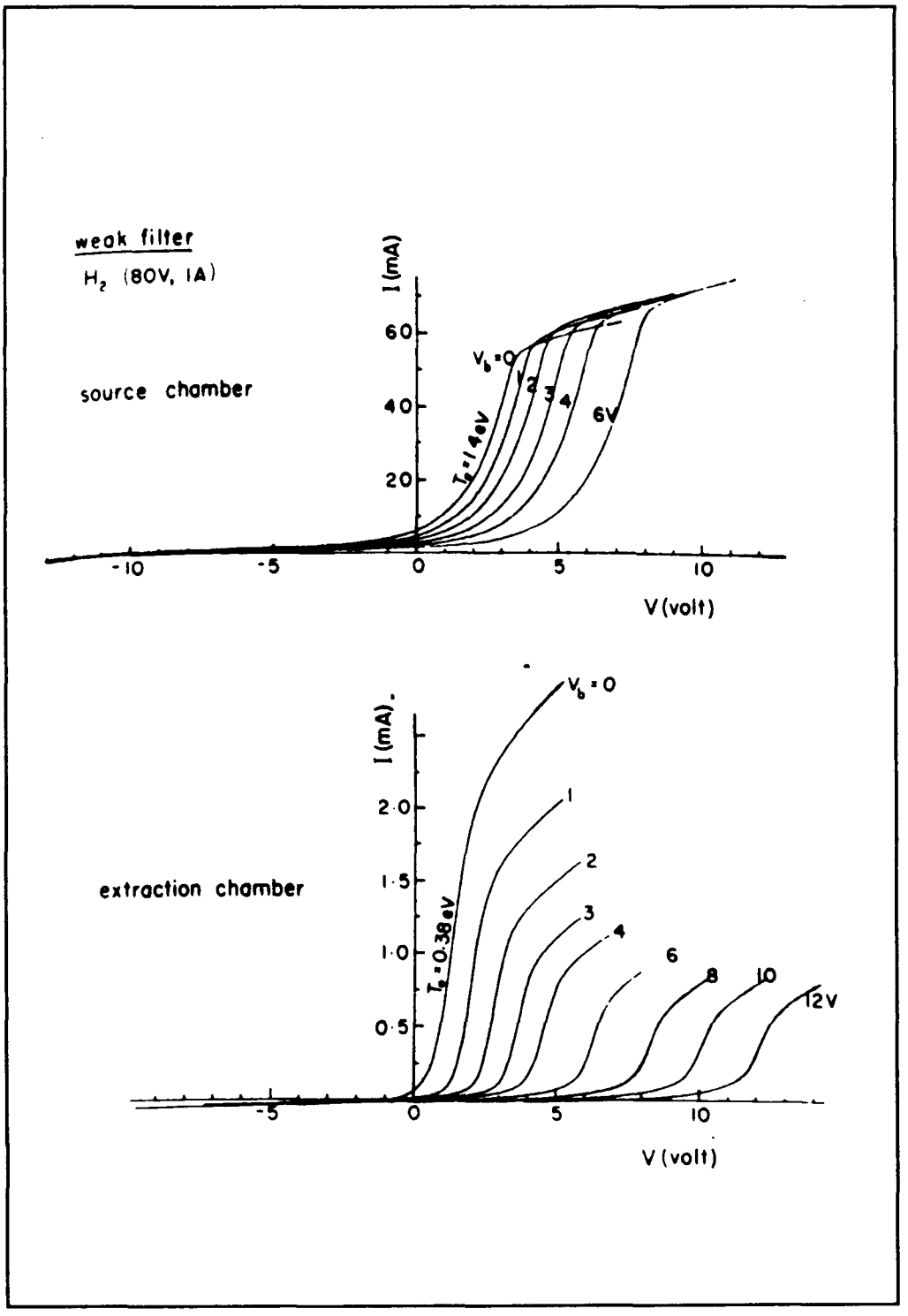

Figure 1-7: Leung's Probe Traces for a Weak Magnetic Filter

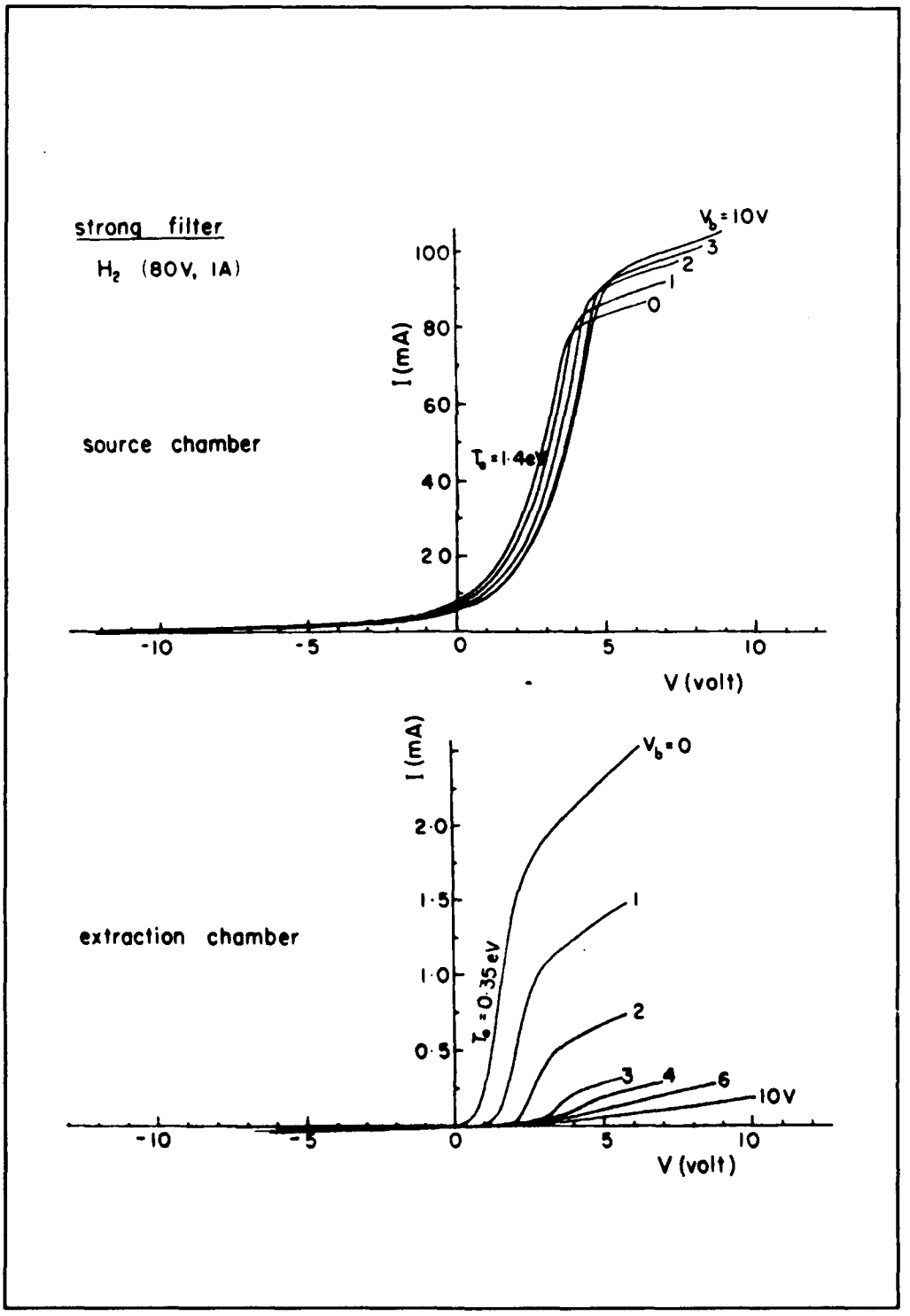

Figure 1-8: Leung's Probe Traces for a Strong Magnetic Filter

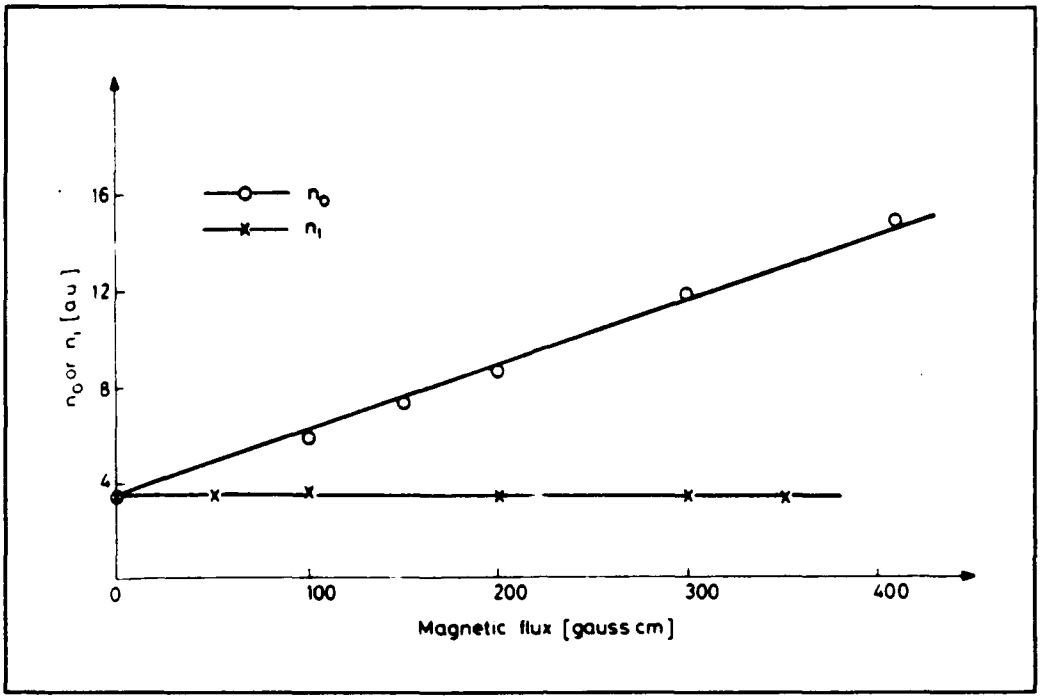

Figure 1-9: Plasma Density Dependence on Magnetic Flux

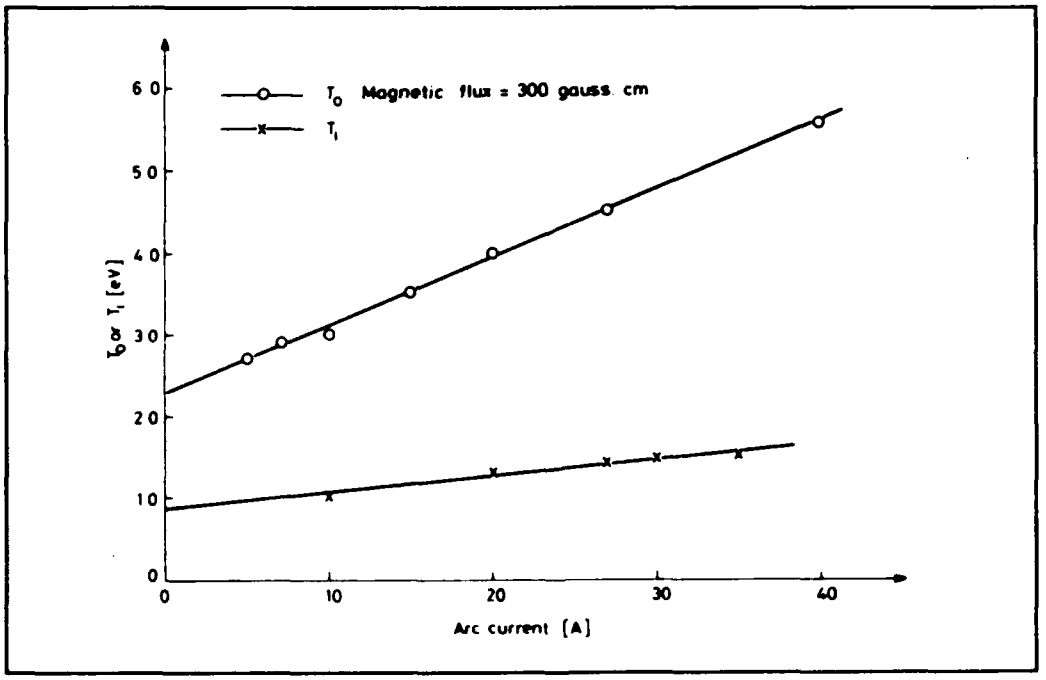

Figure 1-10: Electron Temperature Dependence on Discharge Current

the target chamber density rose by a factor of 2 over that range. Here again V_b = 0 (Holmes, 1982a).

Production and Loss Mechanisms

Production and Loss of H^-. The plasma in the source chamber consists of three positive ion species -- H^+, H_2^+, and H_3^+ -- and the negative ion H^-, together with both energetic and thermal electrons (Mordin, 1983). The emitted energetic electrons are accelerated through the sheath which forms at the tungsten filaments and acquire an energy equal to the difference between the filament voltage and the plasma potential (this is typically over 100 V). They have sufficient energy to excite molecular hydrogen vibrationally.

Variations in target chamber plasma densities and electron temperatures are of great importance to the production of H^- by dissociative attachment of vibrationally excited H_2. The largest cross sections for this process are for the higher vibrational levels of H_2, $v > 7$. For these vibrational levels, the cross sections peak at electron energies of less than 1 eV (Mordin, 1983: 57, 63).

The importance of low electron temperatures to this process was demonstrated by Leung *et al* in 1986. In an experiment the electron temperature in the extraction chamber was reduced from 1.0 eV to 0.5 eV by the injection of cold (0.5 eV) electrons. It was found that the plasma density in the extraction chamber increased by a factor of 3, and the H^- yield improved by more than a factor of 4. The increased yield is attributed to the reduction of electron temperature in the extraction chamber (Leung, 1986).

But even at higher electron temperatures the H^- production rate is sensitive to $H_2(v)$ (vibrationally excited H_2) populations. Theoretical calculations by Wadhera show that the dissociative attachment rate increases by four orders of magnitude from the fourth to the eleventh vibrational levels for a range of electron temperatures $T_e > 1$ eV, so it is advantageous to maximize the populations of the higher vibrational levels (Mordin, 1983).

Negative hydrogen ions can also be produced by polar dissociation to molecular hydrogen and dissociative recombination of H_2^+ and H_3^+:

Polar dissociation: $H_2 + e \rightarrow H^- + H^+ + e$

Dissociative recombination: $H_2^+ + e \rightarrow H^- + H^+$

$H_3^+ + e \rightarrow H^- + H_2^+(v)$

These processes, however, are negligible compared to dissociative attachment of vibrationally excited molecular hydrogen (Mordin, 1983).

Recent experiments in a cesium-seeded discharge have indicated that H^- may be produced in substantial amounts at the plasma electrode, *via* a wall process (Walther, 1988).

Loss mechanisms include losses to the walls, mutual neutralization with positive ions and collisional electron detachment. (This is yet another reason that T_e in the extraction chamber should be low. The electron temperature should be comparable to or less than the collisional detachment threshold energy of 0.75 eV (Mordin, 1983: 74).) In the source chamber, wall losses for H^- should be small when the plasma potential is positive, as is usually the case. In the extraction chamber,

the wall loss rate will be governed by the plasma potential profile (Mordin, 1983). The collisional electron detachment rate can be a function of the choice of wall material. For low pressure discharges, secondary electrons formed from energetic electron bombardment of the anode along the cusp lines can decrease H^- yield. When primary electrons are present in the extraction chamber, wall material with a high work function must be selected in order to decrease secondary electron emissions. Aluminum appears to be the best choice (Leung, 1985a).

Regardless of the wall material, collisional electron detachment plays a major role in H^- destruction in the source chamber. The importance of this effect was shown by Leung and Bacal who measured the ratio of H^- to electrons in the source chamber of a device to be 0.02 when the filaments were placed in the magnetic field free region near the center of the chamber and 0.15 when the filaments were placed in the region of intense magnetic field strength, thereby magnetically confining energetic electrons near the walls (Leung, 1984b). (It should be noted that negative ions will congregate to the center of a discharge where the space potential is high.)

As the cross section for collisional electron detachment has a peak for electron energies near 10 eV, this process is negligible in the extraction chamber where few energetic electrons exist. Moreover, as stated previously, the thermal electrons in the extraction chamber are at a lower temperature (Mordin, 1983).

Mutual neutralization with positive ions can be the dominant loss process for negative hydrogen ions in the extraction chamber. As mutual neutralization is dependent upon the relative velocities of the interacting

particles (Bruneteau, 1985), the strength of the process is related to the pressure, plasma density, and the plasma potential profile (Bacal, 1984).

Negative hydrogen ions may also be lost through collisions with either atomic or molecular hydrogen. Stripping by molecular hydrogen frequently excites the molecular hydrogen vibrationally, leading in turn to the production of H^- through dissociative attachment. Dissociation through impact with atomic hydrogen is generally negligible due to the low atomic hydrogen density (Mordin, 1983).

Production and Loss of $H_2(v)$. Vibrationally excited molecular hydrogen is created through collisions of $H_2(v = 0)$ with high energy electrons (called E-V interactions) through an intermediate electronic state, and through collisions with thermal electrons (called e-V interactions) which generally raise or lower the vibrational quantum number by one. In addition, there exists considerable experimental evidence that recombinative desorption of atomic hydrogen on the walls is an important source of $H_2(v > 0)$, at least for v up to 5 (Cadez, 1988; Eenshuistra, 1988). This process would be of most importance in the high pressure regime. Atomic hydrogen produced in the source chamber would pass into the extraction chamber with relative ease due to its long mean free path, and there form $H_2(v)$. Calculations have indicated, however, that recombinative desorption should be important only up to level $v = 2$ (Bacal, 1988).

Another process (referred to as the S-V process) can produce $H_2(v)$: H_2^+ or H_3^+ ions are neutralized on the wall to produce $H_2(v)$. Hiskes speculates that 1/3 of H_2^+ ions reflect from the walls as $H_2(v)$ (Bacal, 1988).

As to loss mechanisms, calculations have shown that wall de-excitation is more important for vibrational levels with v less than 4, while V-T (vibrational-translational energy transfer) rates are more important from there on (Mordin, 1983) (although more recent work indicates that wall de-excitation may dominate up to v=13 or higher (Bacal, 1988)). This is true for low (I_d = 10 A) discharge currents. When the current is raised to 1000 A, however, ionization becomes the dominant loss mechanism (Bacal, 1988).

For production, it is believed that the E-V process controls the production in the range v > 6 at 10 A discharge current, and for v > 2 at I_d = 1000 A. For discharge currents less than 100 A, the e-V process dominates production up to v = 6 (Bacal, 1988).

Production and Loss of H^+. The primary creation process for H^+ is dissociative ionization of molecular hydrogen by electron impact. Losses are due to wall neutralization and mutual neutralization with H^- (Mordin, 1983).

Production and Loss of H_2^+. The dominant production process for H_2^+ is direct ionization of $H_2(v = 0)$. It is lost to the walls and through collisions with neutral H_2 which results in the creation of H_3^+ (Mordin, 1983).

Production and Loss of H_3^+. This ion is created through collisions of H_2^+ with $H_2(v = 0)$. It is lost through wall collisions, through dissociative recombination with thermal electrons, through dissociation *via* impact with energetic electrons, and through recombination with H^- (Mordin, 1983).

Production and Loss of H. The most important creation processes for atomic hydrogen are dissociation of molecular hydrogen *via* energetic electron impact and the collision of neutral hydrogen molecules with H_2^+ which results in the creation of H_3^+ and H. The only significant loss process for H is diffusion to the walls (Mordin, 1983).

Production and Loss of Electrons. The high energy electrons emitted from the tungsten filaments are degraded in energy by inelastic collisions and by Coulomb collisions with thermalized electrons. The electron-electron collisions lead to a Maxwellian distribution for the low energy portion of the electron energy distribution function (EEDF). For energies greater than 15 eV, the EEDF is proportional to the discharge current I_d. Its shape has been characterized as far from Maxwellian (Hiskes, 1985), but others assert that a second, high temperature Maxwellian energy distribution function is a good approximation to the high-energy portion of the EEDF (Hopkins, 1988). Electrons are thus produced at the filaments and through ionization. They are lost to the walls in the source chamber and through the filter to the extraction chamber where they move to the extraction electrode. Electrons may also be lost through dissociative attachment to $H_2(v)$ and attachment to ions.

High Power Discharges and Models

Yield Dependence on Discharge Current. One important feature of tandem multicusp ion sources was discovered experimentally in 1983 (York, 1984). This was the fact that the extracted H^- beam current increases almost linearly with the discharge current I_d. Bretagne *et al* have calculated the electron energy distribution function in a low pressure

(4 mTorr) source and have shown that the pumping rates for the higher vibrational levels scale as I_d (Bretagne, 1986: 1211). These facts reinforce the idea that the main source of H^- in the plasma is the dissociative process, but they also introduce a difficulty. York *et al* found that, when the discharge current was increased above 160 amperes, the source pressure was too low to keep the beam stable and quiet, and so had to be increased (York, 1984: 682). At this pressure, the beam current was 38 mA/cm^2.

Optimum Chamber Lengths at Low Pressures. An experiment was performed to determine the optimum lengths for the source and extraction chambers (Leung, 1985). When the source was operated at a pressure of 1.5 mTorr with a discharge current of 3 A and a discharge voltage of 80 V, it was found that the extracted H^- current rapidly increased when the distance from the filter to the plasma electrode was reduced to less than 4 cm. In addition, the extracted electron current was reduced, presumably because electrons were trapped in the filter magnetic field. The experimenters determined that H^- was being formed in the filter region. This determination was made by inserting a movable extractor in the source. It was found that H^- yield increased by a factor of 6 as the extractor was moved from the edge of the source to a position near the filter plane. Finally, it was found that the H^- yield was not especially sensitive to the size of the source chamber, except when the source chamber became so small that the filaments resided in the filter magnetic field, in which case H^- production was increased substantially. The important variation was that the optimum operating pressure of the source - the pressure at which H^- density was at a

maximum - rose with decreasing source chamber length (see Figure 1-11). The curve labelled a is for a source chamber with length 20 cm, that labelled b has a source chamber 16 cm in length, and curve c is for a source chamber so short that the filaments have begun to enter the magnetic field of the filter. This result indicated to those conducting the experiment that larger source chambers would enhance H^- yields, since stripping would be reduced.

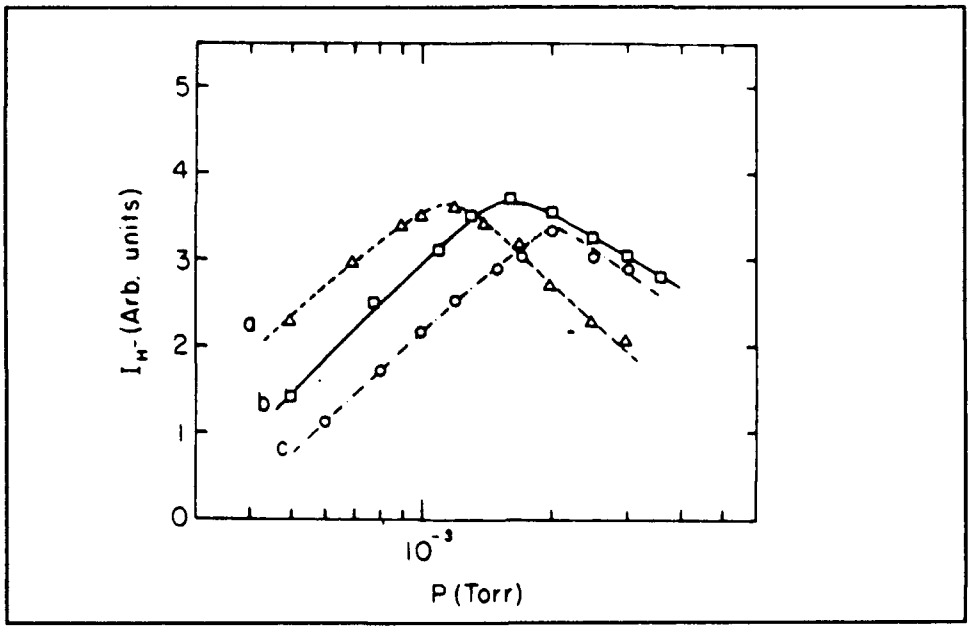

Figure 1-11: Dependence of Maximum H^- Current on Pressure

Emphasis on Small Scale Lengths. Some time before that experiment was conducted, Hiskes and Karo had modelled an H^- source to determine the optimum extractable H^- current as a function of H_2 and electron densities (Hiskes, 1984). According to this model, optimum extracted H^- current densities will occur when the product $n_e R = 10^{13}$ electrons cm^{-2} where n_e is the electron number density and R is a sys-

tem scale length, usually the length of the source chamber or the source chamber radius; and when the product $N_2R = 10^{14}$ to 10^{15} molecules cm^{-2}, where N_2 is the number density of molecular hydrogen. The model was extended in the next year (Hiskes, 1985) to include the effects of molecular ion surface neutralization, with particular emphasis on the length of the extraction chamber. The model predicted that the largest concentrations of H^- would occur for small Z/R, where Z is the extraction chamber length. (Hiskes (Hiskes, 1987) commented upon Leung's (Leung, 1985) discovery that extracted H^- current densities were higher near the filter plane. Although Hiskes' model assumed that $H_2(v)$ and H^- were attenuated by collisions in the extraction chamber, Hiskes remarked that Leung's source was operated with electron densities too low to provide the requisite number of H atoms to provide that attentuation. He surmized that Leung's effect was due to the rapid fall of electron density through the filter.) The model also predicted that, for a source of scale length R_o, which provides an H^- current density j_o, by decreasing the source scale length to R_b while increasing all densities by a factor of R_o/R_b, the current densities would increase to $j_b = (R_o/R_b)j_o$. On the basis of this scaling, Hiskes concluded that source sizes must be scaled down from the typical R = 10 cm scale length to provide sufficient current densities for fusion applications (Hiskes, 1987).

Model of a Large Source. In contradiction to this conclusion, Holmes *et al* (Holmes, 1987) developed a source which provides sufficient current density for fusion applications (57 mA/cm^2) by increasing the dimensions of the source. (Hiskes' 1984 model had predicted that, for a system of scale length R = 10 cm, the maximum extracted negative

ion current density would be about 8 mA/cm^2 (Hiskes, 1984: 1935).) The source was configured as shown in Figure 1-4 with dimensions of 55 cm by 31 cm by 20 cm. Several results from this experiment are noteworthy.

First, it was shown that the effective wall loss area A_p for the primary electrons was only 170 cm^2 out of the total wall surface area of 5000 cm^2. This was determined by measuring the change in the ratio of I_d to $n_p \upsilon_p$ (where n_p is the number density of primary electrons and υ_p is their mean velocity) with variations in the gas pressure. The equation

$$I_d = \frac{e n_p \upsilon_p}{4} A_p + e n_p N_2 \upsilon_p \sigma_{in} V \tag{1.1}$$

establishes the equality of primary electron production at the filaments to losses at the cusps and through inelastic collisions (with cross section σ_{in}) and with neutral molecular hydrogen (N_2 being the H_2 number density) through the volume V of the plasma. At low pressure, then

$$\frac{4 I_d}{e n_p \upsilon_p} = A_p \tag{1.2}$$

and so variations in source pressure allow measurement of A_p.

Second, it was found that positive ion current density is practically independent of gas pressure at high (> 3 to 5 mTorr) gas pressures, and this can be explained in terms of the confinement of energetic primary electrons. Since, by Eq (1.1), at high N_2,

$$I_d = e n_p N_2 \upsilon_p \sigma_{in} V \tag{1.3}$$

the product $n_p \upsilon_p$ varies as N_2^{-1} at constant I_d. But the rate of production of ions is governed by $n_p \upsilon_p N_2 \sigma_{ion}$, where σ_{ion} is the cross section for ionization; and losses are linear in n_I, the number density of positive ions, and independent of terms appearing in the rate of production. So, for ions,

$$n_p \upsilon_p N_2 \sigma_{ion} = \frac{n_I}{\tau_I} \tag{1.4}$$

where τ_I is a characteristic positive ion destruction time; and so n_I is constant in N_2 and linear in I_d.

Third, when the source was operated at 10 mTorr pressure with I_d = 1000 A, the H^- density in the extraction chamber was about 2.8 x 10^{11} cm^{-3} and approximately 1/2 the density of positive ions in the source. In sources operated at low discharge currents (about 10 A), the H^- density is usually about 0.1 times the electron density in the extraction chamber (Leung, 1984b) (see Figure 2-3). The negative ion density was seen to rise linearly with I_d until it saturated at high discharge currents (about 1000 A, but lower for lower operating pressures). This saturation is likely due to the reduction in H_2 density at higher discharge currents (Bacal, 1988). The H^- density also rises with increasing source pressure, though the rate of increase decreases as the source pressure increases.

Fourth, it was found that $n_I n_- / n_e$ scales linearly with N_2. This result is derived by Holmes *et al* on the assumption that the dominant loss

processes for H^- in the extraction chamber are mutual recombination with H^+ and collisions with H. Since atomic hydrogen is produced through dissociation of H_2 by impact with primary electrons and by collisions between H_2 and H_2^+ resulting in H_3^+ and H,

$$\frac{N_H}{\tau_H} = n_p S_d N_2 + n_p N_2 \langle \sigma \upsilon \rangle_{DI} + N_2 < \sigma \upsilon (3^+, H) > n_2 \qquad (1.5)$$

where N_H is the number density of atomic hydrogen, τ_H is the atomic hydrogen recombination time for wall collisions, S_d is the dissociation rate for the process $e + H_2 \rightarrow 2H + e$, n_2 is the number density of H_2^+, $<\sigma\upsilon>_{DI}$ is the rate coefficient for $e + H_2 \rightarrow H + H^+ + e$, and $<\sigma\upsilon(3^+,H)>$ is the rate coefficient for the process $H_2 + H_2^+ \rightarrow H_3^+ + H$. For high pressures, it is well known that

$$n_2 = \frac{n_p < \sigma \upsilon (2^+) >}{< \sigma \upsilon (3^+, H) >} \qquad (1.6)$$

(Mordin, 1983: 177) (this result is easily obtained from the balance equation for H_2^+) where $<\sigma\upsilon(2^+)>$ is the rate coefficient for the process $e + H_2 \rightarrow H_2^+ + 2e$. So Eq (1.5) can be written as

$$\frac{N_H}{\tau_H} = n_p S_d N_2 + n_p S_i N_2 \qquad (1.7)$$

where S_i is the ionization rate, $<\sigma\upsilon(2^+)> + <\sigma\upsilon>_{DI}$.

Also, since the primary creation process for H^+ is dissociative ionization of H_2,

$$\frac{n_I}{\tau_I} = n_p S_i N_2 \tag{1.8}$$

Then

$$\frac{N_H}{n_I} = \left(1 + \frac{S_d}{S_i}\right)\frac{\tau_H}{\tau_I} \tag{1.9}$$

This ratio will prove useful later.

The balance equation for H^- is written as

$$N^* n_e \langle \sigma v \rangle_{DA} = n_I n_- \langle \sigma v \rangle_{+-} + N_H n_- \langle \sigma v \rangle_{H^-} \tag{1.10}$$

where n_e is the number density for thermal electrons, N^* is the number density of vibrationally excited molecular hydrogen, $\langle \sigma v \rangle_{DA}$ is the rate coefficient for dissociative attachment of electrons to vibrationally excited hydrogen molecules, $\langle \sigma v \rangle_{+-}$ that for mutual recombination of H^- to H^+, and $\langle \sigma v \rangle_{H^-}$ the rate coefficient for stripping of H^- by atomic hydrogen. Using Eq (1.9), Eq (1.10) is written as

$$N^* n_e \langle \sigma v \rangle_{DA} = n_I n_- \langle \sigma v \rangle_m \tag{1.11}$$

where

$$\langle \sigma v \rangle_m = \langle \sigma v \rangle_{+-} + \langle \sigma v \rangle_{H^-} \cdot \frac{\tau_H}{\tau_I}\left(1 + \frac{S_d}{S_i}\right) \tag{1.12}$$

Then, by writing the rate equation for vibrationally excited molecular hydrogen,

$$\frac{N^*}{\tau^*} + N^* n_p \langle \sigma \upsilon \rangle_D = n_p N_2 \langle \sigma \upsilon \rangle_p \tag{1.13}$$

where τ^* is the wall loss time for for vibrationally excited H_2, $\langle \sigma \upsilon \rangle_D$ is the rate coefficient for its destruction and $\langle \sigma \upsilon \rangle_P$ for production. Since the wall loss term is small for high discharge currents,

$$N^* = N_2 \frac{\langle \sigma \upsilon \rangle_P}{\langle \sigma \upsilon \rangle_D} \tag{1.14}$$

and

$$\frac{n_I n_-}{n_e} = N_2 \cdot \frac{\langle \sigma \upsilon \rangle_P \langle \sigma \upsilon \rangle_{DA}}{\langle \sigma \upsilon \rangle_D \langle \sigma \upsilon \rangle_m} \tag{1.15}$$

Measurements show that, in fact, $n_I n_- / n_e$ is linear in the source pressure. Figure 1-12 displays Holmes' measurements of this relation (Holmes, 1987).

Fifth, Holmes *et al* go on to state that, if the dominant loss process for H^- were electron detachment, n_- would be proportional to N_2. This is easy to see. If electron detachment were the dominant loss process, then the H^- balance equation would read as

$$N^* n_e \langle \sigma \upsilon \rangle_{DA} = n_e n_- \langle \sigma \upsilon \rangle_{eD} \tag{1.16}$$

where $\langle \sigma \upsilon \rangle_{eD}$ is the rate coefficient for electron detachment. Substituting Eq (1.14) for N^* into Eq (1.16)

$$n_- = N_2 \cdot \frac{\langle \sigma \upsilon \rangle_P \langle \sigma \upsilon \rangle_{DA}}{\langle \sigma \upsilon \rangle_{eD} \langle \sigma \upsilon \rangle_D} \tag{1.17}$$

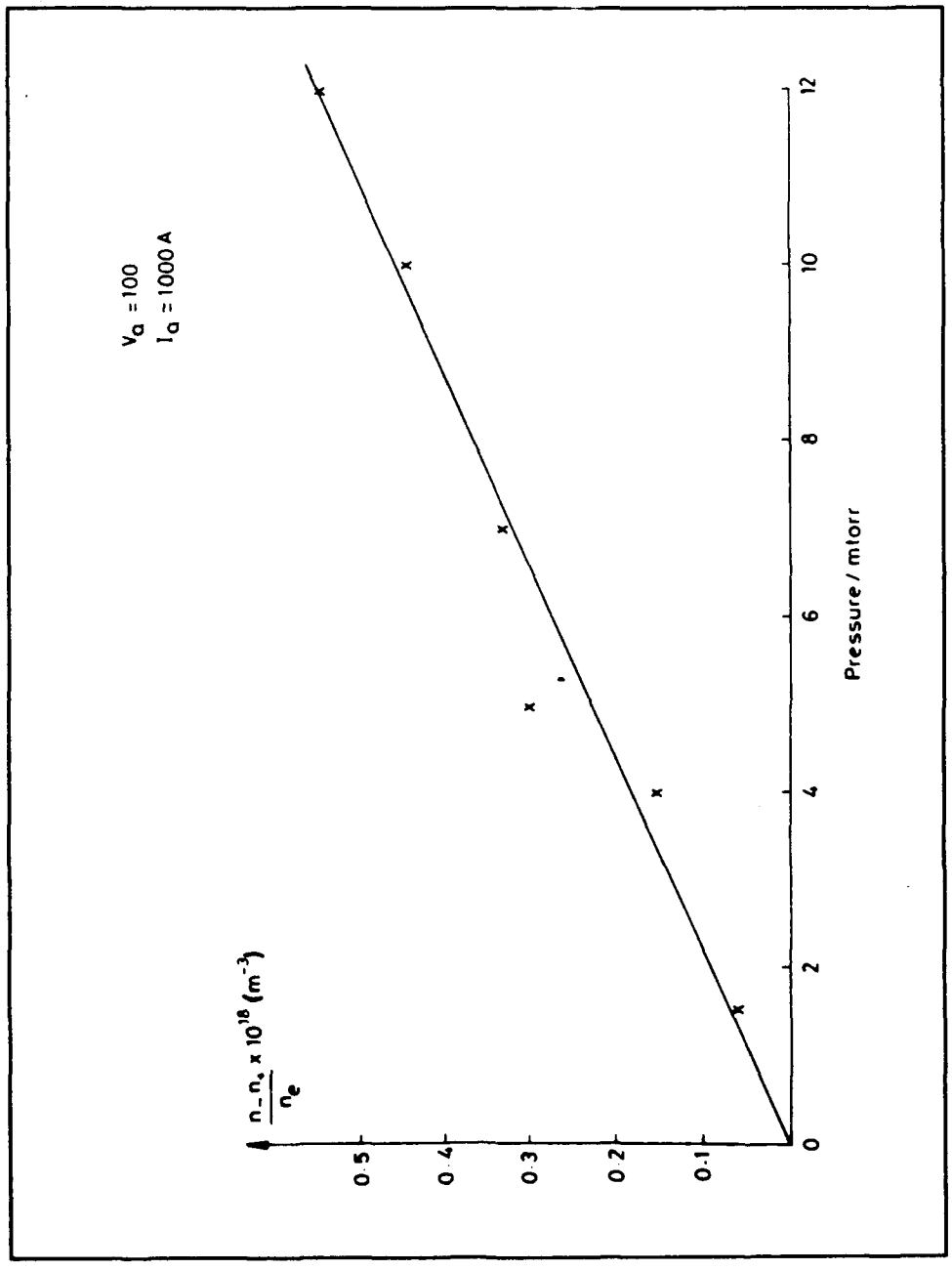

Figure 1-12: Dependence of $n_i n_-/n_e$ on Pressure

Although n_- does rise with N_2, the relation is not linear.

Sixth, it was remarked by the authors that the primary electron density is independent of the potential applied to the plasma electrode, and so N^* and N_H are independent of V_b.

Seventh, the ratio of $n_I n_-$ to n_e was measured at various values of n_e by varying the potential applied to the plasma electrode. Since $n_I n_-$ rises linearly with n_e, it is concluded that stripping of H^- by atomic hydrogen is not as important a loss process as mutual neutralization. Figure 1-13 displays Holmes' measurement of the dependence of $n_I n_-$ on n_e (Holmes, 1987). This conclusion appears to have been reached by investigating the scaling implied in Eq (1.10) when the term for mutual neutralization losses is neglected. Then,

$$N^* n_e \langle \sigma \upsilon \rangle_{DA} = N_H n_- \langle \sigma \upsilon \rangle_{H^-} \tag{1.18}$$

Then n_e is proportional to n_-, or $n_I n_e$ is proportional to $n_I n_-$. By noting that $n_I = n_- + n_e$, it is seen that if stripping were dominant, then $n_I n_-$ should vary as $n_e(n_e + n_-)$. But this variation is not observed. If, instead, mutual neutralization is the dominant process, then the scaling $n_I n_-$ proportional to n_e is immediate from Eq (1.10). (Note: Eq (1.15) appears to be perfectly general on first sight, showing that $n_I n_-$ is proportional to n_e regardless of the relative sizes of the terms for mutual neutralization and stripping by atomic hydrogen. However, τ_I, which appears on the right-hand side of Eq (1.15) inside of the term $\langle \sigma \upsilon \rangle_m$, as is plain from Eq (1.12), must be dependent upon the bias voltage of the plasma electrode: the electrode potential causes changes

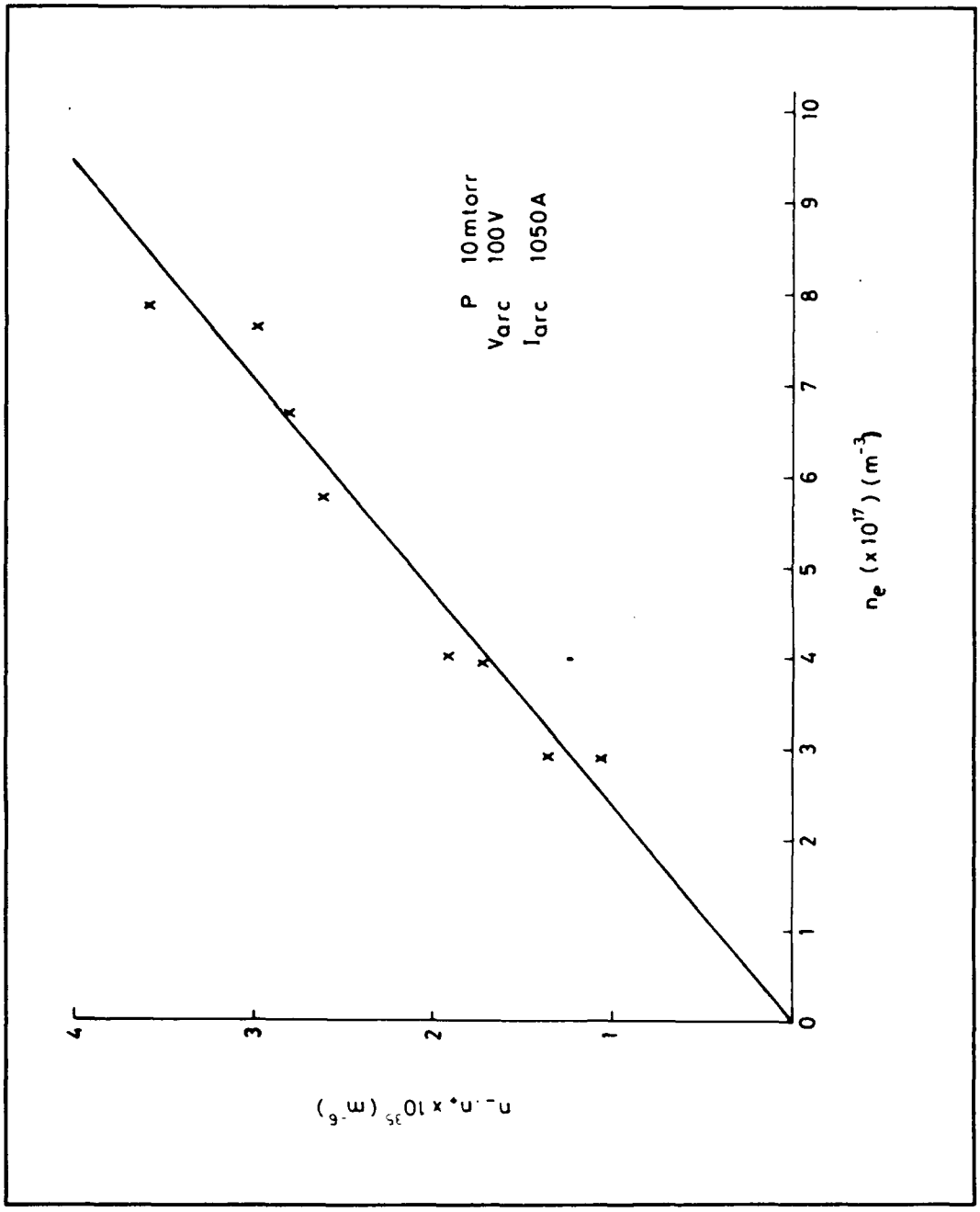

Figure 1-13: Dependence of n_-n_+ on n_e

in the potential profile through the filter and across the target chamber, and could conceivably effect the loss times for positive ions. So Eq (1.15) predicts a linear rise in $n_I n_-$ with n_e only if the mutual neutralization term in Eq (1.12) dominates.)

Model Including Filter Effects. On the basis of this measurement (Figure 1-13), Green *et al* (Green, undated) neglect processes involving atomic hydrogen in their model of the source. This model is very similar to Holmes' model just discussed. The greatest dissimilarity is in the fact that Green includes the effects of the filter to relate source and extraction chamber parameters. Green's equation for the balance of H^- production and destruction processes is

$$\frac{n_-}{\tau_-} + n_- n_I^{(2)} \langle \sigma v \rangle_{+-} = n_e^{(2)} N^* \langle \sigma v \rangle_{DA} \qquad (1.19)$$

This differs from Eq (1.10) in that, on the basis of Holmes' results, Green has neglected the effects of atomic hydrogen; he has instead included a term n_-/τ_- for wall losses. The superscripts "2" in $n_e^{(2)}$ and $n_I^{(2)}$ refer those densities to the target chamber; any H^- created in the source chamber is assumed to be destroyed at these high discharge currents. Green states the condition for neutrality in the target chamber

$$n_- + n_e^{(2)} = n_I^{(2)} \qquad (1.20)$$

and he introduces a parameter α which relates the positive ion density on the two sides of the filter:

$$\alpha = \frac{n_I^{(2)}}{n_I^{(1)}} \tag{1.21}$$

where $n_I^{(1)}$ is the positive ion density in the source chamber.

By solving Eq (1.19) for the ratio $n_e^{(2)}/n_-$ and substituting an expression for N^* from Eq (1.13) and an expression for n_p from Eq (1.4), it is found that

$$\frac{n_e^{(2)}}{n_I} = \left[\frac{1}{n_I^{(2)}\tau_-} + <\sigma\upsilon>_{+-}\right]\frac{1}{<\sigma v>_{DA}}\left[\frac{\tau_I}{\tau^*}\frac{S_i}{<\sigma\upsilon>_P}\frac{n_I^{(2)}}{n_I^{(1)}} + \frac{n_I^{(2)}}{N_2}\frac{<\sigma\upsilon>_D}{<\sigma\upsilon>_P}\right] \tag{1.22}$$

Then, introducing α for $n_I^{(2)}/n_I^{(1)}$ and $n_I^{(2)}/n_- - 1$ for $n_e^{(2)}/n_-$,

$$\frac{n_I^{(2)}}{n_-} = \left[\frac{1}{n_I^{(2)}\tau_-} + <\sigma\upsilon>_{+-}\right]\frac{1}{<\sigma v>_{DA}}\left[\frac{n_I^{(2)}}{N_2}\frac{<\sigma\upsilon>_D}{<\sigma\upsilon>_P} + \frac{\tau_I}{\tau^*}\frac{S_i}{<\sigma\upsilon>_P}\alpha\right] \tag{1.23}$$

Since the n_-/τ_- term in Eq (1.19) is significant only for very low densities, it is neglected, and Green writes

$$\frac{1}{n_-} = \left[\frac{<\sigma\upsilon>_{+-}}{<\sigma\upsilon>_{DA}}\frac{S_i}{<\sigma\upsilon>_P}\frac{\tau_I}{\tau^*}\alpha\right]\frac{1}{n_I^{(2)}} + \left[\frac{<\sigma\upsilon>_{+-}}{<\sigma\upsilon>_{DA}}\frac{<\sigma\upsilon>_D}{<\sigma\upsilon>_P}\right]\frac{1}{N_2} \tag{1.24}$$

Green tests this equation by measuring $1/n_-$ as a function of $1/j_I$ in the extraction chamber, and finds good agreement.

In order to use Eq (1.24) to maximize n_- in the extraction chamber, it is necessary to understand 1) how α varies with the magnetic filter induction and extraction electrode bias voltage V_b, 2) whether any ion species can be transported preferentially across the filter to maximize $<\sigma\upsilon>_{+-}$, and 3) how to transport electrons across the filter so as to maximize $<\sigma\upsilon>_{DA}$, since the dissociative attachment rate is a function of

electron temperature. These are fundamentally questions of plasma transport, the subject of the present study.

Discussion of Plasma Transport

Goal and Utility of This Work. Initially, the major goal of this work was to calculate the fluxes of the charged particles in the plasma to the walls in the source chamber and through the filter to the walls in the extraction chamber. It was thought that these fluxes, once known, would allow for calculation of the plasma potential in the source chamber. The method to be employed would involve writing an equation for electron creation and loss, and this equation would inevitably involve the difference between the potential on the anode V_a and the plasma potential V_p. For instance, equating the production of electrons to their losses at the line cusps in a cylindrical-source,

$$\frac{I_d}{e} + n_p \upsilon_p \sigma_{ion} V = \frac{1}{4} n_e \upsilon_e W_e L \exp(-(V_p - V_a)/T_e) \qquad (1.25)$$

with W_e the leak width for electron losses to cusps of total length L, and T_e the electron temperature. The idea, then, was to analyze the total electron loss, both at the cusps and *via* diffusion through the magnetic field at the anode and *via* diffusion through the magnetic filter field into the extraction chamber.

The goal was not, however, simply to calculate the plasma potential. Analysis of the fluxes should also allow calculation of the variation of the plasma density in the source chamber with both the magnetic induction of the filter field and the bias voltage on the extraction electrode.

(See Figure 1-9 for an example of how the filter magnetic field strength can effect the source chamber plasma density.) Knowledge of these variations, along with knowledge of the plasma potential, would considerably improve detailed numerical calculations of the species densities in the source chamber, as in Bailey, 1987; Bell, 1987; Bretagne, 1986; and Hiskes, 1982. In these calculations, one normally is interested in populations of vibrationally excited molecular hydrogen and, therefore, in densities of both thermal and primary electrons; both of these densities are inextricably related to electron losses due to transport out of or to the walls of the source chamber.

In addition, the evidence suggests that the great majority of H^- in the source is produced in the extraction chamber at the edge of the filter field. The electron temperature in the extraction chamber is sufficiently low to enhance the dissociative attachment process and too low to strip H^-. An analysis of electron transport through the filter should produce a model of the temperature fall, and knowledge of precisely how the fall occurs and how it varies with the final chamber electron density would doubtless be valuable in any attempt to optimize H^- production. Also, the final chamber electron density (or ion density, as in Green's formulation (Eq (1.24))) itself must be known as a function of the filter field strength, source chamber density, and plasma electrode bias voltage in order to be useful in analysis of H^- production. This is due to the fact that the H^- production rate $n_e N^* \langle \sigma \upsilon \rangle_{DA} V$ is linear in the final chamber electron density.

Quite apart from utilitarian motives, one is struck with curiousity regarding the electron transport through the filter upon first noticing the

fact that the plasma potential falls from the source to the extraction chamber. This indicates, of course, that the electrons are moving through the filter with relative ease in comparison to the ions. And yet the ion flow is not much diminished by the presence of the filter. The ion gyroradius is, even at the highest filter field strengths, on the order of centimeters, which indicates that one or two collisions with neutrals would suffice to move an ion across the filter: but the electron gyroradius is on the order of tenths to hundredths of centimeters.

It was found that the majority of experimental data related to charged particle motion across the magnetic fields in tandem sources, though scanty, was related to the magnetic filter. As the difficulty of the problem became clear, the goal of this effort was progressively reduced from calculating the densities and potential in the source on the basis of fluxes out of the source chamber to understanding the flow of the plasma through the filter. And, even so, only a general understanding of electron transport through the filter has been achieved.

Scale Lengths/Frequencies. Since the plasma density in the source chamber can be anywhere between 10^{11} and 10^{12} cm^{-3} for low pressure and high pressure discharges respectively, and the thermal electron temperature ranges from 1 eV to 5 eV, the Debye length can be from 2 x 10^{-3} cm for low pressure discharges to 1.6 x 10^{-3} cm for high pressure discharges. In the extraction chamber, these lengths increase by a factor of $(5/3)^{1/2}$ to $(10/3)^{1/2}$, since the plasma density falls by a factor of 5 to 10 from the source to the extraction chamber and the temperature falls by a factor of about 3. The plasma frequency can be between

5.5×10^9 sec^{-1} in the extraction chamber of a low pressure discharge to 5.5×10^{10} sec^{-1} in the source chamber of a high pressure discharge.

For electrons, the mean free path for electron-ion collisions is 21 cm in the extraction chamber of a low pressure discharge, 23 cm in the source chamber of a low pressure discharge or the extraction chamber of a high pressure discharge, and about 60 cm in the source chamber of a high pressure discharge. The electron gyroradius, however, is much less than 20 cm even in the low magnetic field near the center of the discharge: magnetic induction magnitudes must be as low as 0.1 Gauss for the electron gyroradius to reach 20 cm.

The mean free path for electrons in electron-neutral collisions can be estimated by using the momentum transfer cross section data of Figure 1-14 (McDaniel, 1964). For electron energies between 0.5 and 5.0 eV, this cross section is about 10^{-15} cm^2. The mean free path ranges from 50 cm in a low pressure (1 mTorr) discharge to 5 cm at high pressures (10 mTorr), assuming a molecular hydrogen temperature of 500 degrees Kelvin (Bacal, 1988). This indicates that electron-neutral collisions may dominate electron transport in high density discharges operated at high discharge currents. The cause of this can be found in the rise in source chamber electron temperature with discharge current, considering that the electron-ion mean free path increases as T_e^2.

The three species of positive ions are found in the discharge in varying proportions. The relative concentrations of H^+, H_2^+, and H_3^+ are a function of the discharge current. Figure 1-15 (Ehlers, 1982b) shows that, at low discharge currents (I_d < 15 A) the dominant ion species extracted is H_3^+, but for I_d > 15 A the H^+ percentage is highest.

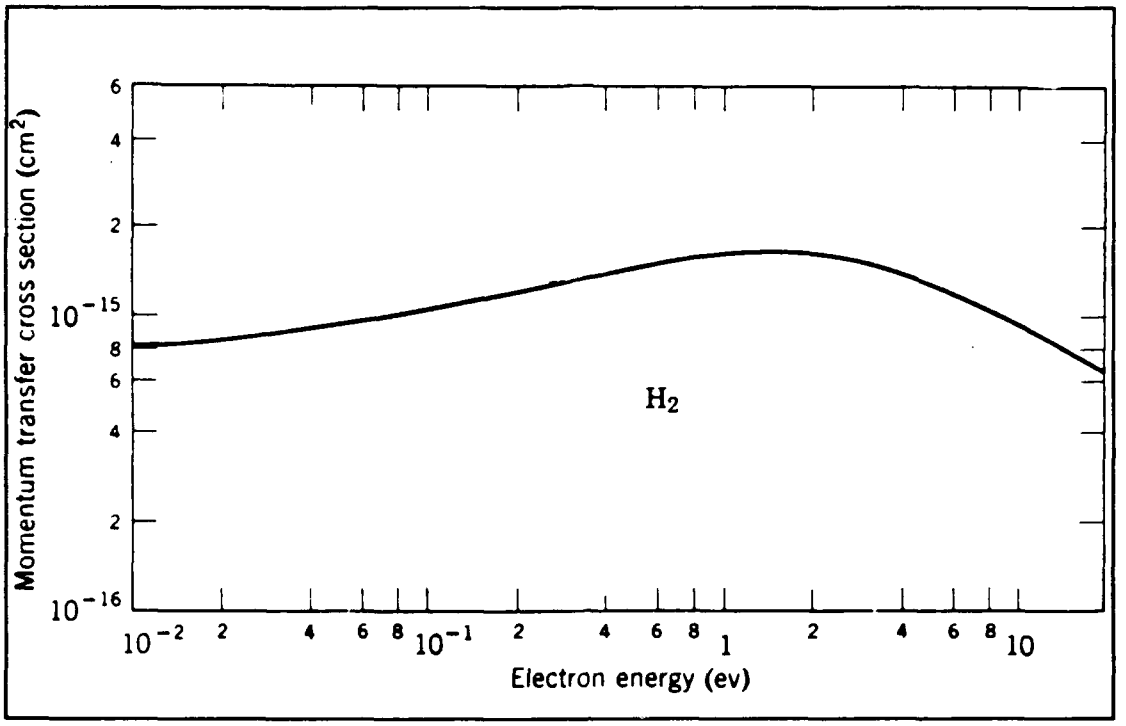

Figure 1-14: Electron-H_2 Momentum Transfer Cross Section

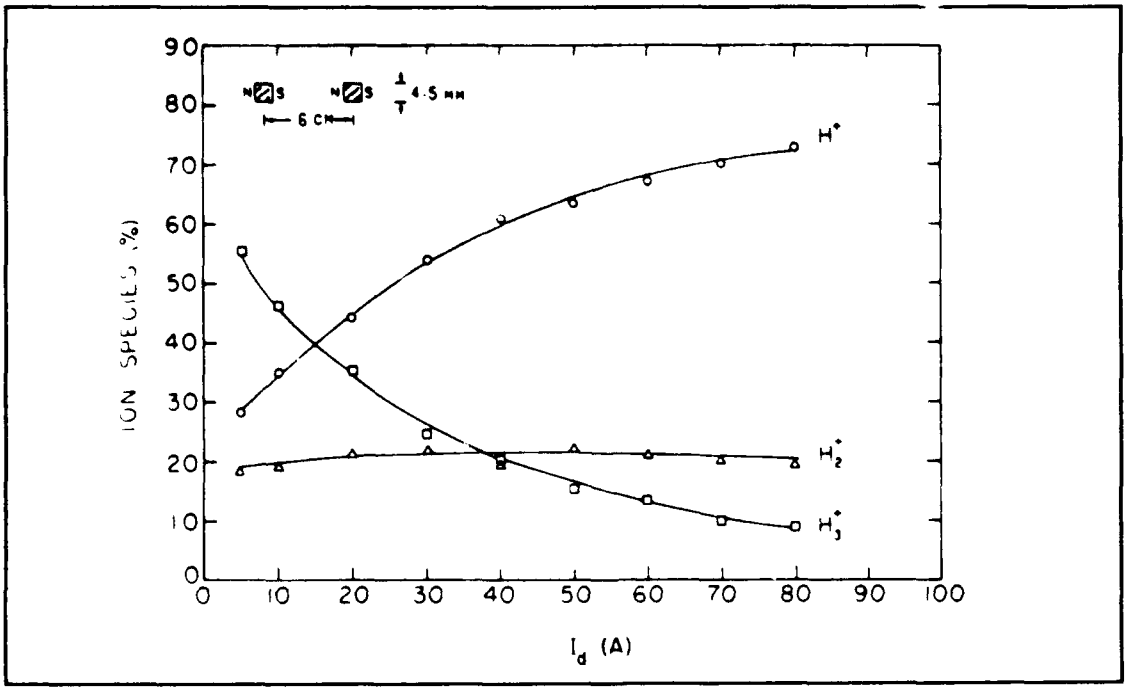

Figure 1-15: Relative Concentrations of Positive Ion Species

The ion temperatures are not well known. In a recent model (Bacal, 1988), the H^+ temperature is taken to be 0.35 eV, equal to the temperature of atomic hydrogen. This estimate is apparently based on the assumption that the temperature of an ion is equal to the energy of formation. In like manner, therefore, the temperatures of H_2^+ and H_3^+ can be tentatively estimated. Since H_2^+ collects very little energy in formation from ionizing electrons, the temperature of H_2^+ is taken to be equal to the molecular hydrogen temperature, 0.04 eV. The temperature of H_3^+ can be estimated by examining the reaction $H_2 + H_2^+ \rightarrow H_3^+ + H$, by which the vast majority of H_3^+ is created. This reaction is exothermic with approximately 0.44 eV of available kinetic energy (Mordin, 1983). The energy should be shared with 75% going to H and 25% to H_3^+. Hence, the temperature of H_3^+ is about 0.11 eV.

The accuracy of these estimates depends upon the ratio of the mean time for a collision with the walls to the mean time between collisions with neutral hydrogen molecules. If collisions with H_2 are more likely, then the average ion energy could better be estimated as the difference in plasma potential over the ion's mean free path, whether that path length is twice the ion gyroradius or the distance between hard collisions.

Using tabulated cross sections for ion elastic collisions with H_2 (Smith, 1987), the mean free paths and collision frequencies for ion neutral collisions can be calculated. (At these low ion energies, the elastic collision cross sections are reasonable extrapolations, not measured values (Smith, 1987).) Denoting the mean free path for H^+ - H_2 collisions as L_{1o}, that for H_2^+ - H_2 collisions as L_{2o}, and that for H_3^+ - H_2 col-

lisions as L_{3o}, with the corresponding collision frequencies denoted as ν_{1o}, ν_{2o} and ν_{3o}, the results are shown in Table 1-1 for an assumed H2 temperature of 500 degrees K. With these mean free paths, it is obvious that each ion will suffer multiple collisions before striking a cusp. And yet, the energy of formation can be an accurate estimate of the temperature. Although ions are reflected from the source chamber walls, they pass through the filter with relative ease. Thus, a substantial percentage of the ions may exit the source chamber at an energy near the energy of formation.

	1 mTorr	10 mTorr
L_{1o} (cm)	10	1
L_{2o}	17	1.7
L_{3o}	17	1.7
ν_{1o} (x 10^4 sec^{-1})	9.5	95
ν_{2o}	1.3	13
ν_{3o}	3.4	34

Temperature is assumed to be the energy of formation.

Table 1-1: Ion-Neutral Mean Free Paths and Collision Frequencies

(At low ion energies, the ion elastic collision cross section for H_2^+ may be smaller than the cross section for the process $H_2^+ + H_2 \rightarrow H_3^+ + H$. The mean free path L_{2o} given in Table 1-1 may thus be an overestimate of the actual H_2^+ mean free path.)

The ion energy may therefore be estimated loosely as the minimum of the potential gradient in the source and the energy of formation. For

the purpose of estimating the relative magnitudes of ion-neutral and ion-ion collisions, the ion temperature for H_2^+ and H_3^+ will be taken to be 0.1 eV. The value 0.1 eV is a guess based upon observed changes in the plasma potential of about 0.1 eV over the width of the source (Bacal, 1985a). The temperature of H_3^+ is taken to be 0.35 eV.

The effects of ion-ion collisions on ion motion will be discussed in Chapter V. Here, it suffices to present the collision frequencies for ion-ion collisions for both low pressure, low discharge current and high pressure, high discharge current environments. The ion-ion collision frequency is given by (Hinton, 1983: 158)

$$\nu_{\alpha\beta} = \frac{4\sqrt{2\pi}}{3} \frac{n_\beta e^4 \ln(\lambda)}{(T_\alpha/m_\alpha + T_\beta/m_\beta)^{3/2} m_\alpha} (1/m_\alpha + 1/m_\beta) \qquad (1.26)$$

The term $\ln(\lambda)$ is the Coulomb logarithm, equal here to approximately 7. (Incidentally, this equation reduces to the appropriate equation for electron-ion collisions if the subscript α refers to electrons.) Table 1-2 presents calculations for the collision frequencies. For the low pressure column, the total ion density was estimated at 1×10^{11} cm^{-3}. H_3^+ is taken to account for 60% of the positive charge, H^+ 30%, and H_2^+ the remaining 10%. At high pressures, the distribution is 70% H^+, 20% H_2^+, and 10% H_3^+ of the total positive ion number density equal to 1×10^{12} cm^{-3}.

Since the cross section for elastic scattering of ions from neutrals varies little in the low energy range, the data of Table 1-1, calculated for ion temperatures equal to their energy of formation, should be reasonably accurate, and can be compared with the frequencies of Table 1-2. The

conclusion to be drawn is that, in the source chamber at all pressures, ion-ion collisions are more important than ion-neutral collisions for H_2^+ and H_3^+. At low pressures in the extraction chamber, however, the results will be lowered by a factor of 5 to 10, depending upon the positive ion density decrease, and so ion-neutral collisions could equal ion-ion collisions in importance.

	Low Pressure	High Pressure
ν_{12}	2.8	56
ν_{13}	16	27
ν_{21}	42	99
ν_{23}	50	82
ν_{31}	2.7	63
ν_{32}	5.5	110

Frequencies x 10^{-4} sec^{-1}

Table 1-2: Ion-Ion Collision Frequencies

The energetic electrons from the filaments have a mean free path for elastic collisions with neutrals equal to 250 cm and a collision frequency of 2 x 10^6 sec^{-1} at low pressures. These electrons do not exist in large numbers in the extraction chamber, as has been shown experimentally (Hopkins, 1987). In calculations to follow, it will be assumed that electron fluxes are not altered beyond the source chamber

edge of the filter field due to processes involving energetic electrons. That is, source and sink terms for electrons will be considered to be zero through the filter and into the extraction chamber. That this is a valid assumption for source terms can be shown by way of an example. Holmes (Holmes, 1982b) measured an electron current through the magnetic filter of about 1 ampere. If it were supposed, as an overestimate, that the entire discharge current of about 5 A was injected into the magnetic filter in the form of energetic electrons, very few would ionize H_2 while within the filter magnetic field. Assuming a path of 4 cm within the filter for each energetic electron and an ionization cross section of 10^{-16} cm^2 (Tarawa, 1990), the electron current created in the field is at most $I_d \times 4/L_i = I_d \times 4N_2\sigma_{ion} = 8 \times 10^{-3}\ I_d$. Here L_i is the mean free path for ionization. This value is at most a factor of 10^{-2} below the current flowing through the filter, and so is negligible.

Loss of electron flux through the filter and in the extraction chamber due to recombination with ions and dissociative attachment will also be neglected. The loss of electrons through these processes over a cross section of the source will be compared with the flux. The electron loss per unit area is

$$\frac{V}{A}\{n_e n_I \langle \sigma\upsilon \rangle_R + n_e N^* \langle \sigma\upsilon \rangle_{DA}\} \tag{1.27}$$

with A the cross-sectional area of the source and $\langle \sigma\upsilon \rangle_R$ the reaction rate coefficient for recombination of electrons with ions. As an extreme case, $N^* = 10^{-3}N_2$ and $\langle \sigma\upsilon \rangle_{DA} = 10^{-8}$ cm^2 (Mordin, 1983: 63). In a low pressure discharge, $n_e = 10^{10}$ cm^{-3}, so the second term in brack-

ets yields 10^{12} cm^{-3} sec^{-1}. The cross section for recombination may approach 10^{-14} cm^2 at low electron temperatures, so the first term is about 10^{13} cm^{-3} sec^{-1}. Thus, the loss of electrons per unit area is at most 10^{14} cm^{-2} sec^{-1}, which is a factor of 100 below the flux measured in Holmes' experiment (Holmes, 1982b). There Holmes drew an electron current in excess of 1 A to the extraction electrode area of 197 cm^2.

As an aside, it should be noted that electron losses in the extraction chamber through these processes imply that the flux through the filter must balance the electron thermal flux to the plasma electrode plus losses due to recombination and dissociative attachment. If these processes are ignored, the minimum flux through the filter is being underestimated slightly. This should be kept in mind in anticipation of the results of Chapter II.

Mathematically, these calculations can be related to the continuity equation

$$\frac{dn}{dt} = -\nabla \cdot \underline{\Gamma} + \frac{\delta n}{\delta t} \tag{1.28}$$

It has been shown above that, for electrons, $\Gamma_x >> |\delta n/\delta t\ \Delta x|$ beyond the edge of the filter field, or Γ_x = a constant.

Both ionization and recombination effects are important at lower values of the flux, such as when the extraction electrode is shielded by a magnetic field or is biased to a low voltage. And, of course, they will be of consequence for ion motion, since the ion flux is much lower than the electron flux under most circumstances.

Outline of Efforts and Results

Thermal electron transport through the magnetic filter will be treated first, in Chapters II, III, and IV.

In Chapter II it will be shown that electrons diffuse across the magnetic filter at a rate higher than one would expect from a classical diffusion mechanism. Evidence from three experiments will presented in support of that conclusion. It will also be shown that the electron-ion collision frequency derived by Holmes is larger by a factor of about 17 than the collision frequency generally quoted in the literature.

Chapter III is concerned with whether Holmes' derivation is valid. It will be shown that the cause of the discrepancy is Holmes' procedure. He assumes a particular functional form of the diffusion coefficient and then averages, rather than following the standard approach of computing the mean square displacement upon collisions. Also, an equation for the flux will be derived from the Fokker-Planck equation. It will be shown that this equation does not provide sufficient flux to account for the results of experiments discussed in Chapter II, but that there are conditions where the electron flux may be driven by ion acoustic or related turbulence resulting in a flux equation with the same functional form.

Chapter IV will demonstrate from experimental data that the flux to the extraction electrode rises in a way consistent with the temperature gradient term in the flux equation acting as a drag term. Nothing definite can be concluded about the functional dependence of the collision frequency itself on temperature or plasma density, except that a variety of functional forms may fit the data reasonably well. An equation for

the cooling of electrons as they pass from source to extraction chambers will be derived and shown to be in reasonable agreement with the data, both at low values of flux through the filter where inelastic collisions are an important consideration and higher values of the flux where the energy flux variation depends primarily on the electric field.

In Chapter V, the primary electron and positive ion transport through the filter will be examined. A model of the source will be presented in order to predict extracted positive ion species percentages. The model will incorporate a particular view of positive ion and primary electron transport, and will thus constitute an indirect test of ion transport theory.

Chapter VI is a summary of these results and an outline of future research projects in this area.

Chapter II - Evidence of Enhanced Diffusion

Introduction

In magnetic multicusp negative hydrogen ion devices with magnetic filters, sometimes called tandem devices, electrons diffuse across the magnetic field of the filter at a rate higher than what one would expect from a classical diffusion mechanism. Evidence for enhanced diffusion through the filter can be found in experiments performed by Leung and Bacal (Leung, 1984b), Holmes (Holmes, 1982b), and Ferreira *et al* (Ferriera, 1989).

In what follows, each of these experiments will be discussed in some detail. For the Leung and Bacal experiment, a calculation will be made of the final chamber electron number density n_2. The value of n_2 so calculated is a factor of 350 lower than the value Leung and Bacal measured in the experiment. The implication to be drawn is that either the rate of electron diffusion through the filter is greatly enhanced above the classical (electron-ion) value, or the electron flux to the plasma electrode is far below its thermal value $1/4\ n_2 \overline{\upsilon}$, or both effects are at work.

For the Holmes experiment, Holmes' derivation of a classical electron-ion collision frequency a factor $9\pi^{1/2}$ higher than the generally accepted value will be rehearsed, as will measurements in agreement with the derived result.

The Ferriera experiment will then be briefly addressed. The credible results from that experiment are the measurement of an enhanced (three orders of magnitude) electron diffusion coefficient through a magnetic picket fence and the measurement of an ion-sound-like wave spectrum in the magnetic filter region.

Evidence from Leung and Bacal's Experiment

In the experiment conducted by Leung and Bacal, the magnetic filter had a maximum strength of about 35 G. A profile of the magnetic field from source to extraction chambers is shown in Figure 2-1. Although this information is not given in the manuscript itself, the authors state that the configuration of the filter is the same as in a previous experiment, documented in Leung, 1983. In that earlier paper, it was stated that "the filter was arranged according to the optimized geometry found in a previous investigation," and this geometry is given in Ehlers, 1982b. The inference can be made from Table 1 and Figure 3 of Ehlers, 1981c, that near the magnetic surfaces, the filter field strength is 76 G, but in between two magnets the maximum filter field strength is 35 G. The field extends 4 cm to either side of the plane of the filter magnets. The filter field is generated by an array of permanent magnets as depicted in Figure 2-1. Electrons are magnetized throughout this region.

The maximum electron flux through the filter should occur when the unshielded circular plate at the end of the target chamber (the plasma electrode) draws the greatest current, and this will be the case when the plate bias voltage, V_b, is very nearly equal to the plasma potential in the target chamber, V_p. Incidentally, the relation $V_b = V_p$ is also characteristic of the optimum configuration of the source for H^- extraction, so it makes excellent sense to attempt to understand the electron flow to the extraction chamber with these parameters (Leung, 1984b).

One factor which makes this experiment valuable for investigation of electron flow is that there is no stray magnetic field shielding the target chamber end plate. Such a field does arise when plasma is extracted from

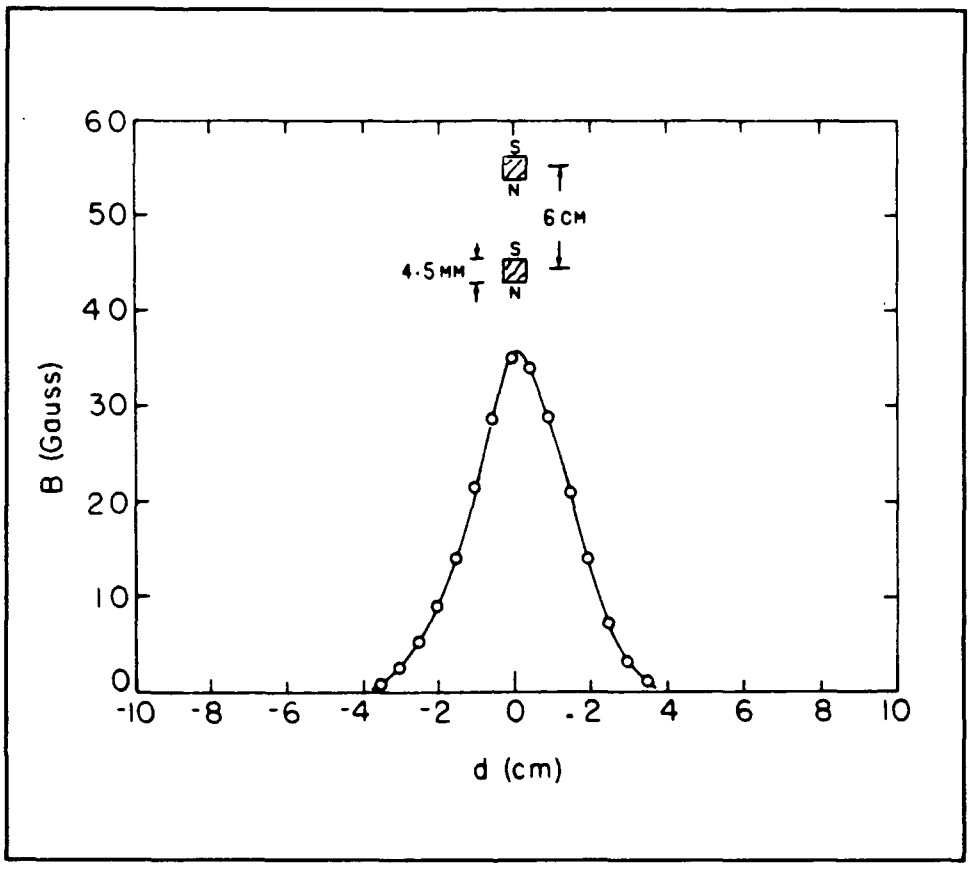

Figure 2-1: Profile of the Filter Field

a small opening in the end plate and separated magnetically into constituents (Bacal, 1987). A stray field as high as 20 G parallel to the end plate can be formed just inside the target chamber. In this experiment, no plasma was extracted; instead, plasma constituent number densities were measured using a photodetachment technique. Even without the separation magnets, there may remain a small residual magnetic field near the center of the plasma due to the side-wall magnets. The effect of this field will be considered at the end of this section.

When the plate bias voltage V_b is raised to 2.5 V, there is little potential fall between the plasma and the wall. The plasma density in the source chamber is given as $n_1 = 1.2 \times 10^{11}$ cm^{-3}, while the density in the extraction chamber is $n_2 = 1.7 \times 10^{10}$ cm^{-3} (see Figure 2-2). It is well known that the electron temperature decreases as the electrons flow from the source chamber to the target chamber (Holmes, 1982a; Ehlers, 1981) and that the fall is typically by a factor of 2 to 3 for sources configured in this way (Leung, 1983). (See Figures 1-6 through 1-8 for the temperature fall.) The source chamber electron temperature is generally about 1.0 eV to 1.5 eV, so the final chamber electron temperature is about 0.5 eV. In the calculation which follows, the electron flow in the target chamber to the end plate can be diminished at most by a factor of exp $[e(V_b - V_p)/T_e]$ or exp(-1/5), since the difference $V_b - V_p \approx -0.1$ V. Also, it is important to remember that a temperature fall acts to oppose the flow of electrons from the source to the extraction chamber (Golant, 1961). But this inhibiting effect of the electron temperature gradient will be ignored, and the magnetic field strength will be assumed to be 35 G uniformly across the filter plane at its maximum value (although it rises to 76 G near the magnet faces). Finally, the inhibiting effect of the electric field between source and target chambers will be ignored. The plasma potential drops two to three tenths of a volt from the source to the extraction chamber (see Figure 1-5). This drop will diminish the electron flux. All of these assumptions are designed to maximize the calculated electron flux to the target chamber. It will be found that, even though the magnetic field strength is underestimated and the retarding effects of the potential and temperature gradients are ignored, the classical collision-driven electron flux is two orders of magnitude too low.

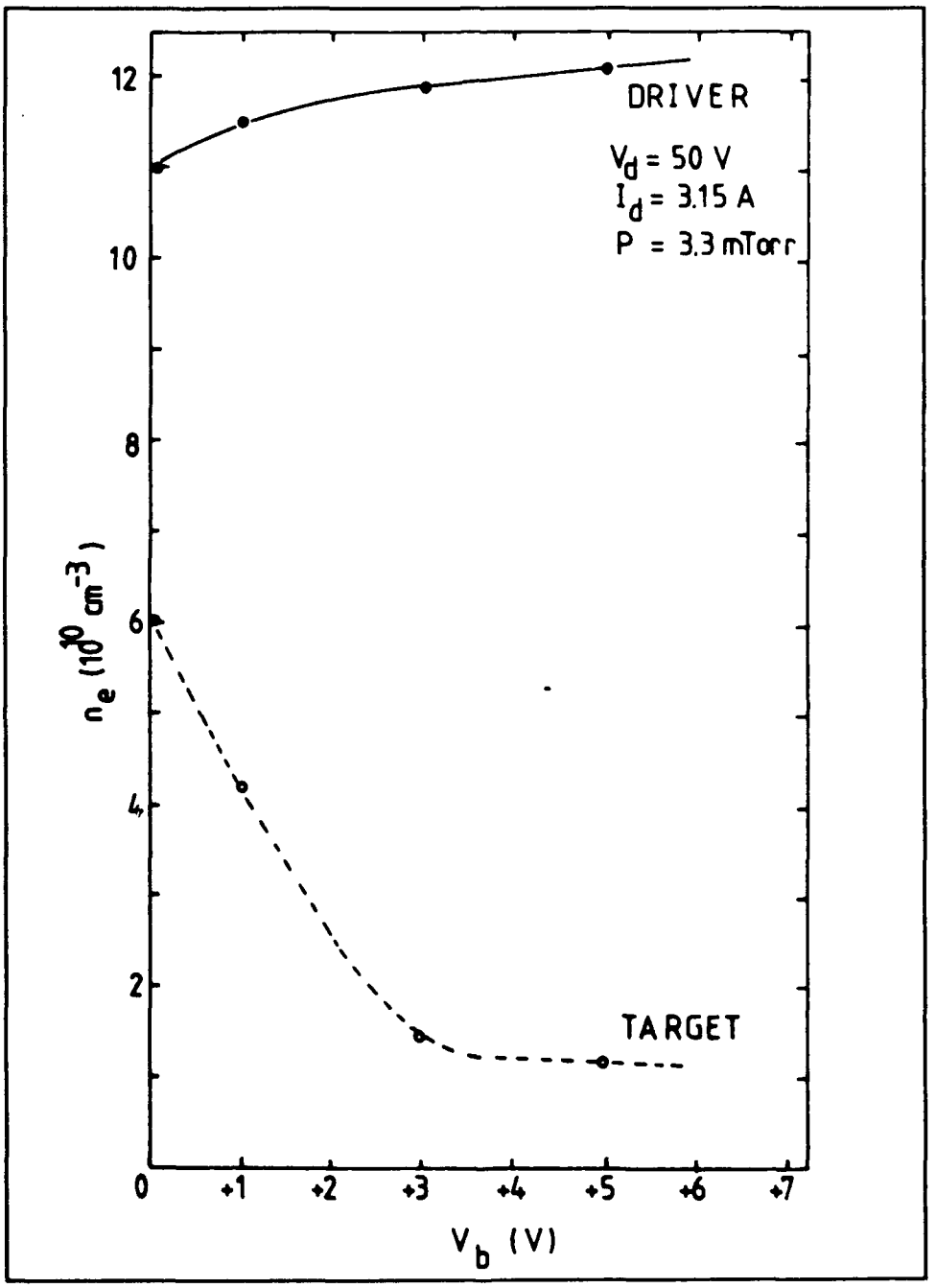

Figure 2-2: Plasma Density Fall in Leung and Bacal's Experiment

Negative hydrogen ions were present in the target chamber with a density about 0.1 that of electrons. Their effect on electron motion will be ignored in this chapter. Figure 2-3 shows the measured ratio of H^- number density to electron number density in the target chamber as a function of the plasma electrode bias voltage.

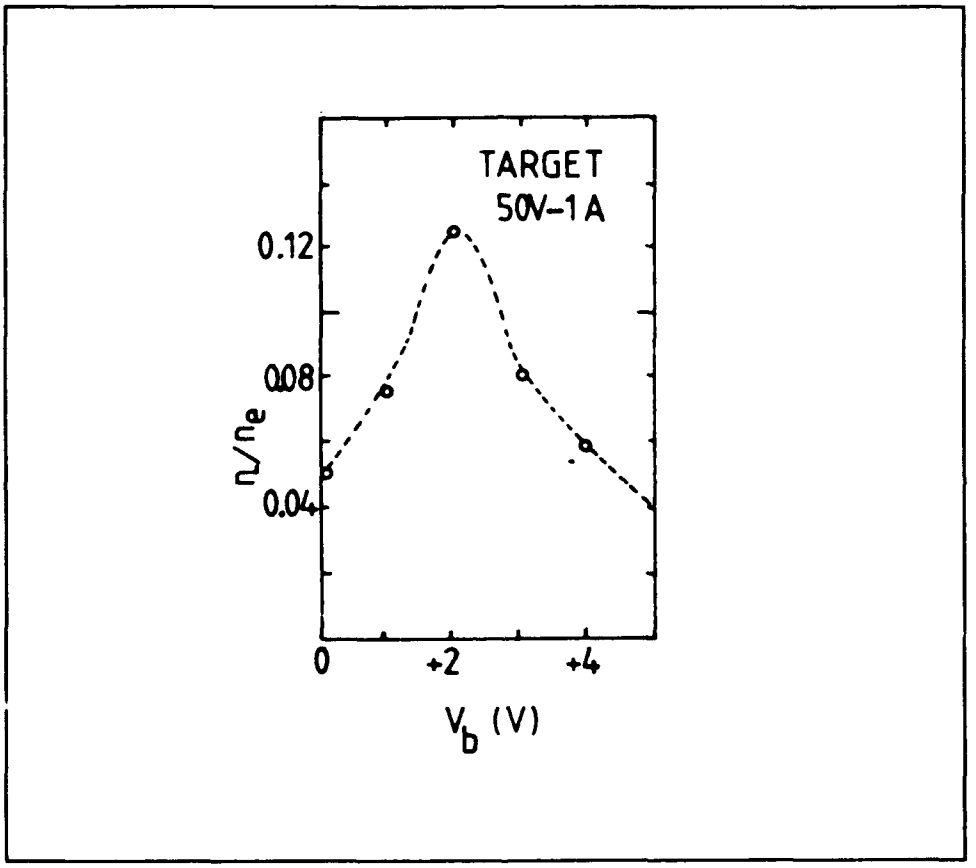

Figure 2-3: Measured Ratio of H^- Ions to Electrons

Figure 2-4 shows the coordinate system employed in the following discussion.

The classical expression for the flux, under the restrictions delineated above, is:

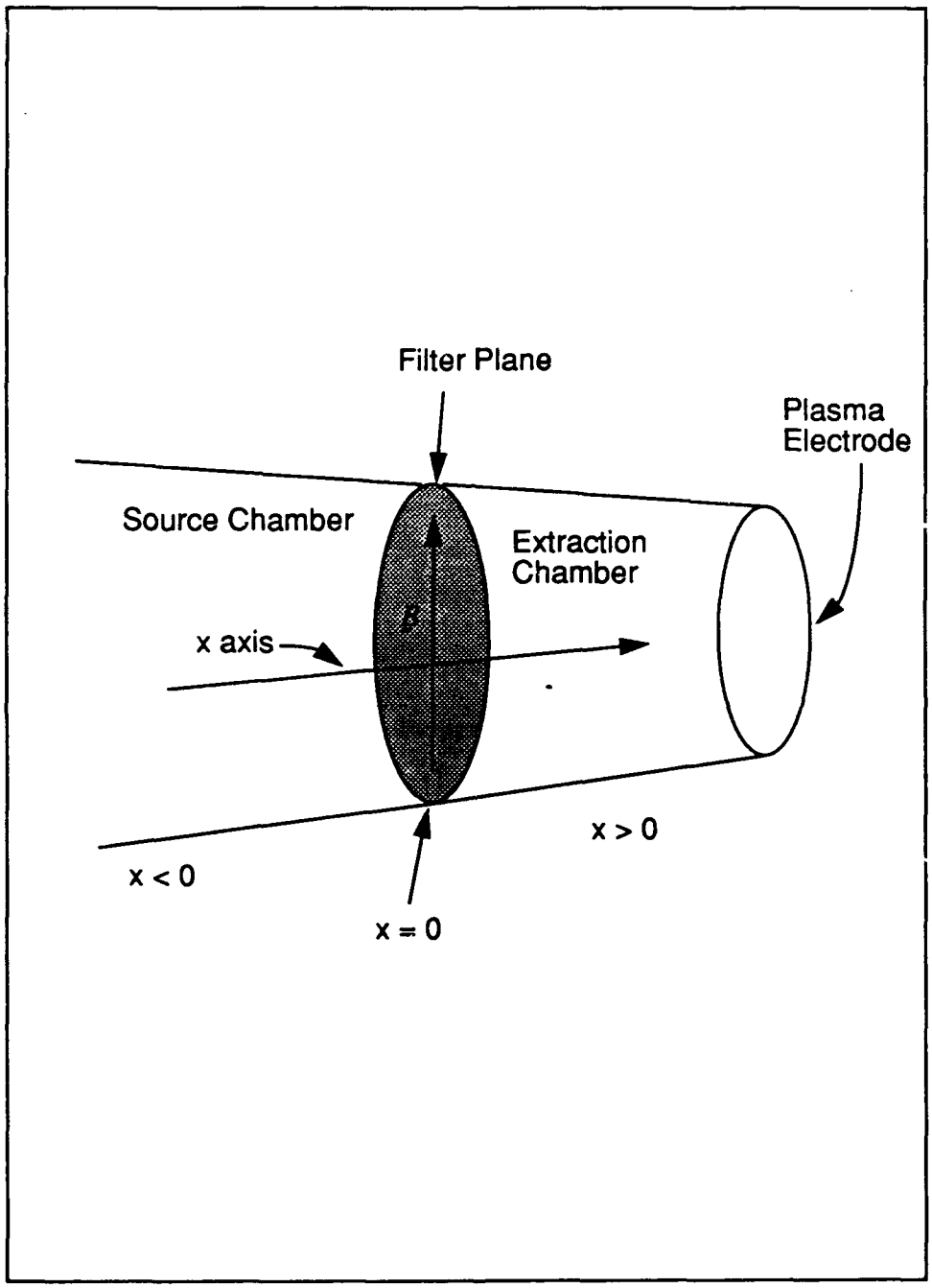

Figure 2-4: Coordinate System

$$\Gamma_x = \frac{-\nu_{el} T_e}{m_e (\nu_{el}^2 + \omega_e^2)} \frac{dn}{dx} \tag{2.1}$$

(Golant, 1963) where x is the dimension along the cylindrical axis of the source, ν_{el} is the frequency of electron-ion collisions under the (here appropriate) assumption that the ion velocity is much less than the electron velocity and averaged over a Maxwellian electron velocity distribution, T_e is the electron temperature in ergs, m_e is the electron mass in grams, n is the plasma density in cm^{-3}, and ω_e is the electron cyclotron frequency, given by $eB/m_e c$, where B is the magnitude of the magnetic induction and c is the speed of light.

With the electron temperature in electron volts, and employing the notation τ_e to indicate the change in units from ergs to electron volts, the electron-ion collision frequency ν_{el} can be written as

$$\nu_{el} = 2.91 \times 10^{-6} \, n \, \frac{\ln(\lambda)}{\tau_e^{3/2}} \tag{2.2}$$

(Department of the Navy, 1983) where $\ln(\lambda)$ is the Coulomb logarithm given by

$$\ln(\lambda) = 23.0 - \ln\left(\frac{n^{1/2}}{\tau_e^{-3/2}}\right) \tag{2.3}$$

It is appropriate to examine the variation of ν_{el} through the magnetic filter. On the source chamber side, $n = 1.2 \times 10^{11}$ cm^{-3} and, although τ_e is not given, we can safely guess that it is about 1.5 eV (Leung, 1983). Then $\ln(\lambda)$ is about 11 and $\nu_{el} = 2 \times 10^6$ sec^{-1}. On the target chamber side, $n = n_2 = 1.7 \times 10^{10}$ cm^{-3}, and, as argued earlier, $\tau_e = 0.5$ eV. Then, in the target chamber, $\nu_{el} = 1.4 \times 10^6$ sec^{-1}.

Since the electron cyclotron frequency $\omega_e = 1.76 \times 10^7 B \text{ sec}^{-1}$, with B in gauss, the ω_e^2 term dominates the ν_{el}^2 term in the denominator of Eq (2.1) even for B as small 1 gauss.

The electron flux Γ_x through the filter can now be approximated. Since the plasma density falls from its initial value to one much lower over the width, roughly 4 cm, of the filter field,

$$\frac{dn}{dx} \cong 1.2\times10^{11}\text{cm}\,\frac{1}{4\text{cm}} = \frac{\Delta n}{\Delta x}$$

and using this value for the variation in electron number density in Eq (2.1), it is found that

$$\Gamma_x \cong 4\times10^{14}\,\text{cm}^{-2}\text{sec}^{-1} \tag{2.4}$$

Assuming, then, a continuity of electron flow through the magnetic filter to the target chamber end plate, the final chamber number density n can be estimated from the expression

$$\Gamma_x = \frac{1}{4}\, n_2\, \bar{\upsilon}\, \xi \tag{2.5}$$

where $\bar{\upsilon}$ is the average electron velocity, $\bar{\upsilon} = (8T_e/(\pi m_e))^{1/2}$, and ξ is a numerical factor expressing the electrostatic shielding of the end plate. It has been estimated earlier that $\xi = \exp(-1/5)$, or about 0.8.

Using the value of Γ_x given in Eq (2.4), Eq (2.5) can be solved for n_2. Hence, $n_2 = 4\Gamma_x/(\bar{\upsilon}\xi) = 2 \times 10^7 \text{ cm}^{-3}$. Of course, in the experiment

n_2 was measured to be $n_2 \approx 2 \times 10^{10}$ cm^{-3} . This indicates that the flow of electrons through the filter substantially exceeds the classical prediction.

If it is objected that the flux has been underestimated because the maximum value of ω_e has been used in the calculation above, the response is twofold. First, the field strength is nearly equal to the maximum value for a width of about 1 cm -- thus, the estimate $n_2 = 2 \times 10^7$ cm^{-3} could be low by a factor of 4, since the filter width was taken to be 4 cm. Second, it is possible to perform the calculation more carefully and to arrive at an equation for the plasma density as a function of x.

Displaying the plasma number density dependence of ν_{el} explicitly by writing $\nu_{el} = d\, n\, T_e^{-3/2}$ (and hence ignoring small variations in ln(λ) with n) with d equal to

$$d = \frac{4\sqrt{2\pi}}{3} \cdot \frac{e^4}{m_e^{1/2}} \cdot \ln(\lambda) \cong 6\times10^{-23}\ \mathrm{cm}^3\ \mathrm{erg}^{3/2}\ \mathrm{sec}^{-1} \qquad (2.6)$$

and applying the knowledge that $\nu_{el} << \omega_e$, Eq (2.1) can be transformed as

$$\Gamma_x = -\frac{d}{m_e\omega_e^2}\ \frac{1}{T_e^{1/2}}\ n\frac{dn}{dx} \qquad (2.7)$$

Writing $\omega_e(x) = \omega_o \exp[-(x/a)^2]$, with ω_o the value of the electron cyclotron frequency at maximum magnetic induction. This should be a fairly good approximation to the shape of the magnetic field. Ignoring the effects of changes in electron temperature or plasma potential on electron transport as before, Eq (2.7) can be integrated, with the result

that

$$n^2(x) = n_1^2 - \beta \frac{a}{\sqrt{2}} \{\Phi(\frac{\sqrt{2}}{a}|x_1|) + \text{sign}(x)\ \Phi(\frac{\sqrt{2}}{a}|x|)\ \} \frac{\sqrt{\pi}}{2} \qquad (2.8)$$

where

$$\beta = \frac{2m_e\Gamma_x\omega_o^2}{d} \cdot \sqrt{T_e} \qquad (2.9)$$

and $\Phi(y)$ is the error function evaluated at y. The coordinate x is taken to be zero at the maximum value of B in the filter plane, is negative in the source chamber and positive in the extraction chamber (see Figure 2-4). Further simplification is possible. The position where source chamber density was measured, x_1, is probably about -4 cm or more, in the magnetic field free region of the source-chamber. Hence,

$$n^2(x) = n_1^2 - \beta \frac{a}{2} (\Phi(\frac{4\sqrt{2}}{a}) + \text{sign}(x)\ \Phi(\frac{\sqrt{2}}{a}|x|)) \sqrt{\frac{\pi}{2}} \qquad (2.10)$$

In order to employ this equation to calculate n_2 , assume that x is some reasonably large (say 4 cm) distance into the target chamber. This distance is chosen because at that point the magnetic induction becomes weak enough for the electron gyroradius to allow electrons to escape from the filter. So

$$n_2^2 = n_1^2 - \beta a \sqrt{\frac{\pi}{2}} \Phi(\frac{4\sqrt{2}}{a}) \qquad (2.11)$$

Writing β again in order to display the dependence upon n_2,

$$\beta = \frac{2m_e\Gamma_x T_e^{1/2}\omega_o^2}{d} = \frac{2m_e\omega_o^2}{d}\ T_e^{1/2}\ \frac{1}{4}\ n_2\ \bar{\upsilon}\ \xi \qquad (2.12)$$

Defining ε by the equation

$$\varepsilon = \frac{2m_e\omega_o^2}{d}\ T_e^{1/2}\ \frac{1}{4}\ \bar{\upsilon}\ \xi\ a\ \sqrt{\frac{\pi}{2}}\Phi\left(\frac{4\sqrt{2}}{a}\right) \qquad (2.13)$$

the expression for n_2^2 can be written as a quadratic:

$$n_2^2 = n_1^2 - \varepsilon n_2 \qquad (2.14)$$

and solved as

$$n_2 = \frac{\sqrt{4n_1^2+\varepsilon^2}-\varepsilon}{2} \qquad (2.15)$$

Using the values accepted earlier for the parameters which appear in Eq (2.13) for ε, it is found that $\varepsilon = 2.8 \times 10^{14}$ cm^{-3}. Since $\varepsilon >> n_1$, it is justifiable to approximate Eq (2.15) with $n_2 = n_1^2/\varepsilon$. With $n_1 = 1.2 \times 10^{11}$ cm^{-3}, $n_2 = 5 \times 10^7$ cm^{-3}. Thus, the revised calculation increases the value of n_2 by a factor of about 3.

Incidentally, knowledge of n_2 allows exact calculation of β, so that Eq (2.10) can be solved for the plasma density as a function of x through the filter field. Figure 2-5 shows the variation in electron number density with x through the filter for the situation discussed above.

The argument above may be summarized as follows. The given source chamber electron density can sustain a classical electron flux through the filter on the order of 10^{14} cm^{-2} sec^{-1} (Eq (2.4)), and demands that the extraction

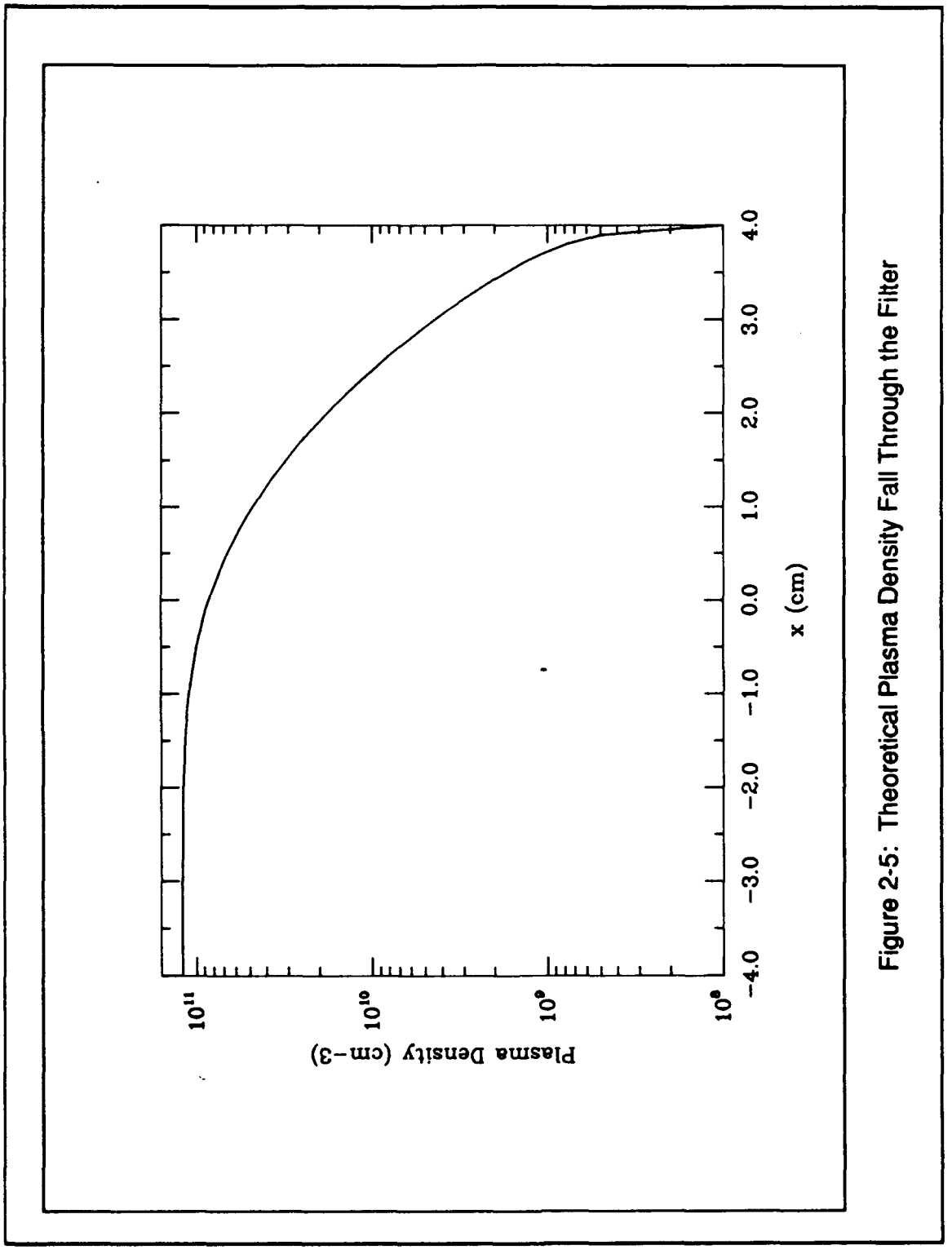

Figure 2-5: Theoretical Plasma Density Fall Through the Filter

chamber electron density be about 10^7 cm^{-3}. The measured final chamber electron density, 10^{10} cm^{-3}, corresponds to an electron flux to the extraction electrode on the order of 10^{17} cm^{-2} sec^{-1}. On the basis of this argument, the flux through the filter must exceed its classical value.

An objection to the argument may be raised. It can be argued that Eq (2.5) overestimates the thermal flux to the extraction electrode. It is not known where in the extraction chamber the electron density n_2 was measured. If the residual magnetic field due to the side-wall confinement magnets or the filter is high enough, the electron mean free path may be much shorter than the target chamber. In that case, the density $n_2 = n_2(x)$ may fall with increasing x, so that the electron density one mean free path away from the extraction electrode may be considerably less than the measured value. Devynck has shown that the electron density may fall by a factor of 3 over a 5 cm distance when there is a residual magnetic field of 5 G (Devynck, 1987). If the plasma density one mean free path from the extraction electrode is much smaller than the measured target chamber value, the electron thermal flux to the plasma electrode, and so the required diffusive flux through the magnetic filter, will also be much smaller.

To avoid this difficulty and more rigorously determine the magnitude of the electron diffusive flux through the magnetic filter, it is necessary to measure the electron current to the extraction electrode. This was done by Holmes in the experiment described in the next section (Holmes, 1982b).

Evidence from Holmes' Experiment

There are some noteworthy differences between Holmes' experiment and that of Leung and Bacal. First, Holmes' filter was not produced by permanent

magnets but by a configuration of wires. Two planes of wires form the magnetic filter. The planes are parallel to the plasma electrode and separated by a distance on the order of 1 cm. The current in one plane is in the opposite direction to the current in the other, forming a fairly uniform magnetic field between them. The field strength is higher, of course, near the wires and between pairs of wires from opposing planes. (Figure 2-6 shows Holmes' measurement of the magnetic field of the filter, with a slight correction to the indicated direction of current flow in the wires.) By varying the current through the filter, Holmes was able to verify the functional dependence of the electron flux on the filter field strength. Second, Holmes gives no indication that he measured the plasma density in the target chamber, but states that he measured the total current to the plasma electrode in the target chamber. As stated near the end of the last section, assuming continuity of current density across the filter region and the target chamber, the current to the plasma electrode gives a definite value for the electron flux through the magnetic filter.

To better understand the functional dependencies verified in this experiment, it is helpful to first examine Holmes' own derivation of the diffusion coefficient.

Holmes begins by assuming a functional form for the diffusion coefficient of

$$D = \frac{\nu_c T_e}{m_e \omega_e^2} \tag{2.16}$$

where T_e is the electron temperature in ergs, m_e is the electron mass in grams, ω_e is the electron cyclotron frequency, and ν_c is the electron-ion

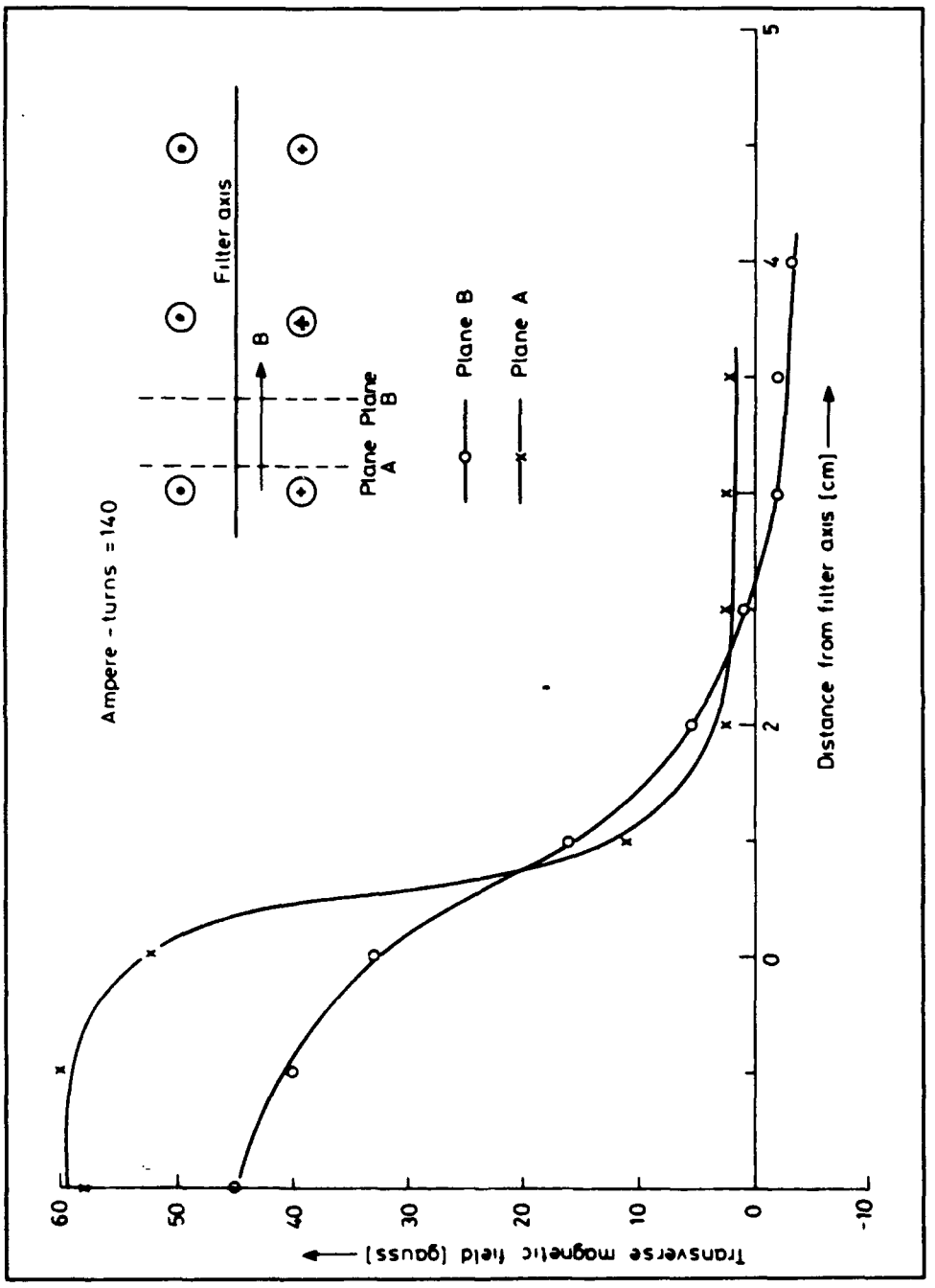

Figure 2-6: Holmes' Filter Field Profile

collision frequency before averaging over the distribution function for electron velocities. Holmes points out that electron-ion collisions dominate electron-neutral collisions under the relevant experimental conditions by a factor of about 30, and he gives the following equation for ν_c:

$$\nu_c = \frac{8\pi e^4 \, n \, \ln(\lambda)}{m_e^2} \left[\frac{\Phi(\chi) - G(\chi)}{\upsilon^3} \right] \tag{2.17}$$

(Holmes' original mks equation has been converted to cgs units) with $\chi = (m_t \upsilon^2/(2T_t))^{1/2}$, where m_t is the mass of the target species (either ions and other electrons) and T_t is the target species' temperature in ergs. This expression is (to within a factor of υ^2) given by Spitzer (Spitzer, 1962) as the result of a derivation for the rate of increase in the square of the change in test particle velocity upon collisions in a direction perpendicular to the original direction. As before, $\Phi(\chi)$ is the error function evaluated at χ, while

$$G(\chi) = \frac{\Phi(\chi) - \chi \frac{d}{d\chi}(\Phi(\chi))}{2\chi^2} \tag{2.18}$$

Before proceeding with Holmes' development, consider the behavior of $\Phi(\chi)$ - $G(\chi)$ for both large ($\chi >> 1$) and small ($\chi << 1$) χ. Since

$$\Phi(\chi) = \frac{2}{\sqrt{\pi}} \int_0^{\chi} dt \, \exp(-t^2) , \tag{2.19}$$

$$\frac{d\Phi}{d\chi} = \frac{2}{\sqrt{\pi}} \exp(-\chi^2) \tag{2.20}$$

So at large χ, $\chi \, d\Phi/d\chi \rightarrow 0$, while $\Phi(\chi) \rightarrow 1$, and $G(\chi) \rightarrow \Phi(\chi)/(2\chi^2)$

$\rightarrow 0$ also. So at large χ, ν_c behaves as $1/\upsilon^3$. At small χ, it is easy to see (by expanding Φ and G in series and retaining only the first few terms), that

$$\Phi(\chi) - G(\chi) \cong \frac{4}{3\sqrt{\pi}}\chi \tag{2.21}$$

Thus, at small χ, ν_c will vary as $1/\upsilon^2$.

Holmes' next step is to average his expression for the diffusion coefficient D Eq (2.16) over a Maxwellian electron distribution function. (Holmes actually linearly combines two terms for ν_c in the numerator of Eq (2.16), one for collisions of electrons with ions and one for collisions of electrons with other thermal electrons. The second of these terms is small, and it will be considered here later, and only in passing.) Converting Holmes' result for the average diffusion coefficient (again, without electron-electron effects) into cgs units,

$$\langle D \rangle = -\frac{\langle \nu_c \rangle T_e}{m_e \omega_e^2} \tag{2.22}$$

where

$$\langle \nu_c \rangle = \frac{24\pi}{\sqrt{2}} \cdot \frac{n e^4}{m_e^{1/2} T_e^{3/2}} \cdot \ln(\lambda) \tag{2.23}$$

This equation for $\langle \nu_c \rangle$ is a factor of $9\pi^{1/2}$ higher than the average collision frequency given by Eq (2.2), re-written here (Golant, 1980) as

$$\nu_{el} = \frac{4\sqrt{2\pi}}{3} \cdot \frac{n e^4}{m_e^{1/2} T_e^{3/2}} \cdot \ln(\lambda) \tag{2.24}$$

It is instructive to attempt to reproduce Holmes' result, Eq (2.23). In order to calculate $\langle \nu_c \rangle$, it is necessary to multiply Eq (2.17) by the normalized Maxwellian electron velocity distribution function, $f(\upsilon)$, given by the following equation:

$$f(\upsilon) = \left(\frac{m_e}{2\pi T_e}\right)^{3/2} \upsilon^2 \exp\left(-\frac{m_e \upsilon^2}{2T_e}\right) \tag{2.25}$$

and integrate over all speeds and angles, or:

$$\langle \nu_c \rangle = \frac{32\pi^2 e^4}{m_e^{1/2}} n \cdot \ln(\lambda) \left(\frac{1}{2\pi T_e}\right)^{3/2} \cdot \int_0^\infty d\chi \cdot \left[\frac{\Phi(\chi) - G(\chi)}{\chi}\right] \exp\left(-\frac{m_e T_i}{m_i T_e}\chi^2\right) \tag{2.26}$$

The challenge, then, is to integrate

$$\int_0^\infty d\chi \cdot \frac{\Phi(\chi) - G(\chi)}{\chi} \cdot \exp(-\alpha\chi^2)$$

where $\alpha = \frac{m_e T_I}{m_I T_e}$. To arrive at Eq (2.23) for $\langle \upsilon_c \rangle$, this integral must deliver a factor of 3/2 $\pi^{1/2}$ for electron-ion collisions and, incidentally, it must yield 0.62/4 $\pi^{1/2}$ for electron-electron collisions to retrieve Holmes' result there.

The simplest way to approach the integral is to employ an infinite series for the error function $\Phi(\chi)$:

$$\Phi(\chi) = \frac{2}{\sqrt{\pi}} \cdot \exp(-\chi^2) \cdot \sum_{n=0}^{\infty} \frac{2^n}{(2n+1)!!} \cdot \chi^{2n+1} \tag{2.27}$$

(National Bureau of Standards, 1964) where $n!!=n(n-2)(n-4)\ldots$

It is a simple matter to show that

$$\frac{\Phi(\chi) - G(\chi)}{\chi} = \frac{\exp(-\chi^2)}{\sqrt{\pi}} \cdot \sum_{n=0}^{\infty} 2^{n+1} \chi^{2n} \left[\frac{1}{(2n+1)!!} - \frac{1}{(2n+3)!!} \right] \qquad (2.28)$$

Then

$$\int_0^{\infty} d\chi \cdot \left[\frac{\Phi(\chi) - G(\chi)}{\chi} \right] \exp(-\alpha\chi^2) = \frac{1}{\sqrt{\gamma}} \sum_{n=0}^{\infty} \frac{1}{2n+1} \frac{1}{\gamma^n} \left(1 - \frac{1}{2n+3}\right) \qquad (2.29)$$

where $\gamma = 1 + \alpha$.

When the field particles are ions, α is very small and the series converges slowly. But when the field particles are electrons also, as in the case when the effects of electron-electron collisions are being taken into account, $\alpha = 1$ and $\gamma = 2$, and Eq (2.29) converges rapidly, within fifty terms, to 0.615. According to Holmes, the integral, in the case of electron-electron collisions, should be $0.62/4\ \pi^{1/2}$. Hence, Holmes' result for this calculation is lower than ours by a factor of $\pi^{1/2}/4$. It is expected that the same discrepancy will occur in the calculation for electron-ion collisions.

The exact result of the integral is dependent upon the values of m_e, m_I, T_e, and T_I which appear in the expression for α. With the ion temperature taken to be 0.1 times the electron temperature, and assuming that the ion mass is that of H_3^+, the series converges slowly. After 30,000 terms, the series yields 5.4.

It is an easy matter to estimate the integral analytically as a check upon the numerical calculation. For $\chi < 2$, $\Phi(\chi)$ - $G(\chi)$ is approximately equal to 0.7χ (see Eq (2.21)). But in that region, $\exp(-\alpha\chi^2)$ is roughly equal to 1 since α is very small. Hence,

$$\int_0^2 d\chi \cdot \left[\frac{\Phi(\chi) - G(\chi)}{\chi}\right] \exp(-\alpha\chi^2) \equiv 1.4 \qquad (2.30)$$

For $\chi > 2$, $\Phi(\chi)$ - $G(\chi)$ can be approximated by 1, and the upper limit of integration is safely placed at the point where $\alpha\chi^2$ is about 1 (that is, at the point where deviations from unity for the exponent begin to become important). This condition is met for χ equal to 235. Then

$$\int_0^{\infty} d\chi \cdot \left[\frac{\Phi(\chi) - G(\chi)}{\chi}\right] \exp(-\alpha\chi^2) \equiv 1.4 + \int_2^{235} d\chi \frac{1}{\chi} = 6.2 \qquad (2.31)$$

It is plain, then, that the value of the integral is nearer to 6.0 than to 6/4 $\pi^{1/2}$. Thus, Holmes' calculation of the diffusion coefficient, understood simply from a computational point of view, is an underestimate of the electron flux by a factor of $\pi^{1/2}/4$.

As shall be shown momentarily, when the right-hand side of the expression for the flux, Eq (2.1), is multiplied by the factor $9\pi^{1/2}$, which is the ratio of Holmes' electron-ion collision frequency to the standard value found in the literature, Eq (2.1) accurately predicts the flux Holmes measured in this experiment. Yet it appears that Holmes' derivation is marred by a small computational error. In addition, the approach taken as a whole is radically different from that normally taken in the theory of electron transport across magnetic fields. This difference will be brought out in Chapter III.

In addition to correctly calculating the experimentally measured electron flux through the magnetic filter, Holmes' expression for the flux preserves what his experiment shows is the correct functional form for the flux, a variation as $1/B^2_{max}$. To demonstrate this, it is necessary to proceed with the derivation.

After calculating the diffusion coefficient, Holmes derives an expression for the flux in much the same way as in the development above leading to Eq (2.8). Beginning with Eq (2.8), assuming that each of the error functions in brackets is equal to one, assuming that $n^2(x) << n_1^2$, solving for Γ_x, and multiplying the right-hand side by a factor of $9\pi^{1/2}$, we have Holmes' equation for the flux:

$$\Gamma_x = \frac{\sqrt{\frac{2}{\pi}}d}{2m_e T_e^{1/2}} \cdot \frac{n_o^2}{a\omega_o^2} \cdot 9\sqrt{\pi} \qquad (2.32)$$

Holmes then performed some measurements to test the validity of this equation. He found that the logarithm of the product $\Gamma_x T_e^{1/2}/n_1^2$ varied inversely with twice the logarithm of the transverse magnetic flux (which is proportional to $\omega_o a$), in agreement with Eq (2.32) (since a is constant for all values of the magnetic flux). Figure 2-7 shows the dependence of the product $I_e T_e^{1/2}/n_1^2$ on the transverse magnetic flux. (There is a typographical error in the figure. The measured slope is -1.97, not 1.97. The theoretical value given by Eq (2.32) is -2.0.) I_e is the total current to the plasma electrode. Lea *et al* (Lea, 1990) have also confirmed that the diffusion coefficient varies as $1/B^2$ at high B, at least for high values of V_b. Figure 1-9 shows Holmes' result from another experiment (Holmes, 1982a) where n_1 was seen to rise linearly with the transverse magnetic flux, as predicted by Eq (2.32).

Holmes also found that $\Gamma_x T_e^{1/2}$ rose linearly with n_1^2 at constant magnetic flux. This result is shown here in Figure 2-8, where the logarithm of the product $I_e T_e^{1/2}$ is shown as a function of the logarithm of n_1^2. The slope was measured to be 0.88. Equation (2.32) predicts a slope of 1.0. These observations verify the functional form of Eq (2.32) but not the magnitude

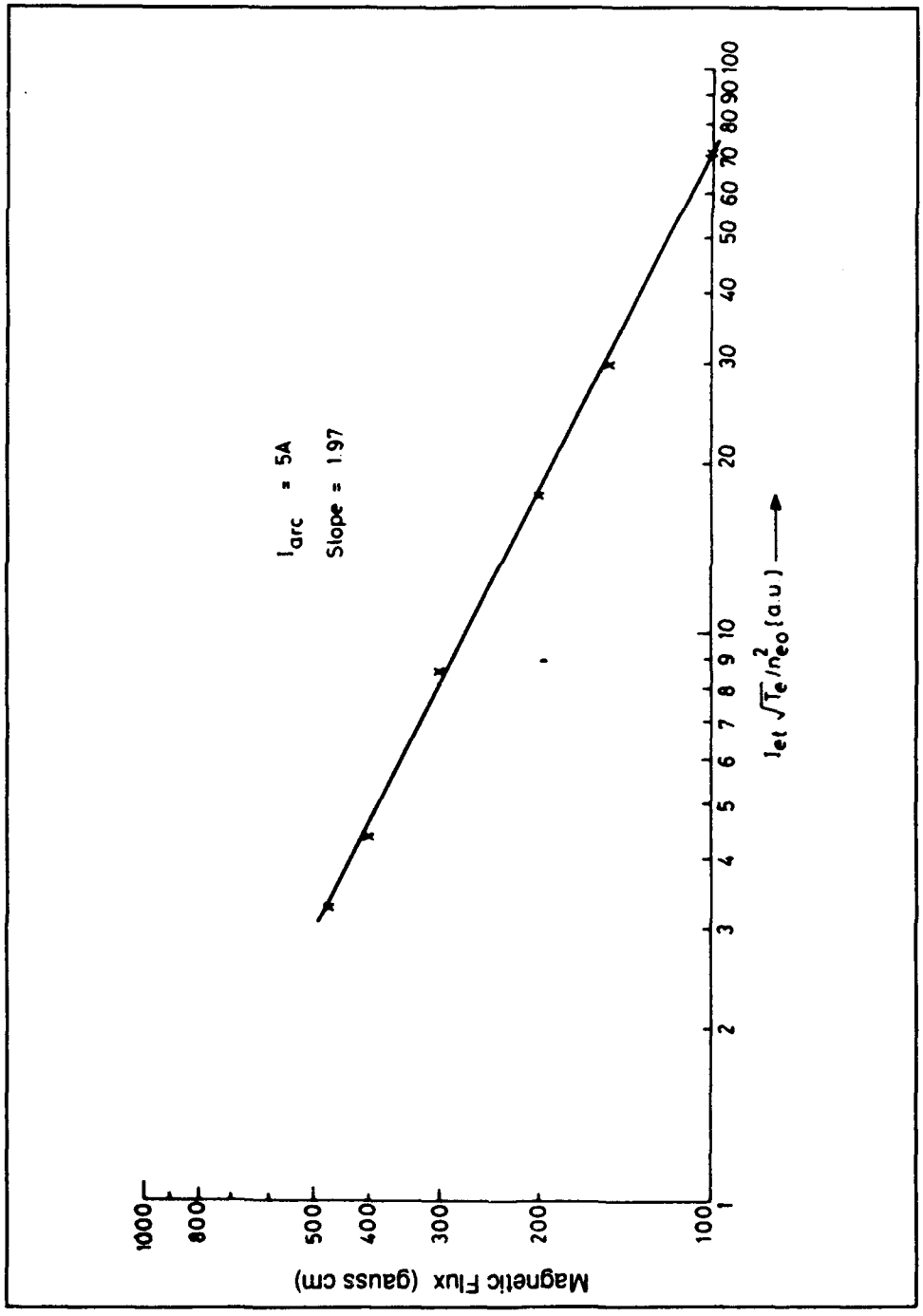

Figure 2-7: Variation of $I_e T_e^{1/2}/n_1^2$ with Transverse Magnetic Flux

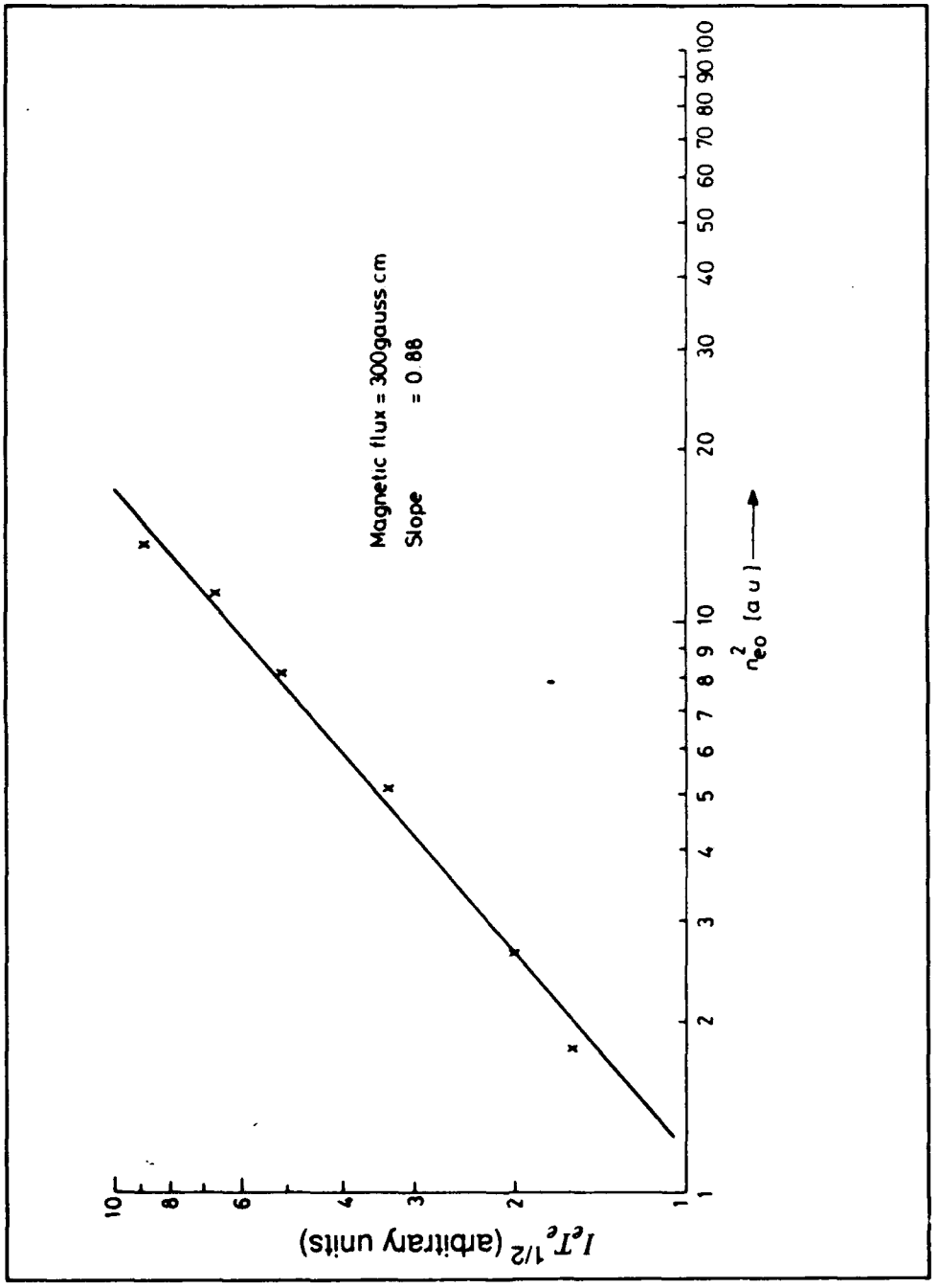

Figure 2-8: Depenaence of $I_e T_e^{1/2}$ with n_1^2

of the collision frequency. That the experimentally measured current matched the value predicted by Eq (2.32) for the appropriate n_1 can only be assumed since the value of the source chamber plasma density is not reported in Holmes' paper (Holmes, 1982b).

It could be objected that, since the plasma density in the source chamber is not constant, Holmes may have measured the plasma density n_1 at a point where it is a factor of four or so lower than its maximum value. The maximum value of n_1 would, under this scenario, provide sufficient diffusive flux through the filter in accordance with Eq (2.32) without the $9\pi^{1/2}$ enhancement factor. The conclusion to be drawn would be that electrons traverse the filter in accordance with a classical Coulomb diffusion coefficient, in contradistinction to Holmes' diffusion coefficient (Eq (2.22)).

The plasma density that enters into the flux equation, however, and drives the electron flux to the extraction electrode, should be measured near the filter plane in the source chamber. This is obvious from the nature of the integral $\Gamma\int_{\text{electrode}}^{x_1} dx\omega_e^2(x) \propto -\int_{n_2}^{n_1} dnn$ deriving from Eq (2.7). The major contribution to the left-hand integral comes near the peak filter induction; this integral is very nearly constant for x_1 not much less than 0 (see Figure 2-4). The right-hand integral must also approach a constant value on the source chamber side of the filter plane. Figure 2-5 shows that Eq (2.8) predicts the source chamber density will be very flat, becoming constant near the filter plane on the source chamber side.

Now in real sources the source chamber plasma density profile is not flat. Measurements show that the density rises to higher values with smaller x (Johnson, 1987: 162). The rise is due to the fact that the plasma must diffuse to the filter, requiring a density gradient into the source chamber. (The

rise is enhanced if plasma loss processes override production near the filter, as they should. Then, $\frac{d\Gamma}{dx}$ will be negative (see Eq (1.28)), so that the flux must be higher deeper into the source chamber, requiring a larger density gradient than if the flux were constant.)

Thus, if Holmes measured the source chamber density away from the filter region, it is likely that the value he used to test Eq (2.32) was too high. Since the value of n_1 deep in the source chamber can be about a factor of 4 higher than n_1 near the filter plane (Johnson, 1987: 162), Holmes' measurements may show that the required enhancement to the classical diffusion coefficient is not a factor of $9\pi^{1/2}$, but is closer to a factor of $(9\pi^{1/2})^2$.

If Holmes' collision frequency is applied to the experiment of Leung and Bacal, described earlier in this chapter, a refined estimate of the target chamber plasma density required to produce a flux to the extraction electrode in balance with the classical flux through the filter can be deduced. Replacing d in Eq (2.13) with $9\pi^{1/2}d$, reducing ε by a factor of $9\pi^{1/2}$, ε decreases from 2.8×10^{14} cm^{-3} to 1.8×10^{13} cm^{-3}. Then the calculation for the final chamber plasma density rises from $n_2 = 5 \times 10^{7}$ cm^{-3} to 8×10^{8} cm^{-3}. This is still a factor of 20 below the final chamber plasma density measured in the experiment. Figure 2-9 displays the variation of electron number density with x for Leung and Bacal's experiment using Holmes' diffusion coefficient. It also shows that the classical diffusion coefficient must be increased by a factor of 350 to yield the measured final chamber electron number density.

As stated earlier, an alternate partial explanation for this wide (factor of 350) discrepancy may be attempted. The actual direct electron flux from the edge of the filter to the end plate can be substantially reduced below the thermal value of $\frac{1}{4}n_2\bar{v}$ by a small residual magnetic field near the center

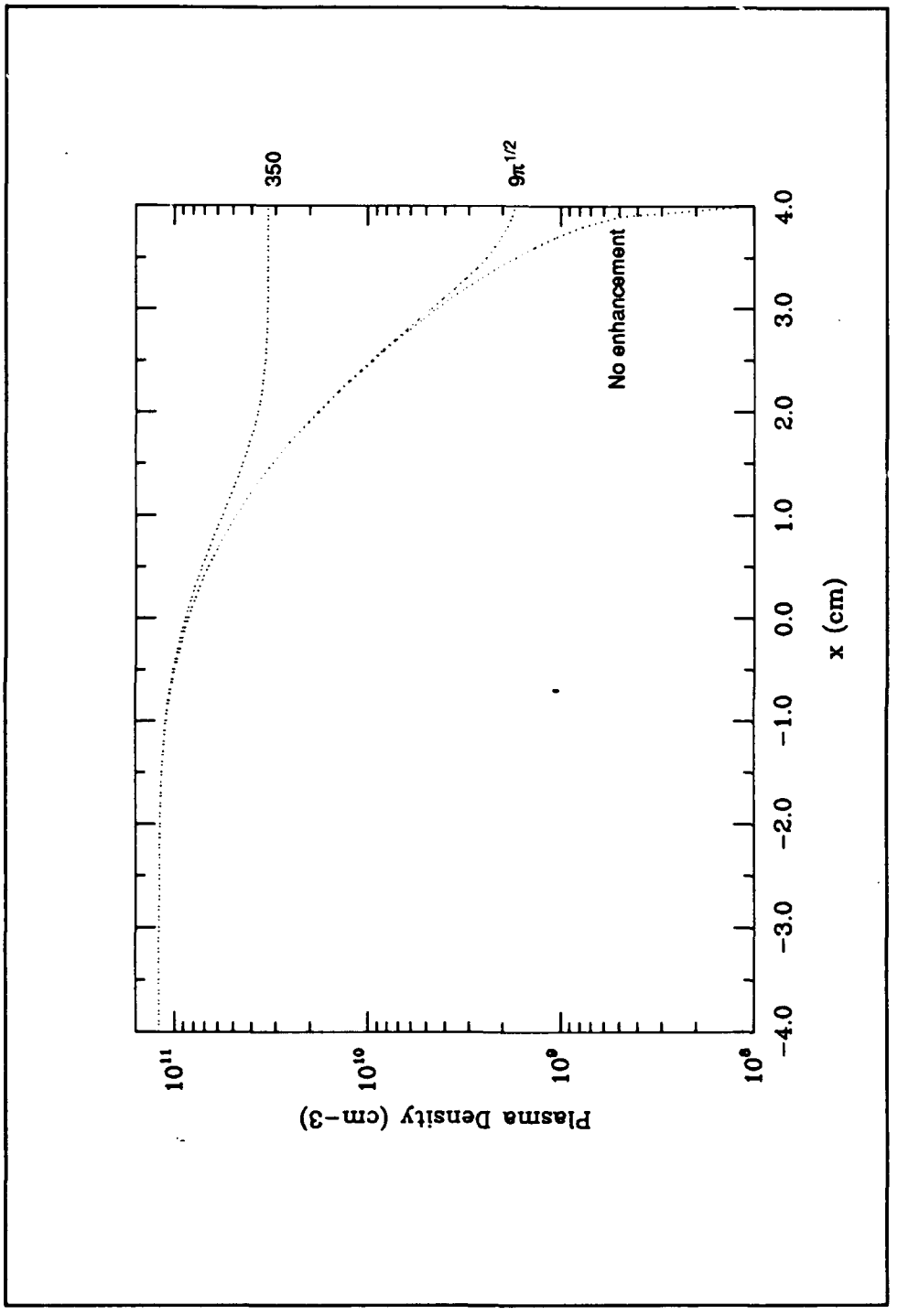

Figure 2-9: Theoretical Plasma Density Profile for Leung's Experiment Using Holmes' Diffusion Coefficient

of the extraction chamber due to the multipole configuration of permanent magnets along the chamber side wall. To determine the degree to which this effect diminishes the thermal flux to the extraction electrode requires simultaneous measurement of the plasma density profile in the extraction chamber and the current to the extraction electrode. In Chapter IV, an estimate is made of the area of the extraction electrode which receives a thermal electron flux for experimental conditions (Leung, 1983) similar to those considered here.

In summary, there is experimental evidence that the electron diffusion through the magnetic filter is anomalously high. These results indicate that the correct functional form for the flux is given as in Eq (2.32), and that there is an enhancement factor of at least $9\pi^{1/2}$ above the classical flux. The high final chamber density in Leung's experiment indicates that either the flux through the filter was enhanced by a factor an order of magnitude higher than $9\pi^{1/2}$, or that the thermal flux to the extraction electrode was diminished by residual magnetic induction.

Evidence from Ferriera's Experiment

The Ferriera experiment was conducted in a source similar in configuration to the Leung and Bacal source (Leung, 1984b). Important differences are: 1) the average plasma density was only about 10^{10} cm^{-3} (compared with 10^{11} cm^{-3} for Leung and Bacal), 2) the peak filter magnetic induction ranged from 230 G to 510 G (compared to 35 G for Leung and Bacal), and 3) the plasma was generated in argon at a pressure of about 0.5 mtorr (compared with hydrogen at 1.5 mtorr for Leung and Bacal). These differences decrease the comparative ability of electrons to cross the filter. The

effect of a decrease in source chamber density and an increase in peak filter magnetic induction is apparent from Eq (2.32): the electron flux is dramatically reduced.

The filter magnetic induction was varied among four different values. The current to the extraction electrode was (presumably) measured, though not reported, for each filter, as were the plasma potential profile and both the source and extraction chamber electron densities. The diffusion coefficient was then calculated from the equation

$$D_{e\perp} = J_{D_e}\left[\frac{e^2 n_{eAV}}{T_{eAV}}\left(\frac{\Delta V}{\Delta x}\right) - e\left(\frac{\Delta n_e}{\Delta x}\right)\right]^{-1} \tag{2.33}$$

where $D_{e\perp}$ is the electron diffusion coefficient, J_{D_e} is the electron current from the source to the extraction chamber, n_{eAV} is the average electron number density, T_{eAV} is the average electron temperature in the filter region, $\frac{\Delta V}{\Delta x}$ is the change in plasma potential and $\frac{\Delta n_e}{\Delta x}$ is the change in electron number density over the width of the filter magnetic field, Δx . The resulting values of the diffusion coefficient ranged from 2 to 6 x 10^4 cm^2 sec. The diffusion coefficient is the same order of magnitude as the Bohm diffusion coefficient (Bohm, 1949), two to three orders of magnitude higher than the classical value.

Nothing definite can be said about the scaling of the diffusion coefficient with magnetic induction or temperature. This is due to the fact that the electron density through the filter was not reported. Instead, the electron saturation current to a Langmuir probe was measured. But to recover the electron density from a measurement of the saturation current requires knowledge of the diffusion coefficient (Bohm, 1949: 54).

It appears that the enhanced diffusion through the magnetic filter is, in this case, due to an ion-sound-like wave interaction. The frequency of peak intensity decreased from 3 MHz at 117.5 G average magnetic induction to 2.5 MHz at 255 G average magnetic induction.

Summary

Evidence for enhanced diffusion through the filter has be found in experiments performed by Leung and Bacal (Leung, 1984b), Holmes (Holmes, 1982b), and Ferreira *et al* (Ferriera, 1989).

In Leung and Bacal's experiment, the final chamber plasma density is so high that, for the flux through the magnetic filter to match the thermal flux to the extraction electrode, the collision frequency must be enhanced by a factor of 350. Alternately, the thermal flux to the extraction electrode may be diminished by a factor of 350 (due to a possible residual magnetic induction), or the two effects of enhancing the collision frequency and diminishing the thermal flux may combine to provide a flux balance.

In Holmes' experiment, the flux through the magnetic filter was measured at (at least) $9\pi^{1/2}$ times the classical rate.

In Ferriera's experiment, performed under conditions of relatively low plasma density and high magnetic induction in an argon plasma, the measured flux exceeded the classical rate by a factor of 10^3.

Chapter III - Transport Theory

Introduction

It was demonstrated in Chapter I that both positive ion and electron collisions are dominated in typical tandem multicusp H^- sources by Coulomb collisions rather than collisions with neutral molecular hydrogen. In Chapter II the derivation of Holmes (Holmes, 1982b), in which an expression for the electron flux through the magnetic filter is developed, was reviewed. There it was noted that Holmes' development is unorthodox. In the present section, a standard theory of charged particle diffusion in a highly ionized plasma is presented and contrasts are drawn to Holmes' derivation. The derivation of the Fokker-Planck equation for a particle in a medium of Maxwellian target particles will be developed in detail in order to deduce the meaning of the terms in Holmes' expression for the electron-ion collision frequency Eq (2.17). Thereafter, the highlights of a standard approach to calculating the electron flux across a magnetic field in a highly ionized plasma will be given; this will serve as a basis for the examination of the relative size of various terms in the equation for the electron flux, on the assumption that the enhanced flux measured in H^- devices may be due to terms generally small in other situations. The equation thus derived will be the standard flux equation for a fully ionized plasma (Shkarofsky, 1966) with a modification to indicate that not all positive ions will experience drift in the filter magnetic field. Finally, an overview of wave-particle transport as derived by Dum (Dum, 1978b) will be presented. It will be shown that it is possible to retain a $1/B^2$ behavior in the diffusion coefficient and

to have a Coulomb-like ∇T drag term in the momentum moment of the Boltzmann equation if the diffusion is driven by ion-sound-like or related turbulence. In Chapter IV, it will become apparent that the correct functional form of the flux must include this ∇T drag term.

The Fokker-Planck Equation

This section in large measure is a repetition of Trubnikov's development (Trubnikov, 1965) of the Fokker-Planck equation.

The starting point for a discussion of charged particle diffusion in a plasma is the Boltzmann kinetic equation for the species α of charged particle under consideration:

$$\frac{\partial f_\alpha}{\partial t} + \nabla \cdot (\underline{v} f_\alpha) + \nabla_v \cdot (\underline{F}^{(e)} f_\alpha) = \left(\frac{\delta f_\alpha}{\delta t}\right)_c \tag{3.1}$$

The function $f_\alpha = f_\alpha(\underline{x}, \underline{v}, t)$, the one-particle distribution function for species α, is defined such that $f_\alpha(\underline{x}, \underline{v}, t)\, d\underline{x} d\underline{v}$ is the probability of finding one particle of species α in the phase-space volume centered at $\underline{x}, \underline{v}$, and whose infinitesimal volume element is $d\underline{x} d\underline{v}$. The term $\underline{F}^{(e)}$ is the external force acting on the particle; usually,

$$\underline{F}^{(e)} = Ze\left\{\underline{E} + \frac{1}{c}[\underline{v} \times \underline{B}]\right\} \tag{3.2}$$

where Ze is the α particle charge (Golant, 1980; Hinton, 1983; Trubnikov, 1965). The term $(\delta f_\alpha/\delta t)_c$ describes the effect of collisions, and it is the central point for discussion in this section.

The collision term appropriate under many circumstances is the Fokker-Planck collision term,

$$\left(\frac{\delta f_\alpha}{\delta t}\right)_c = -\nabla_v \cdot \underset{\sim}{j}^\alpha \tag{3.3}$$

(Allis, 1956: 430) where the flux term j_i^α is given by

$$j_i^\alpha = \frac{F_i^\alpha}{m_\alpha} f_\alpha - D_{ik}^\alpha \frac{\partial f_\alpha}{\partial v_k} \tag{3.4}$$

with $\underset{\sim}{F}^\alpha$ being an entirely different entity from $\underset{\sim}{F}^{(e)}$ of Eq (3.2). This force, $\underset{\sim}{F}^\alpha$, is known as the force of dynamic friction. The tensor D_{ik}^α is called the diffusion tensor in velocity space. (Here and below, the Einstein summation convention is employed for indices i, j and k.)

Since a plasma typically contains multiple charged particle species, terms in Eq (3.4) are equivalent to the sums of individual terms for each target species β:

$$\underset{\sim}{j}^\alpha = \sum_\beta \underset{\sim}{j}^{\alpha/\beta} \tag{3.5}$$

$$\underset{\sim}{F}^\alpha = \sum_\beta \underset{\sim}{F}^{\alpha/\beta} \tag{3.6}$$

$$D_{ik}^\alpha = \sum_\beta D_{ik}^{\alpha/\beta} \tag{3.7}$$

where $\underset{\sim}{F}^{\alpha/\beta}$ is the force of dynamic friction on particles of species α due to particles of species β, and $D_{ik}^{\alpha/\beta}$ is the velocity space diffusion tensor for a particles in a β particle medium. The sum in Eqs (3.5

to 3.7) is over all species that interact with α. The physical meaning of the force of dynamic friction and the diffusion tensor in velocity space can be brought out by examining the derivation of Eqs (3.3) and (3.4). If it is assumed that the distribution function obeys Smoluchowski's law (Wu, 1966):

$$f_\alpha(\underline{v}, t) = \int d\Delta\underline{v} f_\alpha(\underline{v} - \Delta\underline{v}, t - \Delta t)\, Q(\underline{v} - \Delta\underline{v}, \Delta\underline{v}) \tag{3.8}$$

where $Q(\underline{v} - \Delta\underline{v}, \Delta\underline{v})$ is the probability that, in time Δt, the velocity $\underline{v} - \Delta\underline{v}$ changes by a small $\Delta\underline{v}$ to $\underline{v}$ due to collisions. Expanding the integrand in a Taylor series

$$f_\alpha(\underline{v} - \Delta\underline{v}, t - \Delta t)\, Q(\underline{v} - \Delta\underline{v}, \Delta\underline{v}) = f_\alpha Q - \Delta v_i \frac{\partial}{\partial v_i}(f_\alpha Q) \tag{3.9}$$

$$+ \frac{1}{2}\Delta v_i \Delta v_j \frac{\partial^2}{\partial v_i \partial v_j}(f_\alpha Q) + \ldots - \Delta t \frac{\partial}{\partial t}(f_\alpha Q)$$

where $f_\alpha Q = f_\alpha(\underline{v}, t)\, Q(\underline{v}, \Delta\underline{v})$ and noting that $\int d\Delta\underline{v} Q(\underline{v}, \Delta\underline{v}) = 1$, it is apparent that

$$\left(\frac{\partial f_\alpha}{\partial t}\right)_c = -\frac{\partial}{\partial v_i}\{<\Delta v_i> f_\alpha - \frac{1}{2}\frac{\partial}{\partial v_j}(<\Delta v_i \Delta v_j> f_\alpha)\} \tag{3.10}$$

where

$$<\Delta v_i> \equiv \frac{1}{\Delta t}\int d\Delta\underline{v} \Delta v_i Q(\underline{v}, \Delta\underline{v}) \tag{3.11}$$

and

$$<\Delta v_i \Delta v_j> \equiv \frac{1}{\Delta t}\int d\Delta \underset{\sim}{v} \Delta v_i \Delta v_j Q(\underset{\sim}{v}, \Delta \underset{\sim}{v}) \tag{3.12}$$

(Wu, 1966: 52). Then, after some minor manipulation to group terms,

$$\frac{F_i^{\alpha/\beta}}{m_\alpha} = <\Delta v_i>^{\alpha/\beta} - \frac{1}{2}\frac{\partial}{\partial v_j}<\Delta v_i \Delta v_j>^{\alpha/\beta} \tag{3.13}$$

and

$$D_{ik}^{\alpha/\beta} = \frac{1}{2}<\Delta v_i \Delta v_j>^{\alpha/\beta} \tag{3.14}$$

The quantity $<\Delta v_i>$ is obviously the average rate of change in particle velocity due to collisions. And the trace of $<\Delta v_i \Delta v_j>$ is proportional to particle energy loss upon collisions.

The Boltzmann equation with the Fokker-Planck collision term is known as the Fokker-Planck equation. The central condition for applicability of the Fokker-Planck equation is that $\ln(\lambda)$, the Coulomb logarithm, be much larger than 1. This occurs only if the large number of small angle, large impact parameter scattering events have a greater cumulative effect than a few large angle, small impact parameter events (Hinton, 1983). (The reason for this is that, if the collision results in a large velocity change, it is as if a particle were created within an infinitesimal volume element around the final velocity without having passed through the boundary of the volume. Such a process cannot be described mathematically with the divergence of a flux in velocity space (Trubnikov, 1965: 139).) For electrons in a typical H^- volume source, $\ln(\lambda)$ is about 10, so this condition is satisfied. (The Fokker-

Planck equation also fails for especially high velocity particles, for which the Coulomb interaction between two particles is modified by the rest of the plasma in a more complicated way than can be described by static Debye shielding.)

For Coulomb collisions it is possible to derive expressions for $<\Delta v_i>$ and $<\Delta v_i \Delta v_j>$ following Trubnikov (Trubnikov, 1965: 119-124). Consider an α particle incident with relative velocity $\underline{\aleph}$ directed along the z axis upon a medium of β particles with velocity $\underline{v}'$. The number of β particles entering into a particular differential area $\rho d\rho d\phi$ in the x-y plane at impact parameter ρ per unit time with velocity $\underline{v}$ is

$$f_\beta(\underline{v}')\,\aleph\, d\sigma d\underline{v}' \tag{3.15}$$

where $d\sigma = \rho d\rho d\phi$, $\rho = (x^2+y^2)^{1/2}$, and $\aleph = |\underline{v}-\underline{v}'|$. Since the scattering angle is determined by ρ, ϕ, and the relative velocity and since the collisions are elastic, the average Δv_i per unit time, considering all β particles at all velocities, is

$$<\Delta v_i>^{\alpha/\beta} = \int d\sigma \int d\underline{v}' \Delta v_i \aleph f_\beta(\underline{v}') \tag{3.16}$$

Similarly,

$$<\Delta v_i \Delta v_j>^{\alpha/\beta} = \int d\sigma \int d\underline{v}' \Delta v_i \Delta v_j \aleph f_\beta(\underline{v}') \tag{3.17}$$

These equations can be simplified by noting that $\Delta v_i = (m_{\alpha\beta}/m_\alpha)\,\aleph_i$ with $m_{\alpha\beta} = (m_\alpha m_\beta)/(m_\alpha + m_\beta)$ and by writing

$$w_i = \frac{m_{\alpha\beta}}{m_\alpha}\int d\sigma \Delta \aleph_i \aleph \tag{3.18}$$

$$w_{ij} = \left(\frac{m_{\alpha\beta}}{m_\alpha}\right)^2 \int d\sigma \Delta \aleph_i \Delta \aleph_j \aleph \tag{3.19}$$

The difficulty, then, is to calculate the quantities w_i and w_{ij}. From dimensional considerations,

$$w_i = \frac{\aleph_i}{\aleph} A \tag{3.20}$$

$$w_{ij} = \delta_{ij} B + \frac{\aleph_i \aleph_j}{\aleph^2} C \tag{3.21}$$

and the challenge is to compute the scalar quantities A, B, and C. If the scatter is into an angle θ, defined as is usual for spherical coordinate systems as the polar angle, $\Delta \aleph_x = \aleph \sin\theta\cos\phi$, $\Delta \aleph_y = \aleph \sin\theta \sin\phi$, and $\aleph_z = -\aleph(1-\cos\theta)$. But, since it is well known that for the Coulomb interaction $\tan(\theta/2) = \rho_\perp/\rho$ where $\rho_\perp = (e_\alpha e_\beta)/(m_{\alpha\beta}\aleph^2)$, these changes in relative velocity can be transformed as

$$\Delta \aleph_x = 2\aleph \frac{\rho\rho_\perp}{\rho^2+\rho_\perp^2}\cos\phi \tag{3.22}$$

$$\Delta \aleph_y = 2\aleph \frac{\rho\rho_\perp}{\rho^2+\rho_\perp^2}\sin\phi \tag{3.23}$$

$$\Delta \aleph_z = -2\aleph \frac{\rho_\perp^2}{\rho^2+\rho^2_\perp} \tag{3.24}$$

To eliminate the contribution of high-angle scatters, the integrals for w_i and the w_{ij} are performed beginning from a minimum distance

$\rho_{min} = 2\rho_{\perp}$. To avoid divergences, the upper limit is set at a ρ_{max} equal to the Debye length. It is found that (Trubnikov, 1965)

$$w_i = -\left(1 + \frac{m_\alpha}{m_\beta}\right)\left(\frac{4\pi e_\alpha e_\beta}{m_\alpha}\right)^2 \ln(\lambda)\ \frac{\aleph_i}{4\pi \aleph^3} \tag{3.25}$$

(inside of ln(λ), the relative velocity has been replaced with a suitable function of temperature) and

$$w_{ij} = \left(\delta_{ij} - \frac{\aleph_i \aleph_j}{\aleph^2}\right)\left(\frac{4\pi e_\alpha e_\beta}{m_\alpha}\right)^2 \ln(\lambda)\ \frac{1}{4\pi \aleph} \tag{3.26}$$

where w_{zz} is taken to be zero since the integral contained in it converges for an infinite upper limit in ρ. Finally, then, by using the relations $\frac{\partial}{\partial \upsilon_i}\left(\frac{1}{\aleph_i}\right) = \aleph_i / \aleph^3$ and $\frac{\partial^2}{\partial \upsilon_i \partial \upsilon_j}|\underline{\aleph}| = \delta_{ij}/\aleph - (\aleph_i \aleph_j)/\aleph^3$, the following expressions for $<\Delta\upsilon_i>^{\alpha/\beta}$ and $<\Delta\upsilon_i\Delta\upsilon_j>^{\alpha/\beta}$ are generated:

$$<\Delta\upsilon_i>^{\alpha/\beta} = -(1 + m_\alpha/m_\beta)\, L^{\alpha/\beta} \frac{\partial}{\partial \upsilon_i} \varphi_\beta(\underline{\upsilon}) \tag{3.27}$$

$$<\Delta\upsilon_i\Delta\upsilon_j>^{\alpha/\beta} = -2L^{\alpha/\beta} \frac{\partial^2}{\partial \upsilon_i \partial \upsilon_j} \psi_\beta(\underline{\upsilon}) \tag{3.28}$$

where

$$L^{\alpha/\beta} = ((4\pi e_\alpha e_\beta)/m_\alpha)^2 \ln(\lambda) \tag{3.29}$$

and

$$\psi_\beta(\underline{v}) = -\frac{1}{8\pi}\int d\underline{v}' |\underline{v} - \underline{v}'| f_\beta(\underline{v}') \tag{3.30}$$

and

$$\varphi_\beta(\underline{v}) = -\frac{1}{4\pi}\int d\underline{v}' \frac{f_\beta(\underline{v}')}{|\underline{v} - \underline{v}'|} \tag{3.31}$$

where $f_\beta(\underline{v})$ is the distribution function for particles of species β. The functions ψ and φ are known as the Trubnikov potentials. They are, mathematically, apart from constant factors, terms in the series for the well-known Rosenbluth potentials (Trubnikov, 1965). The diffusion tensor in velocity space and the coefficient of dynamic friction for α particles in a medium of β particles can be written in terms of the Trubnikov potentials as

$$D_{ik}^{\alpha/\beta} = -L^{\alpha/\beta}\frac{\partial^2 \psi_\beta}{\partial v_i \partial v_k} \tag{3.32}$$

and

$$\frac{F_i^{\alpha/\beta}}{m_\alpha} = -\frac{m_\alpha}{m_\beta} L^{\alpha/\beta}\frac{\partial \varphi_\beta}{\partial v_i} \tag{3.33}$$

Note also that $\nabla_v^2 \psi = \varphi$.

It is instructive to calculate the Trubnikov potential ψ and the diffusion coefficients $D_{xx}^{\alpha/\beta}$ and $D_{yy}^{\alpha/\beta}$ for the case where there is only one target species β present, which has a Maxwellian distribution function $f_\beta(\underline{v})$, in the coordinate system where the mean β velocity is zero.

$$f_\beta(\underline{v}) = n_\beta\left(\frac{m_\beta}{2\pi T_\beta}\right)^{1/2}\exp(-\chi_\beta^2) = n_\beta\left(\frac{m_\beta}{2\pi T_\beta}\right)^{1/2} f^\circ(\chi_\beta) \tag{3.34}$$

Here, $\underline{\chi}_\beta = (m_\beta/(2T_\beta))^{1/2}\underline{v}$ as in Chapter II. Then

$$f^\circ(\chi_\beta) = \frac{1}{2\pi}\frac{d}{d\chi_\beta}\Phi(\chi_\beta) \equiv \frac{1}{2\pi}\Phi'(\chi_\beta) \tag{3.35}$$

Φ is here, as in Chapter II, the error function, defined by Eq (2.19). Equation (3.30) will be transformed in a similar way prior to integration:

$$\psi_\beta(\underline{v}) = -\frac{1}{8\pi}\int d\underline{v}'|\underline{v}-\underline{v}'|f_\beta(\underline{v}') = n_\beta\left(\frac{2T_\beta}{m_\beta}\right)^{1/2}\psi^\circ(\chi_\beta) \tag{3.36}$$

where

$$\psi^\circ(\chi) = -\frac{1}{8\pi}\int d\underline{\chi}'|\underline{\chi}-\underline{\chi}'|f^\circ(\chi') \tag{3.37}$$

When this integral (Eq (3.37)) is performed, it is found that

$$\psi^\circ(\chi) = -\frac{1}{16\pi}\left[\Phi'(\chi) + (2\chi + 1/\chi)\Phi(\chi)\right] \tag{3.38}$$

In order to calculate $D_{ik}^{\alpha/\beta}$, it is necessary to evaluate

$$D_{ik}^{\alpha/\beta} = -L^{\alpha/\beta}\frac{\partial^2}{\partial v_i \partial v_k}\psi_\beta\Big|_{\chi=\chi_\beta} = -L^{\alpha/\beta}\left(\frac{m_\beta}{2T_\beta}\right)^{1/2}\frac{\partial^2}{\partial v_i \partial v_k}\psi^\circ\Big|_{\chi=\chi_\beta} \tag{3.39}$$

In a straightforward manner this yields

$$D_{ik}^{\alpha/\beta} = -L^{\alpha/\beta}\left(\frac{m_\beta}{2T_\beta}\right)^{1/2}\left[\delta_{ik}\frac{1}{\chi}\frac{d}{d\chi}\psi^\circ + \frac{\chi_i\chi_k}{\chi^2}\left(\frac{d}{d\chi^2}\psi^\circ - \frac{1}{\chi}\frac{d}{d\chi}\psi^\circ\right)\right] \tag{3.40}$$

This is simple to evaluate when the coordinate system is chosen properly. Taking the z axis parallel to $\underset{\sim}{\chi}$, then $D_{ik}^{\alpha/\beta}$ will be diagonal. In that coordinate system, $\chi_i = 0$ unless $i = 3$, and $\chi_i\chi_k = 0$ unless $\chi_i\chi_k = \chi_3^2 = \chi^2$. Hence,

$$D_{xx}^{\alpha/\beta} = D_{yy}^{\alpha/\beta} = -L^{\alpha/\beta} n_\beta \left(\frac{m_\beta}{2T_\beta}\right)^{1/2} \frac{1}{\chi}\frac{d}{d\chi}\psi^\circ\Big|_{\chi=\chi_\beta} \tag{3.41}$$

And employing Eq (3.38) it is found that

$$\frac{1}{\chi}\frac{d}{d\chi}\psi^\circ = \frac{-1}{8\pi\chi}\left(\Phi(\chi) - \frac{\Phi(\chi) - \chi\Phi'(\chi)}{2\chi^2}\right) = -\frac{1}{8\pi}\left(\frac{\Phi(\chi) - G(\chi)}{\chi}\right) \tag{3.42}$$

an expression very similar to Eq (2.17), the term Holmes employed for the electron-ion collision frequency before averaging over the test particle distribution function. And this is, of course, exactly what is expected, since Holmes takes for ν_c, $1/\upsilon^2$ times Spitzer's $<(\Delta w_\perp)^2>$, which is equivalent of $<(\Delta\upsilon_x)^2> + <(\Delta\upsilon_y)^2>$. Hence, Holmes' ν_c is actually $D_{xx}^{\alpha/\beta}/\upsilon^2$. But the question remains of whether his is a legitimate approach to calculating the transport of electrons across a magnetic field.

For completeness, the diffusion coefficient $D_{zz}^{\alpha/\beta}$ is written

$$D_{zz}^{\alpha/\beta} = L^{\alpha/\beta} n_\beta \frac{G(\chi_\beta)}{4\pi\upsilon} \tag{3.43}$$

Since $\nabla_\upsilon^2\psi_\beta = \varphi_\beta$,

$$\varphi_\beta(\underset{\sim}{\upsilon}) = -n_\beta \frac{\Phi(\chi_\beta)}{4\pi\upsilon} \tag{3.44}$$

and the force of dynamic friction can be written, from Eqs (3.33) and (3.44) as

$$\frac{1}{m_\alpha}F_i^{\alpha/\beta} = \frac{m_\alpha}{m_\beta}L^{\alpha/\beta}\left(\frac{m_\beta}{2T_\beta}\right)\frac{n_\beta}{2\pi}\frac{\upsilon_i}{\upsilon}G(\chi_\beta) \tag{3.45}$$

This is as far as Trubnikov goes in his presentation. But it is possible to write the diffusion coefficient in velocity space as

$$D_{ij}^{\alpha/\beta} = \frac{n_\beta L^{\alpha/\beta}}{8\pi\upsilon^3}\{\Phi A_{ij} + GB_{ij}\} \tag{3.46}$$

where

$$A_{ij} = \delta_{ij}\upsilon^2 - \upsilon_i\upsilon_j \tag{3.47}$$

$$B_{ij} = 3\upsilon_i\upsilon_j - \delta_{ij}\upsilon^2 \tag{3.48}$$

Next, the collision integral $-\nabla\cdot\underset{\sim}{j}^{\alpha/\beta}$ will be written:

$$-\nabla\cdot\underset{\sim}{j}^{\alpha/\beta} = \frac{n_\beta L^{\alpha/\beta}}{8\pi}\frac{\partial}{\partial\upsilon_i}\{\frac{2m_\alpha}{T_\beta}\frac{\upsilon_i}{\upsilon}Gf_\alpha + \left(\frac{\Phi A_{ij} + GB_{ij}}{\upsilon^3}\right)\frac{\partial f_\alpha}{\partial\upsilon_j}\} \tag{3.49}$$

Incidentally, this result reduces to Braginskii's collision integral (Braginskii, 1965: 239) in the limit of $\chi_\beta >> 1$. In that limit, $\Phi \to 1$ and $G \to 1/(2\chi^2)$.

In summary, Trubnikov's derivation of the Fokker-Planck equation has been presented and the conditions of its applicability have been stated. The equation should apply to the electrons in the plasma, but

not to the positive ions. The Trubnikov potential derivation was presented, and the Trubnikov potentials were employed to deliver the Fokker-Planck collision term for any species α in a medium of Maxwellian β particles in the frame of reference where the directed velocity of the β particles is zero.

A moments approach (based on the work of Grad (Grad, 1949; Golant, 1980)) to obtaining an expression for the electron flux will be highlighted; but first a short digression to consider the (position space) diffusion coefficient as given by the mean square displacement per unit time. This consideration of the particle's mean square displacement upon collisions will make it plain why Holmes' appropriation of $D_{xx}^{\alpha/\beta}/\upsilon^2$ for the collision frequency before averaging is incorrect.

Excursus on the Mean Square Displacement

The vector $\underline{\rho}_b = \underline{b} \times \underline{\upsilon}/\omega$ is directed from the center of the Lamor circle to the particle position. The vector $\underline{b}$ is a unit vector in the direction of the magnetic field $\underline{B}$, here taken along the z axis, $\underline{\upsilon}$ is the particle velocity, and ω is the cyclotron frequency. Upon a collision, the Lamor center, with position given by $\underline{r}$, is moved a distance given by

$$\Delta \underline{r} = -\Delta \underline{\rho} = \underline{b} \times \Delta \underline{\upsilon}/\omega \qquad (3.50)$$

(see Figure 3-1).

Here, the motion of particles in the x direction is investigated. The change in the Lamor center position along x is

$$\Delta x = -(\Delta \underset{\sim}{\rho}_b)_x = (\Delta v_y)/\omega \tag{3.51}$$

It can be shown, in much the same way as in the derivation of the Fokker-Planck equation, that the flux Γ_x of charged particles is given by

$$\Gamma_x = n\langle \Delta x \rangle - \frac{1}{2}\frac{\partial}{\partial x}[n\langle (\Delta x)^2 \rangle] \tag{3.52}$$

for small $\Delta x/\Delta t$, where here, as in the previous section, $\langle \Delta x \rangle$ is $\overline{\Delta x}/(\Delta t)$.

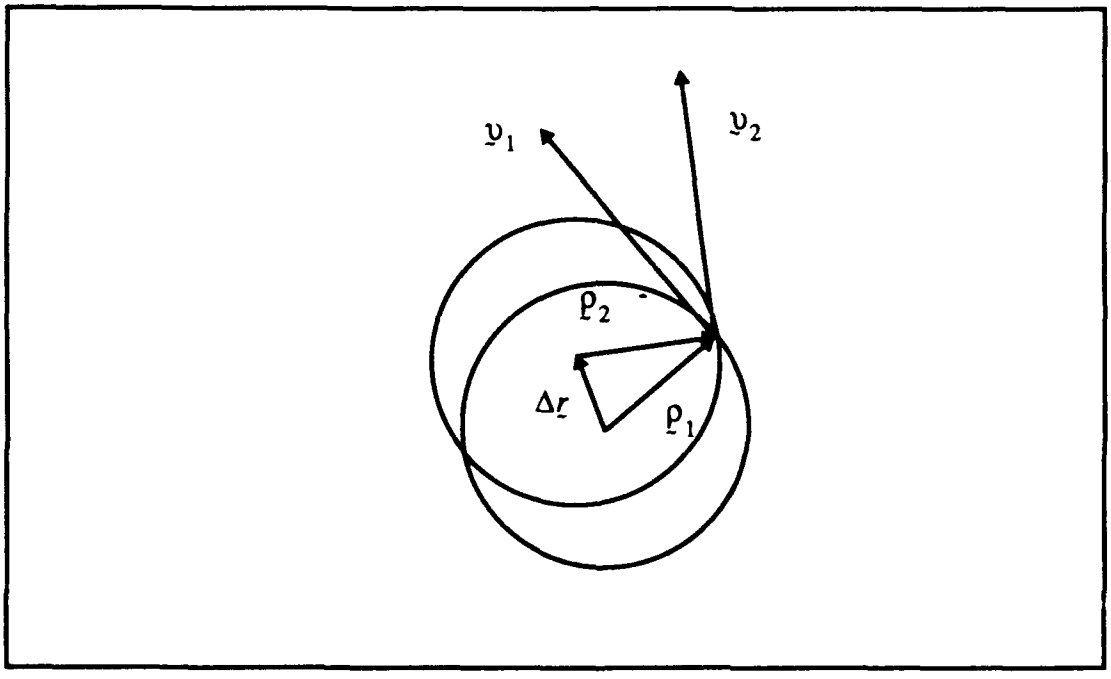

Figure 3-1: Geometry of Lamor Center Displacements

The diffusion coefficient is

$$D = \frac{1}{2}\langle (\Delta x)^2 \rangle = \frac{1}{2}\frac{\langle (\Delta v_y)^2 \rangle}{\omega^2} \tag{3.53}$$

It is tempting to substitute here $D_{yy}^{\alpha/\beta}$ from Eq (3.41) into Eq (3.53)

as Holmes has done (Holmes, 1982b). However, the coordinate system here is different from the one employed earlier. That system was tied to the particle velocity, with z along the direction of motion for each α particle individually. The coordinate system here is the same for all particles. For random collisions, it is expected therefore that

$$<(\Delta v_y)^2> = \frac{1}{3}<(\Delta v)^2> = \frac{2}{3}\{D_{xx}^{\alpha/\beta} + D_{yy}^{\alpha/\beta} + D_{zz}^{\alpha/\beta}\} \tag{3.54}$$

So the diffusion coefficient, before averaging over the α particle distribution function, is

$$D = \frac{1}{3}\{D_{xx}^{\alpha/\beta} + D_{yy}^{\alpha/\beta} + D_{zz}^{\alpha/\beta}\}\frac{1}{\omega^2} = \frac{1}{3}\{n_\beta L^{\alpha/\beta}\frac{\Phi}{4\pi v}\}\frac{1}{\omega^2} \tag{3.55}$$

(Compare with Eqs (2.16) and (2.17). Holmes is averaging a function of $1/v^3$, which makes a larger contribution at small v than the function of $1/v$ given in Eq (3.55).) The average diffusion coefficient is then

$$\langle D\rangle = \frac{4\pi}{3}\left(\frac{m_\alpha}{2\pi T_\alpha}\right)^{3/2}\int_0^\infty dv v^2\left\{\frac{n_\beta L^{\alpha/\beta}\Phi(\chi_\beta)}{4\pi v}\right\}\frac{1}{\omega^2}\exp\left(\frac{-m_\alpha v^2}{2T_\alpha}\right) \tag{3.56}$$

Since $\Phi(\chi_\beta) \approx 1$ except for extremely small v ($v^2 < 2T_b/m_b$) (assuming here that the β particles are heavy ions), the result is

$$\langle D\rangle = \frac{\nu_{\alpha\beta}T_\alpha}{m_\alpha\omega^2} \tag{3.57}$$

with $\nu_{\alpha\beta}$ given by Eq (2.24) with $\alpha = e$ and $\beta = I$. That is, this approach yields the classical diffusion coefficient.

One can also employ this method to estimate the effect of the change in the magnetic field strength through the filter on the electron motion. That is, since B is not a constant, $\Delta x \approx (\Delta \upsilon_y)/\omega - (\upsilon_y \Delta\omega)/\omega^2$. Since $\Delta\omega \approx \frac{d\omega}{dx}\Delta x$, then

$$\Delta x \cong \frac{\Delta \upsilon_y}{\omega}\left(1 + \frac{\upsilon_y}{\omega^2}\frac{d\omega}{dx}\right)^{-1} \tag{3.58}$$

In the magnetic filter, υ_y is about 10^7 cm sec^{-1} and ω is about 10^9 sec^{-1} with $d\omega/dx$ at most $10^9/2$ cm^{-1} sec^{-1} . This term is very small for that region (strong B) where this discussion makes sense.

In summary, it is clear that Holmes' choice of ν_c as $D_{xx}^{\alpha/\beta}/\upsilon^2$ is incorrect. In addition, it is inappropriate to assume the functional form given by Eq (2.16) and then average over the particle distribution function. The mean square displacement approach results in that functional form, but only after averaging is done. The momentum balance equation for electrons, presented in the next section, may also be used to generate the classical diffusion coefficient, Eq (3.57), in agreement with the mean square displacement approach.

Moments and the Grad Method

In the moments approach an attempt is being made to eliminate the distribution function f_α from the Boltzmann equation (Eq (3.1)) entirely in favor of density, temperature, *etc.* Classical transport equations are obtained by multiplying the Boltzmann equation by 1, momentum, and kinetic energy, *etc.*, respectively, then integrating over velocity. The resulting hydrodynamic equations can be solved for the number density,

temperature, and average velocity at a point provided quantities such as the energy flux, heat flux, viscosity, and force of friction can be related to the temperature, density, and velocity at the same point. The classical transport equations are thus an approximate solution to the Boltzmann equation (Braginskii, 1965: 212). Physically, the approximation asserts that the rate of change of hydrodynamic quantities must depend upon their local values. But this dependence is implausible if particles move substantial distances in short periods of time (Clemmow, 1969). Thus, the Boltzmann moments approach is applicable for the description of classical transport processes when the plasma is collision dominated. That is, the mean free paths must be much shorter than the characteristic length of gradients in temperature or density, *etc.*, in the direction of the magnetic field, and either the mean free path or gyroradius must be much shorter that the characteristic length of gradients in directions perpendicular to the magnetic field (Hinton, 1983). For positive ions in the filter region these conditions are not satisfied, since the ion gyroradius is usually about as wide as the filter field itself, through which the plasma density falls abruptly. For electrons, however, these conditions are plainly met for the direction perpendicular to the filter field. They are also met in the direction along the filter field: in the region near the center line of the plasma, gradients are low (Bacal, 1984: 21). Away from the center line of the plasma, electron motion is restricted by magnetic fields. The Boltzmann moments approach is thus applicable to electron motion both perpendicular to and along the filter field.

The equation most suitable for describing the transport of electrons is the momentum moment of the Boltzmann equation. The momentum

moment is obtained by multiplying the Boltzmann equation by a component of the electron velocity, v_k , and integrating over all velocities. The details of integration and manipulation can be found in many sources (Golant, 1980; Schkarovsky, 1966, *etc.*). The resulting equation can be written as follows:

$$mn\left[\frac{\partial \underline{u}}{\partial t} + (\underline{u}\cdot\nabla)\,\underline{u}\right] = Zen\underline{E} + Znm\omega\,[\underline{u}\times\underline{b}] - \nabla p - (\nabla\cdot\hat{\pi}) + m\frac{\delta(n\underline{u})}{\delta t} \qquad (3.59)$$

For electrons, Z = -1. The variable ω is the electron cyclotron frequency; $\underline{u}$ is the directed velocity defined by

$$\underline{u} = \int d\underline{v}\,\underline{v} f(\underline{v}) = \bar{\underline{v}} \qquad (3.60)$$

The scalar pressure p is defined by $\frac{1}{3}nm\overline{c^2}$. The tensor π_{ij}, called the viscous stress tensor, is defined by $\pi_{ij} = nm\,(c_i c_j - \frac{1}{3}c^2\delta_{ij})$. The vector $\underline{c}$ is defined by the equation $\underline{v} = \underline{u} + \underline{c}$; $\underline{c}$ is the known as the random or peculiar velocity. Equation (3.59) will be simplified following an analysis of the relative size of terms and the elimination of small terms. But first it must be established that the distribution function is nearly Maxwellian: that the random velocity is large in comparison with the directed velocity in the filter field region.

Grad's method for solving Eq (3.59) for the flux capitalizes on the smallness of the directed velocity $\underline{u}$ of the charged particles in comparison with the random velocity. In Chapter II, in the discussion of Leung and Bacal's experiment (Leung. 1984b), it was estimated that the final chamber flux was given by $\Gamma_x = \frac{1}{4}n_2\bar{v}\xi$, with $\xi = 0.8$. Therefore,

the average magnitude of the directed velocity $\underline{u}$ is $u \approx 0.2c$, for the average c. In Chapter IV it will be argued that in addition to electrostatic shielding at the plasma electrode, the magnetic field may decrease the thermal flux by an additional factor of 0.1, so that the directed velocity is actually on the order of $c/50$.

The directed velocity is also small in comparison with the average thermal velocity in Holmes' experiment (Holmes, 1982b). By calculating Holmes' source chamber plasma density from Eq (2.32) by using his measured Γ_x , and by writing $\Gamma_x = n_1 u_1$, u_1 can be found. Then, considering that $\Gamma_x = n_2 u_2$, the rise in u through the magnetic filter can be estimated by assuming a reasonable value for n_2 .

From Figure 2-6 it is apparent that the characteristic width a of Holmes' filter field is about 1.5 cm. Employing this value in Eq (2.32), with an electron flux of 3×10^{16} cm^{-2} sec^{-1} at a magnetic flux equal to 300 gauss cm, the source chamber electron number density is $n_1 = 4 \times 10^{11}$ cm^{-3} . Since the total flux (1 ampere to an effective area of 197 cm^2) is only 3×10^{16} cm^{-2} sec^{-1}, the directed velocity is about 8×10^4 cm sec^{-1}. If the electron density falls by a factor of 10, as it did in Leung and Bacal's experiment (Figure 2-2), the final chamber density is 4×10^{10} cm^{-3} and the directed velocity rises to 8×10^5 cm sec^{-1}. The average velocity of electrons is about 7×10^7 cm sec^{-1}, so the thermal velocity is high with respect to the directed velocity, at least through the filter.

On the basis of this calculation, then, it is surmized that the Grad method of computing the collision term to the momentum equation (or to any other moment of the Boltzmann equation) should apply.

To simplify Eq (3.59), note first that the term $\frac{\delta n_e \underline{u}}{\delta t}$ is roughly equal to $-m_e \nu_{el} n_e (\underline{u}_e - \underline{u}_I)$ plus terms of comparable magnitude, as shall be demonstrated shortly. (Incidentally, ν_{el} is given by Eq (2.24).) All smaller terms can be set to zero. For large electron fluxes, this collision term can be approximately 10^{-4} dynes/cm^3. The pressure term is on the order of 10^{-2} dynes/cm^3. The electric field term is perhaps an order of magnitude lower than the pressure term, and the magnetic field term is comparable to the pressure term.

The hydrodynamic acceleration, the left-hand side of Eq (3.59), is about 10^{-6} dynes/cm^3. So this term can be ignored. The divergence of the stress tensor, $\nabla \cdot \hat{\pi}$, is another term involving the directed velocity. The largest terms in π_{ij} , for strong magnetic fields, are of the form

$$0.73 \frac{n_e T_e}{\nu_{el}} W_{ij} \quad . \tag{3.61}$$

where

$$W_{ij} = \frac{\partial u_i}{\partial x_j} + \frac{\partial u_j}{\partial x_i} - \frac{2}{3} \delta_{ij} (\nabla \cdot \underline{u}) \tag{3.62}$$

For large magnetic fields, only the diagonal terms are appreciable (Braginskii, 1965). The only significant component of the electron directed velocity is along the x axis. Hence,

$$W_{xx} \approx \frac{4}{3} \frac{\partial u_x}{\partial x} \quad , \quad W_{yy} = W_{zz} = -\frac{2}{3} \frac{\partial u_x}{\partial x} \tag{3.63}$$

The derivatives of π_{ij} with respect to y and z are practically zero, so

the only non-zero viscous stress term in Eq (3.59) is $\frac{\partial \pi_{xx}}{\partial x}$. This term is of the same order of magnitude as the collision term.

In order to apply the Grad method to Eq (3.59), an expression must be found for $\frac{\delta (n_e \underline{u})}{\delta t}$. Initially, it will be assumed that only Coulomb collisions are important. Elastic collisions with neutrals and inelastic collisions will be taken up later in the chapter. Taking the velocity moment of the right-hand side of the Boltzmann equation,

$$\frac{\delta (n_e u_k)}{\delta t} = \int d\underline{v} v_k \left(\frac{\delta f_e}{\delta t}\right) \tag{3.64}$$

where f_e is the electron distribution function. Substituting the expression for $\frac{\delta f_e}{\delta t}$ from Eq (3.10) and integrating by parts,

$$\frac{\delta (n_e u_k)}{\delta t} = -\int d\underline{v} \left\{ <\Delta v_k>^{e/I} f_e - \frac{1}{2} \frac{\partial}{\partial v_j} (<\Delta v_k \Delta v_j>^{e/I} f_e) \right\} \tag{3.65}$$

where the symbol I indicates a species of ion. The second term in Eq (3.65) integrates to zero since $<\Delta v_k \Delta v_j>^{e/I} f_e$ goes to zero on the surface at infinity. Substituting an expression for $<\Delta v_k>^{e/I}$ from Eq (3.27) together with Eq (3.44), Eq (3.65) becomes

$$\frac{\delta (n_e u_k)}{\delta t} = -\left(1 + \frac{m_e}{m_I}\right) L^{e/I} \left(\frac{n_I}{4\pi}\right) \frac{m_I}{T_I} \int d\underline{v} \left(\frac{v_k}{v}\right) G(\chi_I) f_e \tag{3.66}$$

As in the integration of Eq (3.56), $\Phi \approx 1$ except for very small v, so $G(\chi_I) \approx 1/(2\chi_I^2)$ is a good approximation to G for $v > ((2T_I)/m_I)^{1/2}$. For velocities smaller than this, the leading power of χ in G is χ^1. This can be seen by examining the series for Φ in Eq (2.27). So there

is no large contribution to the integrand at small velocities and it can be safely assumed that

$$\frac{\delta(n_e u_k)}{\delta t} = -\left(1+\frac{m_e}{m_I}\right) L^{e/I} \frac{n_I}{4\pi} \int d\underline{\upsilon} \frac{\upsilon_k}{\upsilon^3} f_e \tag{3.67}$$

In the Grad method, the distribution function is expanded in a series whose coefficients involve moments such as n, T, u_k, *etc.*:

$$f = n\left(\frac{m}{2\pi T}\right)^{3/2} exp\left(-\frac{mc^2}{2T}\right)\left[1 - \sum_k q_k \frac{mc_k}{nT^2}\left(1-\frac{mc^2}{5T}\right)\right] \tag{3.68}$$

(Golant, 1980: 164), where $\underline{q}$ is the heat flux vector defined by $q_k = \frac{1}{2} m \overline{c^2 c_k}$. This expansion is a special case of a more general expansion which includes terms linear in elements of the viscosity tensor. However, from the mathematical form of the expansion (not shown here), it is plain that the non-zero (diagonal) elements of the viscosity tensor are coefficients of terms that will integrate to zero in Eq (3.67).

By expanding the integrand of Eq (3.67) in a Taylor series about $\upsilon_k = c_k$, it can be shown that

$$\frac{\delta(n_e \underline{u})}{\delta t} = -\nu_{eI} n_e (\underline{u} - \underline{u}_I) + \frac{3}{5}\frac{\nu_{eI}}{T_e}\underline{q}_e \tag{3.69}$$

(Golant, 1980) where ν_{eI} is given by Eq (1.26) and u_I is the directed velocity of the species of ions. It remains to substitute into Eq (3.69) an expression for the heat flux. For conditions where the energy of directed motion is much less than the energy of random motion, the heat flux moment equation is

$$\frac{5}{2}\frac{n_e T_e}{m_e}\nabla T_e + \omega_e \underline{q}_e \times \underline{b} = -1.87\nu_{el}\underline{q}_e + \frac{3}{2} n_e T_e \nu_{el}(\underline{u} - \underline{u}_I) \tag{3.70}$$

Then, solving for $\underline{q}_e$

$$\underline{q}_e = -\frac{1}{\omega_e}\underline{b} \times \frac{5}{2}\frac{n_e T_e}{m_e}\nabla T_e \tag{3.71}$$

where only the largest term, comparable to the first term on the left-hand side of Eq (3.69), has been retained. (Of course, a larger term exists, but it is in the direction of the magnetic field. The interest here is in transverse directions.)

For electrons, then, Eq (3.59) may be written as

$$en_e\underline{E} + n_e m_e \omega_e \underline{u} \times \underline{b} + \nabla p_e + \nabla \cdot \hat{\pi} + m_e n_e \nu_{el}(\underline{u} - \underline{u}_I) \tag{3.72}$$

$$+\frac{3}{2}\frac{\nu_{el}}{\omega_e}\underline{b} \times \frac{n_e}{m_e}\nabla T_e = 0$$

where all the vectors (except $\underline{b}$) are in a plane perpendicular to $\underline{b}$. In the case where a similar equation can be written for the ion momentum balance, separate equations for $\underline{u}_e$ and $\underline{u}_I$ may be derived. Here, however, that is impossible; but Eq (3.72) can be written in a form which brings out the functional form of the flux in the x (source chamber to extraction chamber) direction. Eliminating $\underline{u} \times \underline{b}$ in the usual way (by first taking the cross product of Eq (3.72) with the unit vector in the direction of the magnetic induction, hence producing a second equation involving $\underline{u} \times \underline{b}$), it is found that

$$-m_e n_e (\omega_e^2 + \nu_{el}^2) u_x = e n_e \nu_{el} E_x + \nu_{el} \frac{dp_e}{dx} + \nu_{el} \frac{d\pi_{xx}}{dx} - \frac{3}{2} \nu_{el} n_e \frac{dT_e}{dx} - m_e n_e \nu_{el}^2 u_{I_x} \quad (3.73)$$

$$+ m_e n_e \nu_{el} \omega_e (\underline{u}_I \times \underline{b})_x$$

It is difficult to assign a value to the last term in Eq (3.73) since a fluid momentum equation for the ions cannot be written. Since collisions occur infrequently for positive ions, it is expected that they will drift with a velocity approximately equal to

$$\underline{u}_I^d = \frac{e}{m_e \omega_e} (\underline{E} \times \underline{b})$$

(the usual $\underline{E} \times \underline{B}$ drift velocity). But as only a fraction of the ions are trapped within the filter field, the last term in Eq (3.73) can be approximated as

$$(g - 1) e n_e \nu_{el} E_x$$

with g a positive factor less than 1. When g is 1, no ions are trapped in the filter field; and when g is zero, all are.

Braginskii (Braginskii, 1965: 218) shows that

$$\pi_{xx} = -\frac{0.73}{3} \frac{n_e T_e}{\nu_{el}} \frac{\partial u_x}{\partial x} \quad (3.74)$$

This can be written, under the assumption of constant flux, as

$$\pi_{xx} = \frac{0.73}{3} \frac{T_e}{\nu_{el}} n_e u_x \frac{1}{n_e} \frac{dn_e}{dx} \quad (3.75)$$

Finally, then, the equation for the electron flux is

$$\Gamma_x = -\frac{\nu_{el}}{m_e\left(\omega_e^2+\nu_{el}^2-0.24\frac{\nu_{el}}{m_e}\frac{d}{dx}\left(\frac{T_e}{\nu_{el}}\frac{d}{dx}ln\,(n_e)\right)\right)}\times\left(geE_x+\frac{dp_e}{dx}-\frac{3}{2}n_e\frac{dT_e}{dx}\right. \quad (3.76)$$

$$\left.-m_e\nu_{el}\frac{n_e}{n_I}\Gamma_{I_x}\right)$$

where Γ_{I_x} is the ion flux in the x direction. As the ion flux is not likely to exceed 10^{16} cm^{-2} sec^{-1} (using Bohm's estimate of

$$\Gamma_{I_x} = n_I\left(\frac{T_e}{m_I}\right)^{1/2}\exp\left(-\frac{1}{2}\right) \quad (3.77)$$

for the flux to the extraction electrode (Bohm, 1949)), the last term on the right-hand side of Eq (3.76) is extremely small in comparison to the electric field and gradient terms. The term from the stress tensor in the denominator is at least 5 orders of magnitude smaller than ω_e^2 at high magnetic inductions, so this term can also be ignored. The electron flux should then be given by

$$\Gamma_x = -\frac{\nu_{el}}{m_e(\omega_e^2+\nu_{el}^2)}\left(geE_x+\frac{dp_e}{dx}-\frac{3}{2}n_e\frac{dT_e}{dx}\right) \quad (3.78)$$

summed over all ion species. This is essentially Eq (2.1), written under the assumption of negligible electric field and small temperature gradients, both of which, it is apparent from Eq (3.78), act to slow the electron flux through the filter.

The effects of electron-electron collisions on the electron flux have not been considered in the foregoing discussion. Shkarofsky (Shkarofsky,

1966: 288) shows that the velocity moment of like particle collision integrals is zero to first order. Therefore, there can be no sizeable contribution from electron-electron collisions. (To the extent that further terms in Eqs (3.9) and (3.10) can be ignored, electron-electron collisions can be disregarded.)

As noted in Chapter I, the mean free path for electron-ion collisions is only a factor of 2 higher than that for electron-neutral collisions in a low pressure discharge. Hence, there is reason to expect a contribution from collisions with neutrals of the same order of magnitude as the contribution from electron-ion collisions. The electron-neutral collision frequency is about 10^6 p(mTorr)/1 mTorr sec^{-1}. The electron-ion collision frequency given by Eq (2.2) is about 3 x 10^6 sec^{-1}. Golant (Golant, 1961) derives an expression for the electron flux across a magnetic field by utilizing an expansion of the electron distribution function in Laguerre polynomials. His result, in the high magnetic field limit, and omitting ion pressure terms, is:

$$\Gamma_x = -\frac{\nu_{ea}(\nu_{ea}+\nu_{el})}{\omega_e^2}\Gamma_{I_x} - \frac{\nu_{el}+\nu_{ea}}{m_e\omega_e^2}T_e\frac{dn_e}{dx} - \left(\frac{\nu_{ea}-\frac{1}{2}\nu_{el}}{m_e\omega_e^2}\right)n_e\frac{dT_e}{dx} \qquad (3.79)$$

$$-\frac{\nu_{ea}}{m_e\omega_e^2}en_eE_x$$

This reduces to Eq (3.78) as $\nu_{ea}\rightarrow 0$ and the high ω_e limit is taken in Eq (3.78), apart from the fact that g, for Golant, must equal 0 since all ions are assumed trapped within the magnetic field. Assuming, as in Chapter II, that temperature gradients and the electric field are unimportant, Eq (3.79) can be integrated. For simplicity, assume a Gaus-

sian magnetic field of characteristic width a and integrate from negative to positive infinity. The result is

$$\Gamma_x = \frac{\sqrt{\frac{2}{\pi}}}{m_e \omega_o^2 a}\left(\frac{d}{2T_e^{1/2}}(n_1^2 - n_2^2) + \nu_{ea}(n_1 - n_2)T_e\right) \tag{3.80}$$

where ω_o is maximum electron cyclotron frequency. The second term on the right-hand side is of the same order of magnitude as the first, so the increase in flux is much less than the factor of $9\pi^{1/2}$ measured by Holmes. Using Eq (3.80) on the example given on page 2-12, the final chamber density rises from 5 x 10^7 cm^{-3} with only electron-ion collisions considered to 7 x 10^7 cm^{-3} when electron-neutral collisions are included.

To estimate the contribution of inelastic collisions, consider the relatively likely vibrational excitation of H_2 from v=0 to v=1. Given a reaction rate of 10^{-9} cm^3 sec^{-1} (Tawara, 1990) and a pressure of 1.0 mTorr with a gas temperature assumed to be 500 degrees Kelvin, the inelastic collision frequency for this process is 2 x 10^4 sec^{-1}. This is two orders of magnitude lower than the electron-neutral elastic collision frequency and so is inconsequential.

If the vibrational temperature of the neutrals were equal to the electron temperature, it is expected that the superelastic collision frequency for the v=1 to v=0 vibrational transition would approach the inelastic collision frequency given immediately above. Typically, the superelastic collision frequency will be smaller than the inelastic collision frequency. An electron which experiences a superelastic collision will have an increased Δv_y (see Eq (3.53)) due to the gain in energy. This energy gain, to-

gether with the electron's initial energy, will result in a Lamor radius of about 0.1 cm in a 35 G magnetic filter. The gain in energy is thus far too small to send the electron directly across the filter field. The energy gain required to do that is roughly 200 eV. And, because the Coulomb collision frequency speed dependence is $1/\upsilon^3$, the rate at which it experiences Coulomb collisions will decrease. Indeed, since the Coulomb diffusion coefficient varies as $\nu T \sim T^{-1/2}$, it is expected that electrons which have experienced superelastic collisions will have a relatively difficult time traversing the filter.

Drifts and Motion Along Field Lines

Neo-classical diffusion in toroidal fusion plasmas is the result of two effects: drifts which, between collisions, carry charged particles a distance large in comparison to the Lamor-radius, and the existence of trapped particles near the outer edge of the torus (Stacey, 1981; Galeev, 1968; Frieman, 1970; Rutherford, 1970a and b). The resulting diffusion coefficient varies as $1/B^2$ but is an order of magnitude or more higher than the classical counterpart. There should be no analogous trapped particle effects in the magnetic filter, but it is worthwhile to investigate drifts which could increase the electron current through the filter.

Figure 3-2 shows some of the gradient drifts and electric currents that arise near the magnetic filter. The electric field $\underline{E}$ gives rise to an $\underline{E} \times \underline{B}$ drift, discussed above in the simplification of Eq (3.73). Since this drift affects only a fraction 1-g of the ions, a secondary electric field (not shown in Figure 3-2) may be produced. The field would be

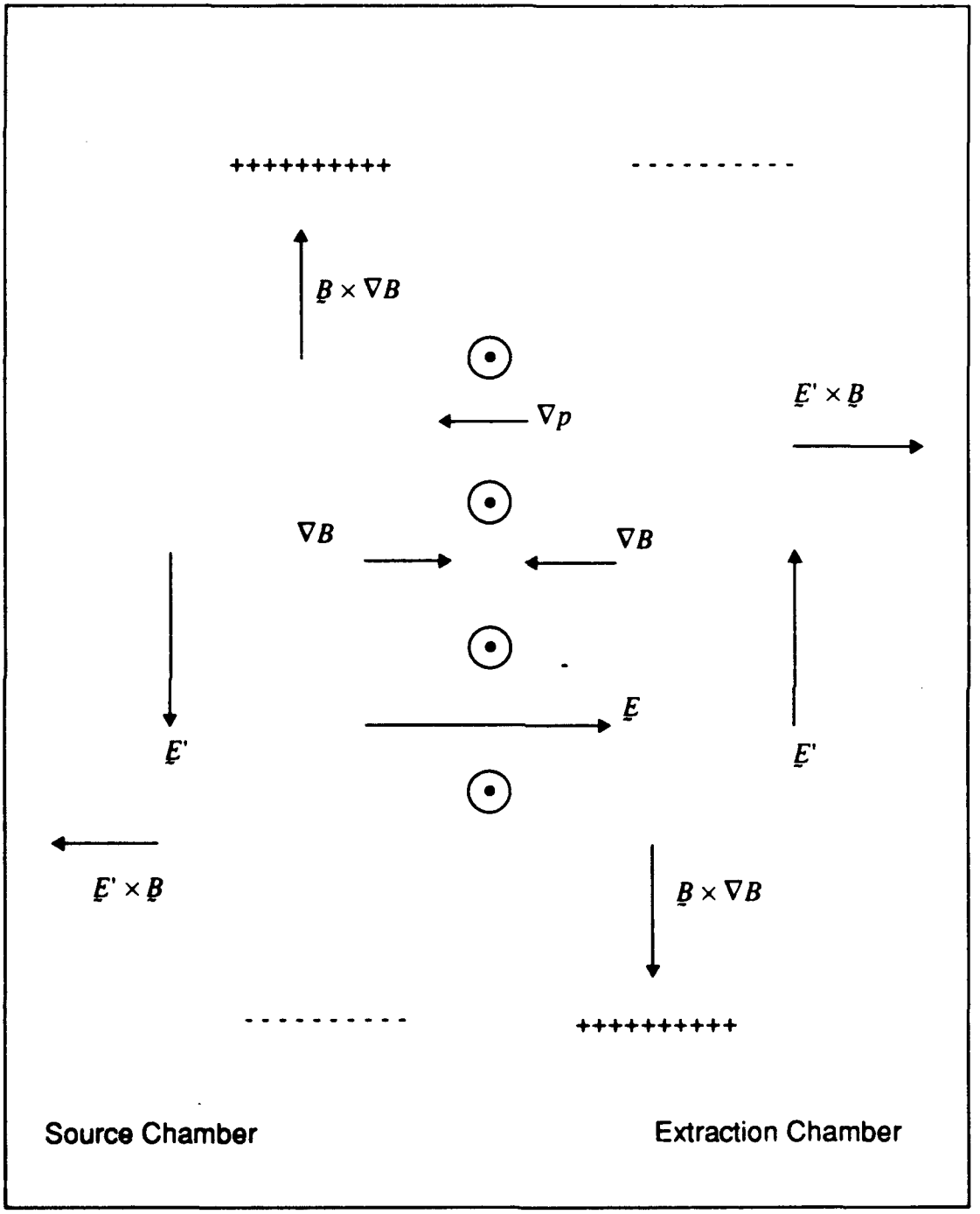

Figure 3-2: Electric Drifts and Gradient Currents Near the Magnetic Filter

directed parallel to the source chamber $\underline{E}'$ and so inhibit motion from the source chamber to the midpoint of the filter.

The gradient of B will be directed toward the filter plane. So in the source chamber, the gradient B drift will drive positive ions to the top of the page and electrons to the bottom. The resulting electric field, $\underline{E}'$, causes an electric drift (denoted by $\underline{E}' \times \underline{B}$) whose effect will be to drive electrons and positive ions back into the source chamber. In the extraction chamber, the gradient drift drives electrons to the top of the page and positive ions to the bottom. The resulting electric field causes an electric drift of charged particles into the extraction chamber. If, then, electrons can diffuse as far as the filter center line, they should receive assistance from the $\underline{E}' \times \underline{B}$ drift as they proceed farther into the extraction chamber.

There will also be a pressure gradient drift near the filter. The pressure gradient is directed from extraction to source chamber. Thus it will tend to counter the effect of the $\underline{B} \times \nabla B$ drift in the source chamber and accelerate it in the extraction chamber. Because of the comparatively rapid changes in B, it is concluded that the gradient B drift effects are more important.

The net effect of drifts in the source chamber is to oppose the motion of charged particles toward the extraction chamber. In the fluid approach taken in the previous section, the induced electric field was assumed to be zero.

Electrons may move along the magnetic field lines. In this way the mean displacement upon collisions can be very much greater than the electron Lamor radius. Any assistance received from this effect will

approach zero near the filter plane, since the curvature of the field lines also decreases. It is near the filter plane that the magnetic induction is high and an enhancement to classical diffusion is required.

The magnetic field lines between the filter magnets may be deformed by by the presence of confinement magnets on the source chamber end plate. The rippling of the field lines can also increase the mean square displacement upon collisions. However the net effect of this must be small: for an electron near the filter plane, a collision will simply carry the electron to a field line near the previous one. This field line should parallel the first, so no advantage is gained over the case where the field lines are straight.

Anomalous Diffusion

It appears, then, that classical diffusion theory cannot account for the electron flux through the filter as measured by Holmes (Holmes, 1982b). That the expression for the flux given by Eq (3.78) incorporates the generally-accepted form of the diffusion coefficient is well attested by the literature. Chandrasekhar (Chandrasekhar, 1961: 193) agrees with Eq (3.78) to within a factor of 2 in the limit of high B, no electric field or temperature gradients. (The factor of 2 comes in because these early calculations required magnetized ions in a fully ionized plasma. Under those conditions, it is well known that the diffusion is ambipolar (Golant, 1980: 311). The ambipolar diffusion coefficient is, if the electron and ion temperatures are equal, twice the coefficient given in Eq (3.78).) Chandrasekhar's result was obtained 4 years earlier by Longmire and Rosenbluth (Longmire, 1956: 509). Golant (Golant, 1980: 311) gives an

expression for the electron flux which is, in all pertinent details, identical to Eq (3.78). Braginskii (Braginskii, 1965: 249-251) also agrees with Eq (3.78), as does Hinton (Hinton, 1983: 180).

Jimbo (Jimbo, 1984) observed anomalous (Bohm scaling) diffusion in a reflex-type negative hydrogen ion source. The source was operated at a pressure of about 10 mTorr with magnetic inductions ranging from 1500 to 5000 G. The anomalous diffusion of H^- was found to enhance H^- production in the device.

Holmes' measurements (Holmes, 1982b), and those of Lea (Lea, 1990), clearly establish that the diffusion coefficient in the tandem multipole source varies with temperature, magnetic induction and plasma density as the classical diffusion coefficient. This rules out Bohm diffusion. The Bohm diffusion coefficient is written as

$$D_B = \frac{1}{16}\frac{T_e}{m_e\omega_e} \tag{3.81}$$

(Bohm, 1949). This coefficient provides the linear rise of source chamber density with magnetic induction shown in Figure 1-9, but could not reproduce the scaling with temperature and magnetic induction shown in Figures 2-7 and 2-8. Incidentally, the flux through a magnetic filter predicted by use of Eq (3.81) agrees fairly well with the value measured by Holmes (Holmes, 1982b) at 300 G cm.

In addition, there are theoretical reasons for scepticism as regards diffusion due to collective effects. For a two-dimensional plasma, the $1/B^2$ behavior of the cross-field diffusion coefficient depends upon the ratio of the change in particle position upon collision to the Debye length.

When the change in particle position upon collision is larger than a Debye length, different particles are encountered on each gyration and all encounters can be treated as independent (Okuda, 1973). A mathematical expression for this condition can be derived for a two-dimensional plasma employing quantities developed earlier in this chapter. The condition for collisional dominance of the diffusion coefficient (a classical functional form) may be written as

$$(<(\Delta x)^2>)\,\tau_c \geq \lambda_D^2 \tag{3.82}$$

where τ_c is the mean time between collisions and λ_D is the Debye length. Using Eq (3.53) for the relation between $<(\Delta x)^2>$ and $<(\Delta v_y)^2>$, and averaging, the result is

$$\left(\frac{\omega_p}{\omega_e}\right)^2 \geq 1 \tag{3.83}$$

where ω_p is the plasma frequency and ω_e is the electron cyclotron frequency. (To achieve this simple equation the electron Debye length has been employed. The condition would be more stringent had the smaller (ion) Debye length been used.) In the source chamber of a low pressure plasma, ω_p is about 10^{10} sec^{-1} and ω_e is 6×10^8 sec^{-1} in a typical filter. So

$$\left(\frac{\omega_p}{\omega_e}\right)^2 \cong 280 \tag{3.84}$$

Thus, the plasma passes the rather stringent (two dimensional) condition

for classical behaviour. Since particles in a three-dimensional plasma can move along the magnetic field lines, collective effects must be far less likely.

In Jimbo's experiment, described above, the electron density was around 10^{12} cm^{-3}, corresponding to a plasma frequency of 6×10^{10} sec^{-1}. For a magnetic induction of 1500 G, the cyclotron frequency is about 3×10^{10} sec^{-1}, and the ratio of Eq (3.83) becomes roughly 4.

In Chapter II, the results of Ferriera's experiment (Ferriera, 1989) were briefly presented. It is not clear from the data, but it is possible that the diffusion coefficient there also had Bohm scaling. The ratio of Eq (3.83) in that experiment was roughly 2.

This consideration indicates that the filter magnetic field in low power discharges is far too weak for Bohm scaling to arise. The same is doubtless true for high power discharges, where plasma densities are about an order of magnitude higher, while the filter field has approximately the same maximum induction. Could anomalous scaling with magnetic induction be observed in the source chamber across the confinement magnetic fields? The confinement fields along the anode wall are typically on the order of kilogauss. But there the fact that electrons have direct access to the anode at the cusps makes anomalous diffusion less plausible.

Weak Turbulence

Ion acoustic and related turbulence is characterized by small phase velocity $\omega/(k\upsilon_e) \ll 1$ and short wavelength $(k\upsilon_e)/\omega_e \gg 1$. The existence of an ion sound spectrum in a magnetic picket fence was verified by

Ferriera (Ferriera, 1989) under conditions of low ω_p/ω_e . This fact, along with the consideration that such spectra can be generated by electron-ion drifts, ion-ion drifts, beams and gradients (Dum, 1978b; Melrose, 1986: 229), makes ion-sound-like and related turbulence a plausible candidate explanation for the observed electron transport rates across the magnetic filter in negative hydrogen ion sources.

Anomalous diffusion of ions due to ion sound instability was treated by Spitzer as early as 1960 (Spitzer, 1960; Bernstein and Kulsrud, 1960; Hoh, 1962). In Spitzer's theory, the electric field is characterized by a phase which is a statistical function of time. Drummond and Rosenbluth parted from Spitzer in assuming that the electric field is composed of a superposition of coherent plane waves (Drummond and Rosenbluth, 1962). As a result it was seen that diffusion was due to resonance between particle and phase velocities.

Theories of turbulent plasma separate into two groups. Weak turbulence theory supposes that the turbulent spectral function $W(\underline{k})$ is composed of randomly phased plane waves (Kadomtsev, 1965). In weak turbulence theory, waves may be damped by either velocity space electron diffusion, which removes the instability's source of free energy - this is the quasilinear theory (Vedenov, 1963; Goldman, 1984) - or by wave-wave scattering and induced scattering off thermal ions (Goldman, 1984; Melrose, 1986). In strong turbulence theory, nonlinear wave structures may be used instead of plane waves as the building blocks for turbulence, or one goes beyond the usual random phase approximation to admit phase coherence and renormalization effects (Goldman, 1984).

The condition for applying weak turbulence theory is that the energy density of the turbulence W is much less than the energy density of the the particle species $n_e T_e + n_I T_I$. This condition is satisfied if 1) the free energy driving the instability is small compared with the species' thermal energy and 2) the fluctuations generated by the instability have wavelengths of the order of or less than the ion gyroradius. Relatively large fluctuation energy densities are found experimentally only at larger wavelengths (Gary, 1980). Ion acoustic turbulence is short in wavelength. It is expected that gradient-induced drift velocities in the filter magnetic field region will be small in comparison to the electron thermal velocity. Consequently, the free energy driving the instability should be small in comparison with the electron thermal energy, and weak turbulence theory should apply.

The scattering of electrons by the turbulent ion acoustic and related spectra can be treated with the Fokker-Plank equation, as was done earlier in this chapter for electron-ion collisions. The electron-wave force of dynamic friction $\underset{\sim}{F}^{e/w}$ and the velocity space diffusion tensor $D_{lm}^{e/w}$ are, of course, very different from their Coulomb counterparts. Since the electron wave force of dynamic friction, due to the spontaneous emission of ion sound waves, is only a small correction to the electron-ion force of dynamic friction $\underset{\sim}{F}^{e/w}$, it will not be considered here (Dum, 1978b). The unmagnetized quasi-linear velocity space diffusion tensor is given by

$$D_{lm}^{e/w} = \frac{8\pi^2 e^2}{m^2} \int d\underset{\sim}{k} W(\underset{\sim}{k})\, \delta(\omega_k - (\underset{\sim}{k} \cdot \underset{\sim}{v}))\, \frac{k_l k_m}{k^2} \tag{3.85}$$

where $W(\underset{\sim}{k})$ is the energy density of the turbulent spectrum in d^3k about

$\underline{k}$ and $\underline{v}$ is the electron velocity, $\underline{v} = \underline{c} + \underline{u}$, the sum of the random and directed velocities.

C. T. Dum argues that the unmagnetized form of the resonance condition may be used for weakly turbulent spectra which are sufficiently broad in $\underline{k}$ (Dum, 1978b). The wave-particle correlation time will then be short compared with the electron's gyro period.

Dum (Dum, 1978a) has carried out detailed calculations of the wave-particle transfort coefficients for electrons in ion sound and related turbulence. He has found that, provided the electron distribution function stays close to Maxwellian and the turbulence is isotropic, the effect of turbulence on electron transport is obtained by substituting enhanced values of Z, the ion charge, and T_I, the ion temperature, in the classical transport equations (Braginskii, 1967; Epperlein, 1986). What this implies for electron transport is that ion acoustic and related turbulence enhances the collision frequency appearing in the transport equations but retains the classical functional form. Thus, the ∇T term in the flux equation will act as a drag term as in Eq (3.78), even while the collision frequency ν_{ew} depends upon a positive power of T_e . (The fact that, for Coulomb collisions, the temperature gradient acts as a drag term is ascribed to the fact that $(\nu/T)\,((\partial\nu)/(\partial T))$ is negative (Golant, 1980: 285).)

(There is, of course, no guarantee that the turbulent spectrum in the magnetic filter of an H^- source, supposing that one exists, is isotropic. Lacking detailed knowledge of the spectrum, this assumption is made for simplicity. An additional complicating factor, as Dum points out (Dum, 1978b), is that the turbulence may react upon the initial Max-

wellian electron distribution so that the electron distribution function approaches an $\exp(-ac^5)$ dependence on c (a is a constant). Measurements of the electron energy distribution function have shown no profound divergence from a Maxwellian. In what follows it will be assumed that the electron distribution function is nearly Maxwellian.)

Dum's results will not be reproduced here. (Dum reduces the Fokker-Plank equation to a system of equations for an isotropic and a small anisotropic part of the electron distribution function, and computes moments from these (Dum, 1978a).) Instead, to display how the form of the of the transport equations remains Coulomb-like for ion-acoustic wave-particle transport, the Grad expansion of the electron velocity distribution function, Eq (3.68), will be used in conjunction with Eq (3.64) for the velocity moment of the collision integral, Eq (3.3) for the rate of change in the distribution function due to collisions, and Eq (3.85) above for the wave-particle velocity space diffusion tensor, to generate the collision term in the momentum moment of the Boltzmann equation, Eq (3.59). It will be shown that Eq (3.69) for $(\delta(n_e\underset{\sim}{u}))/(\delta t)$ is reproduced by the isotropic ion acoustic or related spectrum with the substitution $\nu_{el} \rightarrow \nu_{ew}$. Given this, and assuming that Eq (3.70) for $\underset{\sim}{q}_e$ is correct with $\nu_{el} \rightarrow \nu_{ew}$, Eq (3.78) with $\nu_{el} \rightarrow \nu_{ew}$ is then obviously the appropriate equation for electron flux under the influence of isotropic ion acoustic or related turbulence.

From Eq (3.64)

$$\frac{\delta(n_e u_k)}{\delta t} = \int d\underset{\sim}{v} v_k \left(\frac{\delta f_e}{\delta t}\right)_c \tag{3.86}$$

From Eq (3.3) and Eq (3.4), and considering only wave-particle interactions,

$$\left(\frac{\delta f_e}{\delta t}\right)_c = \frac{\partial}{\partial \upsilon_l} D_{lm}^{e/w} \frac{\partial f_e}{\partial \upsilon_m} \tag{3.87}$$

where the friction force has been assumed negligible. Integrating Eq (3.86) by parts,

$$\frac{\delta (n_e u_l)}{\delta t} = -\int d\underline{c} D_{lm}^{e/w} \frac{\partial f_e}{\partial \upsilon_m} \tag{3.88}$$

Now

$$\frac{\partial f_e}{\partial \upsilon_m} = \frac{\partial f_e}{\partial c_m} = -\frac{m_e}{T_e} c_m f_e + f_e^{\circ} \left[-q_m \frac{m_e}{n_e T_e^2} \left(1 - \frac{mc^2}{5T_e}\right) + \frac{2}{5} q_k \frac{m_e c_k}{n_e T_e^2} \frac{m_e}{T_e} c_m \right] \tag{3.89}$$

where $f_e^{\circ} = (m_e / (2\pi T_e))^{3/2} \exp\left[-(m_e c^2)/(2T_e)\right]$. It will turn out that, by symmetry, terms involving $c_m q_k c_k$ will integrate to zero. Eq (3.88) can then be rewritten as

$$\frac{\delta (n_e u_l)}{\delta t} = \frac{\delta (n_e u_l)^{(0)}}{\delta t} + \frac{\delta (n_e u_l)^{(1)}}{\delta t} \tag{3.90}$$

$$\frac{\delta (n_e u_l)^{(0)}}{\delta t} = \int d\underline{c} \frac{m_e}{T_e} D_{lm}^{e/w} c_m f_e^{\circ}$$

$$\frac{\delta (n_e u_l)^{(1)}}{\delta t} = \int d\underline{c} D_{lm}^{e/w} q_m \frac{m_e}{n_e T_e^2} \left(1 - \frac{m_e c^2}{5T_e}\right) f_e^{\circ}$$

By transferring the Dirac delta function in the diffusion tensor to a delta function involving the angle $\hat{k} \cdot \hat{c}$ (the angle between the vectors

$\underline{k}$ and $\underline{c}$) and the quantity $\omega^\circ = (\omega_k - (\underline{k}\cdot\underline{u}))/(kc)$ (ω_k is the frequency of the plane wave with wave vector $\underline{k}$), it is straightforward to show that

$$\frac{\delta(n_e u_l)^{(0)}}{\delta t} = \int d\underline{c}\frac{4\pi^2 e^2}{m_e^2}\int d\underline{k}W(\underline{k})\,\theta(\omega^\circ)\frac{k_l}{k^2}\frac{(\omega_k - (\underline{k}\cdot\underline{u}))}{kc}\frac{m_e}{T_e}f_e^\circ \qquad (3.91)$$

where $\theta(\omega^\circ) = 1$ for $-1 \le \omega^\circ \le 1$, 0 otherwise. Since $|\omega^\circ| \ll 1$ for ion acoustic turbulence, the condition $\theta(\omega^\circ)$ may be dropped from the integrand of Eq (3.91). If $W(\underline{k})$ is isotropic, this may be written as

$$\frac{\delta(n_e\underline{u})^{(0)}}{\delta t} = -\int d\underline{c}\frac{m_e}{T_e}f_e^\circ\frac{c^2}{3}\nu_{ew}(c)\,(\underline{u}-\underline{u}_w) \qquad (3.92)$$

where

$$\nu_{ew}(c) = \int d\underline{k}W(\underline{k})\left(\frac{4\pi^2e^2}{m^2c^3}\right)\frac{1}{k} \qquad (3.93)$$

Equations (3.92) and (3.93) together define the electron-wave collision frequency and the wave spectrum drift velocity $\underline{u}_w$. Note that the electron-wave collision frequency has the same $1/c^3$ speed dependence as the electron-ion collision frequency. Integrating Eq (3.92),

$$\frac{\delta(n_e\underline{u})^{(0)}}{\delta t} = -n_e\nu_{ew}(\underline{u}-\underline{u}_w) \qquad (3.94)$$

with

$$\nu_{ew} = \frac{4\pi}{3}(2\pi)^{1/2}\frac{e^2}{m_e^{1/2}T_e^{3/2}}\int d\underline{k}W(\underline{k})\frac{1}{k} = \frac{4\pi}{3}(2\pi)^{1/2}\frac{e^2}{m_e^{1/2}T_e^{3/2}}W\langle\frac{1}{k}\rangle = \qquad (3.95)$$

$$\frac{1}{3}\left(\frac{2}{\pi}\right)^{1/2}\pi\frac{W}{n_e T_e}\left\langle\frac{\omega_p}{k\upsilon_e}\right\rangle\omega_p$$

with υ_e being the electron thermal velocity $(T_e/m_e)^{1/2}$. Similarly,

$$\frac{\delta(n_e\underline{u})^{(1)}}{\delta t} = \frac{3}{5}\underline{q}\frac{\nu_{ew}}{T_e} \tag{3.96}$$

If, as stated earlier, the substitution $\nu_{el}\rightarrow\nu_{ew}$ holds for the collision term of the heat flux moment equation, as it should, Eq (3.78) for the flux is transformed by $\nu_{el}\rightarrow\nu_{ew}$. Compare Eq (3.69) and following.

Actually, the electron-ion and electron-wave collision frequencies can be combined into a summary collision frequency $\nu_s = \nu_{el}+\nu_{ew}$:

$$\nu_s = \frac{1}{3}\left(\frac{2}{\pi}\right)^{1/2}\left[3Z\frac{\ln(\lambda)}{\lambda}+\pi\frac{W}{nT_e}\left\langle\frac{\omega_e}{k\upsilon_e}\right\rangle\right]\omega_e = \left(\frac{2}{\pi}\right)^{1/2}Z^{\circ}\frac{\ln(\lambda)}{\lambda}\omega_e \tag{3.97}$$

where λ is given by

$$\lambda = \frac{\lambda_D}{Ze^2}3T_e \tag{3.98}$$

with $\lambda_D = (T_e/(4\pi n_e e^2))^{1/2}$, the electron Debye length.

More careful calculations by Dum (Dum, 1978a) show that if the turbulence is so weak that the electron distribution function remains essentially a Maxwellian, the effect of turbulence on the classical transport coefficients can be modelled by replacing Z and T_I with Z° and T_I° where Z° is the effective ion charge and T_I° is the effective ion temperature.

Plainly, then, the electron-ion collision frequency is enhanced by the ratio $\frac{Z^\circ}{Z}$. If it is supposed that wave-particle transport is about $9(\pi)^{1/2}$ times as effective as particle-particle transport in the filter (as was shown in Chapter 2), then $(Z^\circ)/Z$ is about $9(\pi)^{1/2}$. For this value of Z° , the transport coefficients may be well approximated by using the coefficients which correspond to $Z^\circ = \infty$ (see, for instance, Tables II, III and IV in Epperlein (Epperlein, 1986)). The coefficients which enter the expression for the flux (Eq (3.78)) are not functions of Z° .

The electron diffusion coefficient may be written as

$$\langle D \rangle = \frac{\nu_{el} + \nu_{ew}}{m_e \omega_e^2} T_e \approx \frac{\nu_{ew} T_e}{m_e \omega_e^2} \tag{3.99}$$

Although there is a formal $1/B^2$ scaling here, the actual scaling is dependent upon how $W\langle 1/k \rangle$ varies with B (see Eq (3.97)). Again, ν_{ew} varies explicitly with $T_e^{-3/2}$, but $W\langle 1/k \rangle$ may also be a function of the electron temperature. Equation (3.99) was obtained formally by Vedenov, who introduced a term describing collective electron-ion friction into the electron momentum balance equation (Vedenov, 1968: 99).

The actual dependence of ν_{ew} on T_e and B depends on the source of the instability and the damping mechanism. S. Peter Gary (Gary, 1980) has calculated the electron-wave collision frequency for the universal drift instability, which is driven by the electron diamagnetic drift, for the case where the electron distribution function stays close to Maxwellian. Attention is drawn here to this collision frequency because it is an instance where the wave-particle transport diffusion coefficient retains its $1/B^2$ behavior. Gary shows that the electron-wave cross field

diffusion coefficient for the universal drift instability is

$$\langle D \rangle = \frac{4\pi}{9} \frac{T_e^{4/3}}{m_e \omega_e^2} \left| \frac{\nabla n_e}{n_e} \right| \frac{m_i^{1/2} T_i^{1/6}}{(1 + T_i/T_e)} \tag{3.100}$$

or

$$\nu_{ew} = \frac{4\pi}{9} \frac{T_e^{1/3}}{m_e} \left| \frac{\nabla n_e}{n_e} \right| \frac{m_i^{1/2} T_i^{1/6}}{(1 + T_i/T_e)} \tag{3.101}$$

The ion temperature enters the expression because it is assumed that damping is due to wave-ion interactions. This collision frequency can easily be on the order of 10^8 sec^{-1} for typical H^- source parameters, two orders of magnitude higher than the classical electron-ion frequency.

Summary

In this chapter the transport properties of electrons across a magnetic field under the influence of collisions with either ions or ion acoustic turbulence have been examined. It has been shown that Holmes' value of the electron-ion collision frequency is high by a factor of $9\pi^{1/2}$. The wave-particle equation for the flux mimics the Coulomb (electron-ion) flux equation, and will provide a much larger flux. In Chapter IV it will be shown that the $-\nabla T_e$ drag term, common to both electron-ion and electron-wave transport, is necessary in order for the flux through the magnetic filter rise with increasing extraction electrode bias voltage with the extraction chamber thermal flux.

Chapter IV - Temperature Gradient Effects and Electron Cooling

Introduction

In Chapter III it was shown that the appropriate classical expression for the electron flux is

$$\Gamma_x = -\frac{\nu_{el}}{m_e(\omega_e^2+\nu_{el}^2)}\left(gen_eE_x+\frac{dp_e}{dx}-\frac{3}{2}n_e\frac{dT_e}{dx}\right) \qquad (3.78)$$

as long as the ion flux is not very much greater than the electron flux. Employing this relation and an equation for the electron heat flux it is possible to relate the temperature fall through the filter to the plasma density fall. The development of a mathematical expression based upon the classical transport coefficients will be presented in a section to follow. But first, the relevant experimental data will be discussed. These data will then be employed in an analysis of the functional form of the flux to determine whether the classical expression (Eq (3.78)) shows the correct variation with changing V_b.

It will be concluded that Eq (3.78) properly describes the variation in Γ_x with changing V_b . Some ambiguity will remain, however. While the results of the present chapter will reinforce the conclusion that the electron flux across the magnetic filter is enhanced, it will not be possible to decide from these scaling considerations between electron-ion and electron-wave scattering as the mechanism which drives the diffusion. What will be plain is that the temperature gradient term must be a drag term for the filter flux to vary as the thermal flux to the extraction electrode.

Presentation of the Data

As seen in Chapter I, the final chamber electron temperature is a function of the extraction electrode bias voltage. By analyzing the probe traces of Figure 1-7 (Leung, 1983) the electron temperature and plasma density in both the source and extraction chambers can be discerned and compared with the theory to be developed. Figure 1-7 is chosen for analysis rather than Figure 1-8 since it is difficult to extract information from the extraction chamber probe traces in the strong filter case. Shown in Table 4-1 are the source and extraction chamber electron densities, temperatures and plasma potentials given by the probe curves of Figure 1-7. The densities are given in arbitrary units (found by scaling the saturation current with the electron temperature), while the temperatures are in electron volts and the plasma potentials are in volts. V_b is the voltage applied to the extraction electrode, as before; ϕ_1 is the plasma potential in the source chamber and ϕ_2 is the plasma potential in the extraction chamber. $\Delta\phi_p$ is the change in plasma potential, ϕ_1-ϕ_2 , and $\Delta\phi_w$ is (the change in potential at the extraction electrode wall) ϕ_2-V_b .

It should be noted that T_1 in Table 4-1 is 0.3 eV higher than the value reported for the Langmuir probe trace with V_b = 0 in Figure 1-7.

The six data points for the extraction chamber electron temperature show a rise in that temperature with increasing extraction electrode bias voltage. But as that voltage is increased, the ratio n_2/n_1 falls. This behavior of T_2 as a function of n_2/n_1 is not accounted for by the expression developed by Holmes (Holmes, 1982a) to explain extraction

chamber electron cooling, but can be anticipated upon careful consideration of the analysis of Ogasawara (Ogasawara, 1990).

V_b	ϕ_1	ϕ_2	$\Delta\phi_p$	$\Delta\phi_w$	n_1	n_2	n_2/n_1	T_1	T_2	T_2/T_1
0	3.6	1.5	2.1	1.5	4.2	.32	.076	1.7	0.4	0.24
1	4.2	2.4	1.8	1.4	4.5	.21	.047	1.7	0.5	0.3
2	4.8	3.1	1.7	1.1	4.7	.15	.032	1.7	0.5	0.3
3	5.4	4.1	1.3	1.1	4.8	.12	.025	1.7	0.6	0.35
4	6.4	5.1	1.3	1.1	5.0	.11	.022	1.7	0.7	0.42
6	7.9	6.8	1.1	0.8	5.1	.08	.016	1.7	0.8	0.48

Table 4-1: Source and Extraction Chamber Densities, Temperatures and Potentials

Holmes' relation between the plasma density fall and electron cooling is

$$\frac{2a}{3}\ln\left(\frac{n_1}{n_2}\right) = \frac{(T_1 - T_2)}{T_2} \tag{4.1}$$

where a is a parameter found experimentally to be 2.5 . Thus, according to this equation, the ratio T_1/T_2 rises with n_1/n_2. However, according to Leung's data (Figure 1-7), n_1/n_2 rises while T_1/T_2 falls as V_b is increased.

Holmes did not test his equation with V_b variations. In his experiment, V_b was constant at the anode voltage, V_b = 0.0 V. Also,

in his derivation, he assumed that the potential variation between chambers was negligible, and this is far from true for the data of Table 4-1.

The relation between n_2/n_1 and T_2/T_1 given by the data of Table 4-1 is

$$\frac{n_2}{n_1} = 0.003\left(\frac{T_2}{T_1}\right)^{-2.15} \tag{4.2}$$

This is an empirical relation found from a log-log plot of the data.

Bezverbaja (Bezverbaja, 1988: 230) also found that the ratio of extraction to source chamber electron temperatures rose as the ratio of extraction to source chamber electron number densities fell. For the Bezverbaja experiment, the empirical relation is

$$\frac{n_2}{n_1} = 0.001\left(\frac{T_2}{T_1}\right)^{-5.0}. \tag{4.3}$$

so plainly the multiplicative factor and the exponent are functions of the discharge parameters.

Ogasawara's equation for the cooling will be presented in a later section. It will be found that Ogasawara's approach allows for the phenomena of of rising n_1/n_2 with falling T_1/T_2.

Effective Area of the Extraction Electrode

As discussed in Chapter II, the residual magnetic field in the target chamber can decrease the electron mean free path and result in spatial variation in electron density. The electron density required to compute the thermal electron flux to the extraction electrode is the electron den-

sity one mean free path away from the extraction electrode. Mathematically, a decrease in the electron density is equivalent to a decrease in the effective area of the extraction electrode. An attempt will be made in this section to deduce the extraction electrode effective area, and so to determine to what extent thermal flux calculations based upon measured values of the extraction chamber electron density typically overestimate the actual thermal flux to the extraction electrode.

The data of Table 4-1 allow an estimate to be made of the effective area of the extraction electrode. Such an estimate will be required in order to approximate the electron densities listed in Table 4-1. The electron flux to the walls of the source must always exceed the ion flux by an amount equal to the discharge current I_d:

$$\Gamma_e^a A_e^a + \Gamma_e^b A_e^b - (\Gamma_I^a A_I^a + \Gamma_I^b A_I^b) = \frac{I_d}{e} - \Gamma_p A_p^a \qquad (4.4)$$

where A_e^a is the effective area of the anode for thermal electrons, A_e^b is the effective area of the plasma electrode for thermal electrons, and A_p^a is the effective area of the anode for filament (primary) electrons. Quantities subscripted "*I*" refer to positive ions. Negative hydrogen ions are neglected, since they are at low temperature and high mass relative to the electrons and, under most conditions, are shielded from the walls by potential gradients. Assuming that the ion flux is equal to the Bohm expression, the balance equation can be written as:

$$n_1\left(\frac{T_1}{2\pi m}\right)^{1/2}\exp\left(-\frac{\phi_1}{T_1}\right)A_e^a + n_2\left(\frac{T_2}{2\pi m}\right)^{1/2}\exp\left(-\frac{\Delta\phi_w}{T_2}\right)A_e^b \qquad (4.5)$$

$$-0.6n_1\left(\frac{T_1}{m_I}\right)^{1/2}A_I^a - 0.6n_2\left(\frac{T_2}{m_I}\right)^{1/2}A_I^b = \frac{I_d}{e} - \Gamma_p A_p^a$$

As the potential on the extraction electrode is raised, electrons are drawn out of the plasma at a rate sufficient to raise the plasma potential in the source chamber. This decreases the value of the first term in Eq (4.5) rapidly; by the time that V_b is 3 V, ϕ_1 is about 5.4 V, and the electron flux to the anode has fallen to 4 x 10^{-2} times the thermal value, making it comparable to the positive ion flux to the anode. The $\Gamma_I^b A_I^b$ term will be much smaller than all others at high values of V_b, so it is expected that

$$n_2\left(\frac{T_2}{2\pi m}\right)^{1/2}\exp\left(-\frac{\Delta\phi_w}{T_2}\right)A_e^b \approx \frac{I_d}{e} - \Gamma_p A_p^a + 0.6n_1\left(\frac{T_1}{m_I}\right)^{1/2}A_I^a \qquad (4.6)$$

$$+ n_1\left(\frac{T_1}{2\pi m}\right)^{1/2}\exp\left(-\frac{\phi_1}{T_1}\right)A_e^a$$

Since the primary electron flux to the cusps should be little effected by changes in plasma potential, and since I_d is a constant, Eq (4.6) provides a means of estimating A_e^b in terms of A_e^a using the values given in Table 4-1 for high V_b. (A_e^b is an unknown quantity due to the magnetic shielding from the confinement magnets on the anode.)

It is found that $A_e^b/A_e^a \approx 18$. (To do this calculation, use the fact that $4A_e = A_I$ (Cho, 1990).) But A_e^a is $W_e L$, where L is the total cusp length and W_e is the cusp leak width given by $4(r_e r_I)^{1/2}$, where r_e is

the electron and r_I is the ion gyroradius. Using the maximum strength of the confinement magnets (3600 G), this gives A_e^b = 30 cm^2 .

It is also possible to estimate A_e^b using the electron currents extracted by Leung and Ehlers (Leung, 1983) from a 0.15 by 1.3 cm^2 opening in the plasma electrode (see Figure 4-1). These electron cur-

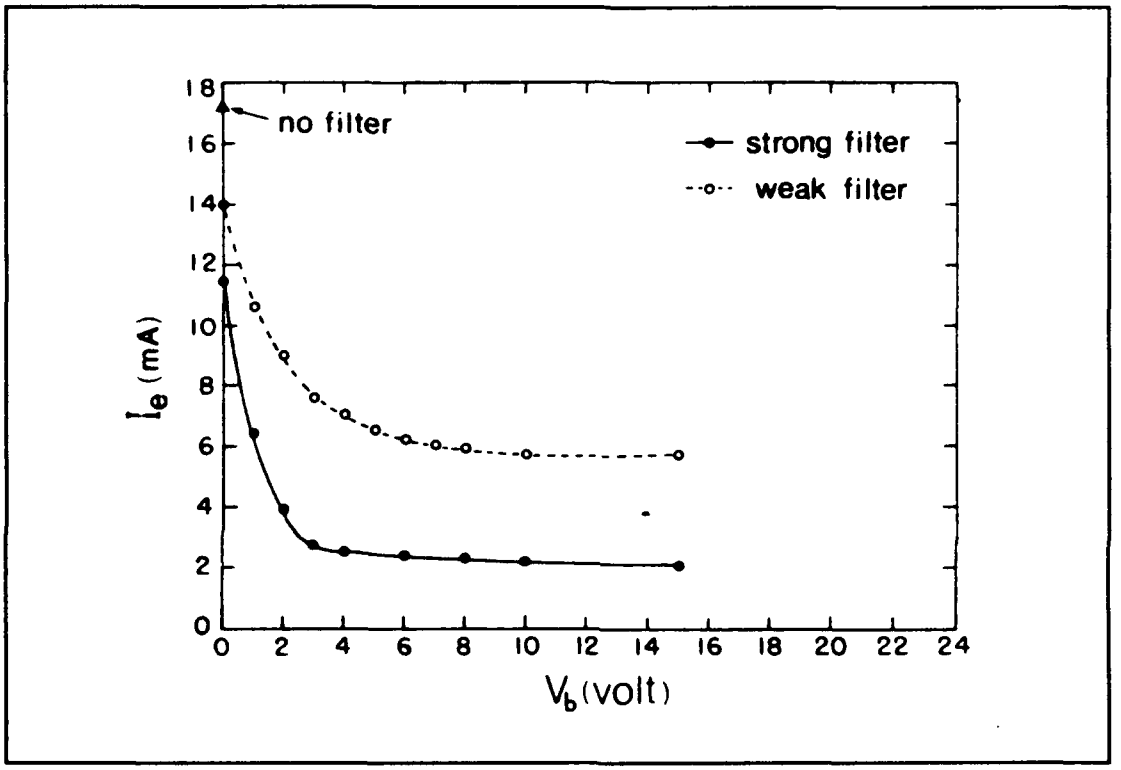

Figure 4-1: Extracted Electron Current as a Function of V_b

rents were extracted from a discharge operated under conditions identical to those for which the data of Table 4-1 apply, for two different magnetic filters and without a filter. When the source was operated without a filter, the extracted current was 17 mA. This current is due mainly to primary electrons, since it remains constant with variations in the plasma electrode potential. Supposing the loss area of the plasma electrode

to be large compared to the wall cusps, the maximum current to the plasma electrode is approximately equal to the discharge current. Assuming, then, that the extracted current density is constant over the effective area of the plasma electrode, this indicates that the maximum effective area of the plasma electrode is about 11 cm^2.

It is difficult to transfer this condition to thermal electrons, since, although they are turned in their paths by lower values of magnetic induction, they also have the ability to diffuse across a magnetic field due to their higher collision frequencies. When a filter is inserted in the device, the primary electrons are prevented from entering the extraction chamber and the current to the plasma electrode varies with applied potential. For the case of a filter, with maximum magnetic induction of about 35 Gauss, the extracted current was 6 mA at high values of V_b. Assuming, then, that there is no sheath at the plasma electrode (the absence of such a sheath having been demonstrated by Bacal and Hillion (Bacal, 1985b)), the maximum effective area of the plasma electrode is 33 cm^2. A larger area than this would imply a current to the plasma electrode in excess of the discharge current. The plasma density responsible for that 6 mA current is about 1×10^{10} cm^{-2}. Since the data of Table 4-1 were taken with the source configured with this filter, and operated under the same discharge conditions as when the current of 6 mA was extracted, this value will be used in subsequent calculations in this chapter to scale the source and extraction chamber densities. A value of n_1 or n_2 equal to 1.0 in Table 4.1 will be assumed to be 1×10^{11} cm^{-2}.

When the strong filter was used, the maximum effective area rises to 93 cm^2. This condition is, of course, superfluous.

A rough estimate of A_e^b is therefore 20 cm^2. Where the thermal flux to the extraction electrode is computed in the following, it will be scaled down by the ratio of this effective area (20 cm^2) to the effective area of the filter quoted by Holmes (Holmes, 1982b), 200 cm^2. This much smaller estimate of the effective size of the extraction electrode has an important implication for the analysis of Chapter II. There it was found that Holmes' experiment (Holmes, 1982b) required an enhancement to the flux by a factor of $9\pi^{1/2}$. The data of Leung and Bacal's experiment (Leung, 1984b), however, necessitated an enhancement by a factor of 350, assuming an effective extraction electrode area of 200 cm^2. This enhancement is reduced to a factor of 35 if the effective area is 20 cm^2, bringing the two experiments to near agreement.

Analysis of the Effect of Temperature Gradients on the Flux

The data of Table 4-1 put certain constraints upon the functional form of the flux. In fact, they show that the functional form of the flux given in Eq (3.78) matches the thermal flux to the plasma electrode as a function of variations in the plasma electrode potential, with the exception, of course, that the flux described by Eq (3.78) is much too small.

Assume that

$$\Gamma_x = -\frac{v_I}{m\omega^2}\left(T\frac{dn}{dx} - \frac{1}{2}n\frac{dT}{dx} - en\frac{d\phi}{dx}\right) \tag{4.7}$$

which is essentially Eq (3.78) with the subscripts "*e*" dropped and with *g* equal to 1 (no ions trapped). Next, the data of Table 4-1 imply, roughly, that

$$e\frac{d\phi}{dx} \approx \frac{3}{2}\frac{dT}{dx} \tag{4.8}$$

Substituting this value for $d\phi/dx$ into Eq (4.7),

$$\frac{\Gamma_x m\omega^2 T^{1/2}}{d} = -n\frac{dn}{dx} + \frac{2n^2}{T}\frac{dT}{dx} \tag{4.9}$$

where *d* is given by Eq (2.6).

This differential equation can be solved with the result that

$$n^2(x) = \left(\frac{T(x)}{T_1}\right)^4 n_1^2 - \left(\frac{T(x)}{T_1}\right)^4 \int_{x_1}^{x} dx \frac{\Gamma_x m\omega^2}{d} T^{1/2} \left(\frac{T(x)}{T_1}\right)^{-4} \tag{4.10}$$

Since the integral term is negative, the flux through the filter is positive only if

$$\frac{n_2}{n_1} < \left(\frac{T_2}{T_1}\right)^2 \tag{4.11}$$

This condition is not met for V_b equal to 0.0 V in Table 4-1. Physically, this means that, assuming Coulomb collisions drive the flux, and that the ion drift eliminates none of the electric field effect on the flux, the gradient in number density multiplied by the temperature must be higher than twice the temperature gradient times the number density in order for the flux to be positive.

In general, the sign and size of the numerical coefficient of the dT/dx term (assuming that the potential gradient has already been eliminated) must be such that, if α is the numerical coefficient of dT/dx in an equation like Eq (4.9), then

$$\frac{n_2}{n_1} < \left(\frac{T_2}{T_1}\right)^{\alpha} \tag{4.12}$$

From the data of Table 4-1 it is clear that $\alpha < 1.8$ for these data.

It follows then that if $g = 0$, so that the ion $\underline{E} \times \underline{B}$ drift eliminates the electric field dependence of the flux in Eq (4.7), Eq (4.12) becomes $n_2/n_1 < (T_2/T_1)^{1/2}$. This condition is met by all of the data of Table 4-1.

Holmes' (Holmes, 1982a) data also obeys the condition for positive flux (Eq (4.12)). Holmes measured the variation of $\ln(n_1/n_2)$ with $(T_1 - T_2)/T_2$ and found it to obey Eq (4.1). One data point (the one closest to being in violation of Eq (4.12) with $\alpha = 1/2$) validating Holmes' expression had $\ln(n_1/n_2)$ at about 0.2 and $(T_1 - T_2)/T_2 = 1/3$. This corresponds to $n_2/n_1 = 0.82$ and $T_2/T_1 = 0.75$. If the electric field term makes a contribution (if g is not zero and there is an electric field directed from the source to the extraction chamber), then α becomes larger than 1/2. With the given data point, the maximum value of α is 0.69. Since the value of g depends upon the strength of the magnetic field, this should not be taken as an upper bound on α.

Strictly speaking, there are conditions where the flux may be negative, such as when the potential on the extraction electrode is very negative and secondary electrons are generated by ion impact. Under such conditions, incidentally, the extraction chamber temperature rises

as V_b falls, probably due to the generation of secondary electrons (Ehlers, 1981).

It will be seen in the next section that the flux form with $\alpha > 0$ has the feature of increasing flux with increasing T_2, as is measured experimentally.

Comparison of Various Models of the Diffusive Flux with the Thermal Flux to the Extraction Electrode

In addition to remaining non-negative, the flux through the filter must equal the thermal flux to the extraction electrode. This requirement can yield insight into the physical mechanism driving the enhanced flux through the filter. The expression for the flux through the filter must thus be of the correct magnitude, and it must vary with changes in V_b in the same way as the thermal flux to the plasma electrode.

The flux through the filter, Γ_f , will be compared with the flux to the plasma electrode, Γ_b , for the values of V_b given in Table 4-1, for various values of α. In the first comparison, a Coulomb-like diffusion coefficient will be assumed. The number density 1.0 will be taken to be 1×10^{11} cm^{-3} , and all other densities will be scaled accordingly. The expression for the flux through the filter Γ_f is a generalization for arbitrary α of Eq (4.10):

$$\Gamma_f = \frac{\sqrt{\frac{2}{\pi}}d}{2ma\omega_o^2} \frac{1}{T_2^{1/2}} \left(\frac{T_2}{T_1}\right)^{2\alpha} \left(n_1^2 - \left(\frac{T_2}{T_1}\right)^{-2\alpha} n_2^2\right) \qquad (4.13)$$

This equation has been derived assuming

$$\int_{x_1}^{x_2} dx \frac{2m\omega^2 T^{1/2}}{d} \left(\frac{T(x)}{T_1}\right)^{-2\alpha} \approx T_2^{1/2} \left(\frac{T_2}{T_1}\right)^{-2\alpha} \int_{-\infty}^{\infty} dx \frac{2m\omega^2}{d} \tag{4.14}$$

This assumption is probably not very good since the electron temperature at the point where the magnetic field strength is high is probably somewhat higher than T_2, but the assumption allows the effect of the falling electron temperature through the magnetic filter on the electron-ion collision frequency to come through. Taking electron cooling into account thus causes a change in the expression for the flux from that given in Eq (2.32), for which the temperature was assumed to be equal to the source chamber temperature. Numerically, with a maximum magnetic induction of 35 G,

$$\Gamma_f = 1.37\times10^{14} \left(\frac{T_2}{T_1}\right)^{2\alpha} T_2^{1/2} \left(n_1^2 - \left(\frac{T_2}{T_1}\right)^{-2\alpha} n_2^2\right) \text{ cm}^{-2} \text{ sec}^{-1} \tag{4.15}$$

when the temperatures and densities are as given in Table 4-1. The flux to the extraction electrode is, similarly,

$$\Gamma_b = 1.67\times10^{17} n_2 T_2^{1/2} \exp\left(-\frac{\Delta\phi_w}{T_2}\right) \text{ cm}^{-2} \text{ sec}^{-1} \tag{4.16}$$

In Table 4-2, the values of Γ_f and Γ_b are given for various values of V_b and α.

So, when α = -2 , the flux at highest bias is high by at least one order of magnitude, and decreases as V_b increases, whereas Γ_b increases with V_b. This is due to the fact that, when α is negative, the temperature gradient helps to drive the electrons across the filter. As V_b rises, the temperature gradient is less, and this assistance di-

minishes. On the other hand, Γ_f increases with V_b when $\alpha > 0$. As V_b increases and the temperature gradient becomes smaller, the inhibiting effect of the gradient decreases, and electrons cross the filter with increasing ease. Thus, positive values of α show the best agreement with Γ_b , in that they increase with increasing V_b. They are, however, too small.

		Γ_f				
V_b	Γ_b	α=-2	α=-1	α=0	α=1	α=2
0	8	12,500	690	38	1.9	-0.1
1	15	5250	450	39	3.3	0.2
2	20	5720	490	43	3.7	0.27
3	25	2630	330	41	5.0	0.6
4	32	1420	240	41	6.9	1.1
6	44	810	180	40	8.8	1.9

fluxes x 10^{-14} cm^{-3} sec^{-1}

Table 4-2: Comparison of Extraction Electrode to Filter Fluxes for Coulomb-Like Diffusion Coefficients

The best agreement between the slope of Γ_b and that of Γ_f is found for $\alpha \approx 1.1$. For that value of α, g = 0.4 or 60% of the ions are magnetized. There, the ratio Γ_b/Γ_f is nearly constant at about 6. The enhancement to the classical collision frequency required by this result is somewhat lower than Holmes' factor of $9\pi^{1/2}$. One might have expected a larger enhancement factor, since Holmes' flux equation ignored temperature and potential gradients. These are precisely the effects

which reduce the magnitude of the flux and give it the proper slope with V_b variations. On the other hand, it should be recalled that Eq (4.15) overestimates the positive influence of the temperature fall by assigning the value of the final chamber temperature to the temperature at peak magnetic field strength. Lower temperatures increase the collision frequency and result in a higher flux.

It was shown in Chapter III that the temperature gradient drag effect, so characteristic of Coulomb collisions, can occur for wave-particle transport. If $W\langle 1/k\rangle$ is a constant, independent of n, T, ω , *etc.*, then the wave particle transport scales exactly as Coulomb transport, but can proceed at a substantially higher rate. Thus, $\alpha \approx 1.1$ is a reasonable fit for electron transport due to ion acoustic turbulence, supposing $W\langle 1/k\rangle$ does not vary with extraction electrode bias voltage.

Negative values of α are included in Table 4-2 for comparison. For Coulomb collisions it is incorrect to assume $\alpha < 1/2$. An interaction between electrons and excited states of molecular hydrogen could, perhaps, cause Γ_f to vary as n^2 (as with Coulomb collisions) with $\alpha < 0$. This could occur only if the density of the excited states were a linear function of the electron density. The variation of this flux with V_b cannot be concluded from an examination of Table 4-2. This is due to the fact that Eq (4.24) supposes a Coulombic dependence of the collision frequency on the temperature, which results in a multiplicative factor of $T_2^{1/2}$. A different temperature dependence would necessarily change this factor. Some indication of the range of temperature dependence of the collision frequency consistent with $\alpha < 0$ can be deduced in the following way. The expression for the flux may be written as

$$\Gamma_f = -\frac{\nu}{m\omega^2}\left(T\frac{dn}{dx} + n\left(1 + \frac{T\partial\nu}{\nu\partial T}\right)\frac{dT}{dx} - \frac{3}{2}g\frac{dT}{dx}\right) \tag{4.17}$$

This equation can be established upon examining the thermal force term in the momentum equation (Golant, 1980: 300). Eq (4.17) assumes the validity of Eq (4.8). Then

$$\alpha = \frac{3}{2}g - \left(1 + \frac{T\partial\nu}{\nu\partial T}\right) \tag{4.18}$$

This gives the familiar results for Coulomb collisions. Thus $\alpha = 2$ when $g = 1$ (no magnetized ions) and $\alpha = 1/2$ when $g = 0$ (all ions magnetized). Consider the inelastic collisions discussed above, and assume $g = 0$. Then $\alpha < 0$ when $(\partial\nu)/(\partial T) > -\nu/T$. If the collision frequency depends upon a positive power of the temperature, then $\alpha < 0$. The diffusion coefficient will increase in magnitude with increasing final chamber electron temperature. The support from the temperature gradient term will, however, decrease with increasing final chamber temperature. So, if the diffusion coefficient rise dominates, the flux will increase with increasing V_b, and perhaps match the thermal flux to the plasma electrode. But, even so, the flux due to inelastic collisions should be insignificant. As discussed in Chapter III, inelastic collisions are relatively rare for the cold electrons in the filter region and the extraction chamber, and should have little effect on electron transport.

As a second trial, suppose that the diffusion coefficient depends upon a constant collision frequency, as is the case for electron-neutral collisions and Bohm collisions. First, considering electron-neutral collisions and proceeding as before,

$$\Gamma_f = \frac{\sqrt{\frac{2}{\pi}}\nu T_2}{ma\omega_o^2}\left(n_1 - \left(\frac{T_2}{T_1}\right)^{-\alpha} n_2\right)\left(\frac{T_2}{T_1}\right)^{\alpha} \qquad (4.19)$$

In order to get close to the right order of magnitude, take $\nu = 10^7$ $\sec^{-1}$. (It should be recalled that $\nu \approx 10^6$ $\sec^{-1}$ for electron-neutral collisions.) Numerically, Eq (4.19) becomes

$$\Gamma_f = 9.2\times10^{14} T_2\left(n_1 - \left(\frac{T_2}{T_1}\right)^{-\alpha} n_2\right)\left(\frac{T_2}{T_1}\right)^{\alpha} \text{ cm}^{-2} \text{ sec}^{-1} \qquad (4.20)$$

Table 4-3 gives a comparison of Γ_f and Γ_b for various values of α. Because the collision frequency here is independent of temperature, the columns of Γ_f with $\alpha<0$ do not decrease as rapidly with increasing V_b as those in Table 4-2. The $\alpha=0$ column in Table 4-3 continues to rise with V_b, while the $\alpha=0$ column in Table 4-2 remains fairly constant.

		Γ_f				
V_b	Γ_b	α=-2	α=-1	α=0	α=1	α=2
0	8	280	65	14	2.5	-0.3
1	15	240	70	20	5.1	0.8
2	20	250	73	21	5.7	1.2
3	25	213	75	26	8.7	2.6
4	32	190	78	32	12.6	4.7
6	44	170	80	37	17.1	7.8

fluxes x 10^{-14} cm^{-3} $\sec^{-1}$

Table 4-3: Comparison of Extraction Electrode to Filter Fluxes for Constant Collision Frequency Diffusion Coefficients

The best fit to Γ_b is given by the α=1 column of Table 4-3. The ratio of Γ_b to Γ_f stays at a value close to 2.8 for all six data points. It is difficult to understand, however, given Eq (4.18), how a constant collision frequency diffusion process could have α larger than 1/2. But this is possible for electron transport due to ion acoustic turbulence as shown in Chapter III. For ion acoustic turbulent diffusion, the value of α varies from 1/2 to 2. And it appears to be possible, at least in principle, for ν_{ew} to be constant - that is, if $W\langle 1/k\rangle$ varies as the inverse electron-ion collision frequency.

It is expected that the most rapid transport of electrons through the filter would be due to Bohm diffusion. The Bohm expression corresponds to the α=0 case when the electric field and temperature gradient are ignored. Bohm diffusion, of course, does not scale with temperature or magnetic induction in accordance with Holmes' measurements (Figures 2-7 and 2-8). Numerically, with a magnetic filter of maximum magnetic induction equal to 35 G, Eq (4.20) becomes

$$\Gamma_{\text{Bohm}} = 7\times10^{15}(n_1 - n_2)T_2 \ \text{cm}^{-2}\ \text{sec}^{-1} \qquad (4.21)$$

To analyze the extent of the $(n_1 - n_2)T_2$ scaling agreement with Γ_b the ratios of Γ_b to Γ_{Bohm} are presented in Table 4-4.

This demonstrates that the α=0 scaling agrees well with the slope of the current to the extraction electrode for $V_b \geq 2$ V . The Bohm diffusion coefficient is too high, by a factor of about 7 at high V_b. It would be expected that electric field fluctuations driving the electron diffusion would be strongest at high V_b, when electrons in the source cham-

ber experience the greatest difficulty getting to the anode wall. At low V_b, the anode sheath is small and electrons in the source chamber arrive at the anode with relative ease. There has been speculation that positive ions draw cool electrons acorss the filter (Leung, 1983). But the positive ion flux across the filter decreases as the extraction electrode potential rises, while the electron flux increases. The decrease in positive ion flux is due to the fact that $\Delta\phi_p$ falls with increasing V_b . The electric field between the two chambers is a major contributor to the positive ion flux. An expression for the positive ion flux which incorporates this dependence is given in Chapter V.

V_b	Γ_b	Γ_{Bohm}	Γ_b/Γ_{Bohm}
0	8	110	0 .07
1	15	150	0.1
2	20	160	0.125
3	25	200	0.125
4	32	240	0.133
6	44	290	0 .15

fluxes x 10^{-14} cm^{-3} sec^{-1}

Table 4-4: Comparison of Extraction Electrode to Filter Fluxes for Bohm Diffusion

Inelastic collisions aside, it appears that $\alpha > 0$ is a necessary condition for Γ_f to rise as rapidly as Γ_b with rising V_b. This condition is met naturally for Coulomb collisions because of the temperature de-

pendence of the electron-ion collision frequency, but may also be met for ν_{ew}.

Electron Cooling Equation

It is necessary in order to understand how to optimize H^- production in the extraction chamber to develop an expression which relates the final chamber temperature to the electron density. The point is that the electron density must not be too low, nor the electron temperature too high, to inhibit H^- production, but at the same time the potential difference between the extraction chamber and the extraction electrode must not be so high as to diminish H^- extraction by forcing the negative hydrogen ions away from the extraction electrode to the center of the plasma.

The cooling of the electrons as they cross the magnetic filter is due to the electric field between the source and extraction chambers, elastic collisions with both ions and neutrals, and inelastic collisions. The conducting wall (the plasma electrode) in the extraction chamber absorbs the hotter electrons from the extraction chamber plasma and so also tends to decrease the electron temperature. Electrons are heated by primary electrons largely restricted to the source chamber.

An expression will now be derived which relates the ratio of source to extraction chamber plasma densities to the source and extraction chamber electron temperatures and the potential fall between the chambers. The approach is a generalization of that employed by Ogasawara (Ogasawara, 1990). Ogasawara's equation, however, does not predict

the rise in extraction chamber temperature relative to the source chamber temperature with increasing flux. The equation derived below does.

The flux may be written as

$$\Gamma_x = -D\left(\frac{genE_x}{T} + \frac{dn}{dx} - \frac{1}{2}\frac{n}{T}\frac{dT}{dx}\right) \tag{4.22}$$

where D is given by

$$D = \frac{\nu_I T}{m(\omega^2 + \nu_I^2)} \tag{4.23}$$

Here, subscripts "e" have been dropped: all quantities refer to electrons, and ν_I is the electron-ion Coulomb collision frequency.

The electron energy flux may similarly be written as

$$Q_x = -D\left(genE_x + T\frac{dn}{dx} + 1.91n\frac{dT}{dx}\right) \tag{4.24}$$

or

$$Q_x = \Gamma_x T - 2.41Dn\frac{dT}{dx} \tag{4.25}$$

This is Skharofsky's equation 8-107b (Skharofsky, 1966) generalized for the case when a fraction (1-g) of the ions are magnetized, and assuming that the ion directed velocity is determined by the $\underline{E} \times \underline{B}$ drift (see the discussion on page 3-24).

Solving Eq (4.22) and Eq (4.25) simultaneously results in

$$\frac{d}{dx}\ln n = -\frac{geE_x}{T} + \frac{1}{2}\frac{d}{dx}\ln T + 2.41\frac{\Gamma_x}{Q_x - \Gamma_x T}\frac{dT}{dx} \tag{4.26}$$

In the parameter space of interest to Ogasawara, the electric field term is small in comparison to the density and temperature gradient terms. Using the data of Table 4-1, it is plain that this term must be retained here.

Ogasawara then proceeds to solve for $\ln(n_1/n_2)$ under the assumption that the energy flux Q_x is a constant in x. At very high values of the particle flux and with small variations in the plasma potential, this is a reasonable assumption. That constant Q_x is linear in the particle flux, so that the dramatic rise in particle flux with increasing V_b will not significantly influence the value of the final term in Eq (4.26). But it is clear from Eq (4.21) that $Q_x - \Gamma_x T$ varies as $-Dn\frac{dT}{dx}$, which, for the data of Table 4-1, certainly does not increase in magnitude with increasing V_b nearly as fast as Γ_x. Thus, the final term in Eq (4.26) should increase with Γ_x as V_b rises, and this should lead to the increase in n_1/n_2 with decreasing T_1/T_2 observed experimentally at low pressures and discharge currents.

In the parameter space of interest here, the energy flux is far from constant. From the energy moment equation,

$$\nabla \cdot \underset{\sim}{Q} = -e\underset{\sim}{\Gamma} \cdot \underset{\sim}{E} + \frac{\delta(n\langle K\rangle)}{\delta t} \tag{4.27}$$

with K being the electron kinetic energy. Assuming that the energy flux,

like the particle flux, is directed largely along the cylindrical axis, an expression may be derived for $Q_x(x)$. The last term on the right-hand side, $\frac{\delta(n<K>)}{\delta t}$, is the rate of change in the energy density of the electron gas upon collisions. For the thermal electrons in the source, if the electron and ion thermal velocities are small compared with the electron temperature and if electron energy losses upon inelastic collision are comparable to the initial electron energy, this term is approximately

$$\frac{\delta(n<K>)}{\delta t} = -3\frac{m}{m_I}\nu_I n(T-T_I) - \frac{3}{2}n\nu_{in}T \qquad (4.28)$$

(Golant, 1980: 176-177), where ν_{in} is the total inelastic collision frequency.

The term given by Eq (4.25) is easily of the same order of magnitude as the $e\underline{E}\cdot\underline{\Gamma}$ term regardless of the bias of the plasma electrode. For instance, when the flux is 8 x 10^{14} cm^{-2} sec^{-1} at V_b = 0 V, $e\Gamma\frac{d\phi}{dx} \approx 1.3\times10^3$ cm^{-3} erg sec^{-1} and $-3\frac{m}{m_I}\nu_I n(T-T_I) \approx 1.6\times10^3$ cm^{-3} erg sec^{-1}. The electric field term becomes more important at higher V_b. Inelastic scattering involving the excitation of rotational and vibrational levels of H_2 should be an order of magnitude larger than these terms for particle fluxes in the range 8 to 44 x 10^{14} cm^{-3} sec^{-1}. For instance, one inelastic process which should have a relatively high probability of occurrence is the vibrational excitation of molecular hydrogen from v=0 to v=1, due to the relatively high density of H_2(v=0) and a high reaction rate. The reaction rate for e + H_2(v=0) $\rightarrow$ H_2(v=1) + e is about $<\sigma\upsilon>$ = 10^{-9} cm^3 sec^{-1} (Mordin, 1983: 138). At a pressure of 1.5 mTorr, the collision frequency for this process is about $\nu = N_2<\sigma\upsilon> = 3 \times 10^4$

sec^{-1}. The rate of change in the energy density is then about $1.5nvT$ = 5 x 10^4 cm^3 erg sec^{-1} at V_b = 0 V, roughly one order of magnitude larger than the elastic term given by Eq (4.28) or the electric field term from Eq (4.27). This order of magnitude difference continues to higher values of V_b.

As an order of magnitude estimate on the maximum flux for which the inelastic energy loss term is stronger than the loss associated with work against the electric field, set $e\Gamma_x \Delta\phi_p \leq \frac{3}{2} nvT\Delta x$ at V_b = 0.0 V. The maximum Γ_x is then about 10^{16} cm^{-2} sec^{-1}. The fluxes estimated in this chapter are below this value.

One physical effect omitted in Eq (4.28) is electron heating due to ion sound and related turbulence (Sagdeev, 1979; Dum, 1978b; Dum, 1974). The effect of turbulent heating may be estimated from

$$\frac{\delta (n\langle K\rangle)_w}{\delta t} \cong \int d\underline{v} \frac{mc^2}{2} \left(\frac{\delta f}{\delta t}\right)_w \cong \int d\underline{v} \frac{mc^2}{2} \left\{\frac{\partial}{\partial v_l} D_{lm}^{e/w} \frac{\partial f}{\partial v_m}\right\} \tag{4.29}$$

Assuming that the directed velocity of the turbulent spectrum is zero and the turbulence is isotropic, it is straightforward to show that

$$\frac{\delta (n\langle K\rangle)_w}{\delta t} \cong mn\nu_w u^2 \tag{4.30}$$

where ν_w is the electron-wave collision frequency and u is the electron directed velocity. In order for this heating rate to balance the energy loss rate due to electron-ion collisions,

$$\frac{\nu_w}{\nu_l} > 3\frac{m_e v_e^2}{m_l u^2} \tag{4.31}$$

where υ_e is the electron thermal velocity. For values of the flux typical here, $\upsilon_e/u \approx 10^3$, so Eq (4.31) becomes $\nu_w > 10^3 \nu_I$. A additional order of magnitude in the ratio of collision frequencies is needed for turbulent heating to match cooling through electron-neutral collisions. From the data of Table 4-2, it is plain that, for this experiment (Leung, 1983), $\nu_w/\nu_I \sim 6$, so turbulent heating is insignificant.

Hence, the inelastic collision term is dominant and

$$Q_x(x) = Q_{x_2} - \int_{x_2}^{x} dx \frac{3}{2} n\nu T \tag{4.32}$$

The final chamber value of Q_x may be found by direct computation. It is, assuming no secondary electron emission,

$$n_2 \int_{\left(\frac{2e\Delta\phi_w}{m}\right)^{1/2}}^{\infty} d\upsilon_x \frac{m\upsilon^2}{2} \upsilon_x f(\upsilon_x) = 2\Gamma_x T_2 + \Gamma_x \Delta\phi_w \tag{4.33}$$

(Emmert, 1980) where the lower cut-off in the integral comes from the consideration that, in order to strike the wall, the electron velocity must exceed $(2e((\Delta\phi_w)/m))^{1/2}$, where $\Delta\phi_W$ is the potential drop across the sheath at the plasma electrode.

Incidentally, Ogasawara takes the final chamber value of the energy flux to be equal to $\beta\Gamma T_2$, and he finds that β = 7 gives a good fit for his data. The discrepancy between this value of β and the theoretical value of β = 2 may lie in the contribution of the sheath term $e\Gamma(\Delta\phi_w)$.

Supposing that the inelastic loss term is the dominant term in $Q_x - \Gamma_x T$, it is plain that $\Gamma_x/(Q_x - \Gamma_x T)$ will rise with Γ_x. The equation relating number densities, temperatures and potential gradients is then

found by integrating Eq (4.26):

$$\ln\left(\frac{n_1}{n_2}\right) = -ge\int_{x_2}^{x_1}\frac{E_x}{T} + \frac{1}{2}\ln\left(\frac{T_1}{T_2}\right) - 2.41\int_{x_2}^{x_1} dx\frac{dT}{dx}\frac{\Gamma_x}{\int_{x_2}^{x} dx\frac{3}{2}n\nu T} \tag{4.34}$$

This equation will be used to compute the ratios of source to extraction chamber densities for given values of $\Delta\phi_w$, source chamber densities, and temperatures in both chambers. In order to do that, approximate

$$-ge\int_{x_2}^{x_1}\frac{E_x}{T} \approx g\frac{\Delta\phi_p}{T_1}$$

and assume g=1. Also, take

$$\int_{x_2}^{x} dx\frac{3}{2}n\nu_{in}T \approx hn_1T_1$$

That is, it is assumed that the value of the integral is dominated by the peak value of the integrand. Then choose h as 3.5 x 10^3 cm/sec. This is a not unreasonable value, and gives a decent fit to the data of Table 4-1. The final equation relating densities, temperatures and plasma potential variations is

$$\ln\left(\frac{n_1}{n_2}\right) = \frac{\Delta\phi_p}{T_1} + \frac{1}{2}\ln\left(\frac{T_1}{T_2}\right) + \frac{2.41\Gamma_x(T_1 - T_2)}{3.5\times10^3\,\mathrm{cm/sec}\,n_1T_1} \tag{4.35}$$

A comparison of density ratios computed from Eq (4.35) to measured values appears in Table 4-5.

As can be seen, Eq (4.35), though it suffers greatly from some rather crude approximations, correctly predicts the rise in n_1/n_2 with falling T_1/T_2 as observed in low power discharges.

Physically, what is occurring is this: the incoming energy flux Q_{x_1} is on the order of $\Gamma_x T_1$. The outgoing energy flux is $Q_{x_2} = 2\Gamma_x T_2 + \Gamma_x \Delta\phi_w$. Since the inelastic energy loss across the filter is very large in comparison to the incoming energy flux Q_{x_1}, $Q_{x_1} \gg Q_{x_2}$, and $T_1 \gg T_2$. As the particle flux rises with rising V_b, the inelastic energy loss across the filter decreases relative to the both the incoming and outgoing energy flux terms. Thus, the incoming energy flux and the outgoing energy flux approach the same value, and $T_2 \rightarrow T_1$. The fact that $\Delta\phi_w$ falls as the particle flux rises only serves to enhance this effect. At higher values of the particle flux, one should expect to see very little variation in the extraction chamber temperature as a function of increasing particle flux.

V_b	n_1/n_2 (Measured)	n_1/n_2 (Calculated)
0	13	19
1	21	17
2	31	40
3	40	37
4	45	45
6	64	65

Table 4-5: Comparison of Density Ratios Calculated from Eq (4.35) to Measured Values

Returning to the realm of high relative inelastic energy loss, if the particle flux were to be decreased, say by increasing the peak magnetic induction in the filter, while n_1/n_2 were to rise (the decrease in flux leads to an increase in source chamber plasma density because the plasma is more efficiently confined), then Eq (4.34) predicts that $(dT)/(dx)$ must rise in magnitude. If T_1 does not rise with increasing magnetic induction, then T_2 must fall. This variation in T_2 has, in fact, been observed (Holmes, 1982a). The same behavior should also be observed in the high power discharges where the inelastic loss term is small, as is apparent from Ogasawara's equation (4) (Ogasawara, 1990).

Discussion

The burden of this chapter has been 1) to show that the electron flux through the filter varies as predicted by Eq (4.1) - that is, it is Coulombic to the extent that the temperature gradient acts as a drag term - and 2) to derive an equation describing the decrease in electron temperature from the source to the extraction chamber.

The inferred experimental fluxes to the extraction electrode seem to vary in agreement with Eq (4.1). Nothing definite could be concluded about the functional form of the collision frequency itself, since both constant and Coulomb collision frequencies provided fluxes which increased in a way similar to the extraction electrode thermal flux. The flux rises with increasing V_b with a slope that suggests that temperature gradient acts as a drag on the flux. As the plasma electrode bias voltage increases, the magnitude of this temperature gradient drag falls. The tem-

perature gradient will effect the flux in this way only if the electron collision frequency varies as T^{-p} , where p is a positive number, or for electron-wave scattering as described in Chapter IV.

In order to employ realistic values of plasma densities in these calculations, an estimate was made of the effective area of the plasma electrode. The effective area of the plasma electrode was calculated to be lower by an order of magnitude than the actual area. Since the flux was estimated from the extraction chamber plasma density multiplied by the effective area of the plasma electrode, the fluxes estimated were one order of magnitude lower than they otherwise would have been.

The values of particle flux so calculated were employed to test an equation which describes the cooling of the electron gas as it passes from the source chamber to the extraction chamber. That behavior of the extraction chamber electron temperature as a function of plasma electrode bias voltage itself indirectly served to confirm those estimates of particle flux: had the particle flux been an order of magnitude larger, it is doubtful whether any rise in extraction chamber electron temperature would have been observed as the plasma electrode bias voltage was raised.

The estimated particle flux to the extraction electrode was only one order of magnitude higher than the flux which can be supported by an electron gas obeying Eq (4.1). Thus, this brings the required enhancement to near agreement with Holmes' (Holmes, 1982b) calculation.

The electron cooling equation (Eq 4.31) derived in this chapter was not directly integrable. But it was clear that the last term on the right side rose with increasing particle flux, even when the difference in tem-

peratures fell. This term allows the ratio (source chamber/extraction chamber) of plasma densities to rise while the ratio of temperatures falls. Crude estimates of integrals in the equation were used to attempt to mimic the observed variation in n_1/n_2 as a function of measured variations in temperatures, fluxes, and plasma potentials. Good agreement was found, shown in Table 4-5.

Chapter V - Primary Electron and Ion Motion

Introduction

In this chapter primary electron and positive ion transport through the magnetic filter will be investigated. Direct evidence indicating the mechanism of positive ion transport is not available. It is possible, however, to formulate a model of the source which predicts extracted ion species percentages. These have been measured (Ehlers, 1982b). This model incorporates a particular view of positive ion transport, so the model itself will constitute an indirect test of the ion transport theory.

For positive ions it will be assumed that motion is a ballistic flow across the filter. That is, ions with the greatest energy and highest mass (the largest gyro-radii) traverse the filter with the greatest ease. Under the conditions of the Ehlers experiment, it was often the case that almost all the ions which entered the magnetic filter crossed into the extraction chamber. This was due to a large (1.5 V for a magnetic flux of 104 G cm) potential fall accelerating the ions which arose between chambers. For purposes of predicting ion transport at higher extraction plate bias voltages and lower potential falls, the theory of ion motion will be developed in some detail. Predictions will be made regarding the final chamber ion species percentages for smaller electric potential differences between the two chambers.

The chapter is thus organized as follows. The equation for the ballistic flow of ions across a filter will be derived. Following Hopkins it is assumed that the electron energy distribution function is, to a good approximation, bi-Maxwellian (Hopkins, 1986). The higher temperature

electrons described by the bi-Maxwellian distribution will be termed "primary" electrons with density and temperature n_p, T_p; the lower temperature electrons are called "thermal" electrons with density and temperature n_e, T_e. For primary electrons it will be shown that motion across the filter must be diffusive in nature, but that the classical expression for the flux by diffusion underestimates the primary electron flux by at least one order of magnitude. The density of primary electrons in the source chamber will be inferred from Eq (1.1). This will enable a calculation of positive ion species percentages in the source chamber. The density of primary electrons in the extraction chamber will be ascertained from the extraction electrode floating potentials measured by Ehlers (Ehlers, 1982b). The ion transport equation will be generalized to account for an electric field between the two chambers. Finally, the source chamber positive ion species percentages together with the extraction chamber primary electron percentages will allow calculation of extracted beam percentages. These can be compared with experiment.

In the final section of this chapter, the model will be employed to predict positive ion species densities for a source operated with the extraction electrode at plasma potential.

Ion Flow Equation

Near the end of Chapter I, it was stated that the temperatures of positive ions in tandem multicusp H^- sources are not well known. An argument was presented to show that the temperature of H^+ is between 0.04 eV and 0.35 eV. The smaller value is roughly the energy of molecular hydrogen in the source. The upper value is the energy H^+ gains

upon formation in the process $e + H_2 \rightarrow H^+ + H + e$. The energy of formation of H_2^+ is around the energy of molecular hydrogen. The temperature of H_2^+ is doubtless between 0.04 eV and the energy gained in the electric field between collisions, on the order of 0.1 eV. The energy of formation of H_3^+ is about 0.11 eV (Mordin, 1983: 125). The temperature of H_3^+ is thus between 0.04 eV and 0.11 eV. As a result of the development described below, it will become apparent that accurate knowledge of ion energies is critical for an understanding of their motion across the magnetic filter.

Collisions between different ion species are generally more frequent than collisions between ions and neutrals. So, if one were to propose a theory of ion diffusion across the filter, as has been done by other authors for diffusion along the radial dimension of the source chamber across the wall-shielding magnetic fields (Kock, 1983), collisions with ions of different species would drive the diffusion process for a given ion species. For the filter, however, the theory of diffusion is not mature. The gyro-radius of a typical ion in a typical filter filter field is about 1 cm; yet over a distance of 1 cm the intensity of the filter magnetic field can vary by a factor of 10. Generally, theoretical approaches to diffusion rely upon the relative constancy of the magnetic field throughout the particle orbit. In addition, as has already been remarked in Chapter III, the positive-ions in the filter field region do not meet at least one condition for applicability of the classical transport theory based upon moments of the Boltzmann equation: the ion radii of gyration are long with respect to gradients in the plasma density. So it is questionable whether a momentum balance equation of the form of Eq (3.59) de-

veloped from the Boltzmann equation for each ion species would be logically defensible.

More important, in the case of the magnetic filter, such a procedure is not warranted, since the experimental evidence supports the view that the positive ions move through the filter along kinematically allowed paths. This is true for the case of low discharge pressures (pressures on the order of 1 mTorr) where the filter field strength is not very high. Where the magnetic flux is so high that the direct flux is significantly diminished, collisions must begin to play an important role in ion transport, especially in high power discharges (see Table 1-2). But how to formulate the secondary flux due to collisions is problematic due to the apparent inapplicability of the momentum moment of the Boltzmann equation.

Before proceeding to a discussion of the experimental evidence for the ballistic motion (rather than diffusion) of ions through the filter, a model of that motion, originated by Jones and Bailey (Jones, 1987), will be reviewed. The equations of motion for the ions across the magnetic filter were written under the assumption that there were no collisions to significantly alter the ion paths. This assumption can be justified for Coulomb collisions on the basis that Coulomb collisions result in small scattering angles. For ion-neutral collisions, the mean free path is 10 to 20 cm for low pressure sources (see Table 1-1); since the filter is 4 cm wide, these can be neglected. An additional assumption was that the ions have a Maxwellian velocity distribution function.

The coordinate system employed is displayed in Figure 5-1. The magnetic field is along the z direction. The x axis is from source to

extraction chamber, with $x = 0$ here assigned to the edge of the filter field in the source chamber. The width of the filter field is called Δ. Its cross section in the x-z plane is assumed triangular, as shown in Figure 5-1.

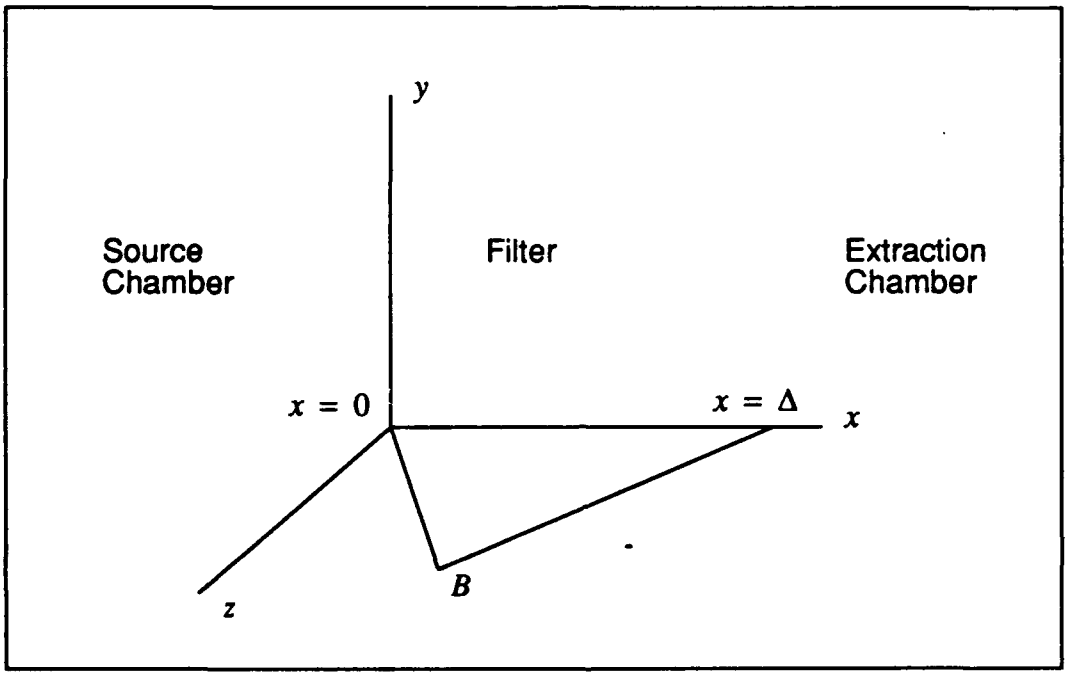

Figure 5-1: Coordinate System for Ion Flux Calculations

The y component of the Lorentz force equation, under the assumption that no electric field is present, is

$$v_y(x) = v_y^\circ - \int_0^x dx' \omega(x') \tag{5.1}$$

where $\omega(x)$ is the ion cyclotron frequency. Substituting this expression into the x-component equation and integrating,

$$v_x^2(x) = v_x^{\circ 2} + 2v_y^{\circ}\int_0^x dx'\omega(x') - 2\int_0^x dx'\omega(x')\int_0^{x'} dx''\omega(x'') \tag{5.2}$$

When the magnetic field is modelled as a triangle of width Δ, the cyclotron frequency is

$$\omega(x) = \begin{pmatrix} \frac{2\omega}{\Delta}x & 0 \le x \le \Delta/2 \\ 2\omega(1-\frac{x}{\Delta}) & \Delta/2 \le x \le \Delta \end{pmatrix} \tag{5.3}$$

where ω is the maximum value of $\omega(x)$. Substituting these values into Eq (5.2) and carrying out the integrations,

$$v_x^2(\Delta) = (v_x^{\circ})^2 + \omega\Delta v_y^{\circ} - \frac{\omega^2\Delta^2}{4} \tag{5.4}$$

In order for the ions to cross the filter, $v_x^2(\Delta) \ge 0$. So the flux through the filter for a particular positive ion species is given by

$$\Gamma_x = n_o\int d\underline{v}\, v_x^{\circ} f(\underline{v}^{\circ}) \tag{5.5}$$

where the subscripts and superscripts "*o*" indicate source chamber values, and *f* is the (supposed Maxwellian) ion velocity distribution function. No attempt will be made to justify the use of a Maxwellian distribution. But, inasmuch as the potential profile of the source chamber is an unknown quantity, the preferable method of generating an ion distribution function, that of Langmuir (Langmuir, 1929; Forrester, 1987), cannot be used. Performing the integration subject to the condition

$$v_x^{\circ 2} + \omega\Delta v_y^{\circ} - \frac{\omega^2\Delta^2}{4} \ge 0 \tag{5.6}$$

results in the following expression for the flux:

$$\Gamma_x = n_o\left(\frac{T}{2\pi m}\right)^{1/2}\left(1-\Phi\left(\left(\frac{m}{2T}\right)^{1/2}\frac{\omega\Delta}{4}\right)\right) \qquad (5.7)$$

Discussion of Measurements

Implications for Ion Diffusion. Leung and Ehlers (Ehlers, 1982b) measured the positive ions species current densities extracted through the plasma electrode of a tandem multicusp source as percentages of the total positive ion current density. The measurements were conducted to optimize the filter for H^+ extraction; the source was being investigated at that time for H^+ production characteristics. To analyze the variation in H^+ percentage with magnetic filter induction and magnetic flux, four different filters were inserted consecutively at the same position in the source. The results of Leung and Ehlers' ion species percentage measurements are displayed in Table 5-1. The discharge current was 10 A for all filters.

Leung and Ehlers define the effective transparency as "the ratio of the ion saturation current density measured by a probe in front of the extraction grids with and without the filter for the same discharge conditions" (Ehlers, 1982b).

A striking feature is the rise in H^+ percentage with increasing filter magnetic field strength and magnetic flux. This rise is partially due to the diminishing production of H_2^+ in the extraction chamber. As the filter becomes stronger, fewer primary electrons penetrate to the extraction chamber and fewer H_2 molecules are ionized. The diminishing presence of primary electrons is indicated by the rise in the floating potential of

the extraction electrode (that is, in the "Plasma Grid Floating Potential" of Table 5-1).

The fact that the H_3^+ percentage falls with decreasing transparency may be partially due to the decrease in the density of H_2^+ in the extraction chamber. The primary production mechanism for H_3^+ requires the generation of H_2^+. It appears, however, that the H_3^+ percentage is falling more rapidly than the H_2^+ percentage. It is a possibility, therefore, that the decrease in H_3^+ in the extraction chamber is due to the relative diminishment in H_3^+ flux into the extraction chamber as compared with the H^+ flux. From Eq (5.7) it is apparent that a relatively high H^+ temperature could keep the H^+ flux high at large values of the magnetic flux.

Filter	B Max (G)	Magnetic Flux (G cm)	Effective Transparency (%)	Plasma Grid Floating Potential (V)	$H^+:H_2^+:H_3^+$
None	--	--	100	-56	24 : 35 : 41
1	40	89	68	-15	30 : 17 : 53
2	76	166	43	-2	41 : 15 : 44
3	35	104	70	-10	35 : 19 : 46
4	20	89	80	-25	26 : 25 : 49

Table 5-1: Effect of Filter Configuration on Ion Species Percentages

Leung and Ehlers stated that the difference in plasma potential between the source and extraction chamber was 1.5 V for Filter 3, which they chose as the optimum filter. Such a large (relative to the ion tem-

perature) potential fall cannot be ignored. It is expected that the potential fall would vary from filter to filter to govern the thermal electron diffusion into the extraction chamber. Equation (5.7) must be generalized to include the effect of the electric field. The generalization will be presented in the section of this chapter entitled "Ion Density Model." There, the relevant chemistry of source will be modelled in an attempt to reproduce the results of Table 5-1. But first, because of the importance of primary electrons in reactions involving ions, primary electron motion into the extraction chamber must be investigated.

In order to account for the variation in ion species percentages with changing magnetic filter strength, primary electron motion across the filter must be understood. As noted above, that primary electrons exist in the extraction chamber is clear from the large negative floating potentials at the lower filter magnetic inductions. At the highest filter field strength, the electrode floats at a relatively high value (-2 V). The filter effectively prohibits most primary electrons from entering the extraction chamber. As the filter magnetic induction or magnetic flux is decreased, electrons cross the filter with increasing ease, and the floating potential decreases. In the following section, primary electron motion will be examined. Due to the scarcity of data, conclusions to be drawn should be considered tentative.

It is worthwhile to note that Filter 1 and Filter 4 had the same magnetic flux, 89 G cm. If the primary electron motion were controlled by an equation of the form of Eq (5.7), the floating potential for the two filters would be identical. The difference in floating potential for two filters with different peak magnetic induction but with the same mag-

netic flux indicates that the primary electrons are diffusing across the filter.

If primary electron motion is governed by a diffusion equation like Eq (2.32), Filter 1 is less easily penetrated that Filter 4. This is due to the fact that the flux varies inversely as the product of the peak magnetic field and the magnetic flux. Thus, the floating potential should be lower for Filter 4 than for Filter 1 as, in fact, it is. (For Holmes' magnetic filter, discussed at length in Chapter II, the characteristic width of the magnetic filter was relatively constant, so that variations in peak magnetic field strength translated directly to variations in the magnetic flux. Here, the characteristic width varies.)

In the following section, it will be shown that the primary electron flow across the magnetic filter (in accordance with Eq (5.7)) is insignificant. The density of primary electrons-in the extraction chamber will be estimated under the assumption that primary electrons diffuse into the extraction chamber. For each filter a comparison will be made between the estimated extr tion chamber primary electron density and the density required to es n the extraction electrode floating potential. From the fact that the classical theory of diffusion is unable to account for the high concentrations of primary electrons in the extraction chamber it will be concluded that the primary electron collision frequency is enhanced by at least one order of magnitude.

Primary Electrons

Ballistic Flow. Equation (5.7) may be employed to determine the number density of primary electrons in the extraction chamber under the

assumption that these electrons are capable of ballistic flow across the filter. Since the primary electron temperature is high in comparison to the potential difference between chambers, Eq (5.7) is valid and the flux through the filter may be written as

$$\Gamma_f^f = n_p^{(1)} \left(\frac{T_p}{2\pi m_e}\right)^{1/2} \left(1 - \Phi\left(\left(\frac{m_e}{2T_p}\right)^{1/2} \frac{\omega_e \Delta}{2}\right)\right) \tag{5.8}$$

where $n_p^{(1)}$ is the density of primary electrons in the source chamber and T_p is the primary electron temperature. The flux to the extraction electrode is

$$\Gamma_b = n_p^{(2)} \left(\frac{T_p}{2\pi m_e}\right)^{1/2} \exp\left(\frac{V_b - \phi_2}{T_p}\right)(1 - \gamma_p) \tag{5.9}$$

where γ_p is the secondary electron emission coefficient for primary electrons. The two fluxes may be equated to give

$$n_p^{(2)} = n_p^{(1)} \left(1 - \Phi\left(\left(\frac{m_e}{2T_p}\right)^{1/2} \frac{\omega_e \Delta}{2}\right)\right) \exp\left(-\frac{V_b - \phi_2}{T_p}\right)\left(\frac{1}{1 - \gamma_p}\right) \tag{5.10}$$

Unfortunately, the temperature and density of the primary electrons were not measured in the experiment under discussion (Ehlers, 1982b). Holmes' probe curves (Holmes, 1982b) indicate that the primary electron temperature in his experiment was 35 eV at an unknown discharge current. In a later experiment, Holmes (Holmes, 1987) measured the primary electron temperature of 40 eV at a discharge current equal to 100 A and a discharge voltage of 100 V. The primary electron temperature for the Ehlers experiment (Ehlers, 1982b) will be assumed equal to 30 eV.

For the weakest of the filters given in Table 5-1, the magnetic flux is 89 G cm. Using this value in Eq (5.10), it is found that the argument of the error function is 4.8. Therefore,

$$\frac{n_p^{(2)}}{n_p^{(1)}} = \frac{(1-\Phi(4.8))}{(1-\gamma_p)} \exp\left(-\frac{V_b-\phi_2}{T_p}\right) = \frac{1\times10^{-10}}{(1-\gamma_p)} \qquad (5.11)$$

The secondary electron emission coefficient for stainless steel is not available, but the secondary electron emission coefficient for iron is near and below 0.5 at these comparatively low energies (Bruining, 1954: 32). It is apparent, therefore, that ballistic motion of primary electrons across the filter is nonexistent. The primary electrons cannot cross the filter except by diffusion.

Primary Electron Density from the Floating Potential. The floating potential column of Table 5-1 indicates that primary electrons exist in the extraction chamber in high numbers. When the floating potential has a large negative value, thermal electron effects may be ignored (this assumption will be defended shortly). The current balance at the plasma electrode may be written as

$$n_p^{(2)}\left(\frac{T_p}{2\pi m_e}\right)^{1/2} \exp\left(\frac{V_b-\phi_2}{T_p}\right)(1-\gamma_p)\frac{A_p^b}{A_I^b} = 0.5 n_I^{(2)}\left(\frac{T_e+T_I}{m_I}\right)^{1/2}(1+\gamma_I) \qquad (5.12)$$

where V_b is the floating potential, ϕ_2 is the plasma potential, $n_I^{(2)}$ is the total positive ion charge density in the extraction chamber, T_e is the thermal electron temperature and m_I is an average positive ion mass. Since ions may also release secondary electrons from the plasma electrode, the secondary electron emission coefficient γ_I is included. Its val-

ue at low ion energies is extremely small, about 10^{-2} (Ray, 1979: 6517). The areas A_p^b and A_I^b are introduced under the assumption that the effective loss area to the extraction electrode may be different (larger) for ions than for primary electrons. The right-hand side of Eq (5.12) contains the generalized Bohm expression for the ion flux (Strangeby, 1986: 43).

The case with no filter will yield a rough estimate of $n_p^{(1)}$. It is found from Eq (5.12) that

$$\frac{n_p^{(1)}}{n_I^{(1)}} = 2\times10^{-2}\frac{A_I^b(1+\gamma_I)}{A_p^b(1-\gamma_p)} \tag{5.13}$$

Assuming no secondary emission and equivalent effective loss areas, with $n_I^{(1)} = 1\times10^{11}$, $n_p^{(1)} = 2\times10^{9}\text{cm}^{-3}$. This is not implausible. This value for the source chamber primary electron density will be of interest in the test of the ability of the classical diffusion rate to cause the extraction electrode to float at the measured value.

Calculations similar to Eq (5.13) may be performed for the Filters 1 through 4. The required value of $n_p^{(2)}/n_I^{(2)}$ for each case is shown in Table 5-2 (second column). In each case it is assumed that the extraction chamber plasma potential is at 1.5 V and that the thermal electron temperature is 0.4 eV.

Also shown in Table 5-2 are estimates of $n_p^{(2)}$ assuming that the positive ion density is 5 x 10^{10} cm^{-3} for all filters. This is an rough selection motivated by the fact that at low plasma electrode bias voltages the extraction chamber plasma density approaches the source chamber density (assumed equal to 1 x 10^{11} cm^{-3}) (see Figure 2-2). The values

of $n_p^{(2)}$ calculated from the floating potential can be compared with those required by classical diffusion theory. Hence, Table 5-2 also displays estimates of $n_p^{(2)}$ based upon a calculation (to be presented shortly) of the diffusive flux.

The contribution of thermal electrons to the floating potential has been ignored in the above calculations. The assumption is that they are too cold to effect the floating potential. That is perhaps not true in the case where V_b = -2 V, depending on the extraction chamber thermal electron temperature.

Primary Electron Density from the Diffusion Equation. The final chamber primary electron density can be calculated using a flux equation similar to Eq (2.32). The primary electron temperature is sufficiently high to make electric field and temperature gradient effects inconsequential. The flux may then be written as

$$\Gamma_f^p = -\frac{\nu_p T_p}{m_e \omega_e^2} \frac{dn_p}{dx} \tag{5.14}$$

A critical question is whether the collisions that drive primary electron diffusion are due to Coulomb collisions or the elastic and various inelastic collisions with neutrals. The Coulomb collision frequency given by Eq (2.2) for 30 eV electrons on a target population with number density 10^{11} cm^{-3} is $\nu_p^C = 2.6\times10^4$ sec^{-1}. The elastic scattering cross section with neutrals may be extrapolated from Figure 1-14. At 30 eV it is approximately 5 x 10^{-16} cm^2. Since the pressure is 1.5 mTorr (Ehlers, 1982b), the elastic collision frequency is about $\nu_p^{el} = 5\times10^6$ sec^{-1}. Inelastic collisions contribute little to the diffusion. The total in-

elastic collision frequency may be estimated from Eq (1.1) and the data presented in Holmes' 1987 paper (Holmes, 1987: 225). The total inelastic cross section is about 7 x 10^{-17} sec^{-1}, so the total inelastic collision frequency is $\nu_p^{in} = 7\times10^5$ sec^{-1}. Plainly, then, elastic collisions should drive the primary electron diffusion across the filter.

Assuming a Gaussian magnetic field profile, Eq (5.14) can be integrated to yield

$$n_p^{(2)} = \frac{\nu_p T_p}{m_e \omega_o^2 a}\left(\frac{m_e}{T_p}\right)^{1/2} n_p^{(1)} \exp\left(-\frac{V_b - \phi_2}{T_p}\right)\frac{1}{(1-\gamma_p)}\frac{A_p^f}{A_p^b} \tag{5.15}$$

under the assumption that $n_p^{(2)} \ll n_p^{(1)}$.

With accurate data for T_p , $n_p^{(1)}$, and ϕ_2 , a more definite evaluation of Eq (5.15) could be performed. As it stands, a rough estimate of the increase in $n_p^{(1)}$ due to the presence of the filter is possible. When a filter is present, primary electrons escape from the source chamber at a slower rate, resulting in a higher equilibrium value. Consequently, there will be larger primary electron flux through the filter than would otherwise have been anticipated. From Eq (1.1) it is plain that, without a filter,

$$n_p^{(1)} = \frac{I_d/e}{\frac{1}{4}\upsilon_p\left((1-\gamma_p)A_p^b + 4\sigma_{in}N_2V_p\right)} \tag{5.16}$$

with σ_{in} about 7x10^{-17} cm^2, and V_p is the discharge volume accessible to primary electrons. Physically, the ratio of volume to area should be approximately equal to the length of the device, so V_p/A_p^b should be about 20 cm. Using this value for V_p/A_p^b , at $I_d = 10\,A$, and with

T_p = 30 eV, the result is $n_p^{(1)}$ = 5.8 x 10^{11} cm^{-1}/A_p^b. The earlier result for the primary electron density for a source without a filter (2 x 10^9 cm^{-3} from Eq (5.13)) is obtained if A_p^b = 290 cm^2.

When a filter is present, the inelastic collision term in Eq (5.16) could dominate. That is, the relative difficulty in crossing the filter can be described mathematically by introducing a small effective cross-sectional area of the filter field. Assuming that this effective area is inconsequentially small, the source chamber density could then rise as high as 1 x 10^{10} cm^{-3}, a value determined solely by the inelastic collision term. This value of the primary electron density, then, will be used in Eq (5.15) in order to calculate the extraction chamber primary electron densities.

In addition, the final chamber plasma potential will be taken to be ϕ_2 = 1.5 V, as before. The area ratio in Eq (5.15) is assumed equal to 1 for purposes of comparison. The resulting values of $n_p^{(2)}$ are compared in Table 5-2 with the estimates generated earlier. The extraction chamber primary electron density computed from current balance to the plasma electrode under the assumption that $n_I^{(2)}$ is 5 x 10^{10} cm^{-3} is given in the third column of Table 5-2. The same density computed on the basis of classical diffusion through the filter and on the assumption that the source chamber primary electron density is 1 x 10^{10} cm^{-3} is presented in the fifth column.

It appears from Table 5-2 that the primary electron diffusion driven by elastic collisions with molecular hydrogen is one order of magnitude too low to account for the measured extraction electrode floating potential. The classical expression for primary electron diffusion provides

an underestimate of the true diffusion rate. Confirmation of this conclusion will be based on the ion density model to be presented in the next section.

Filter	$n_p^{(2)}/n_I^{(2)}$	$n_p^{(2)}$ (x 10^8 cm^{-3})	$n_p^{(2)}/n_p^{(1)}$	$n_p^{(2)}$ (x 10^7 cm^{-3})
None	2.0×10^{-2}	20.0	----------	----------
1	5.0×10^{-3}	2.5	3.4×10^{-3}	3.4
2	3.2×10^{-3}	1.6	6.6×10^{-4}	0.66
3	4.2×10^{-3}	2.1	2.8×10^{-3}	2.8
4	6.9×10^{-3}	3.5	9.6×10^{-3}	9.6

Table 5-2: Extraction Chamber Primary Electron Densities:
Left Columns from Floating Potentials, Right Columns from Diffusion Equation

Ion Density Model

Ion Flow Including Electric Field. In order to show that the ballistic flow of ions results in agreement with the data of Table 5-1, it is necessary to model positive ion production and loss in the extraction chamber. To do so requires a more general version of Eq (5.7), one which accounts for the electric field between the two chambers.

Fortunately, Eq (5.7) can be readily generalized to include electric field effects. It is necessary merely to include the electric field in the Lorentz force equation, Eq (5.1). More generally, then,

$$\Gamma_f^{(i)} = n_i^{(1)} \left(\frac{T_i}{2\pi m_i} \right)^{1/2} \zeta_i \qquad (5.17)$$

where

$$\zeta_i = \frac{1}{2}\left(1 - \Phi\left(\left(\frac{m_i}{2T_i}\right)^{1/2}\left(\frac{\omega_i\Delta}{4} - \frac{2e\phi}{m_i\omega_i\Delta}\right)\right)\right)\exp\left(-\frac{e\phi}{T_i}\right) \qquad (5.18)$$

$$+\frac{1}{2}\left(1 \mp \Phi\left(\left(\frac{m_i}{2T_i}\right)^{1/2}\left|\frac{\omega_i\Delta}{4} + \frac{2e\phi}{m_i\omega_i\Delta}\right|\right)\right)$$

and where ϕ is the difference in electric potential between the extraction chamber edge of the filter field and the source chamber edge (ϕ is negative) and $n_i^{(1)}$ is the source chamber density for a given ion species. The upper (-) sign is taken when the argument of the absolute value is positive, and the lower (+) sign is taken when it is negative.

Figures 5-2 through 5-5 show the variation in $\Gamma_f^{(i)}/n_i^{(1)}$ for four different values of ϕ for the three positive ion species in the source. Temperatures were T_1=0.4 eV, T_2=0.04 eV and T_3=0.04 eV. The assistance of the electric field is felt first by H_3^+, then by H_2^+, and finally by H^+. Large potential falls tend to draw the fluxes up to their thermal values.

Extraction Chamber Balance Equations. Equation (5.17) can be used in the calculation of final chamber species percentages for comparison with the experimental results displayed in Table 1-1. The extraction chamber density for ion species i is given by the balance equation between the flux of species i into the extraction chamber as calculated from Eq (5.17) plus the production rate per unit area in the extraction region on the one hand, and the loss rate per unit area in the extraction region plus the flux to the extraction electrode calculated from

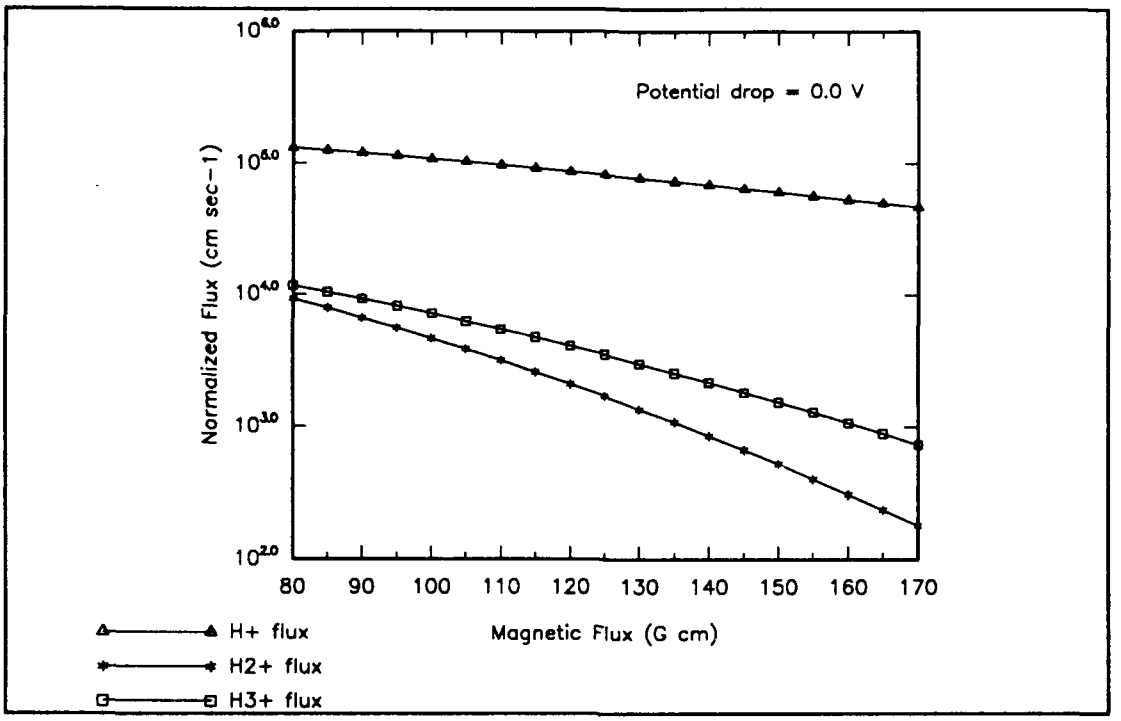

Figure 5-2: Normalized Ion Fluxes for Potential Drop = 0.0 V

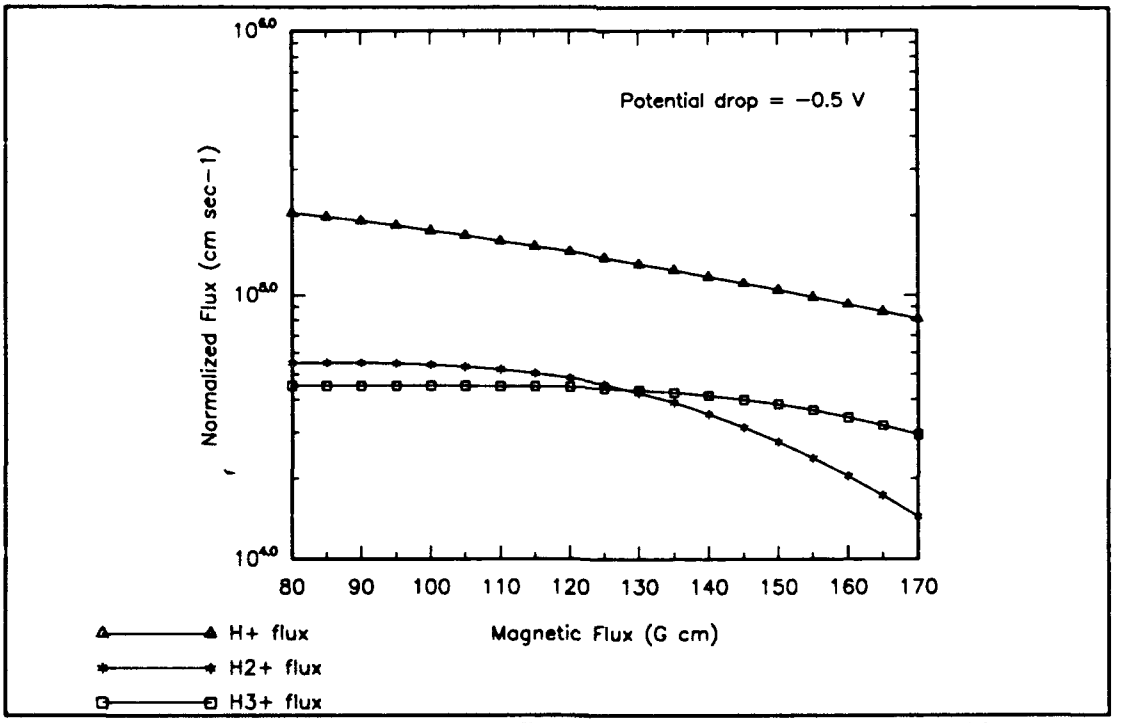

Figure 5-3: Normalized Ion Fluxes for Potential Drop = -0.5 V

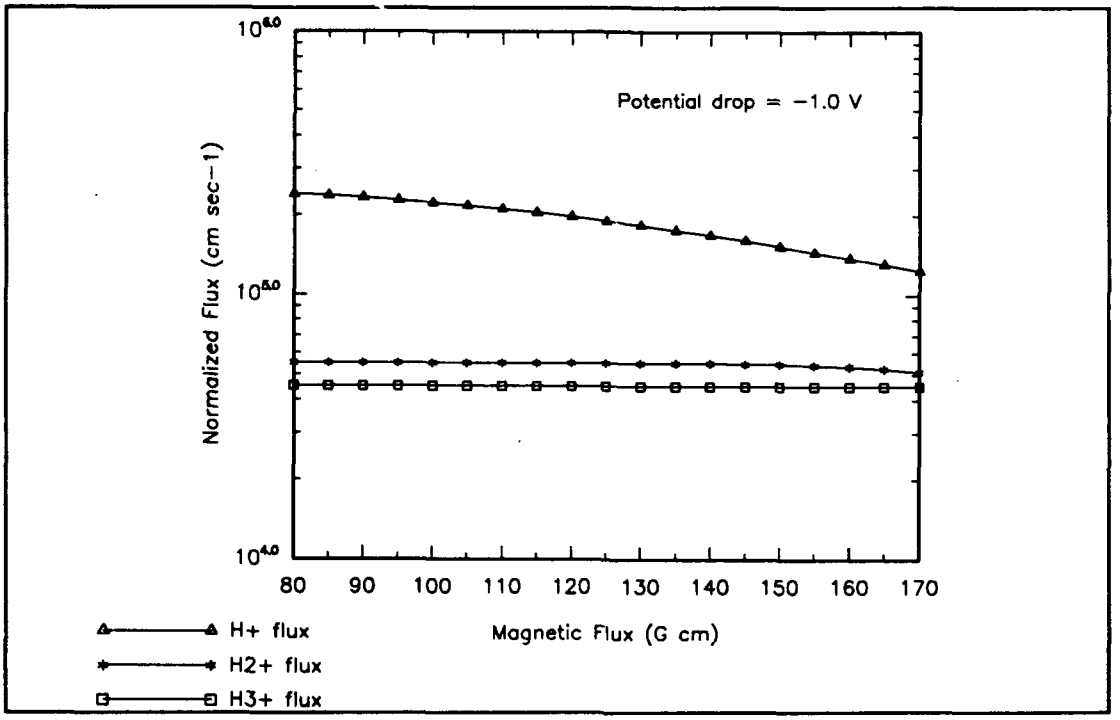

Figure 5-4: Normalized Ion Fluxes for Potential Drop = -1.0 V

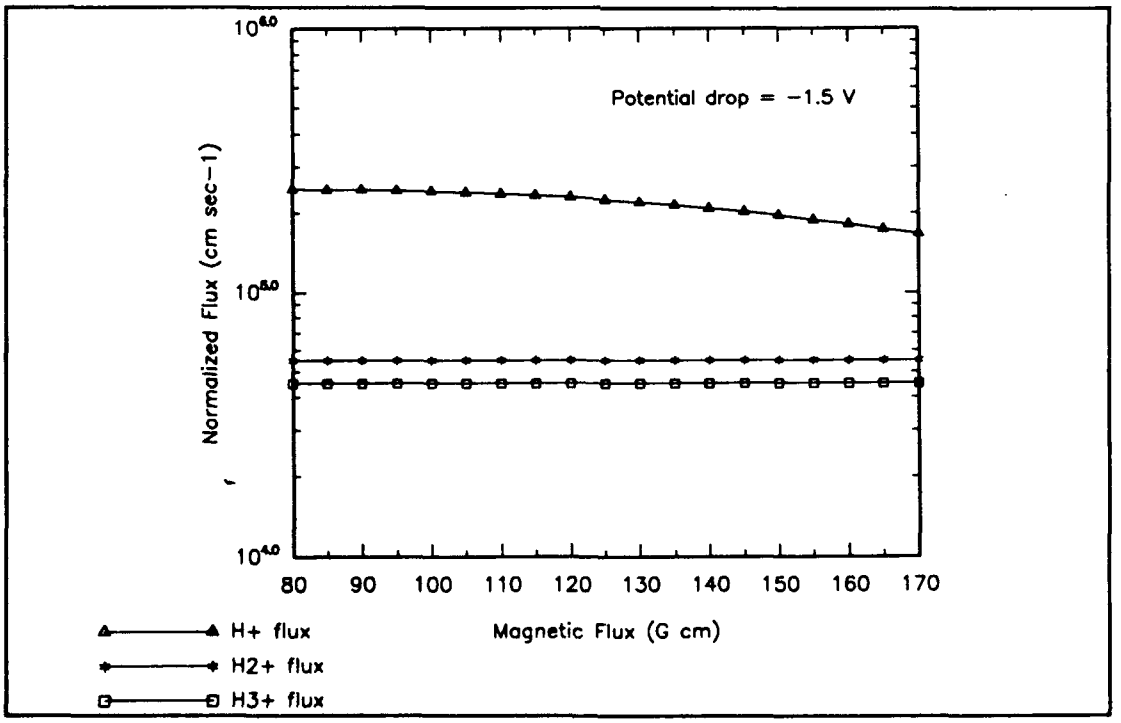

Figure 5-5: Normalized Ion Fluxes for Potential Drop = -1.5 V

$$\Gamma_x^{(i)} = 0.5 n_i^{(2)} \left(\frac{T_e + T_i}{m_i} \right)^{1/2} \tag{5.19}$$

on the other. Here, $n_i^{(2)}$ is the final chamber number density for species i , m_i is the ion mass, and T_e is the electron temperature.

For H^+, the balance equation is simply

$$0.5 n_1^{(2)} \left(\frac{T_e + T_1}{m_1} \right)^{1/2} A_1^b = n_1^{(1)} \left(\frac{T_1}{2\pi m_1} \right)^{1/2} \zeta_1 A_1^f + n_p^{(2)} n_3^{(2)} <\sigma\upsilon(1^+)> V_p^{(2)} \tag{5.20}$$

$$+ n_p^{(2)} N_2 <\sigma\upsilon>_{DI} V_p^{(2)} + n_p^{(2)} n_2^{(2)} <\sigma\upsilon(1^+, H)> V_p^{(2)}$$

A_1^b is the H^+ e .raction chamber wall loss area, A_1^f is the effective area of the filter for H^+ transport, and $V_p^{(2)}$ is the accessible extraction chamber volume for primary electrons.

As stated in Chapter I, the most important production process for H^+ is dissociative ionization of H_2 by primary electron impact. The reaction rate for this process is $<\sigma\upsilon>_{DI} = 3.5 \times 10^{-9}$ cm^3 sec^{-1} (Tawara, 1990: 626). H^+ is also produced by a process wherein primary electrons destroy H_3^+. The reaction rate for this process is $<\sigma\upsilon(1^+)> = 4.2 \times 10^{-7}$ cm^3 sec^{-1} (Tawara, 1990: 629). At high discharge currents dissociative excitation of H_2^+ can become an important source of H^+. The reaction rate for dissociative excitation is $<\sigma\upsilon(1^+,H)> = 1.0 \times 10^{-7}$ cm^3 sec^{-1} (Tawara, 1990: 628).

For H_2^+ the balance equation can be written as

$$0.5n_2^{(2)}\left(\frac{T_e+T_2}{m_2}\right)^{1/2}A_2^b+n_2^{(2)}N_2<\sigma\upsilon(3^+,\mathrm{H})>V_p^{(2)}+ \qquad (5.21)$$

$$n_p^{(2)}n_2^{(2)}<\sigma\upsilon(1^+,\mathrm{H})>V_p^{(2)} = n_2^{(1)}\left(\frac{T_2}{2\pi m_2}\right)^{1/2}\zeta_2 A_2^f+n_p^{(2)}N_2<\sigma\upsilon(2^+)>V_p^{(2)}$$

H_2^+ is lost through the process $H_2 + H_2^+ \rightarrow H_3^+ + H$, for which the reaction rate is $<\sigma\upsilon(3^+,H)> = 1.2 \times 10^{-9}$ cm^3 sec^{-1} (Mordin, 1982: 177). It is formed through direct ionization of H_2 by electron impact. The reaction rate for ionization is written as $<\sigma\upsilon(2^+)> = 3 \times 10^{-8}$ cm^3 sec^{-1} (Tawara, 1990: 620). This is an order of magnitude larger than the dissociative ionization process which generates H^+ (Mordin, 1982).

For H_3^+, the balance equation is

$$0.5n_3^{(2)}\left(\frac{T_e+T_3}{m_3}\right)^{1/2}A_3^b+n_p^{(2)}n_3^{(2)}<\sigma\upsilon(1^+)>V_p^{(2)}+n_e^{(2)}n_3^{(2)}<\sigma\upsilon>_{DR}V_3^{(2)} = \qquad (5.22)$$

$$n_3^{(1)}\left(\frac{T_3}{2\pi m_3}\right)^{1/2}\zeta_3 A_3^f+n_2^{(2)}N_2<\sigma\upsilon(3^+,\mathrm{H})>V_p^{(2)}$$

H_3^+ enters the extraction chamber through the filter, is produced from collisions between H_2^+ and H_2, and is lost to the wall and through collisions with primary electrons resulting in the formation of H^+. At high plasma densities, the dissociative recombination process becomes an important H_3^+ loss mechanism. The symbol $n_e^{(2)}$ indicates the density of thermal electrons in the extraction chamber, while $V_3^{(2)}$ is the extraction chamber volume accessible to both thermal electrons and H_3^+. The ap-

proximate reaction rate for dissociative recombination is $<\sigma\upsilon>_{DR}$= 1 x 10^{-7} cm^3/sec (Tawara, 1990: 629) for cold (~0.1 eV) electrons.

Although the electron temperature T_e is shown in the ion-acoustic velocity terms of Eqs (5.20) through (5.22), its value is not well known. Since ions are accelerated by an electric field from the source to the extraction chamber, they should gain kinetic energy in moving through the filter equivalent to the potential fall. It appears appropriate, therefore, to replace T_e in these equations by $-e(\phi_2-\phi_1)$.

Source Chamber Balance Equations and Primary Electron Diffusion. The above equations allow calculation of the extraction chamber species densities under the assumption that certain other information is available. The extraction chamber density of H^+ depends upon the $n_p^{(2)}$, $n_3^{(2)}$ and $n_1^{(1)}$. Similarly, the extraction chamber density of H_3^+ depends upon $n_2^{(2)}$, $n_p^{(2)}$ and $n_3^{(1)}$. And the extraction chamber density of H_2^+ depends upon $n_p^{(2)}$ and $n_2^{(1)}$. In order to have a useful model, therefore, it is necessary to be able to compute the source chamber ion number densities and to calculate the extraction chamber primary electron density from its source chamber value.

The following method will be employed. The source chamber primary electron density is provided by the following generalization of Eq (1.1):

$$\frac{1}{4}n_p^{(1)}\upsilon_p(1-\gamma_p)A_p^a+\Gamma_f^pA_p^f+n_p^{(1)}N_2\sigma_{in}\upsilon_p=I_d/e \qquad (5.23)$$

where σ_{in} is the total inelastic cross section for primary electrons and Γ_f^p is the flux of primary electrons across the filter given by

$$\Gamma_f^p = -\alpha \frac{\nu_p T_p}{m_e \omega_e^2} \frac{dn_p}{dx} \approx \alpha \frac{\nu_p T_p}{m_e \omega_o^2 a} \left(\frac{2}{\pi}\right)^{1/2} n_p^{(1)} \tag{5.24}$$

where α is an enhancement factor inserted to raise the predicted final chamber primary electron density to its measured value. Without a large α (α about 10 or more), the extraction electrode cannot float at the measured high values. Also, a is, as in previous chapters, the characteristic width of the filter magnetic field and ω_o is the maximum filter electron cyclotron frequency.

Given the source chamber primary electron density, source chamber ion densities may be calculated. The H^+ source chamber density is given by the equation

$$0.5 n_1^{(1)} \left(\frac{T_e + T_1}{m_1}\right)^{1/2} A_1^a + n_1^{(1)} \left(\frac{T_1}{2\pi m_1}\right)^{1/2} \zeta_1 A_1^f = n_p^{(1)} n_3^{(1)} <\sigma\upsilon(1^+)> V_p^{(1)} \tag{5.25}$$

$$+ n_p^{(1)} N_2 <\sigma\upsilon>_{DI} V_p^{(1)} + n_p^{(1)} n_2^{(1)} <\sigma\upsilon(1^+, H)> V_p^{(1)}$$

where A_1^a is the anode loss area for H^+. H^+ is lost to the anode and through the filter, but is created through destruction of H_3^+ by primary electrons, dissociative ionization of H_2, and dissociative excitation of H_2^+.

The H_2^+ source chamber balance equation is

$$0.5 n_2^{(1)} \left(\frac{T_e + T_2}{m_2}\right)^{1/2} A_2^a + n_2^{(1)} \left(\frac{T_2}{2\pi m_2}\right)^{1/2} \zeta_2 A_2^f \tag{5.26}$$

$$+ n_2^{(1)} N_2 <\sigma\upsilon(3^+, H)> V_p^{(1)} + n_p^{(1)} n_2^{(1)} <\sigma\upsilon(1^+, H)> V_p^{(1)} = n_p^{(1)} N_2 <\sigma\upsilon(2^+)> V_p^{(1)}$$

H_2^+, like H^+, is lost to the anode and through the filter. It is also

lost through collisions with H_2 producing H_3^+ and by dissociative excitation producing H^+. H_2^+ is produced by direct ionization of H_2.

For H_3^+ the source chamber particle balance is

$$0.5n_3^{(1)}\left(\frac{T_e+T_3}{m_3}\right)^{1/2}A_3^a+n_3^{(1)}\left(\frac{T_3}{2\pi m_3}\right)^{1/2}\zeta_3 A_3^f+n_e^{(1)}n_3^{(1)}<\sigma\upsilon>_{DR}V_3^{(1)} \qquad (5.27)$$

$$+n_p^{(1)}n_3^{(1)}<\sigma\upsilon(1^+)>V_p^{(1)}=n_2^{(1)}N_2<\sigma\upsilon(3^+,H)>V_p^{(2)}$$

H_3^+ is also lost to the anode and through the filter. In addition, it is lost by dissociative recombination and through interactions with primary electrons which produce H^+. H_3^+ is produced in the destruction of H_2^+ upon collisions with H_2.

These source chamber values of ion densities allow computation of the ion fluxes into the extraction chamber. Several of the ion production processes in the extraction chamber depend upon the density of primary electrons in the extraction chamber. This density is calculated by equating the primary electron flux into the extraction chamber, as given by Eq (5.24), to the primary electron flux to the extraction electrode. (This will be an accurate scheme as long as the dominant loss mechanism for the primary electrons in the extraction chamber is to the walls.) The result is

$$n_p^{(2)}=\alpha\left(\frac{\nu_p T_p}{m_e\omega_o^2 a}\left(\frac{m_e}{T_p}\right)^{1/2}n_p^{(1)}\exp\left(-\frac{V_b-\phi_2}{T_p}\right)\frac{1}{(1-\gamma_p)}\frac{A_p^f}{A_p^b}\right) \qquad (5.28)$$

Since the floating potential is unknown in general, an initial guess is made. The extraction chamber ion densities $n_1^{(2)}$, $n_2^{(2)}$ and $n_3^{(2)}$ are cal-

culated from Eqs (5.20) to (5.22). Then the floating potential is calculated again from the balance of current to the extraction electrode:

$$n_p^{(2)}\left(\frac{T_p}{2\pi m_e}\right)^{1/2}\exp\left(\frac{V_b-\phi_2}{T_p}\right)(1-\gamma_p)A_p^b+n_e^{(2)}\left(\frac{T_e}{2\pi m_e}\right)^{1/2}\exp\left(\frac{V_b-\phi_2}{T_e}\right)A_e^b = \tag{5.29}$$

$$0.5\{n_1^{(2)}\left(\frac{T_e+T_1}{m_1}\right)^{1/2}+n_2^{(2)}\left(\frac{T_e+T_2}{m_2}\right)^{1/2}+n_3^{(2)}\left(\frac{T_e+T_3}{m_3}\right)^{1/2}\}A_I^b(1+\gamma_I)$$

The extraction chamber primary electron density $n_p^{(2)}$ is then recalculated from Eq (5.28) given the revised V_b (ϕ_2 is assumed to be comparatively small, about 1.5 V), the extraction chamber positive ion densities are computed again from Eqs (5.20) to (5.22) given the revised $n_p^{(2)}$, and the floating potential V_b is calculated again from Eq (5.29) *etc.*, until consistency is achieved.

Results and Predictions

Comparison with Table 5-1. Figure 5-6 shows the extracted species percentages predicted by the model described in the previous section for a particular selection of the relevant parameters: ion temperatures, wall loss areas, difference in potential between the chambers as a function of the magnetic flux, and primary electron diffusion enhancement factor α. The ion temperatures were assumed roughly equal to the ion energy upon formation: 0.40 eV for H^+, 0.04 eV for H_2^+ and 0.10 eV for H_3^+. The wall loss area for primary electrons to the anode is taken to be 10 cm^2 based upon the estimated leak width of $4(r_e r_I)^{1/2}$ (where $r_{e/I}$ is the electron/ion Lamor radius) given by Cho (Cho, 1990), while

the loss area to the plasma electrode is assumed to be 250 cm^2. The positive ion loss areas are taken equal to the primary electron loss areas for all species, as are the accessible volumes. The ratio V/A appearing in the figures to follow is the ratio of the accessible volume to the filter or extraction electrode area, the two being assumed equal. V/A is 20 cm in the source chamber and 6 cm in the extraction chamber. These values for V/A are used since Leung and Ehlers state the source chamber together with the filter region in their device is 24 cm long, while the extraction chamber is 6 cm long (Ehlers, 1982b). Since primary electrons and ions are inhibited from entering the end-wall confinement magnetic field in the source chamber, 20 cm seems a reasonable source chamber V/A.

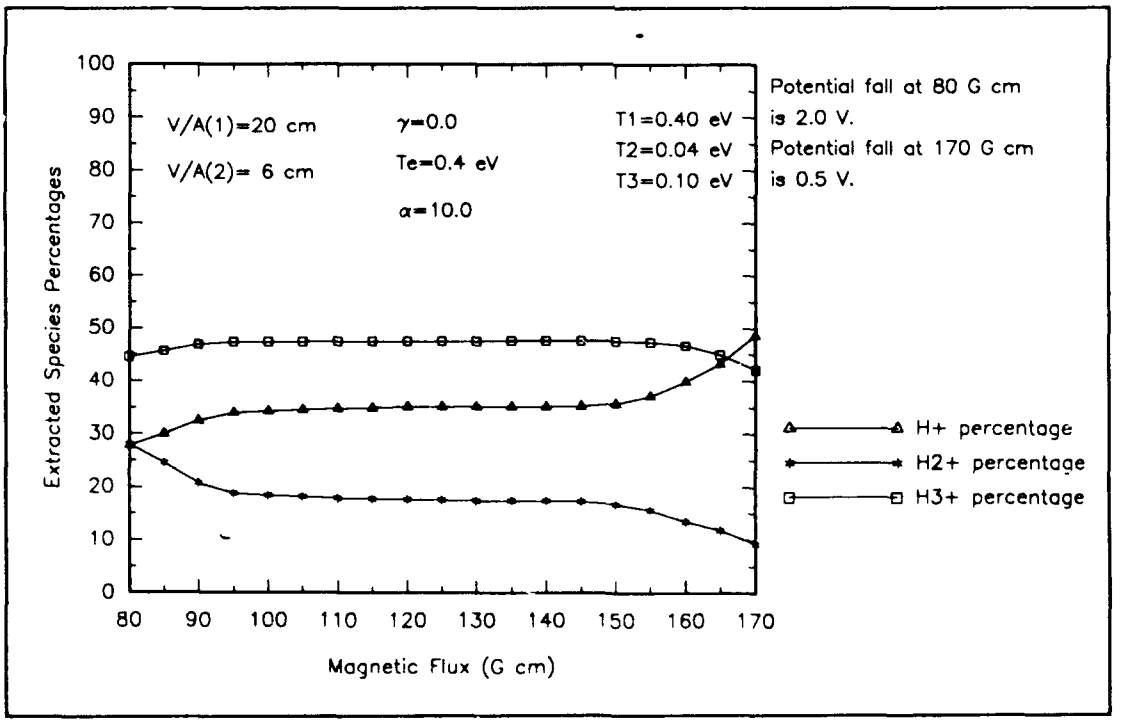

Figure 5-6: Extracted Positive Ion Species versus Magnetic Flux

The potential difference between the two chambers is assumed to be 0.5 V at a magnetic flux of 170 G cm and 2.0 V at 80 G cm (varying linearly with magnetic flux between these values) during the comparison of the model with the data of Table 5-1. This choice of potential fall dependence is motivated by the observation that the potential difference between the chambers increases as the potential applied to the extraction electrode is lowered (see Fig 1-5). Also, it was known that the potential difference between the two chambers had been measured at 1.5 V at 104 G cm (Ehlers, 1982b).

Later, the extracted ion species percentages will be compared with measurements for a single filter (Figure 5-10). In that instance, the potential difference between the chambers is taken to be 1.6 V. In the next subsection, the source is assumed operated with V_b at the plasma potential, and the plasma potential difference is taken to be zero.

The primary electron diffusion enhancement factor α used in the calculations to follow is 10. The only non-zero secondary electron emission coefficient γ used in any of these calculations is that for primary electrons: this is the γ appearing in the figures.

The discharge current is 10 A, as in Table 5-1.

Ions are assumed to exit the plasma with a velocity determined largely by the energy gained in passing from the source to the extraction chambers. The ion velocity is assumed to be equal to

$$v_j = 0.5\left(\frac{-e\phi + T_j}{m_j}\right)^{1/2} \tag{5.30}$$

for ion species j, as long as the difference in potential is larger than the extraction chamber electron temperature.

Figure 5-7 gives the calculated extraction electrode floating potential for the primary electron diffusion enhancement factor α equal to 10. The floating potential here assumes a value of -2 V at about 95 G cm. The data of Table 5-1 show the floating potential at -10 V when the magnetic flux was 104 G cm. This indicates that the primary electron diffusion enhancement factor is somewhat higher than 10. At 89 G cm, the floating potential is -15 V for the narrow, higher-peaked filter (Filter 1) and -25 V for the lower, broader filter (Filter 4). The result shown in Figure 5-7 (-15 V) is consistent with these measurements. (In the calculation of primary electron diffusion, the width factor a was assumed equal to 4 cm. This width agrees reasonably well with the geometry of Filter 1.)

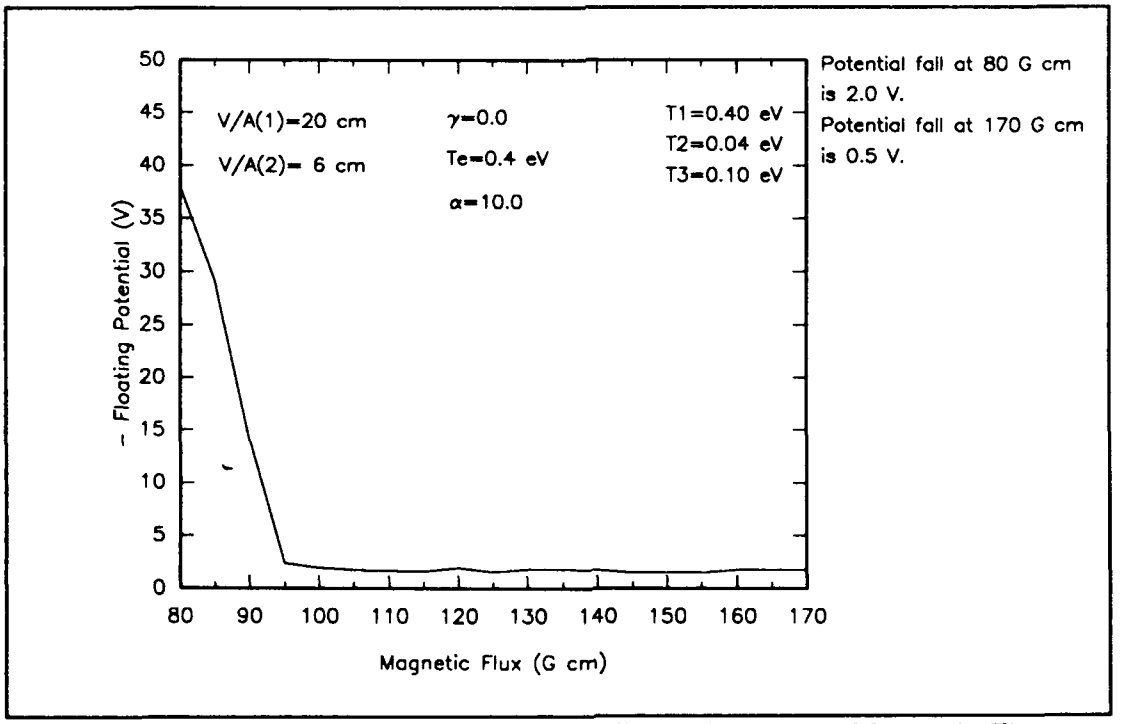

Figure 5-7: Plasma Electrode Floating Potential versus Magnetic Flux

The fair agreement between the measured values of the floating potential and those calculated here reinforce the argument made in an earlier section of this chapter that the rate of diffusion of primary electrons must be enhanced over the classical value by a factor of about 10.

The rapid fall in floating potential at low values of the magnetic flux, caused by the decrease in primary electrons in the extraction chamber, results in rapid variations in the extracted species percentages. At values of the magnetic flux higher than 95 G cm, the floating potential is fairly constant, as are the extracted ion species percentages. Since the potential difference between the chambers is assumed to vary linearly from 2.0 V at 80 G cm to 0.5 V at 170 G cm, at about 150 G cm, the magnetic flux has become strong enough, and the potential fall weak enough, to begin to effect the ion motion. The high H^+ temperature and low mass hold the H^+ flux through the filter high, while first the H_2^+ flux and then later, at higher magnetic fluxes, the H_3^+ flux, fall more rapidly. It is plausible that accurate knowledge of the variation in potential gradient with magnetic flux and filter field width would give better results.

The general features of Figure 5-6 correspond to those of Table 5-1. The H_3^+ percentage falls over a range of the magnetic flux, as the measurements show. The H^+ percentage is an increasing function of magnetic flux, as shown in Table 5-1, and the H_2^+ percentage is a decreasing function of magnetic flux, in agreement with measurements. The percentages themselves are in good agreement with measured values. Table 5-3 compares the measured percentages of Table 5-1 with those predicted by this model.

Filter	Measured $H^+:H_2^+:H_3^+$	Predicted $H^+:H_2^+:H_3^+$
1	30:17:53	33:20:47
2	41:15:44	44:12:44
3	35:19:46	35:18:47
4	26:25:49	33:20:47

Table 5-3: Measures vs Predicted Species Percentages

Figure 5-8 shows the species percentages resident in the extraction chamber for the extracted percentages shown in Figure 5-6. This demonstrates that H_3^+ is still the dominant ion in the plasma even when H^+ is most abundant in the extracted beam.

Several other relevant results: the extraction chamber ion density remains near 4 x 10^{10} cm^{-3} for all values of the magnetic flux, while the source chamber ion density rises gently from 1.9 x 10^{11} cm^{-3} at 80 G cm to 2.3 x 10^{11} cm^{-3} at 170 G cm. (Holmes has measured an increase in source chamber plasma density with increasing magnetic flux.) The extraction chamber primary electron density falls from 2.6 x 10^8 cm^{-3} at 80 G cm to 6.2 x 10^7 cm^{-3} at 170 G cm. The source chamber primary electron density is nearly constant, rising gradually from 1.8 x 10^9 cm^{-3} at 80 G cm to 1.9 x 10^9 cm^{-3} at 170 G cm.

Figure 5-9 is included here to show the effect of a lower H^+ temperature on extracted species densities. With the three ion temperatures equal to the gas temperature (0.04 eV), the species percentage profiles are radically altered. The H^+ percentage falls at high magnetic flux due to the severe diminishment of H^+ flux through the filter. The clear

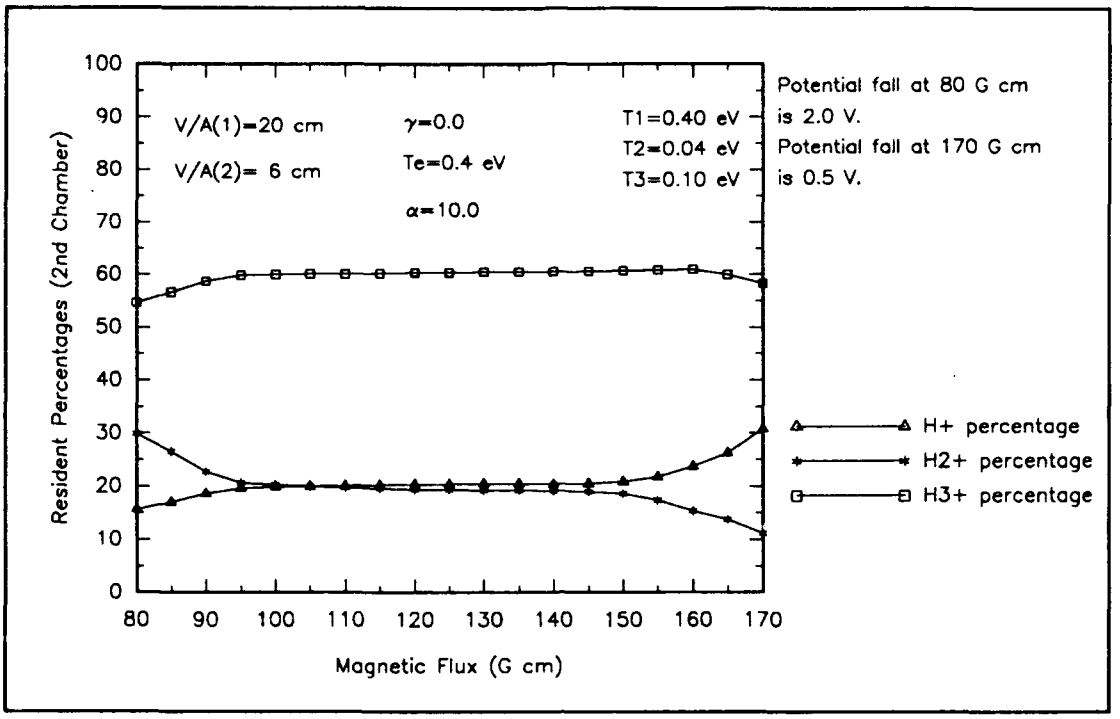

Figure 5-8: Resident Species Percentages versus Magnetic Flux

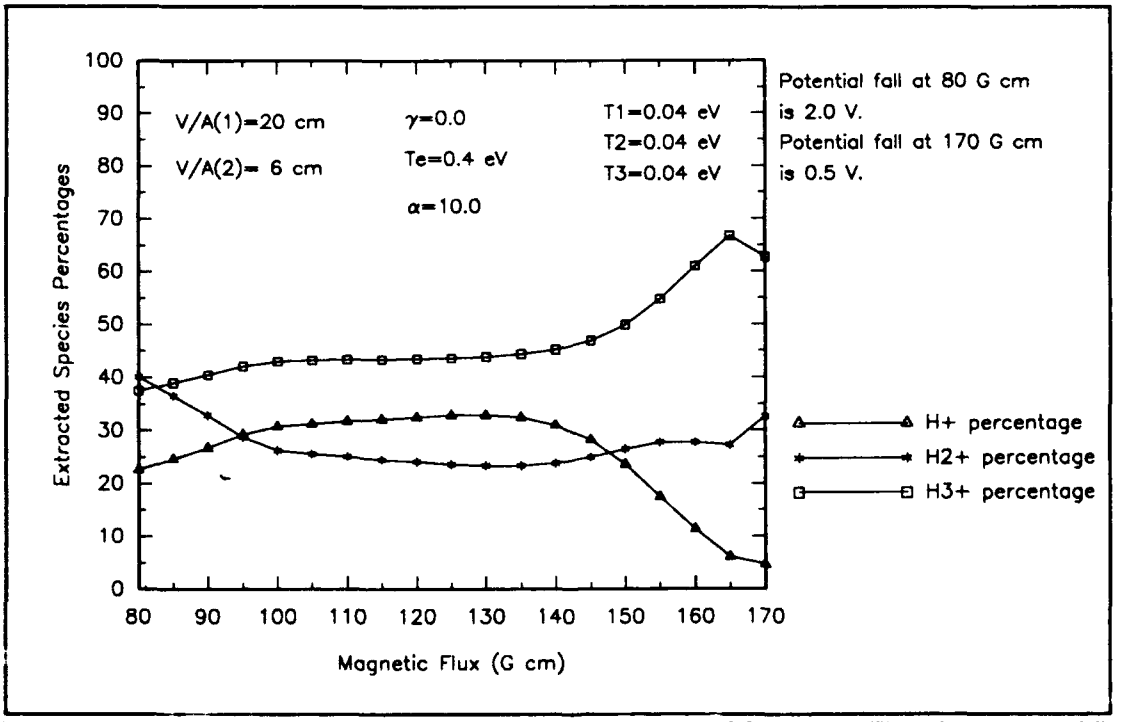

Figure 5-9: Extracted Species Percentages versus Magnetic Flux (T_f=0.04 eV)

implication is that the H^+ temperature must be high relative to that of other positive ion species to account for the observed extracted species percentages: the fall in H^+ percentage at high magnetic flux is not observed experimentally (Figure 1-15).

In Figure 5-10, the extracted species percentages are shown for Filter 3 as a function of the discharge current for the same choice of ion and electron temperatures as above, and for a potential difference between the chambers of 1.6 V (in accordance with the linear variation described above, and nearly equal to the quoted value of 1.5 V (Ehlers, 1982b)), all assumed to be independent of the discharge current. This figure closely resembles the measured ion extraction percentage curves, which were presented earlier in Figure 1-15, and are reproduced here for comparison. The most significant discrepancy between the model and measurement is in the relatively low predicted H^+ percentage and the relatively high H_3^+ percentage at high discharge currents. This discrepancy also resulted in Chan's positive ion model (Chan, 1983). Chan's model is more comprehensive than the model presented here, but was developed for positive ion sources without filters, and so does not include transport between chambers. Chan attributed the discrepancy at high discharge currents to an underestimate of the probability that positive ions form H_2 at the walls. This possibility was discounted completely in the present model since the primary interest here is low discharge current sources.

The agreement with experiment shown here may be taken as indirect verification of the ion and primary electron transport models developed in this chapter. The ion density model may now be applied

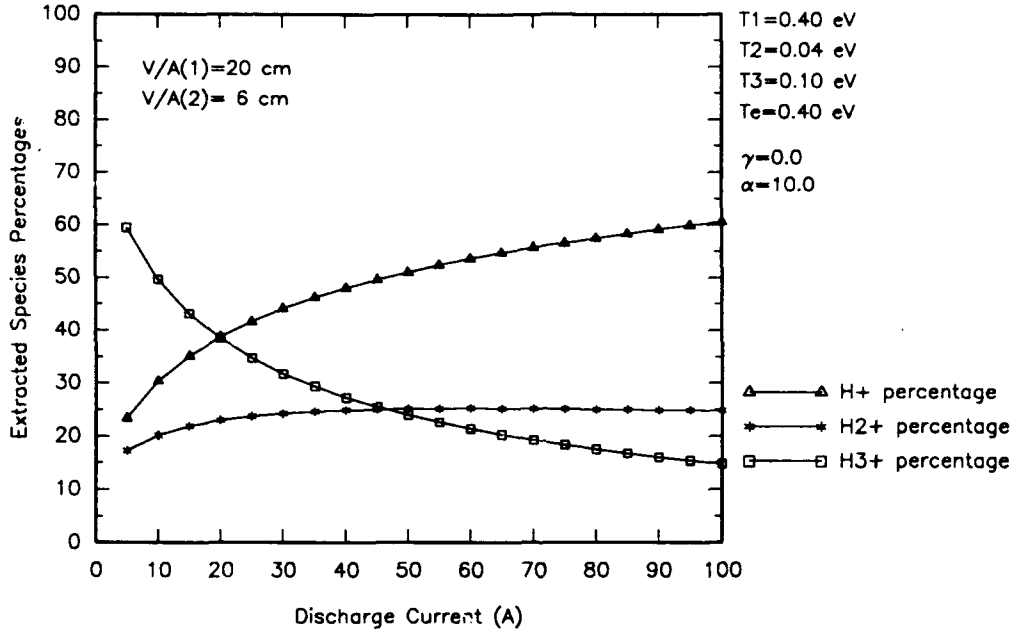

Calculated Extracted Species Percentages versus Discharge Current

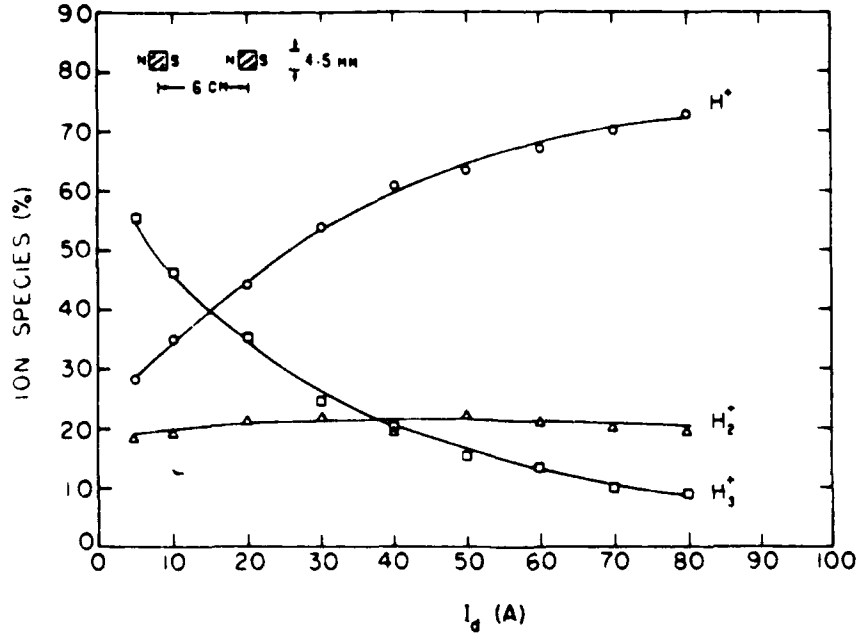

Measured Extracted Species Percentages versus Discharge Current

Figure 5-10: Comparison of Calculated and Measured Species Percentages

to a more interesting case, that of a source configured for extraction of negative hydrogen ions.

Predictions and Implications for Negative Hydrogen Ion Sources. The discussion above was an attempt to validate the ion transport model by direct comparison with experimental data. Here, the model is assumed to be valid, and it will be applied to a source whose extraction electrode is at or near the extraction chamber plasma potential. As discussed in earlier chapters, this is the normal configuration used when negative hydrogen ions are extracted. When the extraction electrode potential is raised so that it approaches the extraction chamber plasma potential, the potential profile is flattened and the negative hydrogen ions can approach the extraction electrode.

When the extraction electrode is held at a fixed value, it is no longer necessary to calculate the extraction chamber primary electron density, floating potential and positive ion density together in an iterative manner. Instead, the primary electron density is calculated directly from Eq (5.28) given the known difference between the plasma potential and extraction electrode potential.

Figure 5-11 shows the predicted variation in extracted ion species percentages as a function of magnetic flux for the case where the extraction electrode is at plasma potential and the plasma potential profile between the two chambers is flat. This figure may be compared with Figure 5-9 (the difference in the secondary electron emission coefficient is negligible, and all other parameters are identical). The model indicates that H^+ will be the dominant extracted species at rather low values

of the magnetic flux when the source is operated with a flat potential profile.

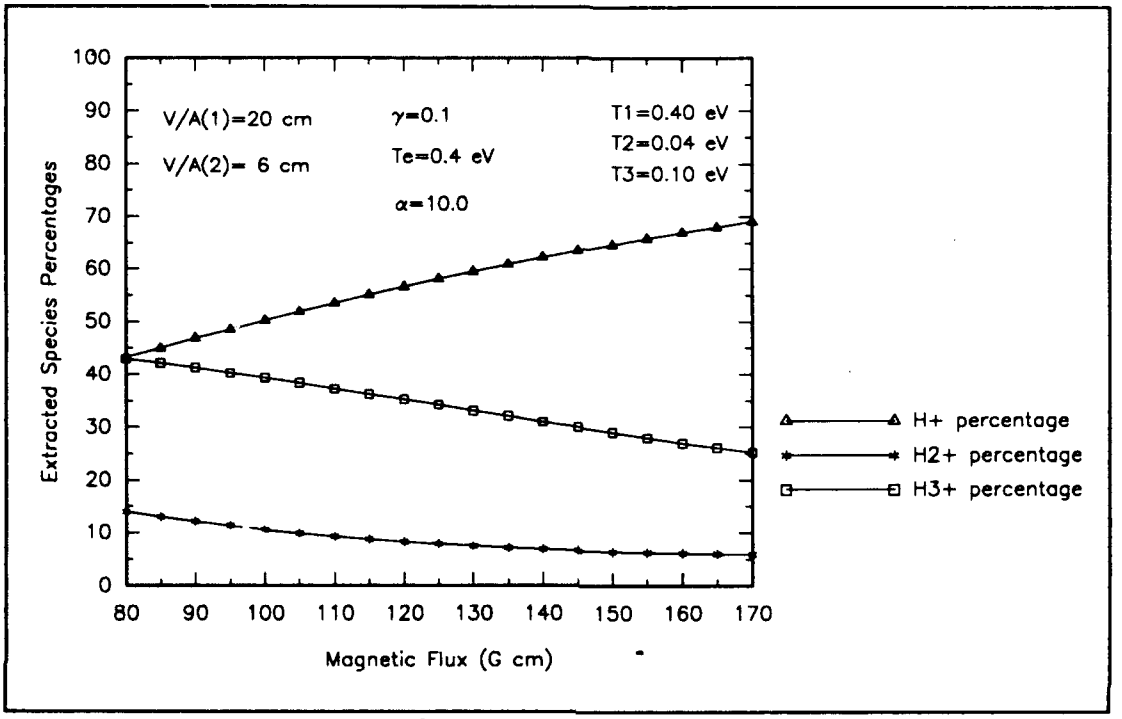

Figure 5-11: Extracted Species Percentages versus Magnetic Flux

Of more relevance to the stoichiometry of the source is the predicted resident species percentages in each chamber. Figure 5-12 shows the resident source chamber ion species percentages as a function of magnetic flux while Figure 5-13 does the same for the extraction chamber. From Figure 5-12 it is clear that H_3^+ is the dominant positive ion in the source chamber for all values of the magnetic flux at this discharge current (10 A).

Figure 5-14 indicates total positive ion densities for each chamber. The source chamber density should be a nearly constant function of magnetic flux, while the extraction chamber density decreases by a factor

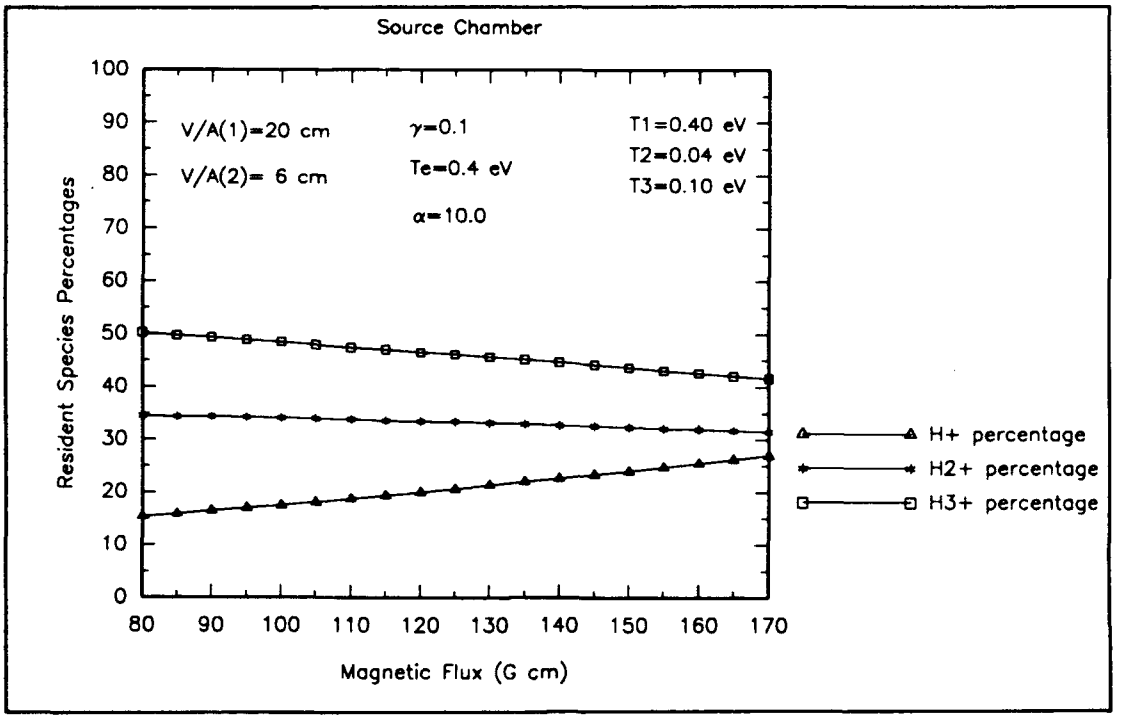

Figure 5-12: Percentages versus Magnetic Flux (Source Chamber)

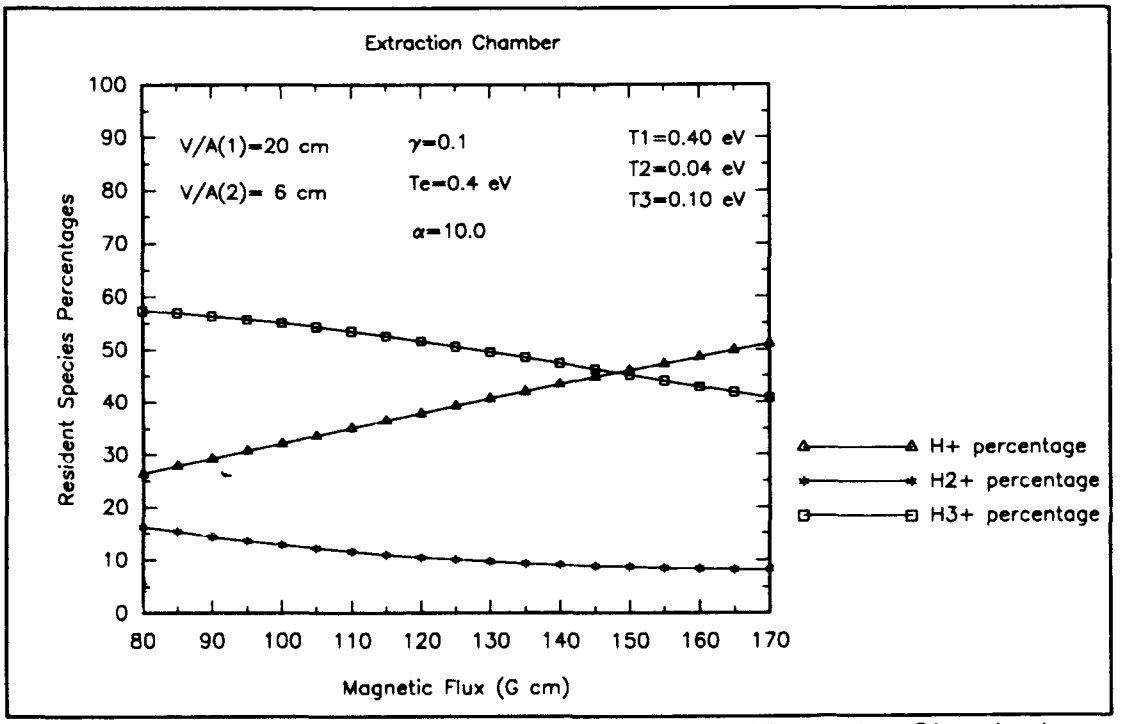

Figure 5-13: Percentages versus Magnetic Flux (Extraction Chamber)

of 3 to 4. This is certainly different from the measurements made by Holmes (Holmes, 1982a) shown earlier in Figure 1-9. There it was found that the source chamber density was an increasing function of the magnetic flux while the extraction chamber density was constant. The difference may be attributed to the fact that, under Holmes' experimental conditions, the plasma potential profile was not flat.

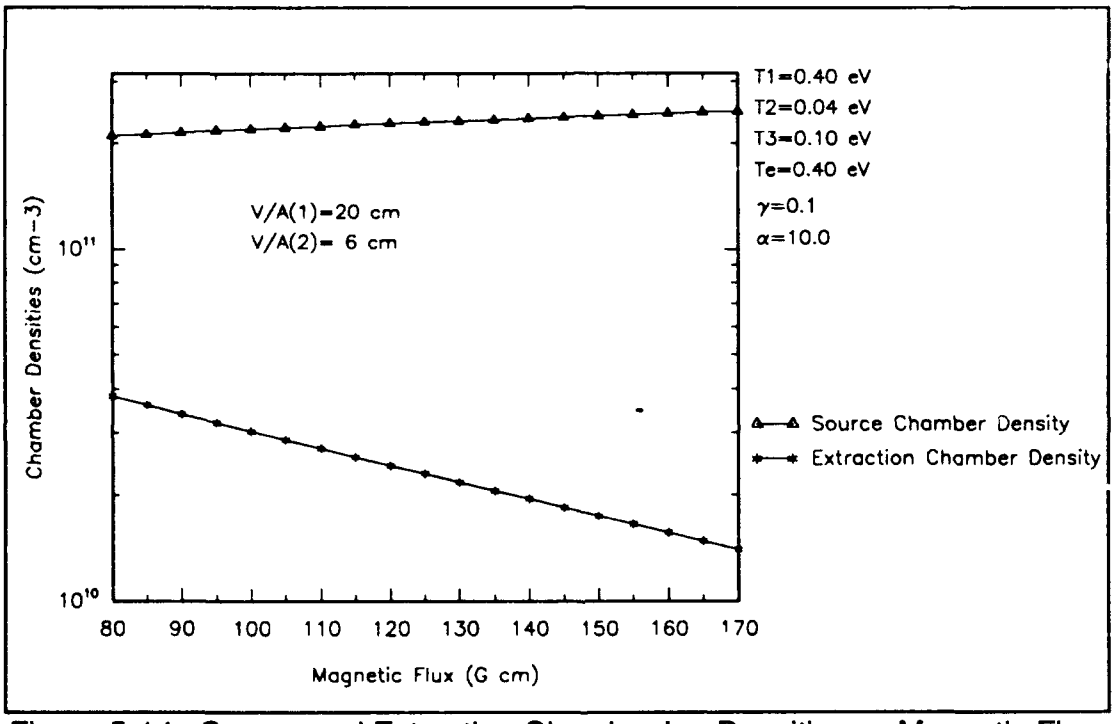

Figure 5-14: Source and Extraction Chamber Ion Densities vs Magnetic Flux

Figure 5-15 indicates the source and extraction chamber values of the primary electron density, given the enhancement factor $\alpha = 10$. The source chamber density is nearly constant, indicating that, even with the enhancement, filter diffusion is not the dominant primary electron loss mechanism. The decline in extraction chamber primary electron

density with increasing magnetic flux is due to the falling primary electron flux across the filter.

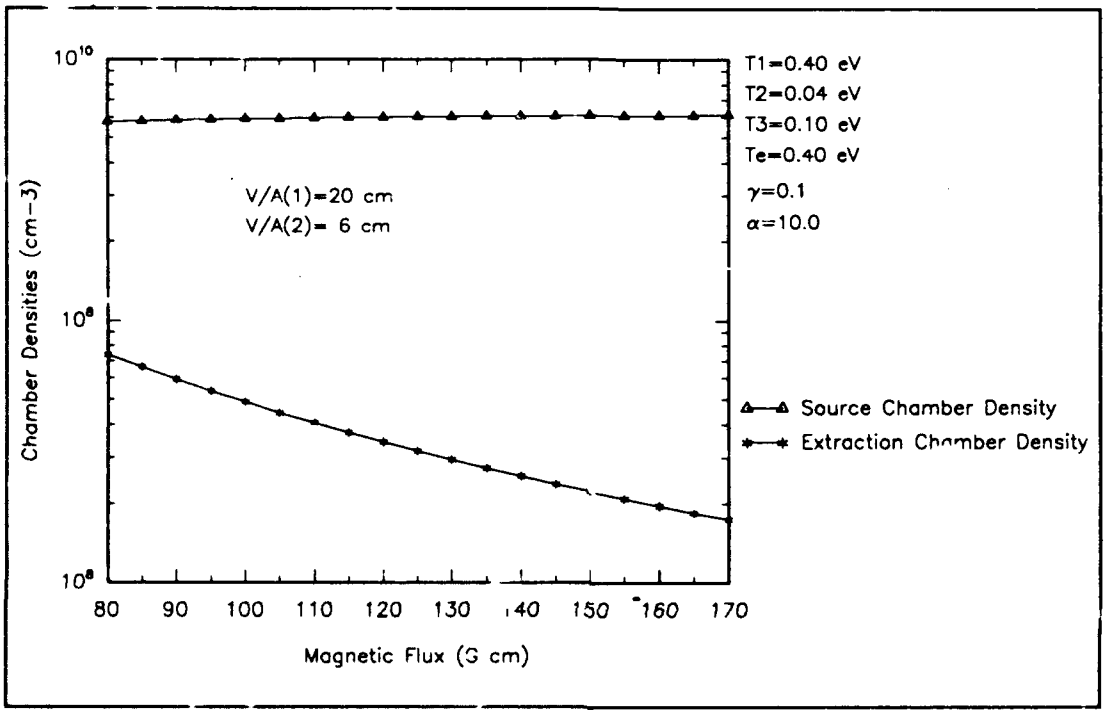

Figure 5-15: Primary Electron Densities vs Magnetic Flux (Two Chambers)

Experimentally, it is doubtless easier to vary the discharge current than the magnetic induction. Figure 5-16 shows the dependence of extracted positive ion species densities upon the discharge current (for a magnetic induction of 100 G cm). As compared to Figure 5-10, the H_2^+ percentage here is considerably lower.

Figures 5-17 and 5-18 display the resident species percentages in the source and extraction chambers respectively. Figures 5-19 and 5-20 show the source and extraction chamber densities of positive ions and primary electrons.

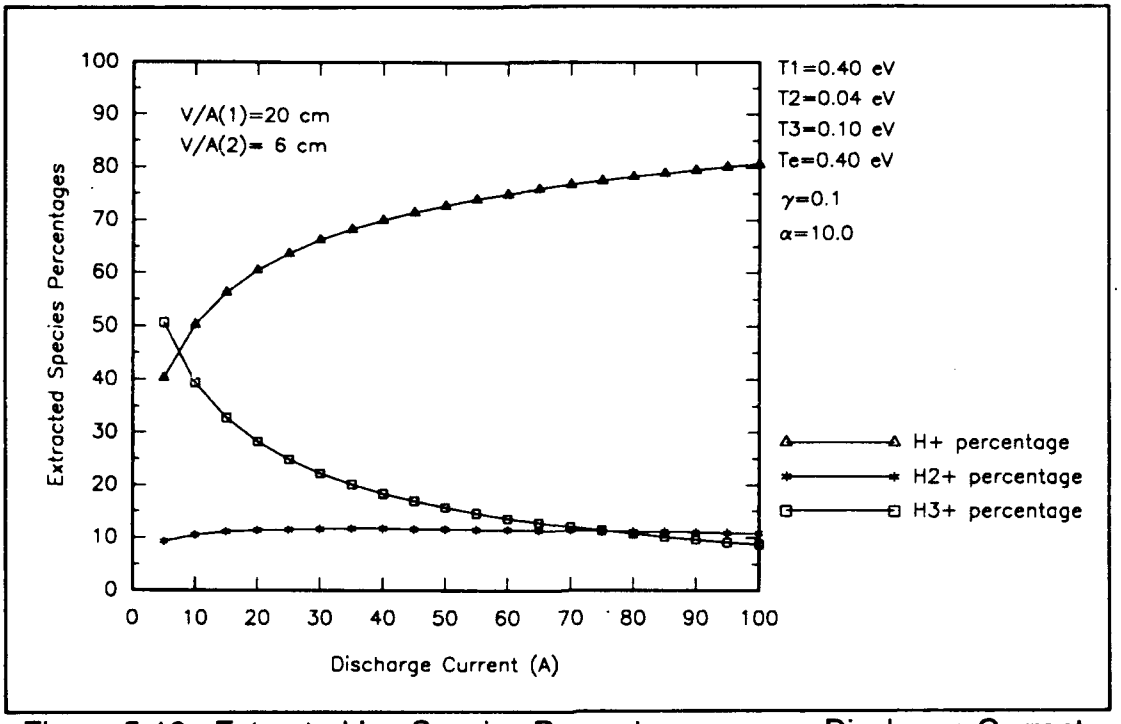

Figure 5-16: Extracted Ion Species Percentages versus Discharge Current

In the positive ion density model, the effect of negative hydrogen ions on the positive ion species' densities has been ignored. For the experiment used to test the model (Ehlers, 1982b), this is probably not a poor simplification. There, primary electrons existed in abundance in both chambers, and consequently the H^- density was probably quite low. When the model is used to predict positive ion densities at high magnetic inductions where the primary electron density in the extraction chamber is low and the H^- density can carry a sizeable fraction of the negative charge in the plasma, the effect of negative hydrogen ions should be included. This cannot be done rigorously, since the H^--H_3^+ neutralization rate has not been measured (Hiskes, 1984). It is possible, however, to draw certain general conclusions about both the effect of large pro-

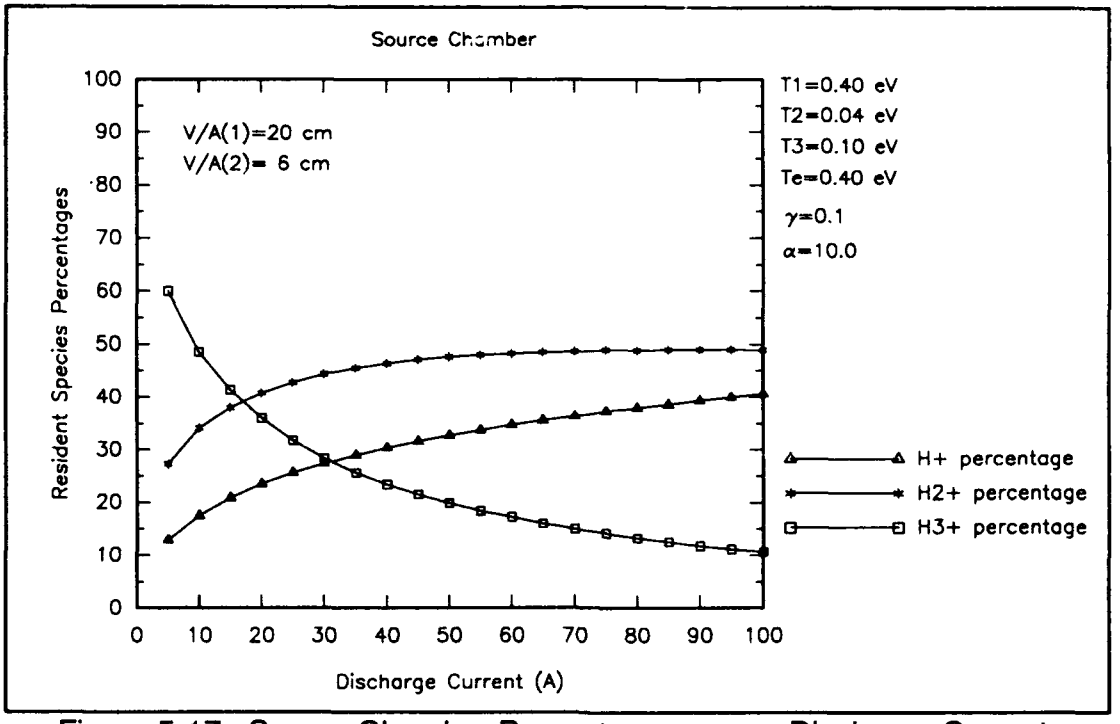

Figure 5-17: Source Chamber Percentages versus Discharge Current

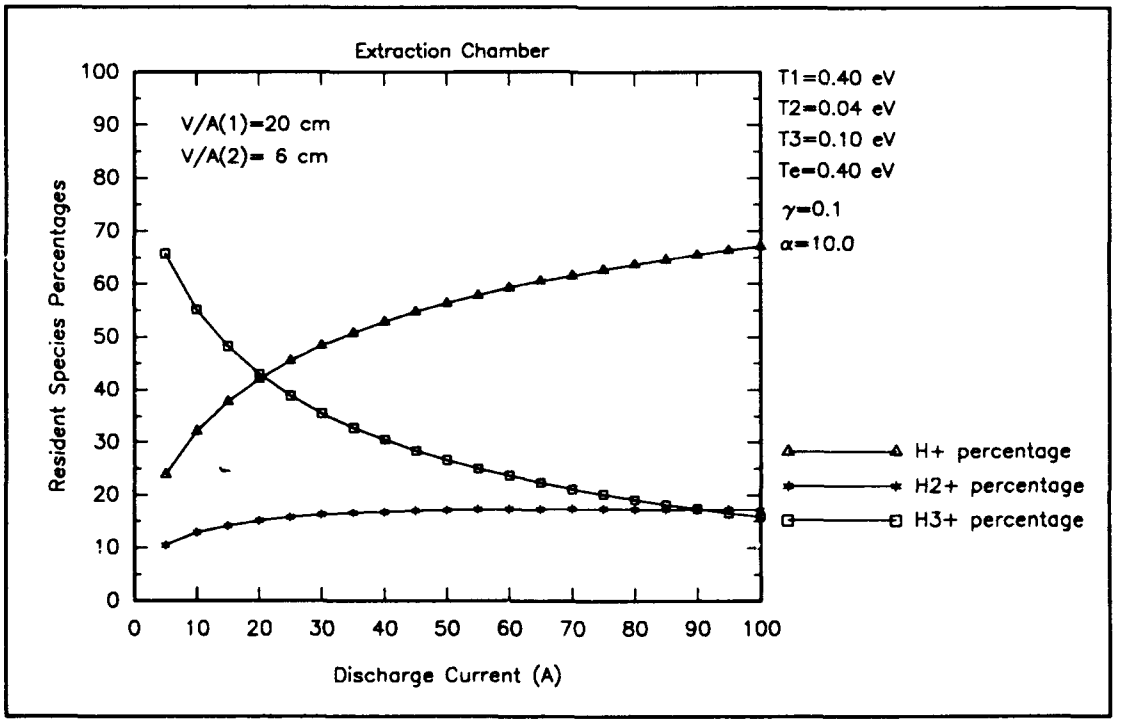

Figure 5-18: Extraction Chamber Percentages versus Discharge Current

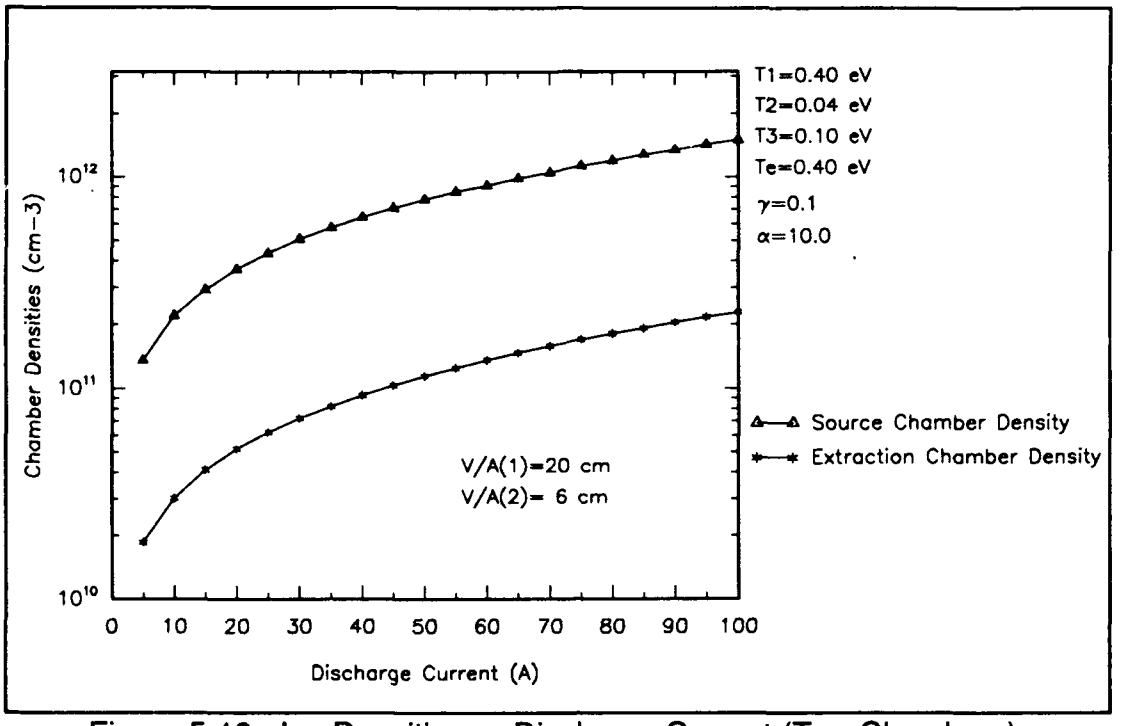

Figure 5-19: Ion Densities vs Discharge Current (Two Chambers)

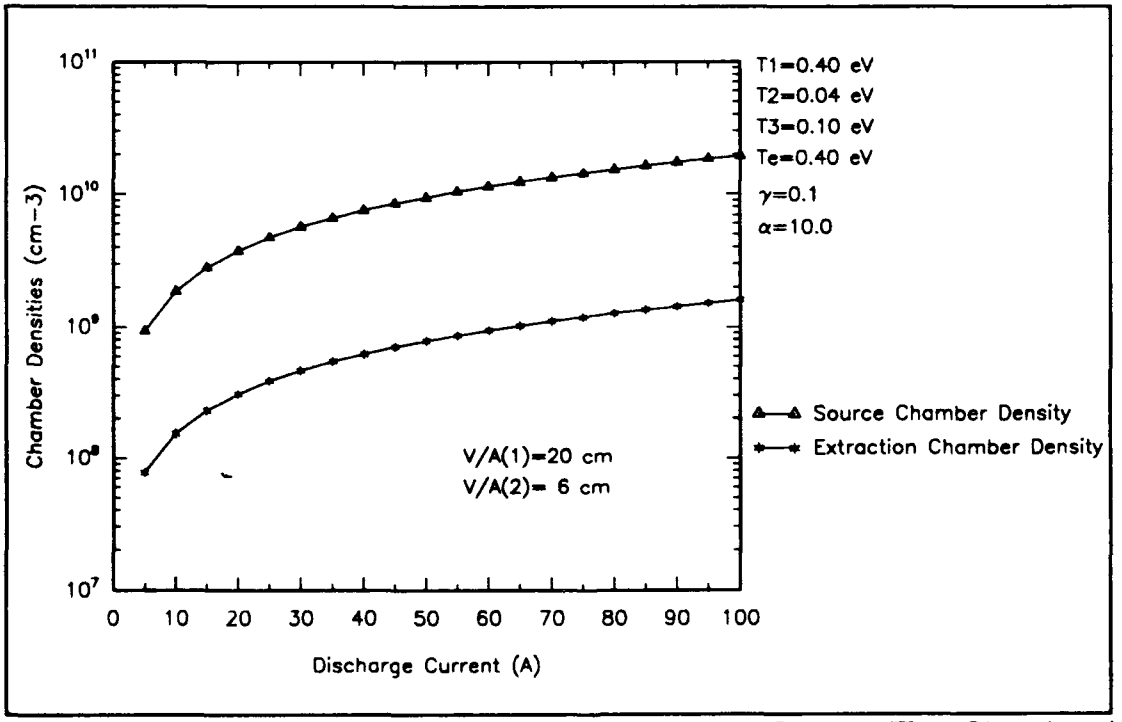

Figure 5-20: Primary Electron Densities vs Discharge Current (Two Chambers)

portions of H^- on the resident positive ion species percentages and the effect of the particular distribution of positive ions on the H^- density.

First, the effect of ion-ion neutralization on the positive ion distribution is slight to nonexistent. The ion-ion neutralization loss rate must be comparable to the positive ion wall loss rate in the extraction chamber for the presence of H^- to be important. For H^+, the ion acoustic velocity is 4.4×10^5 cm/sec. The reaction rate for H^+-H^- neutralization for an interaction energy of 0.3 eV is 3×10^{-8} cm^3/sec (Mordin, 1983), so, with an extraction chamber ratio of volume to area of 6 cm, the density of H^- must exceed 10^{12} cm^{-3} for neutralization to be the dominant loss mechanism. Since the H^- density is usually closer to 10^{10} cm^{-3}, this neutralization process may be ignored.

For H_2^+, the ion acoustic velocity is 2.3×10^5 cm/sec. With an interaction energy of 0.1 eV, the reaction rate for H_2^+-H^- neutralization is about 10^{-7} cm^3/sec. The neutralization loss is smaller than the wall loss as long as the density of negative hydrogen ions is beneath 4×10^{11} cm^{-3}, so in this case also the presence of H^- may be ignored.

The same is probably true for H_3^+. The H_3^+ ion acoustic velocity is 2×10^5 cm/sec. The reaction rate for H_3^+-H^- neutralization is unknown, but is probably about 10^{-7} cm^3/sec (Hiskes, 1984). Thus, the neutralization loss is smaller than wall loss if the H^- density is below about 10^{11} cm^{-3}. In this case the presence of H^- may be ignored. It should be noted that the positive ion density model includes the effect of H_3^+ neutralization due to dissociative recombination with thermal electrons. The reaction rate for dissociative recombination is also about

10^{-7} cm^3/sec, so the correction for neutralization by H^- will be extremely small.

Second, the H^- density is diminished most severely by neutralization with H_3^+. This statement is based on the (speculative) supposition that the H_3^+-H^- neutralization rate is somewhat higher than the neutralization rate for either of the two positive ion types. Plainly, to minimize the loss of H^- through neutralization, it is advantageous to operate the source with a high concentration of H^+. From Figures 5-17 and 5-18 it is plain that higher discharge currents will provide higher relative concentrations of H^+.

To determine properly the optimum discharge parameters, however, requires that the ion density model developed above be expanded to treat the vibrationally excited states of H_2 and the electron distribution function in order to account for other H^- production and loss mechanisms. Such an effort is beyond the scope of this project, whose primary concery is the transport of plasma constituents across the filter magnetic field.

Chapter VI - Summary

Overview of Results

This has been an analysis of charged particle transport in magnetic multicusp negative hydrogen ion sources. The primary interest has been in low power discharges - with H_2 densities of 10^{13} cm^{-3}, plasma densities about 10^{11} cm^{-3}, and discharge currents of 10 A or less - because of the relative copious data in that regime.

The transport of low temperature (~ 1 eV) electrons across the magnetic filter has been of primary interest, since the evidence suggests that classical diffusion theory underestimates the actual electron flux by one to three orders of magnitude. In Chapter II, data from an experiment performed by Leung and Bacal (Leung, 1984b) were analyzed to show that the electron flux through the magnetic filter exceeded the classical electron flux by a factor as large as 350. Measurements by Holmes (Holmes, 1982b) were brought forward to show that the classical electron-ion diffusion rate through the magnetic filter was exceeded by a ratio of about 17. Both of these experiments were performed in hydrogen plasmas confined by multicusp magnetic fields.

Because of limitations in the reported measurements, however, it is difficult to determine the extent of the enhancement to electron diffusion. In the Leung experiment, source and extraction chamber densities were reported, but no axial variations in density were presented. In order to determine the theoretical electron flux through the magnetic filter, it is necessary to measure the plasma density in the source chamber at a point near the filter plane or to compute the flux directly from

a knowledge of the density gradient and density at each point. To determine the thermal electron flux from the extraction chamber electron density, it is necessary to measure the electron density one mean free path (or electron gyroradius) from the extraction electrode. The reported measurement of the source chamber electron density was, in all likelihood, too high (being measured deep in the source chamber), resulting in an overestimate of the classical electron flux across the filter. But the measured extraction chamber electron density was probably also high, resulting in an excessive electron thermal flux to the extraction electrode. The two effects thus offset one another to some extent.

In Holmes' experiment, the difficulty encountered in attempting to compute the thermal electron flux to the extraction electrode from the extraction chamber electron density was surmounted by measuring, instead, the electron current to the extractien electrode. Here again, however, the density profile from source to extraction chamber was not provided. Instead, the reader is assured that Holmes' theoretical flux through the filter is in agreement with the electron current to the extraction electrode. It seems likely that the electron density used to test Holmes' transport theory was measured deep in the source chamber, indicating that Holmes' theory actually underestimates the collision frequency required to drive electron diffusion across the filter.

Also in Chapter II, evidence was presented from Ferriara's experiment (Ferriara, 1989) of electron diffusion across a magnetic filter in an argon plasma. The Ferriara evidence indicates that, in the argon plasma, electron diffusion is being driven by ion acoustic turbulence. The measured electron diffusion rate exceeded the classical diffusion rate

by three orders of magnitude. The experiment was performed at very low plasma and neutral densities and at high peak filter magnetic inductance, so it is difficult to extrapolate these results to a hydrogen plasma.

Holmes had claimed (Holmes, 1982b) that his diffusion coefficient was, in fact, the classical electron Coulomb diffusion coefficient for a fully ionized gas. It was suspected that Holmes' diffusion coefficient exceeded the classical diffusion coefficient by a factor of $9\pi^{1/2}$, and this suspicion was shown to be true in Chapter III. There, the development of the Fokker-Planck equation was rehearsed in order to determine the meaning of the terms appearing in Holmes' collision frequency derivation. It was concluded that Holmes' approach is not standard, and that it exceeds both the diffusion coefficient obtained from examining the mean square displacement of charged particles upon collision in a magnetic field and that obtained from the momentum moment of the Boltzmann equation. This momentum balance equation was examined in considerable detail to determine whether typically small terms might not be large in the relevant parameter space and so produce an enhancement to the electron flux. No such terms were identified.

Next, the geometry of the source in the filter region was scrutinized to identify electron drifts which could increase the electron current through the filter. The net effect of drifts in the source chamber was shown to inhibit the motion of charged particles toward the extraction chamber.

Anomalous diffusion exhibiting Bohm ($1/B$) scaling has been observed in negative hydrogen ion sources (Jimbo, 1984). The conditions

under which this Bohm scaling was observed appear not to exist in typical tandem magnetic multicusp H^- sources. In general, the theoretical considerations of Okuda (Okuda, 1973) suggest that the Bohm diffusion coefficient arises under conditions of low plasma density and high magnetic induction, or $(\omega_p/\omega_e)^2 \sim 1$ or less. Additionally, observations by Holmes (Holmes, 1982b) and Lea (Lea, 1990) support the view that the electron diffusion coefficient in tandem devices has a classical $1/B^2$ scaling with magnetic induction.

The puzzle, then, is how the electron diffusion can retain its classical scaling and yet be one to three orders of magnitude higher than the classical Coulomb diffusion coefficients would predict. A plausible explanation was discovered: that the electron diffusion is driven by ion acoustic or related turbulence. As long ago as 1978 C. T. Dum had shown that, under conditions of weak turbulence characterized by small phase velocities and short wavelengths, the electron diffusion coefficient can retain its classical functional form and yet display considerable enchancement. In fact, provided that the electron distribution function stays close to Maxwellian and the turbulence is isotropic, the effect of turbulence on electron transport is obtained by substituting enhanced values of Z, ion charge, and T_I, ion temperature, in the classical transport equations (Dum, 1978b). An extremely important implication of this result, in anticipation of the analysis of Chapter IV, is that the temperature gradient term in the expression for the charged particle flux (Eq (3.78)) will act as a drag term, just as it does for Coulomb collisions. The scaling of the collision frequency with magnetic induction and temperature, and the value of the enhancement to the collision frequency, de-

pend upon the energy density of the turbulent spectrum, which in turn is a function of the source of the instability and the damping mechanism. An example was given of Gary's theoretical electron-wave diffusion coefficient (Gary, 1980), which retains the classical $1/B^2$ behavior and is two orders of magnitude higher than the classical diffusion coefficient.

The goal of Chapter IV was twofold: 1) to determine whether the classical functional form of the flux (Eq (3.78)) properly describes electron transport through the filter given electron temperature gradient variations, and 2) to relate the electron temperature fall across the filter to the plasma density decrease. Although, as stated earlier, the fact that the electron flux varies as $1/B^2$ in tandem H^- sources has been well established, the flux variation with electric potential and temperature gradients had not, so far as is known, been examined. Data from an experiment by Leung (Leung, 1983) were analyzed which show that the temperature gradient and electric field between the two chambers decreases with increasing extraction electrode bias voltage. The data were used to compute the flux through the magnetic filter as a function of these parameters and to compare that flux with the thermal flux to the extraction electrode. Both an enhanced Coulomb collision frequency and an enhanced constant collision frequency provided sufficient electron flux to the extraction chamber, and the variation of flux with V_b was in good agreement with the thermal flux for both collision frequencies as long as the temperature gradient term in the flux equation acted as a drag term. This occurs naturally for both Coulomb collisions and for electron-wave collisions under the restrictions stated in Chapter III.

An electron cooling equation was written based on the work of Ogasawara (Ogasawara, 1990) whose work was, in turn, based on that of Holmes (Holmes, 1982a). It had been noted that Holmes' electron cooling equation predicted that the ratio of source to extraction chamber electron temperatures (T_1/T_2) must increase if the ratio of densities n_1/n_2 also increases. Leung's data (Leung, 1983) showed instead that n_1/n_2 rises as T_1/T_2 falls when the extraction electrode bias voltage V_b is increased. Holmes had neglected temperature gradients and the electric field in his expression for the flux, so this failure could, perhaps, have been anticipated.

Ogasawara generalized Holmes' expressions for the electron particle flux and energy flux across the filter, and produced a general expression relating electron temperatures and temperature gradients to densities and density gradients (Eq (4.26)). In order to solve this equation, however, Ogasawara assumed that the electric field term was negligible and that the energy flux, like the particle flux, was constant from the source chamber to the extraction chamber. As neither assumption is very good in the parameter space of interest in Chapter IV, the electric field term was retained and an expression written for the variation in energy flux as a function of position. This expression was introduced into Eq (4.26) and the resulting equation was shown to reproduce the observed T_1/T_2 decrease as n_1/n_2 increases, as measured by Leung. The observed temperature-density dependence was seen to be caused by the spatial variation in energy flux, which is due primarily to electron-neutral inelastic collisions.

Having examined thermal electron diffusion for three chapters, attention was drawn to primary electron and positive ion motion in Chapter V. For primary electrons it was shown that motion across the filter must be diffusive in nature, but that the classical expression for the flux due to diffusion underestimates the primary electron flux by at least one order of magnitude. Ion transport was assumed to be due to a ballistic flow, rather than diffusion; that is, ions were assumed to move through the filter along kinematically allowed paths according to the Lorentz force equation. This approach was taken rather than use the Boltzmann momentum moment equation. The momentum moment equation is inapplicable for ions due to the fact that ion gyroradii and mean free paths are large in comparison with the density gradient across the filter.

To test these views of ion and primary electron transport, a source model was developed to predict extracted-ion species percentages. The predicted species percentages were found to be in good agreement with measurements (Ehlers, 1982b), thus providing indirect validation of the charged particle transport models. The model was then employed to make predictions about source constituent species densities when the source is operated at the optimum configuration for H^- extraction.

Potential Research

The analysis of Chapter II points clearly to the need for several types of data. In order to determine the electron flux through the filter, it is necessary to measure the current to the extraction electrode. To test whether classical diffusion can provide that flux, the electron density profile from its peak value in the source chamber through the filter mag-

netic field should also be measured. In addition to the density profile measurement, of course, the electron temperature and plasma potential profiles should also be measured. Simultaneous measurement of these three quantities, along with knowledge of the filter magnetic field profile, allows for the testing of Eq (3.78), the classical electron flux expression.

The electron density and temperature profiles in the extraction chamber for a known flux to the extraction electrode would also be of value. The electron density should be measured up to a point one mean free path from the extraction electrode in order to compare the thermal flux to the extraction electrode with the measured current. This will test whether balancing diffusive flux to thermal flux can provide a simple calculation of the extraction chamber electron density, or whether a complex, spatially dependent simulation is in order.

All of the above measurements should be performed for a variety of filter magnetic inductions and plasma electrode bias voltages. High bias voltage provides the most interesting case, since the electron current is highest there.

The hypothesis that ion acoustic or related turbulence is driving the electron diffusion across the filter can be tested by detecting waves with probes and analyzing the output through use of a spectrum analyzer (Kawai, 1978). These waves could well be localized to the filter region since the source of free energy for the instability is likely to be drifts and gradients in that region, while damping may occur throughout the plasma. If it is found that weak turbulence is the driving mechanism for thermal electron diffusion, the question becomes, "What instability or instabilities generate the turbulence?" That question must be answered

before the electron-wave collision frequency can be calculated, and hence before electron transport in the source can be properly modelled. The same is true for primary electron transport.

Assuming the question of electron transport has been resolved, it appears possible to develop a simple, eclectic model of an H^- source. The model would comprise the positive ion/primary electron model of Chapter V, a generalization of Cho's calculation of the plasma potential in a source (Cho, 1990), a moments computation of thermal and primary electron temperatures in the source chamber after Bailey (Bailey, 1987), the electron cooling equation of Chapter IV, and Green's calculation (Eq (1:24)) of the negative ion density in the extraction chamber (Green, undated).

The positive ion model of Chapter V assumes that electron temperatures and electric potential differences between the two chambers of the device are known. The potential difference between the chambers regulates both ion and electron flux to the extraction electrode and thus serves to enforce charge neutrality within the H^- device. Cho's model of particle and power balance in a multicusp device may be generalized to include the effect of charged particle transport across the filter. Then both source and extraction chamber plasma potentials can be computed on the basis of particle and power balances in the discharge. The solution envisioned is necessarily iterative: electron loss through the filter acts to increase the source chamber plasma potential, but at the same time this loss is a function of the potential gradient between the two chambers (Eq (3.78)).

Although the source chamber plasma density will be given by the positive ion model of Chapter V, information about electron temperatures in the source chamber must be obtained from another source. The source chamber electron temperatures (thermal and primary) can be computed employing a moments approach. This computation, in turn, depends upon the difference in potential between the source chamber plasma and the chamber walls. But, since Cho's calculation of the plasma potential requires knowledge of the electron temperatures, the solution to this part of the problem is iterative also. Once temperatures T_e and T_p are computed, the calculation of the plasma potential must be revised.

Given, then, the source chamber plasma density and electron temperatures, and the difference in potential between the two chambers, the extraction chamber electron density and temperature may be calculated. The ion model of Chapter V gives positive ion density in the extraction chamber. If the model is generalized to allow for the computation of the H^- density in the extraction chamber by employing Green's equation (Eq (1.24)), the extraction chamber electron density follows from charge neutrality. The extraction chamber electron temperature may be computed from Eq (4.26), the electron cooling equation. But, since assumed values for the extraction chamber density and temperature were employed in the generalization of Cho's particle and energy balance equations, here again an iterative approach is mandated.

It is possible that, even if the above converges to a solution for the H^- density in the extraction chamber, the information so gained may not prove useful. Edgley and von Engel (Edgley, 1980) modelled a pos-

itive column with negative ions present and discovered that the density of negative ions was not even approximately constant. Devynck's measurements (Devynck, 1987) and those of Johnson (Johnson, 1987) suggest that the same is true in magnetic multicusp H^- sources: the H^- extraction chamber density is strongly dependent upon position. Yet, it may turn out that the extractable H^- current density will scale in a simple way with the extraction chamber H^- density computed from the eclectic model outlined above.

Care must also be taken with the calculation of the positive ion flux to the extraction electrode under conditions of high negative ion density. Amemiya (Amemiya, 1988) has shown that, if $T_e >> T_I$ or the negative ion temperature T_-, the Bohm form for the positive ion saturation current is not much altered even if $n_-/n_e = 0.9$. But if $n_- >> n_e$, then the positive ion saturation current is governed not by T_e, but by T_I. For flat potential profiles between the two chambers, this modification to the positive ion model may be significant. (It will be recalled that in the Chapter V model, the ion current to the extraction electrode was governed by the difference in potentials between the chambers except when that difference in potential was smaller than the extraction chamber electron temperature, in which case the Bohm form for the positive ion saturation current was employed.)

Appendix: Index of Symbols

A	cross sectional area of the source
A_p	effective wall loss area for primary electrons
A_p^a	effective anode loss area for primary electrons
A_p^b	effective plasma electrode loss area for primary electrons
A_e^a	effective anode loss area for thermal electrons
A_e^b	effective plasma electrode loss area for thermal electrons
A_I^a	effective anode loss area for positive ions
A_I^b	effective plasma electrode loss area for positive ions
A_I^f	effective filter area for positive ion transport
A_p^f	effective filter area for primary electron transport
A_{ij}	$\delta_{ij}\upsilon^2 - \upsilon_i\upsilon_j$
a	characteristic width of filter, about 2 cm
a	parameter relating energy flux to wall, 2.5
$\underline{b}$	unit vector in the direction of $\underline{B}$
$\underline{B}$	magnetic induction
B_{ij}	$3\upsilon_i\upsilon_j - \delta_{ij}\upsilon^2$
$\underline{c}$	random electron velocity, $\underline{c} = \underline{\upsilon} - \underline{u}$
c	speed of light in a vacuum
D^-	negative ionic deuterium
d	6×10^{-23} cm^3 erg$^{3/2}$ sec^{-1}
D	Holmes' diffusion coefficient prior to averaging, or a general symbol for the diffusion coefficient

$\langle D \rangle$	Holmes' D averaged over a Maxwellian electron velocity distribution function
$d\underline{x}$	$dxdydz = d^3x$
$d\underline{\upsilon}$	$d\upsilon_x d\upsilon_y d\upsilon_z = d^3\upsilon$
$d\sigma$	$\rho d\rho d\phi$
$d\phi$	differential polar angle
$D_{e\perp}$	Ferriera's cross-field electron diffusion coefficient
D_{ik}^{α}	i, k th component of velocity space diffusion tensor for particles of species α
$D_{ik}^{\alpha/\beta}$	i, k th component of velocity space diffusion tensor for particles of species α due to collisions with particles of species β
$\underline{E}$	electric field
e	electron
e	magnitude of electric charge
f_α	one-particle distribution function for particles of species α
$\underline{F}^{(e)}$	external force acting on a particle
F_i^{α}	i th component of force of dynamic friction acting on particles of species α
$F_i^{\alpha/\beta}$	i th component of force of dynamic friction acting on particles of species α due to collisions with particles of species β
$f(\underline{\upsilon}^\circ)$	source chamber particle velocity distribution function
$f^\circ(\chi_\beta)$	$\exp(-\chi_\beta^2)$
g	number between 0 and 1. g=0 indicates all ions are trapped in the filter, g=1 indicates that no ions are trapped in the filter
$G(\chi)$	defined by Eq (2.18)
h	3.5×10^3 cm/sec
H	atomic hydrogen

H^-	negative ionic hydrogen
H^+	singly ionized atomic hydrogen
H_2^+	singly ionized diatomic hydrogen
H_3^+	singly ionized triatomic hydrogen
$H_2(v)$	diatomic hydrogen with vibrational quantum number v
$H_2^+(v)$	singly ionized diatomic hydrogen with vibrational quantum number v
H_2	diatomic hydrogen
i	index, vector component, or ionization (as in S_i)
I_d	discharge current
I	designator to indicate ion quantity
I_e	total current to the plasma electrode
j	extracted current density
j_I	total positive ion-current
j_o	extracted H^- current density with scale length R_o
j_b	extracted H^- current density with scale length R_b
j_i^α	i th component of velocity space flux for particles of species α, defined by Eq (3.4)
$j_i^{\alpha/\beta}$	i th component of velocity space flux for particles of species α, due to collisions with particles of species β
j	index, or vector component
k	index, or vector component
$\underline{k}$	wave vector
$\langle 1/k \rangle$	average wavelength of turbulence
L	total cusp length
L_{1o}	mean free path for H^+ - H_2 collisions
L_{2o}	mean free path for H_2^+ - H_2 collisions

L_{3o}	mean free path for H_3^+ - H_2 collisions
L_i	mean free path for H_2 ionization by electrons
$\ln(\lambda)$	Coulomb logarithm
l	index
$L^{\alpha/\beta}$	defined by Eq (3.28)
m_α	mass of particle of species α
m_β	mass of particle of species β
m	particle mass, or index
m_e	electron mass
m_I	ion mass
m_t	mass of test particle
$m_{\alpha\beta}$	$(m_\alpha m_\beta)/(m_\alpha + m_\beta)$
N_2	number density of H_2
n_p	number density of primary electrons
$n_p^{(1)}$	number density of primary electrons in source chamber
$n_p^{(2)}$	number density of primary electrons in extraction chamber
n	charged particle number density
n_o	source chamber ion density (Chapter V)
n_e	thermal electron number density
n_I	positive ion number density
n_-	H^- number density
n_1	Chapter V, H^+ density elsewhere, electron density in source chamber
n_2	Chapter V, H_2^+ density elsewhere, electron density in extraction chamber
n_3	H_3^+ density

$n_1^{(1)}$	source chamber H^+ density
$n_1^{(2)}$	extraction chamber H^+ density
$n_2^{(1)}$	source chamber H_2^+ density
$n_2^{(2)}$	extraction chamber H_2^+ density
$n_3^{(1)}$	source chamber H_3^+ density
$n_3^{(2)}$	extraction chamber H_3^+ density
$n_e^{(2)}$	extraction chamber thermal electron density
$n_I^{(1)}$	source chamber positive ion density
$n_I^{(2)}$	extraction chamber positive ion density
n_t	number density of test particles
N^*	number density of $H_2(v)$
N_H	number density of H
n_β	number density of particles of species β
n_{eAV}	$(n_1 + n_2)/2$, average electron number density
n_o	source chamber particle number density
p	pressure
p_e	electron pressure, $n_e T_e$
Q	probability that, in time Δt , the velocity changes by an amount $\Delta \underline{v}$
$\underline{Q}$	energy flux vector
$\underline{q}_e$	heat flux vector
R	system scale length; R_b and R_o are two values
$\underline{r}$	position vector of Lamor center
r_e	electron Lamor radius
r_I	ion Lamor radius
S_d	rate coefficient for the process e + H_2 → e + 2H

S_i	$\langle \sigma \upsilon (2^+) \rangle + \langle \sigma \upsilon \rangle_{DI}$
T_e	thermal electron temperature
T_α	temperature of species α
T_t	temperature of test particle distribution
t	time
T_{eAV}	electron temperature, average of source and extraction chamber temperatures
T_I°	effective ion temperature, given turbulence
T	temperature
T_1	Chapter V, temperature of H^+ elsewhere, electron temperature in source chamber
$T_1^{(1)}$	temperature of H^+ in source chamber
$T_1^{(2)}$	temperature of H^+ in extraction chamber
T_2	Chapter V, temperature of H_2^+ elsewhere, electron temperature in extraction chamber
$T_2^{(1)}$	temperature of H_2^+ in source chamber
$T_2^{(2)}$	temperature of H_2^+ in extraction chamber
$T_3^{(1)}$	temperature of H_3^+ in source chamber
$T_3^{(2)}$	temperature of H_3^+ in extraction chamber
T_p	primary electron temperature
$T_p^{(1)}$	primary electron temperature in source chamber
$T_p^{(2)}$	primary electron temperature in extraction chamber
$\underline{u}$	directed velocity, especially electron directed velocity
u_I	positive ion directed velocity
$\underline{u}_I^d$	positive ion drift velocity
V_a	anode voltage

V_b	extraction electrode voltage
V_p	plasma potential
v	vibrational quantum number
υ_p	mean velocity of primary electrons
$\bar{\upsilon}$	average thermal electron velocity $((8T_e)/(\pi m_e))^{1/2}$
V	volume of plasma
$\underline{\upsilon}$	electron velocity or velocity of test or α particle
$\underline{\upsilon}'$	velocity of field or β particles
υ_y°	y component of velocity at the source chamber edge of the filter field
υ_x°	x component of velocity at the source chamber edge of the filter field
W_e	leak width for electron losses at cusps
w	wave index
w_i	defined by Eq (3.18)
w_{ij}	defined by Eq (3.19)
W_{ij}	defined by Eq (3.62)
$W(\underline{k})$	energy density of turbulence in $d\underline{k}$ about $\underline{k}$
W	$\int d\underline{k} W(\underline{k})$
x	the distance along the axis of a cylindrical source
y	distance $\perp$ to x axis and $\underline{B}$
z	distance along axis paralled to $\underline{B}$
Z	extraction chamber length
Z	Ze is the species charge

Z°	$Z^\circ e$ is the effective ion charge, given turbulence
α	Chapter I, the ratio $n_I^{(2)}/n_I^{(1)}$
	Chapter II, $(m_e T_I)/(m_I T_e)$, or 1
	Chapter III, particle species index
	Chapter IV, $\frac{3}{2}g-(1+\frac{T\partial\nu}{\nu\partial T})$
β	Chapter II, defined by Eq (2.9)
	Chapters I and III, particle species index
	Chapter IV, a factor governing the energy flux to a boundary, theoretically equal to $2/(1-\gamma)$
$\underline{\Gamma}$	particle flux vector
Γ_x	x component of particle flux
Γ_{I_x}	x component of positive ion flux
Γ_e^a	electron flux to the anode
Γ_e^b	electron flux to the plasma electrode
Γ_I^a	positive ion flux to the anode
Γ_I^b	positive ion flux to the plasma electrode
Γ_p^a	primary electron flux to the anode
Γ_p^b	primary electron flux to the plasma electrode
Γ_f	thermal electron flux through the filter
Γ_b	thermal electron flux to the extraction electrode
Γ_{Bohm}	flux calculated using Bohm diffusion coefficient
Γ_f^p	primary electron flux through the filter
Γ_b^p	primary electron flux to the extraction electrode
γ_p	primary electron secondary electron emission coefficient

γ_I	positive ion secondary electron emission coefficient
Δn	$n_2 - n_1$
Δx	width of filter field, or x component of change in Lamor center position upon collisions
ΔV	change in plasma potential from source to extraction chamber
Δ	width of filter field
$\Delta\phi_p$	$\phi_1 - \phi_2$
$\Delta\phi_w$	$\phi_2 - V_b$
$\Delta\underset{\sim}{\upsilon}$	change in $\underset{\sim}{\upsilon}$ upon collisions
$\langle\Delta\upsilon_i\rangle$	defined in Eq (3.11)
$\langle\Delta\upsilon_i\Delta\upsilon_j\rangle$	defined in Eq (3.12)
$\langle\Delta\upsilon_i\rangle^{\alpha/\beta}$	defined in Eq (3.16)
$\langle\Delta\upsilon_i\Delta\upsilon_j\rangle^{\alpha/\beta}$	defined in Eq (3.17)
$\Delta\underset{\sim}{r}$	change in Lamor center position upon collisions
$\Delta\omega$	change in ω over a change Δx in x
$\frac{\delta f_\alpha}{\delta t}$	rate of change in f_α due to collisions
$\frac{\delta(n_e u_k)}{\delta t}$	defined by Eq (3.64)
$\frac{\delta(n_e \underset{\sim}{\mu})^{(0)}}{\delta t}$	defined by Eq (3.90)
$\frac{\delta(n_e \underset{\sim}{\mu})^{(1)}}{\delta t}$	defined by Eq (3.90)

δ_{ij}	Kronecker delta, $\delta_{ij} = 1$ if $i = j$, 0 otherwise
$\delta(x)$	Dirac delta function of x
$\frac{\delta n\langle K\rangle}{\delta t}$	rate of change in electron energy density upon collisions
ε	defined by Eq (2.13)
ζ_i	defined by Eq (5.18), filter transparency factor
ν_{el}	electron-ion Coulomb collision frequency (see Eq (2.24))
ν_c	defined by Eq (2.17)
$\langle\nu_c\rangle$	Holmes' collision frequency (Eq (2.23))
ν_{ea}	elastic electron-neutral collision frequency
ν_{ew}	electron-wave collision frequency (Eq (3.95))
ν_s	$\nu_{ew}+\nu_{el}$ (see Eq (3.97))
ν_I	ν_{el}
ν_{in}	inelastic collision frequency
ν_p^C	primary electron Coulomb collision frequency
ν_p^{el}	primary electron total elastic collision frequency
ν_p^{in}	primary electron total inelastic collision frequency
π_{ij}	electron viscous stress tensor
ρ	impact parameter
$\rho_\perp$	$(e_\alpha e_\beta)/(m_{\alpha\beta}V^2)$
ρ_{min}	$2\rho_\perp$
ρ_b	$\underline{b}\times\underline{v}/\omega$
σ	cross section
σ_{in}	electron - H_2 inelastic collision cross section
σ_{ion}	total e - H_2 ionization cross section

$\langle \sigma v (3^+, H) \rangle$	rate coefficient for $H_2 + H_2^+ \rightarrow H_3^+ + H$
$\langle \sigma v (2^+) \rangle$	rate coefficient for $e + H_2 \rightarrow H_2^+ + 2e$
$\langle \sigma v \rangle_{+-}$	rate coefficient for H^-, positive ion neutralization
$\langle \sigma v \rangle_{DA}$	rate coefficient for $e + H_2(v) \rightarrow H + H^- + e$
$\langle \sigma v \rangle_{H^-}$	rate coefficient for $H + H^- \rightarrow 2H + e$
$\langle \sigma v \rangle_m$	defined by Eq (1.12)
$\langle \sigma v \rangle_p$	rate coefficient for $e + H_2 \rightarrow H_2(v) + e$
$\langle \sigma v \rangle_D$	rate coefficient for destruction of $H_2(v)$
$\langle \sigma v \rangle_{eD}$	rate coefficient for $e + H^- \rightarrow H + 2e$
$\langle \sigma v (1^+) \rangle$	rate coefficient for production of H^+ through destruction of H_3^+ by energetic electrons
$\langle \sigma v \rangle_{DI}$	rate coefficient for $e + H_2 \rightarrow H^+ + H + e$
$\langle \sigma v (1^+, H) \rangle$	dissociative excitation of H_2^+ by energetic electron impact forming $H + H^+$
$\langle \sigma v \rangle_{DR}$	rate coefficient for dissociative recombination of H_3^+
τ_I	characteristic positive ion destruction time
τ_H	characteristic atomic hydrogen wall loss time
τ^*	$H_2(v)$ wall loss time
τ^-	H^- wall loss time
τ_e	electron temperature in electron volts
τ_c	mean time between collisions
ϕ	Chapter III, polar angle elsewhere, $\phi_2 - \phi_1 = -\Delta\phi_p$
ϕ_1	plasma potential in source chamber
ϕ_2	plasma potential in extraction chamber
$\Phi(\chi)$	error function of χ
φ_β	Trubnikov potential, defined in Eq (3.31)

$\underset{\sim}{\chi}_\beta$	$(m_\beta/(2T_\beta))^{1/2}\underset{\sim}{\upsilon}$
χ	$((m\upsilon^2)/(2T))^{1/2}$
ψ_β	Trubnikov potential, defined in Eq (3.30)
$\psi^\circ(\chi)$	defined by Eq (3.37)
ω	cyclotron frequency
ω_e	electron cyclotron frequency
ω_o	maximum value of ω_e in filter field
ω_p	electron plasma frequency
ω°	$(\omega_k - (\underset{\sim}{k}\cdot\underset{\sim}{u}))/(kc)$
ω_k	frequency of plane wave with wave vector $\underset{\sim}{k}$
$\underset{\sim}{\aleph}$	relative velocity, $\underset{\sim}{\upsilon}-\underset{\sim}{\upsilon}'$ (Chapter III)

Bibliography

Amemiya, Hiroshi. "Probe Diagnostics in Negative Ion Containing Plasma," Journal of the Physical Society of Japan, 57: 887-902 (March 1988).

Allis, W. P. "Motions of Ions and Electrons," Handbuch der Physik, Vol. 21, Berlin: Springer, 1956, 383-444.

Bacal, M. "Volume Production of Hydrogen Negative Ions," Nuclear Instruments and Methods In Physical Research -- Section B: (to be published).

-----. "Analysis of Physical Limitations of Volume Negative Hydrogen Ion Production in Tandem Sources," Proceedings of the 3rd European Workshop on the Production and Application of Light Negative Ions: 112-117 (February 1988).

-----. "Volume Production of H^- Ions at Ecole Polytechnique," Proceedings of the Fourth International Symposium on the Production and Neutralization of Negative Ions and Beams. 246-258. New York: American Institute of Physics, 1987.

-----. "Extraction of Volume-Produced H^- Ions," Reviews of Scientific Instruments, 56: 649-654 (May 1985)a.

-----."Extraction of Volume-Produced H^- Ions from a Hybrid Magnetic Multicusp Source," Reviews of Scientific Instruments, 56: 2274-2278 (December 1985)b.

-----."Negative Ion Production in Hydrogen Plasmas Confined by a Multicusp Magnetic Field," Journal of Applied Physics, 55: 15-24 (January 1984).

-----."Volume Generation of H^- Ions in a Plasma," Physica Scripta, T2/2: 467-478 (September 1982).

Bailey, W. and R. Jones, "Electron Energy Distributions in Magnetic Multicusp Hydrogen Discharges," Proceedings of the Fourth International Symposium on the Production and Neutralization of Negative Ions and Beams. 16-25. New York: American Institute of Physics, 1987.

Bell, David E. A Moment Approach to Modeling Negative Ion Sources. MS Thesis, AFIT/GEP/ENP/87D-2, School of Engineering, Air Force Insti-

tute of Technology (AU), Wright Patterson AFB OH, December 1987 (AD-A188858).

Bernstein, I. A. and R. M. Kulsrud. "Ion Wave Instabilities," Physics of Fluids, 3: 937-945 (November-December 1960).

Bezverbaja, N. K. and others. "Theoretical and Experimental Investigations of Volume Production of Negative Ions," Proceedings of the 3rd European Workshop on Production and Application of Light Negative Ions: 225-230 (February 1988).

Bohm, David. "Qualitative Description of the Arc Plasma in a Magnetic Field," The Characteristics of Electrical Discharges in Magnetic Fields, edited by A. Guthrie and R. K. Wakerling, New York: McGraw-Hill, 1949.

Bonnie, J. H. M. "Scaling Laws for Atomic and Molecular Hydrogen in a Multicusp Ion Source," Physical Review A, 37: 1121-1132 (February 1988).

Braginskii, S. I. "Transport Processes in a Plasma," Reviews of Plasma Physics, Vol 1, New York: Plenum Press, 1965.

Bretagne, J., G. Delovya, M. Capitelli, C. Gorse and M. Bacal, "On Energy Distribution Functions in Low Pressure Magnetic Multicusp Hydrogen Discharges," Journal of Physics D, 19: 1197-1211 (July 1986).

Bruining, H. Physics and Applications of Secondary Electron Emission, New York: Pergamon Press, 1954.

Bruneteau A. and M. Bacal, "Effects of Positive and Negative Ion Energies on H^- Destruction by Mutual Neutralization in Low Pressure Plasmas," Journal of Applied Physics, 57: 4342-4348 (May 1985).

Brynolf, J. and others. "H^- Formation in a Low-Density Plasma in a Magnetic Mirror Field," Proceedings of the 3rd European Workshop on Production and Application of Light Negative Ions: 118-123 (February 1988).

Cadez, I. and others. "Vibrational Excitation of Hydrogen Molecules Produced by Wall Recombination of Hydrogen Atoms," Proceedings of the 3rd European Workshop on Production and Application of Light Negative Ions: 170-174 (February 1988).

Chan, C. F. and others. "Model of Positive Ion Sources for Neutral Beam Injection," Journal of Applied Physics, 54: 6119-6137 (November 1983).

Chandrasekhar, S. Plasma Physics, Chicago, Illinois: University of Chicago Press, 1961.

Cho, M-H. and others. "Particle and Power Balances of Hot-Filament Discharge Plasmas in a Multipole Device," Journal of Applied Physics, 67: 3254-3259 (April 1980).

Clemmow, P. C. and J. P. Dougherty. Electrodynamics of Particles and Plasmas, Reading, Mass.: Addison-Wesley, 1969.

Department of the Navy. NRL Plasma Formulary. Washington D. C.: 1983.

Devynck, P. and others. "Spatial Variation of Negative Ion Density in a Volume H^- Ion Source," Revue de Physique Applique, 22: 753-759 (August 1987).

Drummond, W. E. and M. N. Rosenbluth. "Anomalous Diffusion Arising from Microinstabilities in a Plasma," Physics of Fluids, 5: 1507-1513 (December 1962).

Dum, C. T. "Anomalous Electron Transport Equations for Ion Sound and Related Turbulent Spectra," Physics of Fluids, 21: 956-969 (June 1978)a.

-----. "Anomalous Heating by Ion Sound Turbulence," Physics of Fluids, 21: 945-955 (June 1978)b.

-----. "Turbulent Heating and Quenching of the Ion Sound Instability," Physical Review Letters, 32: 1231-1234 (June 1974).

Edgley, K. W. and A. von Engel. "The Theory of Positive Columns in Electronegative Gases," Proceedings of the Royal Society of London A, 370: 375-387 (March 1980).

Eenshuistra, P. J. and others. "Formation of Vibrationally Excited Hydrogen Molecules by Wall Recombination of Atoms," Proceedings of the 3rd European Workshop on Production and Application of Light Negative Ions: 175-180 (February 1988).

Ehlers, K. W. "High Current Negative Ion Sources," Reviews of Scientific Instruments, 61: 662-664 (January 1990).

-----. "Increasing the Efficiency of a Multicusp Ion Source," Reviews of Scientific Instruments, 53: 1429-1433 (September 1982)a.

-----. "Further Study of a Magnetically Filtered Multicusp Ion Source," Reviews of Scientific Instruments, 53: 1423-1428 (September 1982)b.

-----. "Effects of a Magnetic Filter on Hydrogen Ion Species in a Multicusp Ion Source," Reviews of Scientific Instruments, 52: 1452-1458 (October 1981).

Emmert, G. A. and others. "Electrical Sheath and Presheath in a Collisionless, Finite Ion Temperature Plasma," Physics of Fluids, 23: 803- 812 (April 1980).

Epperlein, E. M. and M. G. Haines. "Plasma Transport Coefficients in a Magnetic Field by Direct Numerical Solution of the Fokker-Plank Equation," Physics of Fluids, 29: 1029 - 1041 (April 1986).

Ferriera, J. L. and others. "Anomalous Particle Diffusion through a Magnetic Picket Fence," Presented at the Spring College on Plasma Physics, Trieste, Italy, 15 May - 9 June 1989 (June 1989).

Forrester, A. T. Large Ion Beams, New York: John Wiley & Sons, 1987.

Frieman, E. A. "Collisional Diffusion in Nonaxisymmetric Toroidal Systems," The Physics of Fluids, 13: 490-496 (February 1970).

Galeev, A. A. and R. G. Sagdeev. "Transport Phenomena in a Collisionless Plasma in a Toroidal Magnetic System," Soviet Physics, JETP, 26: 223-240 (January 1968).

Gary, S. P. "Wave-Particle Transport from Electrostatic Instabilities," Physics of Fluids, 23: 1193-1204 (June 1980).

Golant, V. E. Fundamentals of Plasma Physics, New York: John Wiley & Sons, 1980.

-----. "Diffusion of Charged Particles in a Plasma in a Magnetic Field," Soviet Physics Uspekhi, 79: 161-197 (September-October 1963).

-----. "Diffusion of Charged Particles Across a Magnetic Field in a Three-Component Plasma," Soviet Physics Technical Physics, 5: 831-841 (February 1961).

Goldman, Martin V. "Strong Turbulence of Plasma Waves," Reviews of Modern Physics, 56: 709 - 735 (October 1984).

Grad, H. "On the Kinetic Theory of Rarefied Gases," Communications on Pure and Applied Mathematics, 2: 331-407 (1949).

Green, T. S. and others. "A Model for H^- Production Ion Sources," unpublished.

Hinton, F. L. "Collisional Transport in a Plasma," Basic Plasma Physics, Vol 1, edited by A. A. Galeev and R. N. Sudan, New York: North-Holland, 1983.

Hiskes, J. R. "Review of Progress in the Theory of Volume Production," Proceedings of the Fourth International Symposium on Production and Neutralization of Negative Ions and Beams, 2-15. New York: American Institute of Physics, 1987.

-----. "Optimum Extracted Negative-Ion Current Densities from Tandem High Density Hydrogen Discharges," Journal of Applied Physics, 58: 1759-1764 (September 1985).

-----. "Generation of Negative Ions in Tandem High Density Hydrogen Discharges," Journal of Applied Physics, 56: 1927-1938 (October 1984).

-----. "Hydrogen Vibrational Population Distributions and Negative Ion Concentrations in a Medium Density Hydrogen Discharge," Journal of Applied Physics, 53: 3469-3475 (April 1982).

Hoh, F. C. "Low-Temperature Plasma Diffusion," Reviews of Modern Physics, 14: 267-286 (April 1962).

Holmes, A. J. T. and others. "Multipole Source Scaling Laws," Reviews of Scientific Instruments, 58: 223-234 (February 1987).

-----. "Electron Cooling in Magnetic Multipole Arc Discharges," Reviews of Scientific Instruments, 53: 1523-1526 (October 1982)a.

-----. "Electron Flow through Transverse Magnetic Fields in Magnetic Multipole Arc Discharges," Reviews of Scientific Instruments, 53: 1517-1522 (October 1982)b.

Hopkins, M. B. "Modelling the Effects of Different Magnetic Field Geometries on Ion Source Design," Proceedings of the 3rd European Workshop on Production and Application of Light Negative Ions: 106-111 (February 1988).

-----. "Spatially and Temporally Resolved EEDF Measurements in a Hydrogen Discharge," Proceedings of the Fourth International Symposium on the Production and Neutralization of Negative Ions and Beams. ??-??. New York: American Institute of Physics, 1987.

-----. "Langmuir Probe Technique for Plasma Parameter Measurement in a Medium Density Discharge," Reviews of Scientific Instruments, 57: 2210-2217 (September 1986).

Jimbo, K. "Application of Anomalous Diffusion in Production of Negative Ions," Physics of Fluids, 27: 2752-2761 (November 1984).

Johnson, J. D. Characteristics of a Multipole Volume H- Plasma, PhD Dissertation. The University of Aston, Birmingham, Great Britain, October, 1987.

Jones, R. and W. Bailey, "Diffusion and Free Flow through a Magnetic Filter," Proceedings of the Fourth International Symposium on the Production and Neutralization of Negative Ions and Beams. 106-111. New York: American Institute of Physics, 1987.

Kadomtsev, B. B. Plasma Turbulence, New York: Academic, 1965.

Katsch, M. and K. Wiseman. "Relaxation of Suprathermal Electrons Due to Coulomb Collisions in a Plasma," Plasma Physics, 22: 627-638 (January 1980).

Kawai, Y. and others. "Ion Acoustic Turbulence in a Large-Volume Plasma," Physics of Fluids, 21: 970-974 (June 1978).

Kock, C. and G. Matthieussent. "Collisional Diffusion of a Plasma in Multipolar and Picket Fence Devices," Physics of Fluids, 26: 545-555 (February 1983).

Langmuir, I. and L. Tonks. "A General Theory of the Plasma of an Arc," Physical Review, 34: 876-922 (September 1929).

Lea, L. M. and others. "The Suppression of Electrons Extracted from a Negative Ion Source," Reviews of Scientific Instruments, 61: 409-411, (January 1990).

Leung, K. N. and others. "Enhancement of H^- Production in an Multicusp Source by Cold Electron Injection," Reviews of Scientific Instruments, 57: 321-324 (March 1986).

-----. "Effect of Wall Material on H^- Production in a Multicusp Source," Applied Physics Letters, 47: 227-228 (August 1985)a.

-----. "Optimization of H^- Production in a Magnetically Filtered Multicusp Source," Reviews of Scientific Instruments, 56: 364-368 (March 1985)b.

-----. "Ion Source Operation with Different Magnetic Confinement Geometries," Reviews of Scientific Instruments, 55: 342-345 (March 1984)a.

-----. "H^- Density Measurement in a Tandem Multicusp Discharge," Reviews of Scientific Instruments, 55: 338-341 (March 1984)b.

-----. "Extraction of Volume-Produced H^- Ions from a Multicusp Source," Reviews of Scientific Instruments, 54: 54-61 (January 1983).

Longmire, C. L. and M. N. Rosenbluth. "Diffusion of Charged Particles Across a Magnetic Field," Physical Review, 103: 507-510 (August 1956).

Manheimer, W. M. and others. "Cross Field Thermal Transport Due to Ion Acoustic Waves in Weakly Magnetized Plasmas," Physics of Fluids, 21: 2009-2013 (November 1978).

McDaniel, E. W. Collisional Phenomena in Ionized Gases, New York: John Wiley & Sons, 1964.

McKee, L. Class lecture in Physics 7.54, Physics of Charged Particle Beams, School of Engineering, Air Force Institute of Technology (AU), Wright-Patterson AFB, OH, March, 1986.

Melrose, D. B. Instabilities in Space and Laboratory Plasmas, Cambridge: Cambridge University Press, 1986.

Mordin, A. B. Etude Sur L'Ion Negatif D'Hydrogen Dans Des Decharges A Basse Pression. PhD dissertation, Centre D'Orsay, University de Paris -- Sud, July 1983.

National Bureau of Standards. Handbook of Mathematical Functions, Washington, D. C.: Government Printing Office , 1964.

Ogasawara, M. and others, "Transport Processes through Magnetic Filter in Negative Ion Source," Proceedings of the Fifth International Symposium on the Production and Neutralization of Negative Ions and Beams. 596-602. New York: American Institute of Physics, 1990.

Okuda, H. and J. M. Dawson, "Theory and Numerical Simulation on Plasma Diffusion Across a Magnetic Field," The Physics of Fluids, 16: 408-426 (March 1973).

Phelps, A. V. "Cross Sections and Swarm Coefficients for H^+, H_2^+, H_3^+, and H^- in H_2 for Energies from 0.1 eV to 10 keV," Journal of Physical and Chemical Research Data, 19: 653-675 (May-June 1990).

Ray, J. A. and others, "Absolute Measurement of Low-Energy H^0 Fluxes by a Secondary Emission Detector," Journal of Applied Physics, 50: 6516-6519 (October 1979).

Rutherford, P. H. and others. "Effects of Longitudinal Electric Field on Toroidal Diffusion," Physical Review Letters, 25: 1090-1093 (October 1970)a.

-----. "Collisional Diffusion in an Axisymmetric Torus," The Physics of Fluids, 13: 482-489 (February 1970)b.

Sagdeev, R. "The 1976 Oppenheimer Lectures: Critical Problems in Plasma Astrophysics. 1. Turbulence and Nonlinear Waves," Reviews of Modern Physics, 51: 1-9 (January 1979).

Shkarofsky, I. P. and others. The Particle Kinetics of Plasmas. Reading, Mass.: Addison-Wesley, 1966.

Smith, Kenneth and Alan Glasser, Data Base of Cross Sections and Reaction Rates for Hydrogen Ion Sources, 1987. Los Alamos National Laboratory, LA-UR-87-2736.

Spitzer, L. Physics of Fully Ionized Gases (Second Edition), New York: John Wiley & Sons, 1962.

-----. "Particle Diffusion Across a Magnetic Field," Physics of Fluids, 3: 659-661 (July-August 1960).

-----. "Transport Phenomena in a Completely Ionized Gas," Physical Review, 89: 977-981 (March 1953).

Stacey, W. M. Fusion Plasma Analysis, New York: John Wiley & Sons, 1981.

Strangeby, P. C. "The Plasma Sheath," Physics of Plasma-Wall Interactions in Controlled Fusion, edited by D. E. Post and R. Behrisch. New York: Plenum, 1986.

Swift, J. D. and M. J. R. Schwarr. Electrical Probes for Plasma Diagnostics. New York: American Elsevier, 1969.

Tarawa, H. and others. "Cross Sections and Related Data for Electron Collisions with Hydrogen Molecules and Molecular Ions," Journal of Physical and Chemical Reference Data, 19: 617-636 (May-June 1990).

Trubnikov, B. A. "Particle Interactions in a Fully Ionized Plasma," Reviews of Plasma Physics, Vol 1. New York: Plenum Press, 1965.

Vedenov, A. A. Theory of a Turbulent Plasma, New York: American Elsevier, 1968.

-----. "Stability of a Plasma," Soviet Physics Uspekhi, 4: 336-337.

-----. "Quasilinear Approximation in the Kinetic Theory of a Low-Density Plasma," Soviet Physics JETP, 16: 682-684 (March 1963).

Wadhera, J. M. "Dissociative Attachment to Rovibrationally Excited H_2," Physical Review A, 29: 106-110 (January 1984).

Walther, S. R. Development of L^- and H^- Ion Sources. PhD dissertation. Lawrence Berkeley Laboratory, University of California, Berkeley, California, December 1988.

Weinstock, J. and R. H. Williams. "Nonlinear Theory of Microinstabilities and Enhanced Transport in Plasmas," Physics of Fluids, 14: 1472-1480 (July 1971).

Wells, N. The Development of High-Intensity Negative Ion Sources and Beams in the U.S.S.R., Defense Advanced Research Agency Report R-2816-ARPA, (1981).

Wu, Tan-You. Kinetic Equations of Gases and Plasmas, Addison-Wesley, Reading, Mass.: 1966.

York, R. L. and others. "Extraction of H^- Beams from a Magnetically Filtered Source," Reviews of Scientific Instruments, 55: 681-685 (May 1984).

REPORT DOCUMENTATION PAGE

Form Approved
OMB No. 0704-0188

1. AGENCY USE ONLY (Leave blank)	2. REPORT DATE	3. REPORT TYPE AND DATES COVERED
	December 1991	Doctoral Dissertation

4. TITLE AND SUBTITLE

Plasma Transport in a Magnetic Multicusp Negative Hydrogen Ion Source

5. FUNDING NUMBERS

6. AUTHOR(S)

Ricky G. Jones, Capt, USAF

7. PERFORMING ORGANIZATION NAME(S) AND ADDRESS(ES)

Air Force Institute of Technology, WPAFB, OH 45433-6583

8. PERFORMING ORGANIZATION REPORT NUMBER

9. SPONSORING MONITORING AGENCY NAME(S) AND ADDRESS(ES)

10. SPONSORING MONITORING AGENCY REPORT NUMBER

11. SUPPLEMENTARY NOTES

12a. DISTRIBUTION AVAILABILITY STATEMENT

Approved for public release; distribution unlimited

12b. DISTRIBUTION CODE

13. ABSTRACT (Maximum 200 words)

An analysis of plasma transport through the magnetic filter in tandem magnetic multicusp negative hydrogen ion sources was conducted to determine the mechanism of thermal electron diffusion, explain thermal electron cooling, describe the transport of primary electrons through the filter, and model positive ion species transport. The thermal electron flux was shown to exceed its classical value by one to three orders of magnitude. The flux variation with temperature was best described using a Coulomb-like temperature gradient drag term, consistent with diffusion due to ion-sound-like turbulence. Thermal electron energy flux loss was shown to be dominated by inelastic collisions at low values of the particle flux. Consequently, an equation was derived which correctly reproduces the observed variation in the ratio of source to extraction chamber densities as a function of the ratio of source to extraction chamber electron temperatures. The primary electron flux was found to be one order of magnitude higher than the classical collisional rate. Positive ion species transport was modelled assuming ballistic flow. Ion production and loss mechanisms were used in conjunction with transport to calculate extracted positive ion species percentages. Results were found to be in reasonable agreement with experiment.

14. SUBJECT TERMS	15. NUMBER OF PAGES
Ion Sources, Electron Transport, Turbulent Diffusion, Thermal Diffusion, Plasma Devices, Plasma Waves, Particle Beams	242
	16. PRICE CODE

17. SECURITY CLASSIFICATION OF REPORT	18. SECURITY CLASSIFICATION OF THIS PAGE	19. SECURITY CLASSIFICATION OF ABSTRACT	20. LIMITATION OF ABSTRACT
Unclassified	Unclassified	Unclassified	UL